2016

Impact Behaviour of Reinforced Concrete Beams Strengthened or Repaired with Carbon Fibre Reinforced Polymer (CFRP)

Al-Farttoosi, Mahdi

http://hdl.handle.net/10026.1/6701

http://dx.doi.org/10.24382/1247
University of Plymouth

Impact Behaviour of Reinforced Concrete Beams Strengthened or Repaired with Carbon Fibre Reinforced Polymer (CFRP)

MAHDI HAMEED MOHAMMED AL-FARTTOOSI

PhD 2015

Impact Behaviour of Reinforced Concrete Beams Strengthened or Repaired with Carbon Fibre Reinforced Polymer (CFRP)

by

MAHDI HAMEED MOHAMMED AL-FARTTOOSI

A thesis submitted to Plymouth University in partial fulfilment of the degree of

DOCTOR OF PHILOSOPHY

School of Marine Science and Engineering

Faculty of Science and Engineering

Plymouth University, UK

September 2015

ACKNOWLEDGEMENTS

AUTHOR'S DECLARATION

At no time during the registration for the degree of Doctor of Philosophy has the author been registered for any other University award without prior agreement of the Graduate Committee.

Journal papers under Preparation

Experimental Investigation of Damaged Reinforced Concrete Beams Repaired with Carbon Fibre Reinforced Polymer (CFRP) Strip under Impact Loading.

Impact behaviour of reinforced concrete beams strengthened with carbon fibre reinforced polymer (CFRP) using different strengthening techniques.

Nonlinear Finite Element Analysis (FEA) Model Development for the impact behaviour of damaged Reinforced Concrete Beams Externally Strengthened with CFRP under impact loading

Publications:

AL-FARTTOOSI, M., RAFIQ, Y., SUMMERSCALES, J.AND WILLIAMS, C., 2013. "Nonlinear Finite Element Analysis (FEA) of Flexural Behaviour of Reinforced Concrete Beams Externally Strengthened with CFRP", Proc. of Advanced Composites in Construction ACIC2013 Conf., Queen's University Belfast, pp 200-213.

RAFIQ, Y. AND AL-FARTTOOSI, M., 2013. "Using Model Updating to Predict the Failure of Reinforced Concrete Elements". ASCE Conference on Computing in Civil Engineering-2013: pp. 459-467. (Winner of Prize for the Best Paper).

Rafiq,Y. and Al-Farttoosi, M. 2014. "Predicting the Behaviour of Reinforced Concrete Elements Strengthened with CFRP Using Model Updating Techniques". Computing in Civil and Building Engineering, Orlando Florida.

AL-FARTTOOSI, M., RAFIQ, Y., SUMMERSCALES, J.AND WILLIAMS, C. 2014. "Using Model Updating Techniques to assess bond-slip effects on the behaviour of reinforced concrete beams externally strengthened with CFRP". Intelligent Computing in Engineering, Cardiff, UK, July 16-18. CCCBE, CIBW74 Conference.

AL-FARTTOOSI, M., RAFIQ, Y., SUMMERSCALES, J.AND WILLIAMS, C., 2014," Dynamic impact behaviour of reinforced concrete beams externally strengthened with carbon fibre reinforced polymer (CFRP)". Structural Faults and Repair Conference, Imperial College, London.

AL-FARTTOOSI, M., RAFIQ, Y., SUMMERSCALES, J.AND WILLIAMS, C. 2015," A New Instrumented Drop-Weight Test Machine for Studying the Impact Behaviour of

Reinforced Concrete Beams". The 17th International Conference on Civil, Structural and Earthquake Engineering (ICCSEE 2015), Barcelona, SPAIN, 26-27 October.

RAFIQ, Y., SPEARMAN, J. AND AL-FARTTOOSI, M. 2015." Investigating the load carrying capacity of RC undamaged and damaged beams strengthened with CFRP" ASEMIS Conference, South Korea.

Impact Behaviour of Reinforced Concrete Beams Strengthened or Repaired with Carbon Fibre Reinforced Polymer (CFRP)

Abstract

War, terrorist attacks, explosions, progressive collapse and other unforeseen circumstances have damaged many structures, including buildings and bridges in war-torn countries such as Iraq. Most of the damaged structural members, for example, beams, columns and slabs, have not totally collapsed and can be repaired. Nowadays, carbon fibre reinforced polymer (CFRP) is widely used in strengthening and retrofitting structural members. CFRP can restore the load- carrying capacity of damaged structural members to make them serviceable. The effect of using CFRP to repair the damaged beams has not been not properly addressed in the literature. This research has the aim of providing a better understanding of the behaviour of reinforced concrete beams strengthened or repaired with CFRP strip under impact loading. Experimental and analytical work were conducted in this research to investigate the performance of RC beams strengthened or repaired using CFRP.

To study the impact behaviour of the CFRP reinforced concrete beams, a new heavy drop weight impact test machine has been designed and manufactured to conduct the experimental work. Twelve RC beams were tested experimentally under impact load. The experimental work was divided into two stages; stage 1 (strengthened) and stage 2 (repair). At stage 1, three pairs of beams were tested under impact loading. External bonded reinforcement (EBR) and near surface mounted (NSM) techniques were used to strengthen the RC beams to find the most effective technique. Three pairs of beams were tested in stage 2 (repair). Different degrees of damages were induced using different impact energies. NSM technique was used to repair the damaged beams using CFRP strip. Stiffness degradation method was used to assess the degree of damage in beams due to impact. The study investigated the stiffness, bending load, impact energy, deflection and mode of failure of CFRP strengthened or repaired beams under impact loading. The distribution of the stresses, strains, accelerations, inertia forces, and cracks in the beam under impact loading was also investigated in this study. Empirical equations were proposed in this research to predict the bending load and maximum deflection of the damaged and repaired beams under impact loading.

For validation purposes, finite element analysis was used with the LUSAS package. The FEA results were compared with the experimental load-deflection curves and ultimate failure load results. In this research, to simulate a real situation, different models were used to simulate the bonding between the CFRP and concrete and also between steel bars and concrete. In these FEA models, the bonding between the concrete and the CFRP was modelled using the Drucker-Prager model. To simulate the bonding between steel and concrete, a joint element was used with spring constants to model the bond between steel bars and surrounding concrete. The analytical results were compared with the experimental results.

In most previous research, FEA has been used to simulate the RC beams under impact loading without any damage. In this thesis, a new 3D FEA model was proposed to simulate and analyse the damaged RC beams under impact loading with different degrees of damage. The effect of the damage on concrete stiffness and the bonding between the steel bars and the concrete were investigated in FEA model. The damage was modelled by reducing the mechanical properties of the concrete and the bonding between steel bars and concrete. This thesis has contributed to improving knowledge of the behaviour of damaged beams repaired with CFRP, and the experimental work conducted, together with the numerical analysis, have provided essential data in the process of preparing a universal standard of CFRP design and construction. In the FEA model, the damage to the beams due to impact loading was successfully modelled by reducing the beam stiffness.

TABLE OF CONTENTS

LIST OF TABLES

LIST OF FIGURES

1. Introduction

1.1 Introduction

Structures can be subjected to different types of loading, such as static and dynamic loadings. In a variety of civilian and military applications, the response of concrete to dynamic impact loading is of great interest. For example, (a) nuclear power plants are expected to withstand against the impact loading from any source, such as earthquakes, tsunamis, missiles and explosions, and (b) aircraft take-off and landing apply dynamic loads on airport runways. The design and analysis of these structures requires more understanding of the behaviour of reinforced concrete (RC) structures and structural elements under impact or impulsive loading (Zhang et al., 2010). Trucks, trains and other vehicles can cause dynamic loads when they move over bridges (Duan, 2000). Nowadays, road traffic density is on the increase and the possibility of vehicle impact against bridges and their supports, columns, guards and other structures alongside traffic routes has also increased. Thus, it will be necessary to pay extra attention to these problems (Struck and Voggenreiter, 1975). Figure 1.1 shows different sources of impact loading.

In recent years, the use of fibre reinforced polymer (FRP) has gained particular popularity for strengthening and upgrading existing structural elements (Hamed and Rabinovitch, 2005). FRP has high performance properties, such as low density, high stiffness and strength and ease of installation. In addition, FRP does not corrode and is non-corrosive and composed of nonmagnetic materials. These characteristics make FRP an excellent option for externally reinforcing and retrofitting the structural elements.
Strengthening of RC structures is required to improve their impact performance. FRP has been shown to be a suitable material for impact retrofitting of impacted concrete structures. FRP bonded composite laminate significantly improves the impulse resistance of the strengthened beam and reduces its maximum deflections (Jerome and Ross, 1997, Cantwell, 1999, Tang and Hamid Saadatmanesh, 2003, Erki and Meier, 1999). Also, flexural and shear strength capacity of the structural members and confinement and ductility of the compression members are improved when using FRP composites as external strengthening materials (Khalifa and Nanni, 2000, Shahawy and Beitelman, 1999).

Figure has been removed due to Copyright restrictions.
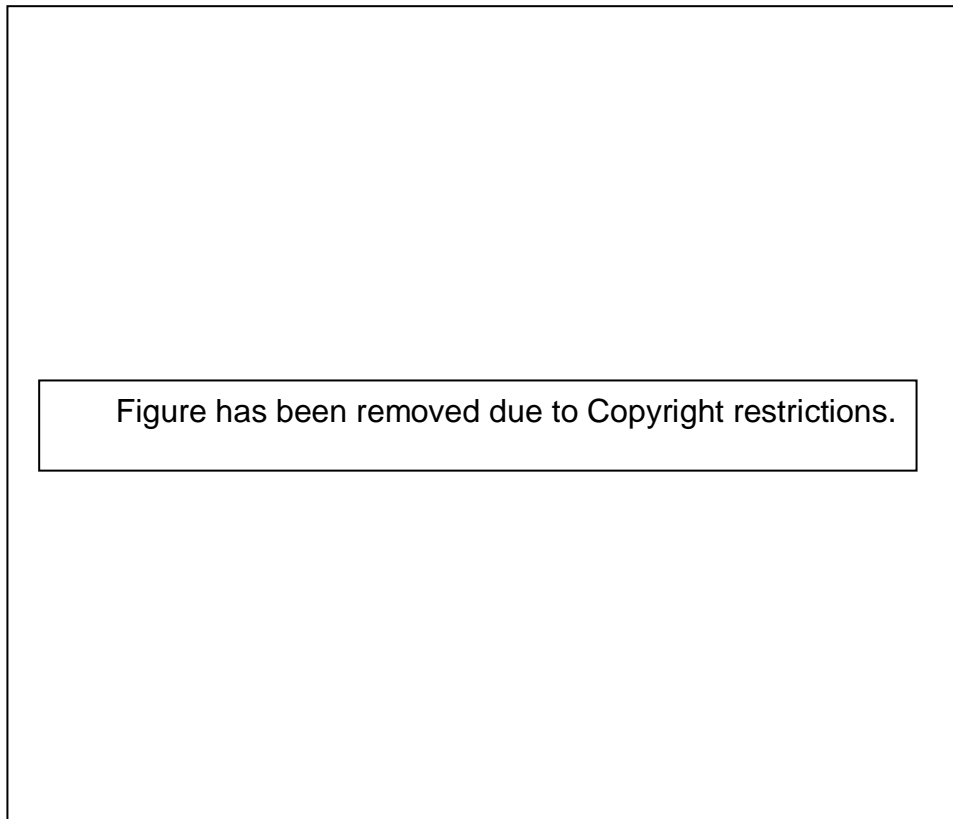
Figure 1.1 Examples of impact loading

1.2 Impact test techniques

The mechanical properties of the structural member depend on many factors, such as the geometry, stiffness, temperature, loading configuration and the applied load rate. The effect of the rate of the loading on concrete structures has been of interest for many investigations. The rate of loading effect was first mentioned by Abrams in 1917 (Banthia, 1987). In impact tests, the storage energy in the striker transfers to the specimen in a very short time, the specimen absorbs the imparted energy by its strain, and when the energy suddenly transfers to the specimen, it develops a high stress in a short time and gives rise to deformation in the specimen.

Several techniques have been used to achieve an impact test, such as free fall dropped weight, ballistic, explosive, Hopkinson bar, Charpy/Izod pendulum test, etc.

Charpy impact test on metallic specimens was conducted by Bluham (1955). The impact in the Charpy test is implemented by a pendulum bob striking the specimen. Basically, a Charpy test is specific to metallic specimen. To use this test machine on concrete specimens, the device has to be modified in terms of the specimen size, hammer and support load (Gopalaratnam et al., 1984).

Hopkinson (1914) first suggested the Hopkinson Pressure Bar (HPB) to evaluate the propagation of stress in the metal bar. Kolsky (1949) developed the Hopkinson test method by using two bars, which are now known as the Split-Hodgkinson bar. In this method, two bars are used and the specimen placed between them, the impulse is generated by one bar and the wave transfers to other bar through the specimen. The stress wave is divided into two parts, the incident wave which reaches the specimen and the reflected wave which will transfer back to the incident bar. The Hopkinson split bar can be used in compression testing and tensile testing (Reinhardt et al., 1986, Davies and Hunter, 1963).

The explosive test has been proposed for structures exposed to the pressure caused by explosions. An explosive test produces a uniformly distributed pressure. This test has faced several problems in terms of quantity of energy and specimen response, and presents significant risks in respect of the health and safety of personnel (Banthia, 1987).

In the drop weight impact test, the hammer rises to a predetermined height and then drops to strike the specimen. An impact test has been recommended by ACI Committee 544 (1982) for specific tests with fixed structural dimensions. The striker consists of a steel ball weight (4.5 kg) with a diameter of 152.4 mm, which hits a specimen of 63.5 mm thickness. The total energy can be obtained by multiplying the number of drops up to failure by the energy imparted to the specimen at each blow. This test also has many problems, such as the arbitrary selection of failure criteria of the specimen and the detection of the first crack depending on operator identification. Furthermore, the ACI test is designed for scaled specimens and it has limitations in the specimen size and the impact energy. The ACI test was used by Swamy and Jojagha (1982) to investigate the impact resistance of steel fibre lightweight concrete. They

concluded that the variation of the number of blows required to induce the first visible crack is very large. The impact resistance of a polypropylene fibre reinforced concrete beams has been investigated by Bader et al (2006), using the impact test recommended by ACI Committee 544.The results showed that the standard deviation and coefficient of variation values were about four times those for compressive. This ACI test requires modifications to increase the accuracy and reduce the large variation. The alternative is to design a new impact test machine to investigate the properties of concrete under high rate loading. In this study, a new heavy drop weight impact test machine has been designed and manufactured to conduct the experimental work (see Chapter 3).

1.3 Damage assessment

The demand for new infrastructures increases every year. Concrete structures can experience different degrees of damage during their service life. There are different loading factors that cause structures deficiency, such as earthquakes and storms hazards, corrosion and accidents. These damages can cause a serious reduction of stiffness and strength of the structures and so more attention needs to be given to repairing and strengthening old and damaged structures. The demand for strengthening and rehabilitation of damaged structures is increasing.

The damage caused by distress of the structures may happen at any single part of the structure. The progress of damage can extend to the whole structure and make it fail early. The damage evaluation is important in selection of the appropriate repairing method.

In Iraq, many buildings and high way bridges have been damaged due to terrorism, wars and combat incidents. The need for upgrading and rehabilitation of structures is increasingly required in any country with the same situation. The structural damages vary from partial to complete damage. Structural repair, instead of demolition, may be more economic and cost effective. The identification of the type and degree of damage is very important for the selection of the appropriate repair technique. The degree of damage can be classified into three categories (Hamad 1993): -

(i) Minor damage: the structures have a slight cracking and no permanent deformation can be observed.

(ii) Intermediate damage: major cracks with some observed permanent deformation

(iii) Major damage: major cracks and significant observed deformation with local damage and spalling and crushing of the concrete

The damage to the structures can be assessed either by visual inspection or by instruments. Damage such as crushing, spalling of concrete, cracking deformations can be evaluated using visual methods while internal damage, such as stiffness reduction, can be assessed using experimental and analytical methods.

The damage may need to be assessed even when there is no obvious visual damage, such as excessive deflection, concrete spalling or visible cracking. Fine cracking may cause internal damage and affect the stiffness and strength of the structural components with consequences for the performance and serviceability of the structures.

Visual assessment is widely used for the evaluation of damage. However, this method can only assess external, and not internal, damage. To evaluate the internal damage, an experimental, analytical or non-destructive test method can be used.

The internal damage within the structures in terms of the reduction of stiffness and strength of the structural component can be deduced using different methods. The practical methods such as stiffness degradation and dynamic excitation methods can be used to assess internal damage.

One of the common methods of detecting the damage location and quantifying the extent of the damage for whole structures is vibration- based damage identification. The damage is identified using dynamic techniques which monitor change in the natural frequency, mode shapes and other dynamic characteristics of the structures.

The stiffness degradation method can also be used to deduce the internal damage. Based on static data, the load deflection path is observed and the damage is assessed by calculating the reduction of the structure stiffness. In this project, the stiffness degradation method was used to assess the damage degree in beams due to impact and to evaluate the enhancement of the stiffness of the repaired damaged beams.

1.4 Fibre Reinforced Polymer (FRP)

Fibre Reinforced Polymer (FRP) composite is formed by embedding continuous fibres in a resin matrix which binds the fibres together. FRP composites mainly consist of resin and reinforcement. Each component plays an important role in FRP properties. The reinforcement is joined together by resin or polymer matrix, which affects the physical properties of the final product.

The common fibre composites mostly used in civil engineering applications are carbon fibre reinforced polymer (CFRP), glass fibre reinforced polymer (GFRP) and aramid fibre reinforced polymer (AFRP). The mechanical properties of fibre reinforced polymer such as the tensile and compressive strength mainly depend on the amount, orientation, length and type of fibres (Luc and Stijn, 2011).Table 1.1 shows the mechanical properties of different types of reinforcement fibres and Figure 1.2 illustrates the stress-strain curves of FRP bars compared to reinforcing steel.

Table 1.1 Mechanical properties of fibres (Luc and Stijn, 2011)

Table has been removed due to Copyright restrictions.

Figure 1.2 Stress-strain curves of FRP bars compared to reinforcing steel (Luc and Stijn, 2011)

CFRP is used in about 95% of strengthening applications in civil engineering (Nordin, 2003).

The major challenges currently facing the modern civil engineering industry are strengthening, upgrading and retrofitting of existing structures (Esfahani et al., 2007). The RC structural members can be strengthened by bonding FRP to the concrete surface using adhesives. However, most of the strengthened members suffer from concrete-FRP interface debonding failure. Externally bonded reinforced FRP (EBR), near surface mounted technique (NSM) and mechanically fastened FRP strengthening (MF-FRP) are the most common techniques for the strengthening of structures. The following sections show FRP techniques used to strengthen structural members.

1.4 .1 Externally Bonded Reinforced FRP Technique (EBR)

The most common technique used for strengthening and retrofitting RC structures is externally bonded reinforcement (EBR) using CFRP. Use of this technique has significantly increased recently.

The following steps are the most common steps applied in practice for strengthening work using EBR technique.

- Prepare the concrete surface using sand blasting or grinding.
- The concrete surface must be cleaned from dust and other contaminates using an air compressor.
- The concrete surface is treated with the primer and allowed to harden. Some laminates do not require primer.
- The adhesive is placed on concrete surface then the fabrics are put in place and, if additional layers are required, the process is repeated. A roller is used to remove the air voids in adhesive layer and to make the fabric straight.
- Alternatively, for the laminate plate bonding strengthening, the epoxy is placed on the laminate surface and the laminate is put in place. Pressure is applied to the laminates by hand or by using a roller to remove air voids and to obtain a uniform distribution of the epoxy. Figure 1.3 shows the strengthening process of a highway bridge.

Figure 1.3 High bridges being strengthened with hand lay-up CFRP laminates

1.4.2 Failure Modes of FRP Strengthened Beams

Several experimental works have been conducted to assess the flexural behaviour of beams externally strengthened with FRP since the early and mid-1990s (Hosny et al., 2006, Khalifa and Nanni, 2000, Gravina and Smith, 2008, Amorn, 2010, Kachlakev and McCurry, 2000, Garden and Hollaway, 1998, Shahawy and Beitelman, 1999, Andreou et al., 2001, Jin, 2004, Ritchie et al., 1991, Saadatmanesh and Ehsani, 1991, Triantafillou and Plevris, 1992, Grace et al., 1999, Grace et al., 2002). In all these studies, the flexural strength of strengthened beams was higher than that of unstrengthened beams. Most of the tests were carried out on small scale strengthening of rectangular beams under four-point loads with FRP sheets. According to ACI subcommittee 440 F (ACI, 2002) for the studies conducted on large scale beams under peeling, shear and flexural loading (Buyukozturk O, 1998, Büyüköztürk and Lee, 1993, Grace, 2004, Triantafillou and Plevris, 1992), the modes of failure cases can be classified as follows:

1- Concrete crushing

2- FRP rupturing after steel reinforcement yielding

3- Concrete crushing after yielding of steel

10

4- FRP debonding

5- Cover delamination

Figure 1.4 illustrates the strengthened beam modes of failure. In addition, shear failure may occur if the shear capacity of beams is low. The FRP has a linearly elastic behaviour. The FRP anchorage force is limited and that leads to non-ductile failure either by debonding of FRP or by shear-tension failure(Gunes, 2002).

Figure has been removed due to Copyright restrictions.
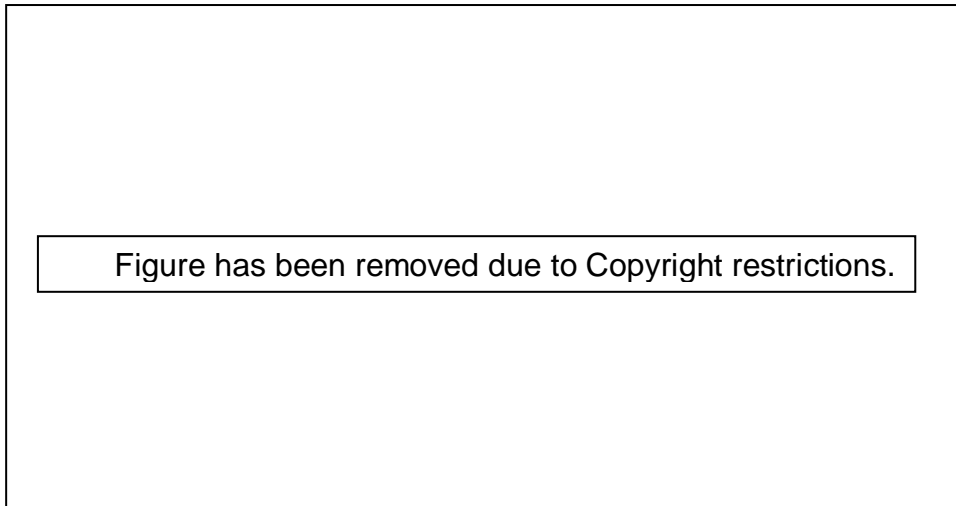
Figure 1.4 Failure modes of strengthening beam

The strength of beams reinforced with FRP decreases when the debonding initiates and propagates beam failure. Most research shows that the debonding initiated at the end of FRP reinforcement and around shear and flexure cracks are due to the concentration of stresses in these areas. It can be prevented by reducing the stress level at the adhesive layer (Gunes et al., 2009, Gunes, 2002, Aram et al., 2008, Oehlers et al., 2008, Au and Büyüköztürk, 2006). Research by Chajes et al.,(1996), Björn, (2003), Chen (2001), Bizindavyi(1999) and Gao et al., (2003), shows four possible modes of debonding failure that may occur in strengthened beams with FRP under shear or flexural loading. These are: (1) cover de-bonding, (2) FRP debonding from FRP end (3) FRP debonding from flexural-shear crack and, (4) FRP debonding from flexural crack. Figure 1.5 shows the fundamental failure mechanisms of beams strengthened with FRP, based on laboratory tests. Figure 1.5 a illustrates the cover debonding mechanism which usually occurs due to high interface stress, low concrete strength and low cracking in shear span. Figures 1.5b shows the potential debonding

failure with debonding initiated at the end of the laminate and propagating toward the centre of the beam. This type of debonding is most likely to occur in beams with high strength concrete and shear capacity. The debonding may occur either at the FRP-concrete interface or within a few millimetres of concrete substrate. If the FRP development length is sufficient or the end of FRP laminate is anchored, the debonding initiates at flexure-shear cracks and propagates toward the beam ends as shown in Figure 1.5c or debonding initiates at flexure cracks if the beam has high shear strength, as shown in Figure 1.5d (Gunes, 2002).

The EBR technique cannot resist the full tensile stress of the FRP material (Nguyen, 2001, Mukhopadhyaya, 2001). Moreover, collisions, freeze/thaw cycles and high or low temperature can cause damage to FRP reinforcement (Täljsten et al., 2003). These problems can be limited by using the NSM technique described in section 1.4.2. More research is needed to study the anchorage, development length and the bond stress distribution in order to make FRP more efficient.

Figure has been removed due to Copyright restrictions.

Figure 1.5 Debonding failure mechanisms (Gunes, 2002)

1.4.3 Near Surface Mounted FRP Technique (NSM)

A major problem with the EBR technique is the CFRP debonding and concrete cover delamination. As a result of this, the EBR technique cannot resist the full tensile stress of the FRP material (Nguyen et al., 2001). The NSM technique was introduced to overcome the drawbacks of the EBR technique and limits the debonding effect. Thus, it is contended that NSM leads to increases in both the flexure and shear strength of the RC members. The NSM technique has been used by many researchers as a promising technique to increase the flexural and shear strength of concrete members (De lorenzis and Nanni,2001).The NSM approach is based on bonding the CFRP laminate or rods in small grooves opened in the concrete cover of the element to be strengthened (Al-Mahmoud et al., 2010) as shown in Figure 1.6. Circular, rectangular and quadrate rebars are mostly used in the NSM technique. In the latter technique, no surface preparations are required and the installation time is less than that of EBR technique.

The most common steps required in the application of the NSM technique are as follows:

- A slit groove is cut in concrete cover.
- A compressed air blower is used to clean the slit.
- CFRP rebars or laminates are cleaned using a suitable cleaner.
- Filling the grove and coating the CFRP rebar with adhesive
- Inserting the CFRP rebars or laminates into the groove, after which a slight pressure is applied on it to allow to epoxy to flow between CFRP and groove borders
- The epoxy adhesive requires time for curing and this must be respected to obtain the full performance of the CFRP.
- Adding concrete cover.

Figure 1.6 shows the installation of the CFRP rod using NSM technique

```
┌─────────────────────────────────────────────────────┐
│                                                     │
│                                                     │
│                                                     │
│       ┌─────────────────────────────────────┐       │
│       │ Figure has been removed due to Copyright restrictions. │       │
│       └─────────────────────────────────────┘       │
│                                                     │
│                                                     │
│                                                     │
└─────────────────────────────────────────────────────┘
```
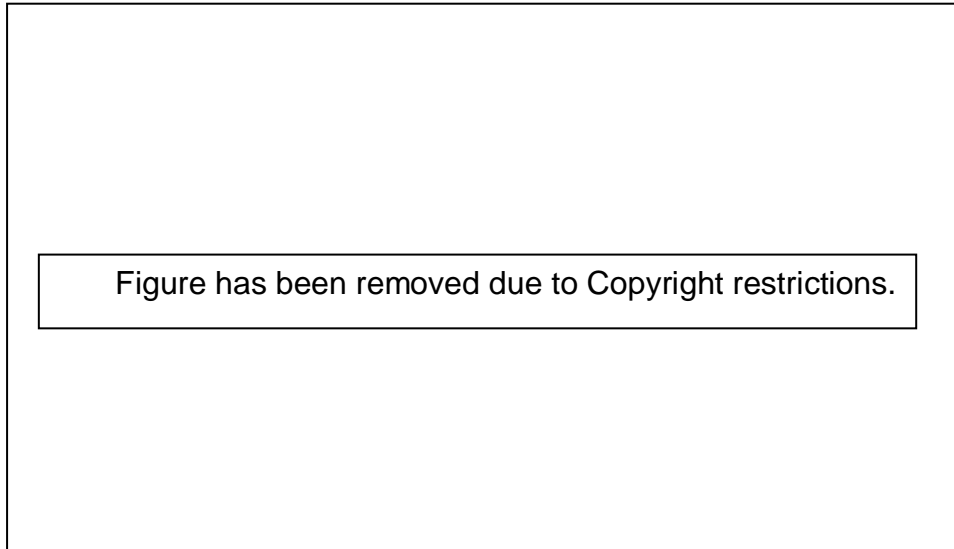
Figure 1.6 NSM-CFRP strengthening technique (Lula, 2011)

Compared to externally bonded FRP reinforcement, the NSM system has a number of advantages (De Lorenzis and Teng, 2007):

• Little concrete surface preparation other than grooving is required, which reduces the time for installation at the site.

• The debonding failure is less frequent when using NSM CFRP strip or rebar is mounted in grooves which increase the bonding surface area with concrete.

• It is easy to anchor NSM bars into adjacent members to prevent debonding failures.

• Pre-stressed FRP rebars can be used in NSM Technique.

• The concrete cover protects NSM bars from accidental impact and mechanical damage, fire, and vandalism.

• The strengthened structure with NSM is less exposed to change in terms of the aesthetic aspect.

1.4.4 End-Anchorage Systems

End-anchorage is one of the most important considerations when retrofitting reinforced concrete beams using CFRP strips. The performance of anchor systems affects the load-carrying capacity of CFRP-retrofitted beam and failure characteristics. The end anchorage technique has been investigated by many researchers (Yoshitake, 2011, Ceroni, 2010, Aram et al., 2008, Ceroni, 2005). It has been concluded that using FRP anchoring is very effective in preventing the premature failure of RC members strengthened with FRP.

Various methods have been used to prevent FRP debonding include clamps, U-shaped stirrups or wraps, anchorage bolts near the end of FRP and staggered multi-layer laminate (Garden and Hollaway, 1998, Garden et al., 1998, Khalifa and Nanni, 2000, Smith and Teng, 2001). Figure 1.7 shows a number of the end anchorage systems that have been used by researchers.

Figure has been removed due to Copyright restrictions.
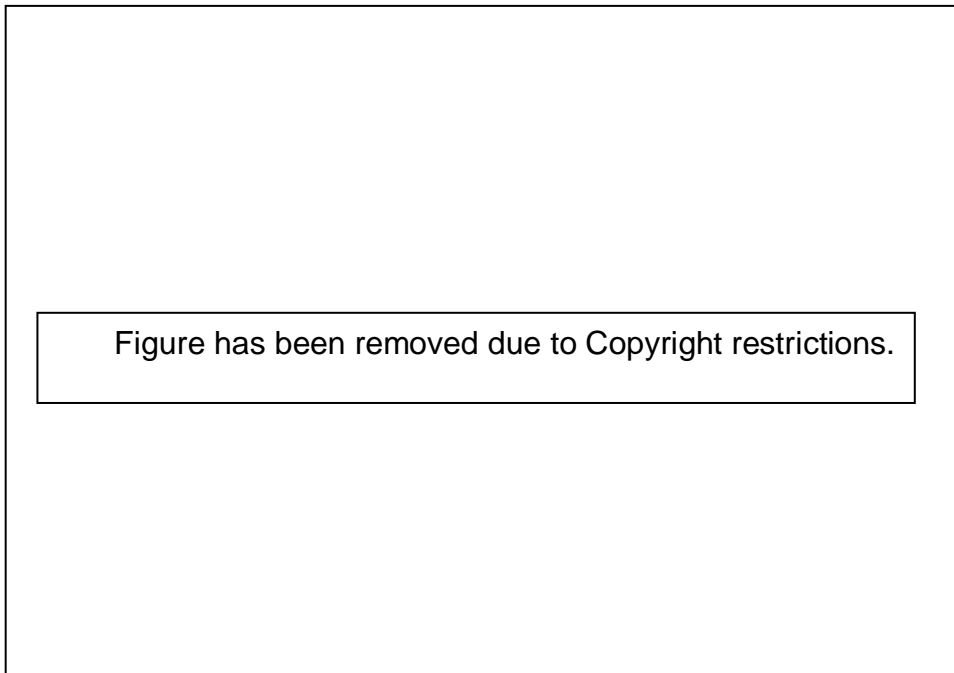
Figure 1.7 Different types of end anchoring systems

1.5 The gap in knowledge

Although a substantial body of work on external reinforcement of concrete beams with CFRP was found in the literature, very little research has been conducted on the behaviour of RC beams strengthened with CFRP under impact loading. There is a gap in knowledge regarding the impact behaviour of RC beams strengthened or repaired with CFRP and there is a need for more experimental and theoretical work to increase our understanding and enhance knowledge in this field (Soeum et al., 2008, Fujikake et al., 2009, Erki and Meier, 1999, Imbeau, 2011).

The external bonded technique (EBR-CFRP) has been used in the research conducted to study the impact behaviour of strengthened reinforced concrete beams under impact loading (Jerome and Ross, 1997, Soeum et al., 2008, Erki and Meier, 1999, Tang and Hamid Saadatmanesh, 2003, Tang and Saadatmanesh, 2005). However, the NSM technique still needs to be investigated. Most structural members experience different percentages of damage when exposed to impact loading during their service life. The studies using CFRP as repairing materials for damaged structural elements due to impact loading are poor.

In most research concerned with numerical analysis, a perfect bond between the steel bars and concrete has been assumed. This affects the numerical results, such as failure load and mode of failure. In reality, there is bond-slip between the steel bars and concrete. In most previous research, FEA models have been used to simulate the RC beams under impact loading without any damage. There is a need to investigate the use of FEA with an appropriate model in order to simulate the damage in structural members and to model the FRP repaired damaged beams under impact loading.

Studies on the behaviour of CFRP composites with concrete structures through various experiments might be the best way to collect data in the process of preparing a universal standard on the CFRP design and construction.

1.6 Research contribution

For RC structures under different conditions, the selection of appropriate strengthening and repairing technique is a very important practical issue. The comparison between the existing techniques assisted in the selection of the most effective system for strengthening and repairing concrete structures.

In this thesis, EBR and NSM techniques were investigated experimentally and analytically and a comparison between them was conducted to find the most effective technique. An experimental and analytical study of work was carried out to investigate the effect of using CFRP on the impact resistance of damaged RC beam in terms of stiffness, impact force, reaction force, deflection and cracking. The acceleration and inertia force distribution of the beam were investigated using two assumptions; linear and sinusoidal distribution. The experimental data were analysed and empirical equations were proposed to find the bending load and maximum deflection of the damaged and repaired beams under impact loading.

In this study, Finite Element Analysis (FEA) was used to simulate and analyse the CFRP strengthened or repaired RC beams under impact loading. To simulate a real life situation, different models were used to simulate the bonding between the CFRP and concrete and also between steel bars and concrete. The analytical results were compared to that of the experimental results. In this study, a 3D FEA model was developed to simulate and analyse the damaged RC beams with different degrees of damage under impact loading. The damage in beams due to impact loading was modelled by reducing the beam stiffness. The concrete elastic modulus, concrete compressive strength and bonding of the steel bars were reduced in the FE models to simulate the beam stiffness reduction due to impact damage.

This thesis has contributed to improve the knowledge and understanding of the behaviour of the strengthened or repaired RC beams under impact loading. A better understanding of impact performance of CFRP strengthened RC beams is significant for the further exploration of the potential application of CFRP in civil structures. The experimental and novel numerical studies conducted in this project have provided essential data for further design-oriented studies.

1.7 Motivation

Reinforced concrete structures can be exposed to impact loading from various sources. They include ocean waves, earthquakes, tornados, crashing vehicles, explosions and missiles. In Iraq and many other countries, war, terrorist attacks and explosions have damaged many structures, including buildings, bridges and infrastructures. Thus, it will be necessary to pay attention to these problems and RC structures will require strengthening and repairing to improve their impact performance. FRP has been shown to be a suitable material to retrofit impacted concrete structures. Carbon fibre reinforced polymer (CFRP) as a strengthening material is widely used nowadays and has attracted much attention. This doctoral study was conducted to investigate the behaviour of reinforced concrete beams strengthened or repaired with CFRP under impact loading.

1.8 Objectives

The main objectives of the research work in this thesis are summarised as follows:
1. To investigate experimentally the dynamic impact behaviour of reinforced concrete beams strengthened with CFRP laminates using two strengthening techniques, which are:

- Externally bonded reinforced FRP (EBR) technique.
- Near surface mounted (NSM) technique

2. To investigate the load–deflection characteristics, location and shape of cracks, mode of failure and load-time history of the strengthened reinforced concrete beams under impact loading.

3. To compare experimental dynamic test results of beams with different types of strengthening technique.

4. To investigate the dynamic behaviour of damaged reinforced concrete beams repaired with CFRP

5. To investigate numerically the dynamic behaviour of reinforced concrete beams strengthened with CFRP under impact loading using nonlinear Finite Element Analysis.

2. Literature Review

2.1 Introduction

The concept of composite materials is an old idea of mixing two different materials to obtain better composite materials (Lopez and Nanni, 2006). Steel plates have been used throughout the world to strengthen and retrofit structural members. Steel plates are bonded to the tension zones to increase the flexural strength of the beams or to increase the compressive strength as in a concrete column jacket. This traditional technique has a numbers of drawbacks. The steel plate can be damaged by corrosion, since alloys typically have limited corrosion resistance. There are difficulties in the installation of the steel plate, as it needs heavy equipment for installation and this takes long time. FRP has been proposed by researchers as an alternative strengthened material to overcome the drawbacks of the steel plates, and also because of the high performance properties of FRP.

In the USA, the interest in FRP reinforcement for concrete structures began in the 1930s. Extensive research on CFRP or GFRP has been conducted in that country. In 2001, general recommendations were presented by the American Concrete Institute for a design of flexural member reinforcement with FRP rebars (ACI, 2002).

In Europe and Japan, parallel research has been carried out on FRP. Experimental work on using FRP in strengthening and retrofitting concrete structures was reported in Germany as early as 1978 (Wolf, 1989). In Switzerland, the research on FRP led to the first application of FRP systems to increase the flexural strength of a bridge (Meier, 1987). In the UK ,the first foot bridge to use glass-fibre composite reinforcement was opened in1995 (Luc and Stijn, 2011). FRP has been used in Japan in more than 100 commercial projects (ACI, 2002). It has also been used in Japan to increase the confinement in columns since 1980s (Fardis, 1981) and its used increased significantly after the catastrophe of the Hypgoken Nanbu earthquake in Japan (ACI, 2002).The design guidelines developed for using FRP system in structures is ongoing in Europe, Japan, Canada and the United States (ACI, 2002, Katsumata et al., 1988).

Many studies have been conducted to investigate the behaviour of reinforced concrete members strengthened with FRP under flexure. The researchers used different techniques to obtain the full performance of FRP composite. In the following sections, the literature is classified in accordance with the techniques used in the strengthening.

2.2 Externally Bonded Reinforced Technique (EBR) studies

Many researchers have used EBR technique in strengthening RC beams. They have investigated the behaviour of the strengthened beams in terms of load carrying capacity, cracks distribution, ductility FRP- concrete bonding and mode of failure. The strengthened beam performance is affected by many parameters, such as size, length, FRP fabric orientation and the mechanical properties of the FRP. This section includes a number of experimental and analytical studies conducted on beams externally strengthened with FRP EBR technique under flexure loading.

Shahawy et al.(1996) conducted an experimental study to investigate the flexural behaviour of RC beams strengthened with EBR-CFRP laminate. Their assessment used different numbers of CFRP laminate on the flexural strengthened beams. Four 2.7 m rectangular RC beams were tested. The beams' cross section was 200 mm width and 250 mm depth. The results showed a significant increase in load carrying capacity for RC beams strengthened with CFRP sheet. A significant reduction in maximum deflection and a considerable increase in flexural strength of strengthened beams were observed using multi-layered CFRP laminated beams. The flexural strength increase was 13.7 % or 92% using two or three-ply CFRP laminates, respectively. All beams were failed by concrete crushing after debonding of CFRP laminate. Flexural strength, curvature and deflection were predicted using 2-dimensional finite element method. In the FE model, the beams section was divided into several layers, represented by concrete, steel bars and CFRP laminate. A good agreement was found between FE and experimental results.

To study different parameters that effected the flexural behaviour of the CFRP strengthened beams, Esfahani et al.(2007). investigated the flexural strength of RC beams strengthened with CFRP sheet. The experimental variables were steel reinforcement ration and length, width and number of CFRP layers. Twelve RC beams and three different steel reinforcement ratios were used. The tested beams' dimensions were 150 mm width, 200 mm depth and 2000 mm length. Three beams were unstrengthened and considered as control beams, while nine beams were strengthened with EBR CFRP laminates. The result showed an increase in flexural strength of RC beams strengthened with CFRP laminates compared with that of the control beams. The experimental results revealed that the increase in flexural strength

calculated using ACI.440-2r-02 and ISIS Canada models is overestimated when using small steel reinforcement ratio compared with the maximum longitudinal reinforcement steel ratio specified in these two guides.

It can be noted from the Esfahani experimental results that the steel bar size affected the percentage of increasing in flexural strength of the strengthened beams. The increase in bar size reduces the load carrying capacity, which increases even with increasing the number of CFRP layer, as shown in Figure 2.1. The reason for that is the debonding of CFRP laminate in strengthened beams. The CFRP debonding in beams with large steel bars occurs faster than that in small steel bar size beams. The large bar size steel bars beams resisted high bending load and this induced high tensile stresses in the steel bars. After the yielding of the steel bar, a high percentage of these stresses transferred suddenly to the CFRP laminate and high concentrated shear stresses developed in the concrete cover. These high stresses caused CFRP de-bonding, either by concrete cover delamination or by separation of the CFRP layers.

Figure has been removed due to Copyright restrictions.
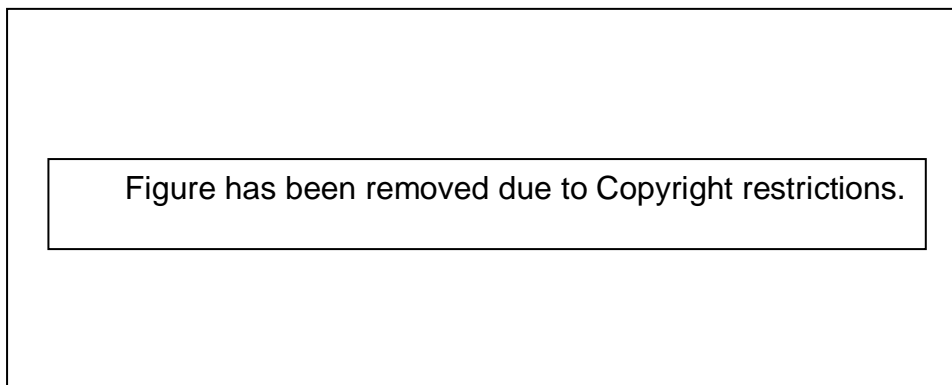
Figure 2.1 Load- deflections curves for tested beams, Esfahani et al.(2007)

Steel plates were once used widely to strengthen concrete structures. Nowadays, FRP is more often employed in strengthening and retrofitting structural members. To study the differences between the two materials in strengthening concrete beams, Jumaat and Alam (2008) carried out an experimental and analytical work to investigate the flexural behaviour of RC beams externally strengthened with CFRP laminates or steel plates. Three 2 m beams were tested statically under four-point loading. All tested beams had size of 125 mm width and 250 mm depth. One beam was a reference beam without any strengthening. Steel plate was used to strengthen the second beam and

CFRP laminate was used with the third beam. The thickness and elastic modulus of steel plate was higher than that of CFRP plate. The strengthened beam with CFRP laminate resisted a slightly higher load and showed less deflection compared to the steel plate strengthened beam. In addition, higher crack load, less reinforcement bar strain and concrete strain were observed with the CFRP strengthened beam compared with the EBR-steel RC beam.

The results of experimental work conducted by Jumaat and Alam (2008) revealed that the flexural strength of the CFRP- strengthened beam was slightly higher compared with the steel plate strengthened beam. The reason for that is the premature debonding failure of the CFRP due to poor bonding between the CFRP and concrete surface. The CFRP beam failed by interfacial debonding close to the CFRP end rather than concrete cover separation, as happened in steel plate strengthened beam. The poor bonding resulted in low transfer stresses between the concrete and the CFRP. The steel plate had a high elastic modulus which made the beam more ductile and had a high beam deflection. In addition to the experimental work, the authors conducted a non-linear finite element analysis to study the behaviour of strengthened RC beams. A perfect bond between the concrete and the steel plate or CFRP laminate was presumed. In the surface meshing, a plane stress was used. The numerical results were compared to the experimental work in terms of the failure mode, ultimate load and mid-span deflection. It was concluded that the numerical ultimate load was higher than that of the experimental as the authors assumed a perfect bond between the concrete and the steel plate. In addition, they assumed a perfect bond between strengthened plate and concrete which resulted in a flexure failure in the FE model, rather than laminate de-bonding, as happened in experimental tests.

Debonding of the FRP is the major problem of EBR technique. That has been observed in experimental tests conducted by many researchers. The NSM technique has been proposed to overcome this problem in EBR technique. The following section reviews some studies conducted on the behaviour of RC beams strengthened with FRP NSM technique under flexure.

2.3 Near Surface Mounted FRP Technique (NSM) studies

Many researchers have studied the use of the NSM technique in strengthening structural members (Barros and Fortes, 2005, Renata, Al-Saidy et al., 2010, Tanarslan, 2011, Rizzo and De Lorenzis, 2009b, Rami, 2012, Foret and Limam, 2008, Al-Mahmoud et al., 2010, Rizzo and De Lorenzis, 2009a, Barros et al., 2006, Sena-Cruz et al., 2011, Barros et al., 2008, Liu et al., 2006, Jung, 2005, Jung, 2007, Kotynia, 2011, Wang et al., 2011). Comparative studies were conducted on RC beams to investigate the differences between the NSM and EBR techniques in terms of flexural strength, deflection, crack distribution and failure mode.

In 2005, Barros and Fortes carried out an experimental programme to study the behaviour of RC beams strengthened with CFRP laminate strip, using the NSM technique. Four series of 1.6 m beams were tested under four point loads. The tested beams had a size of 100 mm width and depth range was between 170 mm and180 mm, due to inaccuracy in the beams' casting. One beam in each series was used as a control without any strengthening. The experimental variables were the number of CFRP strips and the amount of steel reinforcement. Figure 2.2 shows the beams' configuration and details. The results showed that the flexural strength of RC beams strengthened with NSM-CFRP strips increased to between 78% - 91% with respect to the control beam. The failure mode of the strengthened beams was concrete bottom layer separation followed by concrete crushing. A numerical study was conducted to predict the load carrying capacity and corresponding deflection of strengthened beams, and a good agreement was found between theoretical and experimental results.

Figure has been removed due to Copyright restrictions.

Figure 2.2 Tested beams details, Barros and Fortes (2005)

To find the difference between the EBR and NSM techniques on the strengthened beam behaviour under flexure , Jung et al.(2005) carried out a study on flexural strength of RC beams strengthened with CFRP reinforcement. Eight 3.4 m RC beams were tested under four point loads. The size of the beams was 200 mm width, 300 mm depth and reinforced with the same reinforcement ratio. One tested beam was un-strengthened and used as a reference beam; two beams were strengthened with EBR-CFRP laminates; and the remaining five beams strengthened with NSM-CFRP bars. Mechanical interlock (MI) was used as additional strengthening with NSM-CFRP reinforcement to prevent the debonding failure of CFRP as shown Figure 2.3

Figure has been removed due to Copyright restrictions.
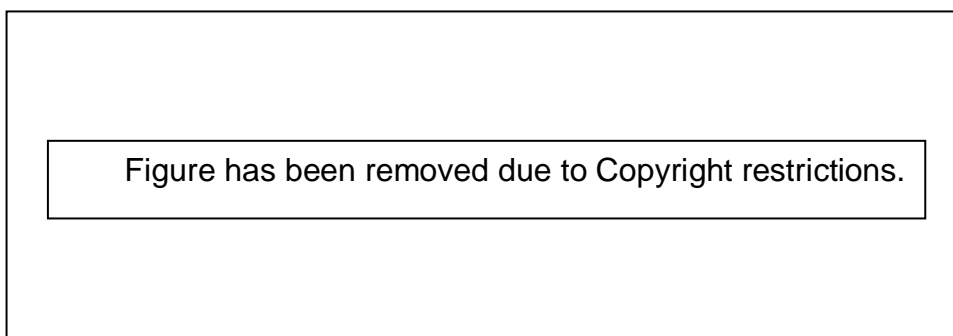
Figure 2.3 NSM-mechanical interlock technique, Jung et al.(2005)

The test results of the NSM-CFRP strengthened beams were compared with the EBR-CFRP technique. The results indicated that the increase in flexural strength of beams

strengthened with NSM-CFRP beams was more than that of those strengthened with CFRP EBR laminate. The increase in ultimate load compared with the control beam was 30-47 % in EBR strengthened beams and 39-65 % in NSM strengthened beams. Furthermore, the mechanical interlock was effective in preventing the debonding failure of NSM strengthened beams. The flexural strength increase of beams strengthened with NSM-CFRP reinforcement and mechanical interlock was 15% above that of NSM strengthened beams without mechanical interlock.

The authors used different percentages of CFRP in beams strengthened with EBR compared with NSM strengthened beams. In addition, the mechanical properties of the CFRP rods and sheets used to strengthen the beams were different. This factor might have affected the tests results and the comparison between the EBR and NSM beams performance. The mechanical interlock could be more useful if it was used with the EBR technique, as the CFRP more likely to debond with the EBR technique than with the NSM technique.

To prevent the FRP debonding in the EBR strengthened technique, the bonding between the concrete cover and composite laminate should be increased. Different methods have been proposed to overcome FRP debonding, such as an end-anchoring system and the NSM technique. Fasteners can be used to bond the CFRP with the concrete cover in addition to the epoxy in EBR technique to increase the bonding between the CFRP and the concrete. This is called the MF-EBR technique. Sena-Cruz et al.(2011) conducted an experiment to investigate the efficiency of different FRP strengthening techniques. The FRP strengthened systems were: external bonded reinforcement (EBR); near-surface mounted (NSM); and mechanically fastened-external bonded reinforced (MF-EBR). RC beams were tested under monotonic and bending fatigue loading. The dimensions of the tested beams were 200 mm width, 300 mm depth and 2 m length. The same longitudinal and transverse reinforcement steel bars were used in all tested beams. The results showed that load carrying capacity was 37%, 88.7% and 85% more than that of un-strengthened beams when EBR, MF-EBR and NSM were used respectively. In addition, the failure mode of beams strengthened with MF-EBR FRP was more ductile than that for EBR and NSM techniques.

 It is clear from the results that there was a slight increase in the MF-EBR strengthened beam compared with EBR –strengthened beams. The fasteners increased the bonding

between the CFRP and concrete. However, they became another source of cracking and de-bonding, because high stresses in concrete are concentrated in the locations of the fasteners, causing many cracks in the concrete cover and leading to CFRP debonding, as shown in Figure 2.4.

Figure has been removed due to Copyright restrictions.
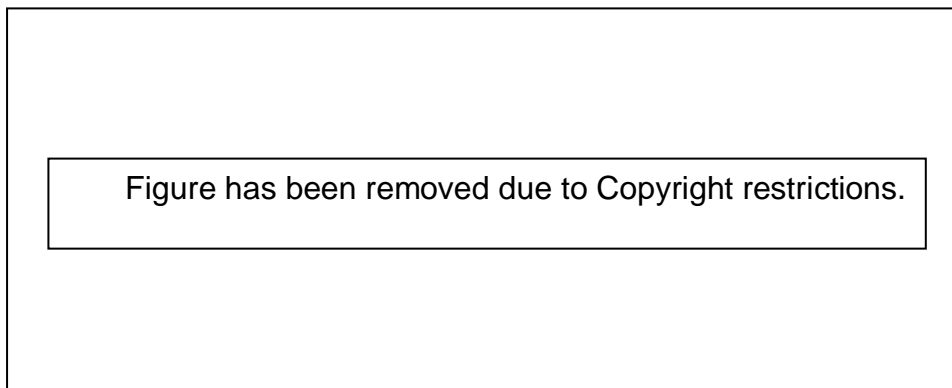
Figure 2.4 MF-EBR strengthened beam failure, Jung et al. (2005)

In 2010, Al-Mahmoud et al. investigated the efficiency of CFRP strengthening on the different type of beams. They studied experimentally the behaviour of RC cantilever beams strengthened with NSM CFRP rods. A number of strengthened cantilever and simple supported beams were tested under flexure load. All beams were taken to failure to study the flexural strength, deflection, cracking and the failure mechanisms of the beams. A simplified analytical model was proposed to model the CFRP de-bonding. The proposed analytical model was compared with the experimental results and the finite element model. The result showed a significant enhancement in the flexural strength of beams with NSM CFRP: the failure modes were the same for cantilever beams and the simple supported beams in a four-point load test. The analytical model had conservative results and showed higher results compared with the experimental and FE results. The author assumed in proposed analytical model a linear elastic behaviour for both concrete and CFRP and assumed a perfect bond between the concrete and the CFRP. These assumptions contrasted with the failure mode noted in experimental tests of the beams. In failure, the CFRP de-bonded from concrete cover due to splitting the resin layer. These assumptions led to high results in analytical results compared to the experimental results, as shown in Figure 2.5.
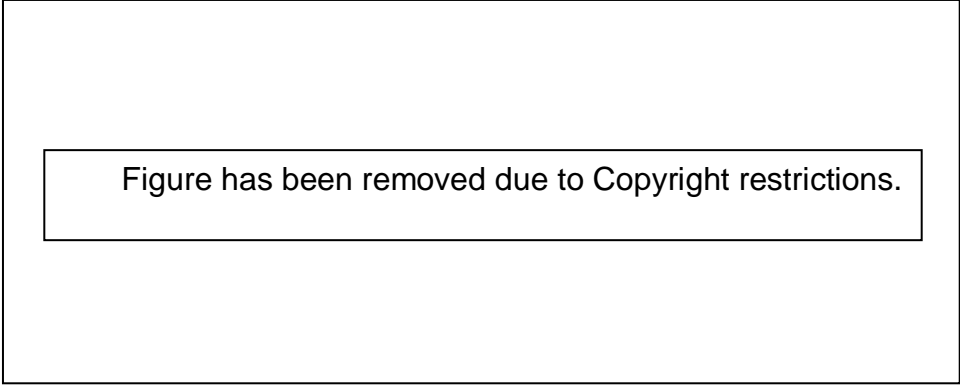
Figure 2.5 Comparison between the experimental, FE and analytical model results, Al-Mahmoud et al.(2010)

CFRP is widely used in research as it has high tensile strength compared with other FRP types such as GFRP. However, CFRP is more expensive and can be cost effective. To investigate different type of FRP in strengthening the RC beams, Sharaky et al. (2014) investigated experimentally the flexural strength of RC beams strengthened using CFRP or GFRP bars in NSM technique. The results were compared with those of the control beams without strengthening. Eight beams were tested experimentally under four-point loading. The tested beams were 160 mm wide x 280 depth mm and 2.4 m clear span. The results showed that the flexural strength of NSM beams was 166 % and 159 % for CFRP and GFRP beams, compared with that of control beams. The results showed that the CFRP- strengthened beams were stiffer than the GFRP beams.

The literature revealed that extensive research has been conducted on strengthened beams under static loading. There is a need to investigate the FRP strengthening on RC beams behaviour under impact loading. Most researchers have used externally strengthened concrete beams, and EBR and NSM technique. In this study, these techniques were adopted to strengthen the simple supported RC beams subjected to impact loading.

2.4 Experimental Studies on Impact Behaviour of Strengthened Reinforced Concrete Beams

Many studies have investigated the dynamic response of RC beams experimentally and analytically under impact load (Fujikake et al., 2009, Saatci and Vecchio, 2009a, Kantar et al., 2011, Roberto, 2009, Saatci and Vecchio, 2009b, Kabir and Shafei, 2009, Chen and May, 2009, Kim et al., 2008, Soleimani and Banthia, 2012, Mohammed, 2012, Mohammed and Parvin, 2011, El-Ariss, 2011, Chen and Hodgkinson, 2011, Beltrami, 2011, Zhang et al., 2010, Ge et al., 2010, Zhou et al., 2009, Saatci, 2007, Kishi et al., 2006, Tang and Saadatmanesh, 2005, May et al., 2005, Abbas et al., 2004, Tang and Hamid Saadatmanesh, 2003, Wang et al., 1996, Banthia et al., 1989, Barr and Baghli, 1988, Banthia, 1987, Swamy and Jojagha, 1982).

Fujikake et al.(2009) studied the dynamic response to the impact load of RC beams experimentally and analytically. The beams were tested under impact load induced by drop weight. The dynamic test program included a study of the effect of weight drop height and the amount of longitudinal reinforcement steel in the beam on dynamic response of RC beams. The two-degrees of freedom mass-spring damper system was used in their dynamic test to simulate the impact load on the RC beam. All tested beams were designed to be an under-reinforced section to allow for an overall flexural failure. The results revealed that increase in the longitudinal steel reinforcement reduced the local failure. In addition, the local damage close to the impact point was affected by the quantity of bottom longitudinal steel reinforcement. A good agreement was observed between analytical and experimental results for RC beams failing in flexure.

To investigate the effect of concrete compressive strength on impact behaviour of RC beams, Kantar et al.(2011) carried out an experimental and analytical study of the impact behaviour of concrete beams. The experimental programme included testing two sets of five beams manufactured using normal and high concrete compressive strength. All beams were tested under impact loading, using a drop hammer from five different heights. The changes in heights, velocity, displacement and energy absorption were recorded. In addition, the failure modes were observed in normal and high strength concrete beams during the impact test. The results revealed that the mode of failure of concrete beams was affected by the compressive strength of concrete. Also,

beams with high compressive strength needed a larger number of drops than that those with normal compressive strength. The normal compressive strength concrete beams also absorbed more energy compared to beams with high strength. Numerical work was conducted, using an ABAQUS finite element model to simulate the tested beams under impact loading. The validation compared the finite element model results with that of experimental tests. Both accelerations and energy were used in this comparison. The results showed a good agreement between the finite element results and the experimental results.

Literature studies on use of FRP composites for strengthening and repairing of RC beams subjected to impact loadings are limited in number.

In 1997, Jerome and Ross investigated the behaviour of plain concrete beams strengthened with EBR CFRP sheets and impulsively loaded to failure. The beams were 76.2 mm square by 762 mm long and without internal steel reinforcement. Different numbers of CFRP panels were used to externally strengthen the concrete samples. All beams were simply supported and a drop weight (43.7 kg) was applied at mid-span to induce an impact force (within duration less than 1 m). A high-speed camera was used to study the failure mechanism of the tested samples. Failure load, mid-span displacement and strains were recorded. The impact test results were compared with static test in terms of bending load, energy absorption and ultimate load. The finite element method was used to study the dynamic behaviour of the test samples. The result indicated that using CFRP to reinforce beams increased the ultimate impact load and decreased the maximum deflection compared to un-strengthened beams. Compared with static results, the impact peak load was always greater than the static load. The static bending energy was greater than that of impact. The experimenters concluded that the beam under impact loading had a fixed capacity to absorb energy and impact compressive strength and displacement. In addition, when the three-ply CFRP was used at the bottom and side of the beams, the highest load, displacement and energy absorption were indicated. Good predictions of the time-displacement behaviour of strengthened beams were achieved when referenced to experimental results.

A different test method was used by Erki and Meier (1999) to study the impact resistance of the strengthened 8.15 m RC beams for flexure. Simply supported beams

(400 mm width, 300 mm depth) were lifted to a given height from one end and dropped to induce impact loading as shown in Figure 2.6. Steel plates were used to strengthen two beams and EBR-CFRP laminates were used for two other beams. The impact behaviour showed that the CFRP laminated beams were more effective compared with the steel plate strengthened beam, although the absorbed energy was less than that of beams strengthened with steel plate. Under the same imported impact energy, the deflection of the CFRP- strengthened beam was less than that of the steel-strengthened beam. In addition, test results indicated that the impact resistance was improved when additional anchoring was used at the end of the CFRP laminates.

Figure has been removed due to Copyright restrictions.
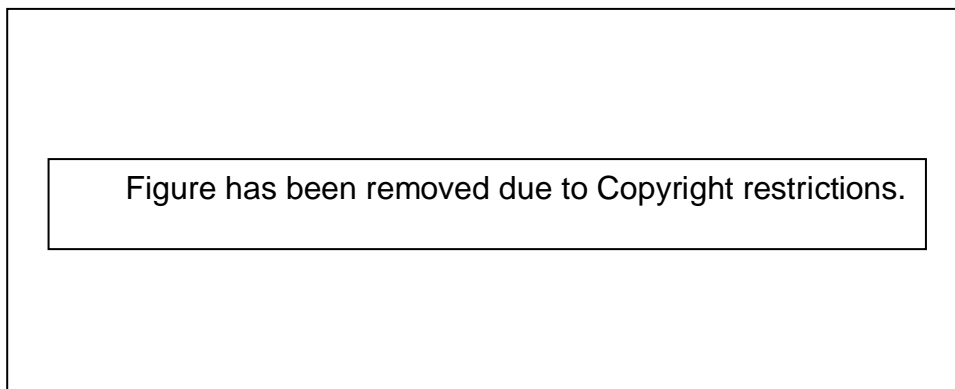
Figure 2.6 impact test mechanism, Erki and Meier (1999)

Capozucca and Nilde (2002) used a non-destructive test method to investigate the dynamic behaviour of RC beams strengthened with CFRP sheets after damage by cracking. The tested beams were damaged by applying static load. During the static test, the permanent state of cracking was recorded on the tensile zone of the section. In the dynamic test, the frequency values were recorded before the damage of the RC beam and after the dynamic test. Flexible springs were used to hang the beams, which simulate the free-free conditions, and an impact hammer was used to induce impulsive load, as shown in Figure 2.7. An accelerometer was used to measure the beam response at different points. The static test results showed an increase in flexural strength and stiffness, with reduced deflection for damaged beams strengthened with CFRP sheet compared to unstrengthened beams. The dynamic test revealed that the CFRP strengthening did not appreciably affect the natural frequency of the strengthened beams.

31

Figure 2.7 Free vibration dynamic test. Capozucca and Nilde (2002)

Despite the CFRP affected slightly the natural frequency of the strengthening beam, other dynamic properties need to be investigated and explored. These aspects include the transfer of dynamic stresses between the concrete and the CFRP strip, shear stresses developing in the adhesive layer and concrete cover due to impact.

2.4.1 The studies of Tang and Hamid Saadatmanesh

In 2003, Tang and Hamid Saadatmanesh investigated the effect of impact load on concrete beams strengthened with fibre reinforced polymer (FRP). Carbon and Kevlar composite materials were used at the top and bottom of tested beams as strengthening materials. Impact tests were carried out on five concrete beams divided as follows: one beam as a reference beam (TB5); two beams strengthened with EBR CFRP laminate (TB2 and TB4); and two beams strengthened with EBR Kevlar laminate (TB1 and TB3). Two layers were used to strengthen the beams, one installed in the top face and another in the bottom face of the beam The size of all tested beams were 95 mm width, 203 mm depth and 1980 mm length. No shear reinforcement was used in any specimen and two 9.8 mm bars were used as longitudinal reinforcement. The impact test was conducted by using a 222 N steel cylinder to induce an impact load on specimens by dropping it from different heights. Two accelerometers were installed at the bottom of the concrete beam mid-span to measure the acceleration of the beam due to impact. Twelve strain gauges were used to measure the strain in the strengthened strip, six on the top face of the beam and six in the bottom. Figure 2.8 shows the setup and distribution of sensors along the beam length.

Figure has been removed due to Copyright restrictions.

Figure 2.8 Test setup and sensors distribution. Tang and Hamid Saadatmanesh (2003)

The impact tests were conducted by repeatedly dropping the mass from the same height and from different heights. Beams TB1 and TB2 were tested by dropping the mass from heights 1.52, 1.83, 2.44, 2.74, 3.05, 3.66 and 3.96 m. Beams TB3 and TB4 were subjected to numbers of impact drops from the same height (1.52 m). For the control beam TB5, the beam was tested by dropping the cylinder from heights 0.305, 0.61, 0.92, 1.22, 1.53, 1, 83, 2.14, 2.44 and 2.74 m.

In impact tests from different heights, comparisons were made between TB1 and TB2 in terms of reaction force and deflection time history for different drop heights. Furthermore, maximum reaction and deflection of TB1 and TB2 were compared for different drop heights. In multi impact test from the same height, the maximum deflection and reaction of TB3 and TB4 were compared. In addition, the reaction force and deflection time history of TB3 and TB4 were compared for different numbers of drops. The individual and cumulative residual deflection under different drop heights was compared between TB1, TB2 and TB5, as shown in Figure 2.9.

Figure 2.9 Deflections of beams TB1, TB2, TB5, Tang and Hamid Saadatmanesh, (2003), a. Individual residual deflection   b. Cumulative residual deflection

The main conclusions of the Tang and Hamid Saadatmanesh research were:

The cumulative and individual residual deflection of CFRP strengthened beam was less than that of the Kelvar strengthened beam under different impact heights. The maximum deflection of the beam and the width and number of cracks were reduced with the increase of the stiffness of the composite laminate. The maximum deflection of TB3 is larger than that of TB1 and TB5 for each individual impact test from different heights and for repetition from the same height. That is because the CFRP beam is stiff, thus increasing the impact and inertia force and reducing the reaction force. The FRP composites significantly enhanced the impact resistance of concrete beams. The RC beams strengthened with CFRP laminates had a higher strength than the RC beams strengthened with Kevlar. The width and number of cracks were reduced by the use of composite laminate. Beams vibration due to impact was another source of cracking. The types, weight, thickness and material properties of the strengthening materials affect impact resistance of the strengthened beams.

Tang and Saadatmanesh (2005) extended their study to investigate the dynamic impact behaviour of beams strengthened with EBR CFRP laminates under impact loading. Twenty seven concrete beams were tested. Two beams without strengthening were used as control beams, while FRP laminates were used to strengthen the remaining beams. The cross section of the tested beams was 205 mm width and 95 mm depth. Two beam lengths were used, 1.98 m and 2.9 m. Figure 2.10 shows the tested beam details. CFRP laminates were used to strengthen 11 beams and Kevlar laminates were used in the strengthening of 12 beams. A steel cylinder drop weight was used to induce an impact force. Two strengthened beams were tested under statically loaded up to failure and the rest of the beams were tested under impact loading. Beam deflection was measured using LVDT installed at both sides of the beam mid-span. Load cell installed at support was used to record the reaction force during the test. Strain gauges were mounted in strengthening plates to measure the strain in composite laminate. Two types of impact tests were conducted: repeated dropped impact from the same height and multi-impact test from different heights.

Figure has been removed due to Copyright restrictions.
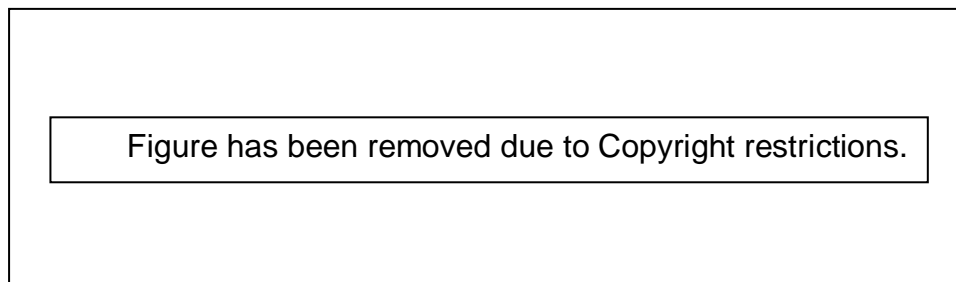
Figure 2.10 Test beams design. Tang and Saadatmanesh (2005)

The experimental results of the strengthened beams were compared with that of control beams in terms of reaction force, deflection, cracking and failure mode. After analysing the tests results, the author concluded the following:

I.   The beams strengthened with CFRP revealed a significantly improved impact resistance. Cracking, flexural strength and initial stiffness of the beams were increased by using composite laminates.

II.   The stiffness for strengthened beams was two to three times that of un-strengthened beams and a 30% decrease in maximum deflection was observed.

III.   The Kevlar strengthened beams were more ductile compared with CFRP strengthened beams and showed high residual deflection.

IV.   The maximum deflection of strengthened beams was less than that under un-strengthened beams.

V.   Flexural and shear cracks were the main types of cracks in the tested beams. Longitudinal cracks in the bottom of the FRP laminate were indicated in the strengthened beams. The failure modes of the tested beams were shear and flexure failure. The type and amount of the FRP used in strengthening affected the mode of failure.

VI.   The reaction force summation under impact loading was greater than the static load.

In a test setup of experimental work conducted by Tang and Hamid Saadatmanesh, accelerometers and LVDT were placed in the mid-span of the beam to measure the acceleration and deflection of the beam. The reading of accelerometers could be affected by cracks in the mid-span and the accelerometers could be damaged. The top layer used to strengthen beams might be damaged due to a direct hit of the mass and this might have affected the test results.

In this PhD study, to avoid possible damage to the sensors due to impact in the beam mid-span, no sensors were placed in the centre of the beam. Alternatively, three dial gauges and accelerometers were installed at equal distances from the support to measure the beam deflection and accelerations. The mid-span deflection and accelerations were then calculated using the extrapolation method.

In the studies of Tang and Saadatmanesh, (2003, 2005), the EBR technique was used to strengthen the beam under impact loading. In this study, two techniques, EBR and NSM, were used to strengthen the RC beams under impact loading. In addition, NSM CFRP was used to repair damaged beams under impact loading.

2.4.2 Soeum et al. (2008). Experimental study

Soeum et al.(2008) experimentally investigated the response to impact loading of RC beams strengthened with CFRP materials. The experimental programme tested twenty RC beams with a size of 160 mm width, 70 mm depth and 1700 mm length under impact load. All tested beams were designed to fail in flexure and classified as follows: four un-strengthened beams as control beams and sixteen beams strengthened with four different types of strengthening schemes of CFRP (TCN, TCC, TLB, and TLC), as

shown in Figure 2.11. The CFRP sheet with a thickness of 0.222 mm and 150 mm width was used in TCN and TCC. For TCC, U-shaped end anchorage was used in addition to the main strengthening system. For TLB and TLC, a 1 mm thick CFRP laminate with a width of 50 mm was used in strengthening. A steel plate with anchor bolts was used to improve the CFRP laminate end anchorages of TLC, while, 0.111mm thickness CFRP laminates were used as an end anchorage system for TLC. Drop weight was used to conduct the impact load and two types of impact test, a single impact test from different heights and repeated impact test from the same height were conducted. In single impact tests, three different drop heights were used, 100 mm, 200 mm and 400 mm, while a 50 mm drop height was used in the repeated impact test.

Figure has been removed due to Copyright restrictions.
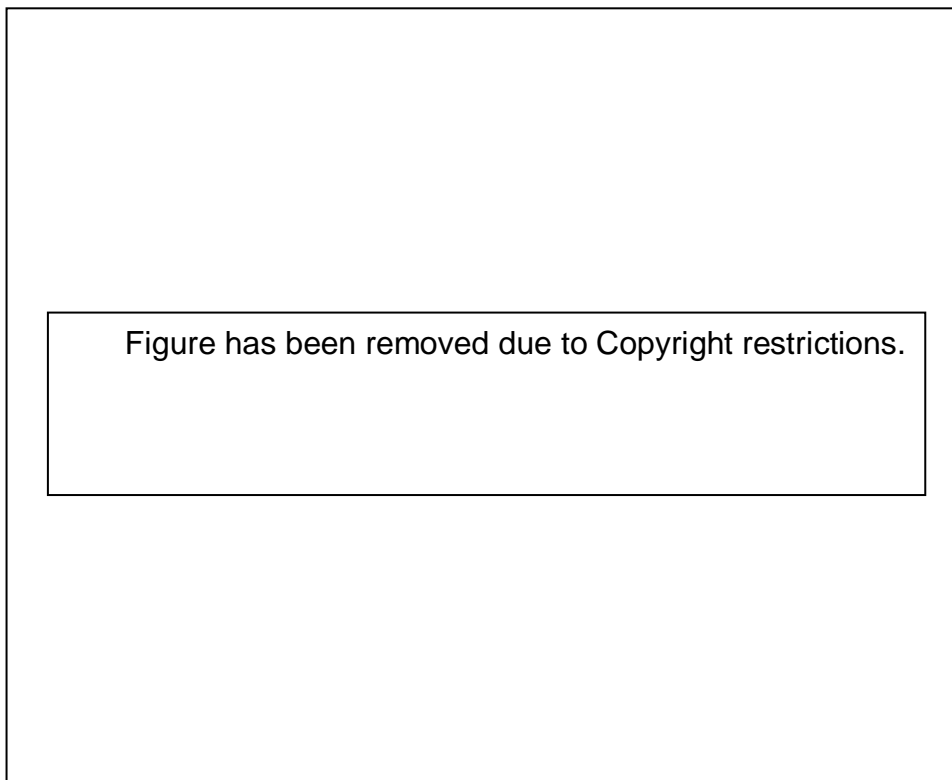
Figure 2.11 Tested beam details. Soeum et al.(2008)

The cracks, deflection and failure mode were investigated for the tested beams and comparison between the results was conducted. A comparison between the tested beams was conducted for each single impact dropped from different heights and for repeated impact from the same height, as shown in the Figure 2.12 and Figure 2.13.
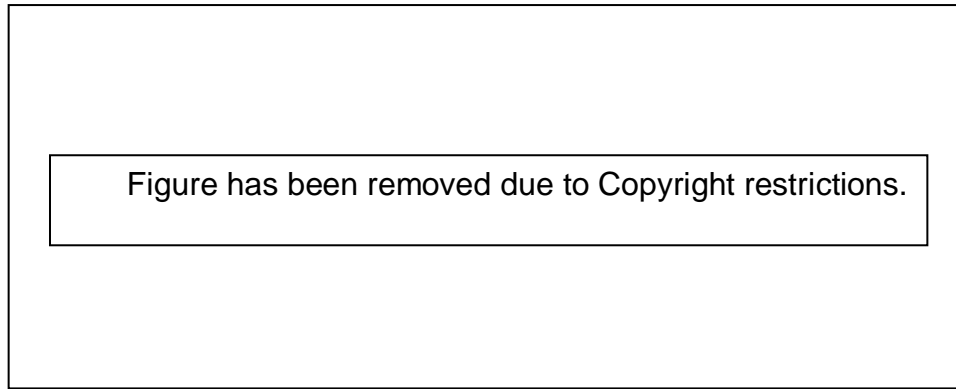
Figure 2.12 Maximum mid-span deflection for the tested beams. Soeum et al.(2008)
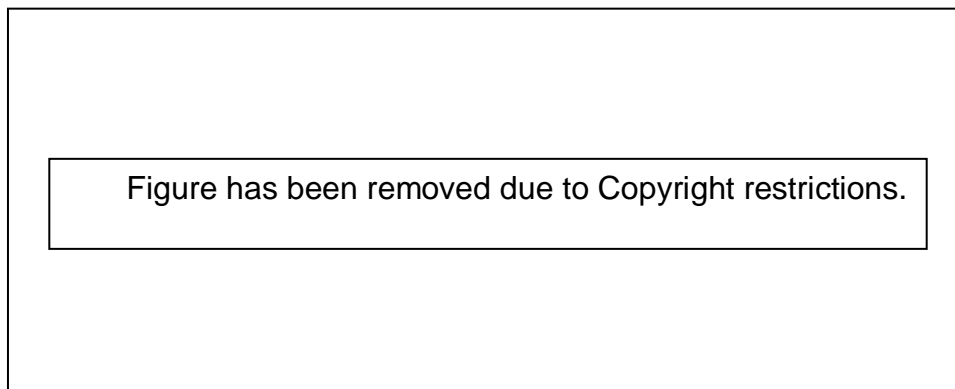
Figure 2.13 Number of blows required to reach 25 mm maximum deflection. Soeum et al.(2008)

The results showed a decrease in crack width for RC beams strengthened with CFRP in flexure by less than 10% with respect to control beam. The smallest maximum deflection was observed in beam TCC, with 50 % reduction compared to the control beam. In addition, the end anchorages prevented the CFRP sheet end from debonding and increased impact resistance. In the case of beams strengthened with CFRP laminates, the steel plate with anchor bolts was shown to be more effective than a U-CFPR sheet as an end anchorage system. Furthermore, an increase in repeated impact load resistance was observed when CFRP was used to strengthen the beams.

The results showed that the strengthened beams can resist weight from twice the drop height of the control beam. This does not mean that the strengthened beams resist

twice the impact force of the un-strengthened beams because the beam was affected by multi impact, causing cracks and deformation that reduce the impact resistance of the beam. However, it might provide some indication that the impact resistance of strengthened beams is higher than that of the control beam.

Appendix A shows the summary of experimental works conducted on concrete beams externally strengthened with FRP under impact loading.

The literature and Appendix A show that most researchers used either the impact test from the same height (repeated impact) or dropped the mass from different heights or used both of methods. In this study, multi-impact test from different heights and repeated from the same height were used to test the strengthened and repaired beams. The comparisons between the tested beam results were conducted for each single impact test to investigate the beams in terms of, impact resistance, reaction force, deflection and cracking.

2.5 Finite element analysis studies on RC beams externally strengthened with CFRP

FEA is low cost method of conducting parametric studies by changing each design parameter in turn to assess the behaviour of structures. It also reduces the time required to analyse the full scale structures and represents an effective alternative tool that compliments the experimental tests. Many finite element analyses have been carried out to study the behaviour of strengthened beams under different kinds of loading.

In 2006, Hoque conducted a parametric study on the effect of FRP properties on failure load and deflection of strengthened beams and plates. He developed a 3-D nonlinear finite element model to investigate the behaviour of the RC beams and plates, either with or without FRP strengthening. The results of the analysis of the developed models were compared with those of the ANSYS software. A good amount of agreement was found between the suggested model results and the ANSYS results. Using FRP to strengthen the RC beams significantly increased the ultimate load and reduced the mid-span deflection.

The nonlinear FEA was used by Jumaat and Alam (2008) to study the behaviour of strengthened RC beams. The experimentally tested RC beams, externally

strengthened with CFRP laminates or steel plates, were analysed using LUSAS software. A perfect bond between the concrete and the steel plate and CFRP laminate was presumed to avoid premature debonding failure. In the surface meshing, a plane stress was used. A good agreement was found between the numerical and experimental results.

The majority of researchers use a perfect bond between steel bars and concrete and between the CFRP and concrete. This affects both the ultimate load and the mode of failure. In reality, there may be bond-slip between the steel bars and the concrete. In EBR strengthened beams, the CFRP are more likely than NSM to debond from the concrete surface, leading to beam failure. Using perfect bond assumption in FE models does not predict debonding failure. In the research conducted for this thesis, the bond between the reinforcement bars and the surrounding concrete was modelled using joint elements that connect the steel reinforcements and concrete through springs. Cohesive elements were used for the interface layer between the concrete and CFRP to simulate the debonding failure.

Mohammed (2012) carried out a large number of numerical studies to investigate the behaviour of reinforced concrete structural members under impact loading. 3D-FEA using ANSYS and LS-DYNA packages was used to conduct the analysis. Various types of structural members were tested numerically, namely RC beams, a slab with an opening and a single hammerhead bridge pier column. A deployable honeycomb energy absorber was proposed and evaluated as a protection system against extreme loading, such as impact and blast loading. The FEA results were compared with the experimental results and a good agreement was found. The results showed that the proposed protection technique was effective and efficient. Using the deployable honeycomb energy absorber can increase the dissipation of energy by 256 to 393% and between 296 to 429 % in mean crushing strength.

In this research, CFRP strip was used to strengthen and repair damaged RC beams under impact loading. A 3-D FE model was developed to analyse the conducted experimental work using LUSAS software.

2.6 Damage assessment and FRP repaired beams

Structures can be exposed to damages from different sources during their life. The damage assessment is important for the selection of the appropriate repairing technique and the choice of suitable material to repair the damaged structures. A great deal ofany research has been conducted to assess the damage to RC beams under static loading.

Benjeddou et al.(2007) investigated the behaviour of damaged RC beams repaired by EBR CFRP laminate. Eight beams of 2 m length were tested under a four-point loading test. The size of the tested beams was 120 mm width and 150 mm depth. The beams were classified as one damaged beam without strengthening as a control beam and damaged beams strengthened with CFRP laminates. The variables were the degree of damage, CFRP laminate width and concrete compressive strength. Four damage percentages were investigated: 0%, 80%; 90: and 100%. The damage degree was defined as the percentage between the applied load causing the beam pre-cracking to the load- carrying capacity of the control beam. The beam was in an elastic state for an 80 % of damage; two cracks appeared at 90 % of damage and the beam behaviour became plastic. For a damage degree of 100 %, more cracks appeared and the beam deflection reached 10.5 mm. CFRP was used to repair the damaged beams and the repaired and the control beam were compared. The results showed a significant increase in strength and rigidity of the strengthened damaged beams compared with that of the control beam. The increase in flexural strength was 44-87 %, depending on the degree of damage. The results showed a slight increase in the repaired beams' load capacity with increase of CFRP width or the compressive strength of concrete. The failure modes of the repaired beams were CFRP peeling off with interfacial debonding.

In the study of Benjeddou et al., the beam was considered to have 80 % damage, and it was still in elastic region and that overestimated. The damage assessment is based on the effect of the damage on the stiffness, ductility and strength capacity of the beams.

The reduction in the beam stiffness can be used to assess the percentage of damage in the structural members. Lakshmikandhan et al. (2013) conducted a study to predict the degree of damage to an RC beam, using a stiffness degradation method. CFRP was used to repair the damaged beam. The beams were then subjected to cyclic

loading. Beam performance and damage were assessed after each cycle to find the degree of damage.

The experimental work included testing six beams (BT0 to BT5) under cyclic and monotonically static four-point test. The tested beams size was 100 mm width, 200 mm depth and 1.5 m length. The experiential work included two stages; the first stage was damage assessment and the second stage was the repair of the damaged beams. Figure 2.14 shows the testing schemes applied on the beams. At the first stage of the experimental work and to assess and evaluate the damage degree, beam BT1 was tested under monotonically loading up to failure to find the ultimate capacity of the beam. The beam BT0 was subjected to cyclic loading to different percentages of the ultimate load, as shown in Figure 2.15. The degree of damage was evaluated with regard to the reduction in the stiffness of the beam by comparing the beam stiffness of BT1 at different loading percentages with the initial stiffness.

Damage percentage=(Ko-Kx)/Ko *100

Where:

Ko= initial stiffness

Kx= stiffness at the certain load percentage of the ultimate load.

The first stage provided data about the stiffness reduction and the corresponding applied loading. These data were used in the second stage of the experimental work to evaluate the beams repaired or strengthened using CFRP. Beams BT2, BT3 and BT4 were damaged to 50-60%, 70-80% and 80-90 % respectively. Beam BT5 loaded to a level of 0-10% so no cracks appeared at the beam. All damaged beams were repaired using NSM CFRP and reloaded up to failure to evaluate the flexure strength. The results of the repaired beams were compared with the results of the control beam BT0 in terms of load deflection curve ductility failure mode. A comparison between the repaired beams with the strengthened beam showed that the repaired beam had a higher load carrying capacity than strengthened beams. The results showed that using the stiffness degradation method successfully predicted the degree of damage.

In the experiment carried out by Lakshmikandhan et al., cycle loading was used to damage the single beam BT0 and, for each cycle, the beam stiffness was measured and compared with the initial beam stiffness, and that was considered as stiffness reduction. It should be noted that the authors neglected the effect of the previous cycles, which the damaged beam and reduced its stiffness. Thus, the damaged degree

calculated by Lakshmikandhan et al. is the cumulative stiffness reduction and not the degree of damage to the specific load.

Figure has been removed due to Copyright restrictions.
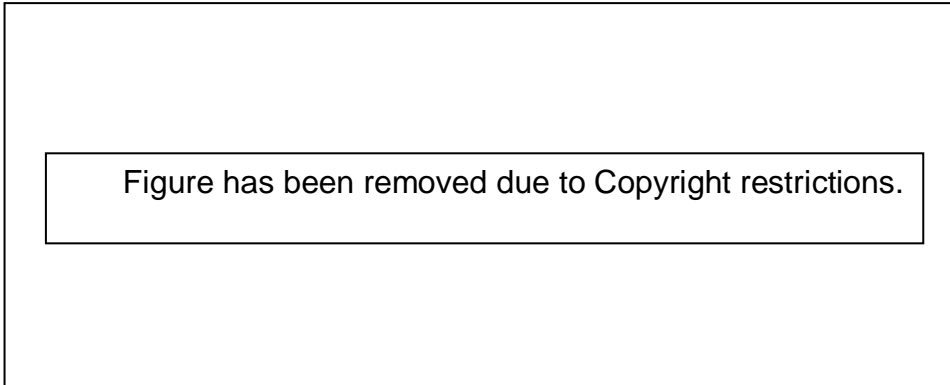
Figure 2.14 The percentages of load applied to the tested beams, Lakshmikandhan et al. (2013)

Figure has been removed due to Copyright restrictions.

Figure 2.15 Cycle loading applied on BT0. Lakshmikandhan et al. (2013)

Roberto (2009) used free vibration tests to study the behaviour of RC damaged beams strengthened with near surface mounted (NSM) CFRP rods under static and dynamic loads. Three 150 mm square section RC beams of length 3.75 m were tested through static and dynamic tests. In the static test, different percentages of damage were

induced on the un-strengthened RC beams, and then NSM CFRP rods were used to strengthen the damaged beams. Free vibration tests were used to obtain experimental dynamic parameters at different states and conditions of damaged and undamaged beams. Flexible springs were used to hang the beams and impulsive load was induced by an impact hammer. The dynamic test results showed that CFRP rods did not prevent the crack development on strengthened beams. The static results indicated an increase of stiffness for beams strengthened with CFRP rods under static test. The strength and ductility of beams were increased when CFRP rods were used as strengthening materials. In addition, compressive concrete failure and cover delamination governed the failure mechanism for all tested beams. The results of the experimental work were compared with those obtained by the non-linear numerical method and a good agreement was obtained between experimental and theoretical results.

The free vibration method cannot precisely determine the damage percentages. It can provide an indication of the damage effect on the beam's behaviour in terms of the cracks distribution and propagation and the natural beam frequency of the damaged beams, which affects beam stiffness.

In this PhD research, the behaviour of damaged beams due to impact was investigated. A stiffness degradation method was used to assess the damage to the beams subjected to impact loading. CFRP strip was used in this study to repair the damaged beams, using NSM technique. The repaired beams were then assessed to evaluate the improvement in their behaviour in terms of stiffness, impact resistance, reaction force deflection and cracking.

Most of the research literature has been conducted on beams damaged by static loading. It is important to pay attention to damage caused by impact loading and to investigate the method of assessment and repair of materials and techniques.

2.7 Steel-concrete bond

Forces can be transferred between concrete and steel in different ways: (i) adhesive (ii) friction between steel bars and (iii) the concrete and the bearing of steel ribs against the concrete (Wang and Liu 2003). The bond between the concrete and steel is significantly affected by concrete properties. Many factors affect the bond between the concrete and steel reinforcement, and it is difficult to separate the contribution of each factor. However, factors such as concrete compressive strength, epoxy coatings, bar

spacing and concrete cover, confinement, relative rib area, bar yield and development length have varying effects on the concrete –reinforcement bars' bonding (El-Hacha et al. 2006). Many published works have reported the ways in which each factor affects the bonding between the concrete and steel reinforcement.

Azizinamini et al. (1993, 1995) used the beam splice test to study the effect of the high concrete strength on bonding between the steel bars and the concrete. They concluded that the mean bonding stress at failure is proportional to the square root of the concrete compressive strength √fc′.

The effect of the concrete strength on the bond was investigated by Esfahani and Rangan (1996), using a splice test and beam-end tests. The results showed that concrete strength affects the crushing in front of the ribs and increases with the decrease of the concrete compressive strength.

Darwin and Graham (1993) and Darwin et al. (1996a, 1996b) investigated the effect of the relative rib area of steel reinforcement on Rr (the ratio of the projected area of the rib to the product of the centre-to-centre rip spacing and the nominal bar perimeter) on the bond. It was concluded that bond strength increases with the increase at the Rr of steel bars.

El-Hacha et al. (2006) and Ogura et al. (2008), after examining the effect of the concrete cover on the binding, concluded that the bond strength increases with an increase of the concrete cover. With minimal concrete cover, a splitting failure is more likely to occur than direct pull-out failure for flexural members. The same conclusion was reached by Hadje-Ghaffari et al. (1994): high bond strength and high ultimate load can be achieved when the concrete cover is increased.

2.7.1 Harajli's bond stress-slip model

Harajli et al., (2002), used regression analysis on test data to generate the monotonic envelope bond stress-slip relationship shown in Figure 2.16. They proposed equations to predicate the maximum bond stress and the corresponding slippage, using both an analytical model and experimental results. The maximum bond stress (Um) and the corresponding slip distance ($s1$) are defined in Equations 2.1 and 2.2 respectively

$$Umax=31.0 \sqrt{fc'}\dots\dots\dots\dots\dots\dots\dots\dots\dots\dots\dots\dots .2.1$$

$$s1= 0.15co \qquad \dots\dots\dots\dots\dots\dots\dots\dots\dots\dots\dots..2.2$$

Where:

$Umax$: maximum bond stress (psi)

$s1$: slip distance (inch)

co: Clear distance between lugs (inch)

fc': concrete compressive strength (psi)

Figure has been removed due to Copyright restrictions.

Figure 2.16 Monotonic envelope model (Harajli et al 2002)

In this study, the bond stress slip relationship (Eq. 2.1) was used to determine the stiffness for spring elements to model the steel bars-concrete bonding in the FEA (See Chapters 7 and 8).

3. Impact test setup and instrumentation

3.1 Introduction

In this study, a drop weight impact test machine was manufactured in the Civil Engineering laboratory at Plymouth University to investigate the impact behaviour of reinforced concrete beams strengthened or repaired with CFRP strip.

The manufactured impact test machine incorporates many instruments, including accelerometers, load cells, dial gauges and a high speed camera. Various data results were obtained from the test, such as impact load, acceleration, displacement and reaction force vs. time curves. The mass and drop height were varied in order to induce different impact energies. To prevent vertical movement and rebounding of the simply supported beam ends during the impact test, a modified support (yoke) was made and used successfully during the impact test. The manufactured drop weight impact apparatus is described below:

3.2 Preliminary design of drop weight impact test machine

The test frame, instrumentation and data acquisition system of the impact machine are described in the following sections.

3.2.1 The impact test machine frame

The impact test machine components were supported using a steel frame tower with four alignment bars used to guide the hammer during lifting and dropping. These guidelines were made of 50mm diameter circular steel bar. A number of ball bearings was used between the hammer and the guide bars to give the hammer a smooth vertical movement and accurate alignment. The machine included a mechanical chain hoist to lift the impactor and a hand held control box containing a latch assembly to hold the hammer at the required height until release when the impact test is started. When released, the weight falls due to gravity and strikes the beam precisely at a given point. Figure 3.1 illustrates the details of the test machine and Figure3.2 shows the test frame and guide rails.

A debris curtain was used for safety to protect the operators and other facilities in the lab from damage due to potential flying debris caused from the collision between the hammer and the specimens. In addition, Plexiglas sheet was used to protect and

allow the high speed camera to record the impact moment and the subsequent effects on the specimens.
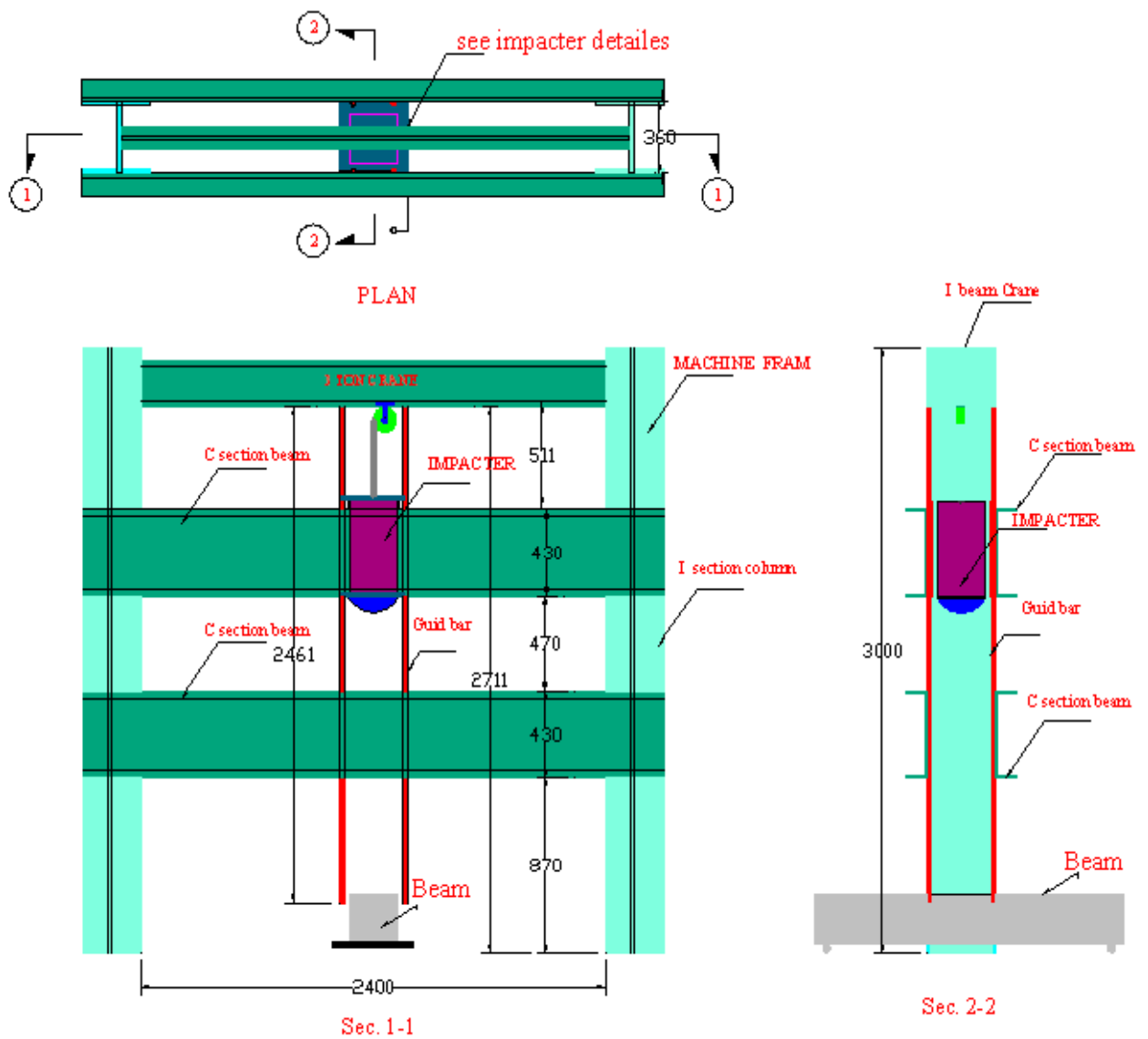
Figure 3.1 Schematic diagram of the test machine

Figure 3.2 The impact Test Machine

3.2.2 The Impact Hammer

The hammer comprises a container with dimensions of 460 x260 x 260 mm. The container encloses a number of 10 kg steel plates, each with dimensions of 250x 250 x25 mm. The drop mass, including the container, can be increased by 10 kg increments up to 200 kg and the mass can be dropped from a height of up to 2 m. A 125 mm hemispherical solid steel hammer head was used to transfer the impact energy from the dropped hammer to the specimen. Figure 3.3 shows the impact hammer. The total applied dropped mass is the summation of the container, steel head and the weight of the steel plates.

Figure 3.3 The Impact hammer

3.2.3 Design and manufacturing of the yoke at the supports

In this study, simply supported beams were tested under impact loading. During a short period of impact, the support-ends experienced rebounding when the hammer struck. This was due to the support losing contact with the beam ends. Thus, the load cell at the support did not record the correct data. To prevent this vertical movement and rebounding, a steel yoke was used in the support to restrain the vertical movement of the beam ends, while at the same time allowing rotation motion.

Figure 3.4 illustrates details of the steel yoke and beam support. It consisted of two arms connected to the support by a pin to allow the end to rotate. A top plate was used to hold the beam end in place and to prevent it from moving vertically. The reaction force was recorded using the load cell mounted at the support. To allow the beam to move horizontally at the roller end, a number of small diameter steel bars were placed between the top plate and top face of the beam and between the bottom face of the beam and the support, as shown in Figure 3.4.
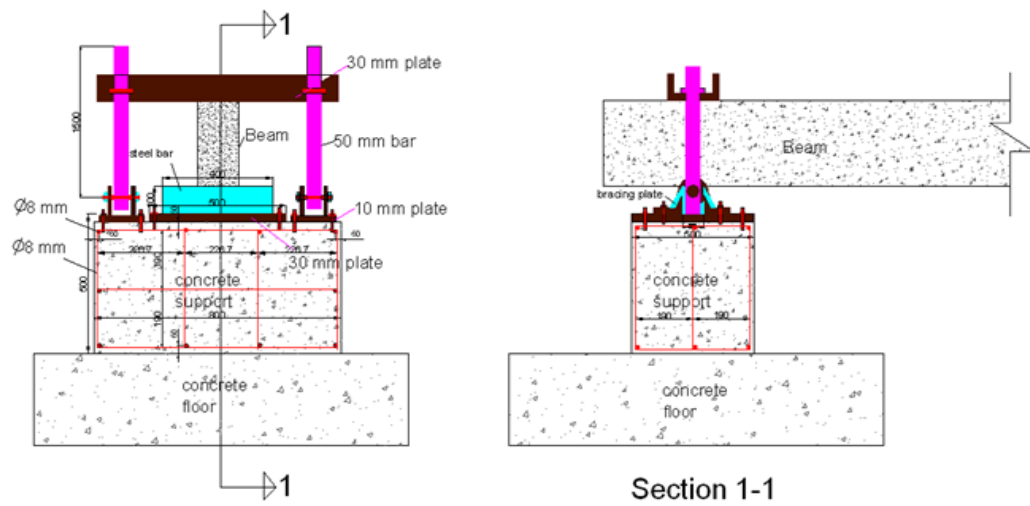
Bin support
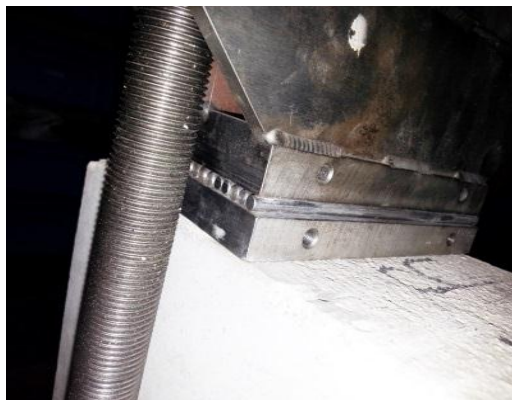
roller support

Figure 3.4 Details of steel yoke and beam support

3.2.4 Instrumentation

The impact test was conducted to measure several parameters: impact force, acceleration of the specimens and the support reactions. To obtain the required data, the instrumentation included accelerometers, load cells and a high speed camera. Table 3.1 shows the type of the sensors and the parameters that they measured in carrying out this research

Table 2.1 Types of sensors and the parameters

Parameter	Sensors
Impact force	Accelerometer
Acceleration	Accelerometer
Reaction force	Load cell
Deflection	Dial gauge

- **Accelerometers**

Two types of 70 kHz frequency response accelerometers with a resolution of 0.1 g, manufactured by PCB Piezotronics Company, were used in the impact machine. The first type was a piezoelectric sensor model with an acceleration capacity of range $\pm$ 1000 g. The second type of accelerometer was the piezoelectric sensor model 353B15 with an acceleration capacity of range$\pm$500 g. The technical data for the accelerometers are shown in Appendix B.1.

- **Load cell**

Load cell model 204C, manufactured by PCB Piezotronics Company, was used to measure the reaction force developed due to impact. One load cell was installed on the yoke support as shown in Figure 2.5. The load cell maximum force capacity measurement was 177 kN. The technical data of the load cell is shown in Appendix B.2.
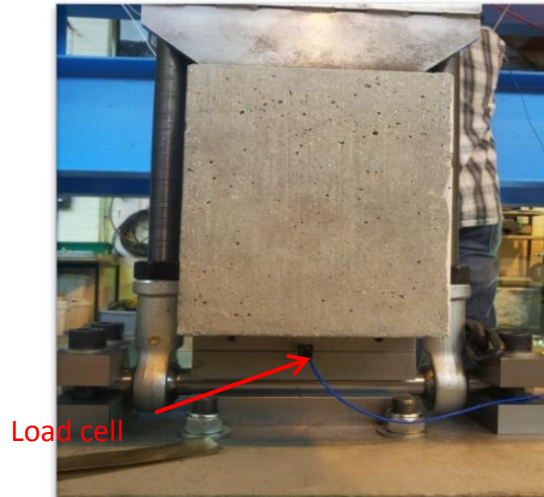
Figure 3.5 Load cell at support

- **High-speed video system**

The NAC's HotShot 1280 pci digital high-speed video system with 1000 frames per second was used to record the impact test and the moment of impact between the hammer and the specimens (see Figure 3.6). The recorded film was initially stored in the memory of the camera and then transferred to the computer hard drive. Appendix B.3 shows the technical data sheet of the high-speed camera.

Figure 3.6 High speed camera

- **Data acquisition system**

A data acquisition system produced by the National Instruments Company was used in the impact test. The sampling rate of the data logger was 50 kHz. The data were collected and viewed using Lab View software.

3.4 Beam deflection measurment

Three methods were used to measure the deflection under the impact loading point: accelerometers, a high speed camera and dial gauges. In the first method, dial gauges were used to find the maximum and residual deflections of the beam during the impact at different points along the beam length. A linear extrapolation was used to find the deflection at the beam mid-span.

In the second method, accelerometers were placed at certain distances along the beam length to measure accelertation, velocity and deflection. The deflection at any time was found by double integration of the acceleration at each accelerometer installed in the beam. No accelerometers were installed at the point of the impact, so as to prevent damage due to impact. To find the deflection under the impact load point, a linear extrapolation of displacement from other points was used.

The third method used to measure the maximum deflection at the mid-span of the beam was the high-speed camera. Measurements were indicated at the mid-span of the beams, as shown in Figure 3.7. A steel wire attached to the guide bars was the datum placed at the the same level of the bottom face of the concrete beam before the impact. The maximum deflection was found at mid-span by inspection of each frame recorded by the high-speed camera and by reading the measurments indicated by the datum.
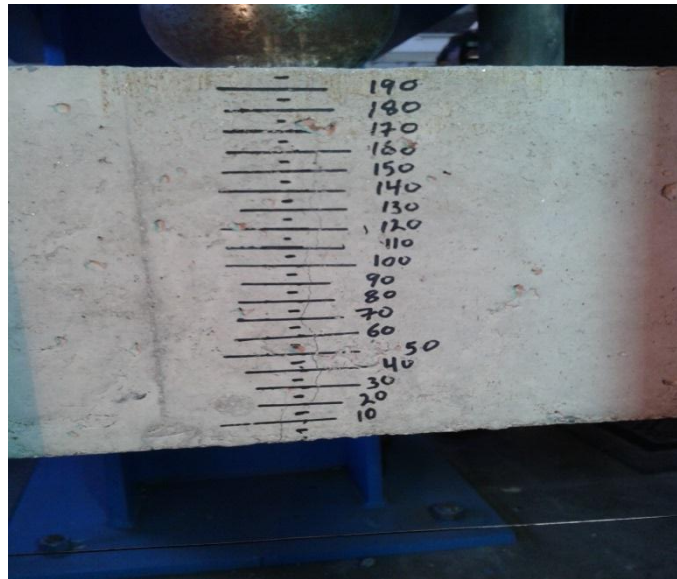
Figure 3.7 Scale for deflection measurements at mid-span of the beam

3.5 Preliminary impact tests

A trial impact test was implemented on one RC beam to commission the impact test machine and the testing procedure. The single beam tested at the trial stage had a clear span of 3000 mm and 2Ø12 mm steel reinforcement bars were used at both the bottom and top faces of the beam. The shear reinforcement was an 8 mm bar with 115 mm spacing. Figure 3.8 shows the beam details and distribution of sensors along the beam length. The compressive strength of the concrete was 30 MPa. The impact test was started by dropping the mass from a low height and increased gradually until beam failure.

For this test, one 353B15 (500 g) accelerometer was placed on the striker to measure the impact force on the impactor, as shown in Figure 3.9. The accelerometer 353B11 (1000 g) was used to measure the acceleration at the beam during the impact (see Figure 3.10).

impacter

Accelerometer →

Accelerometer

1

500 mm

3000 mm

1

100 mm

Ø12 mm

Ø8@115mm

Ø12 mm

200 mm

Section 1-1
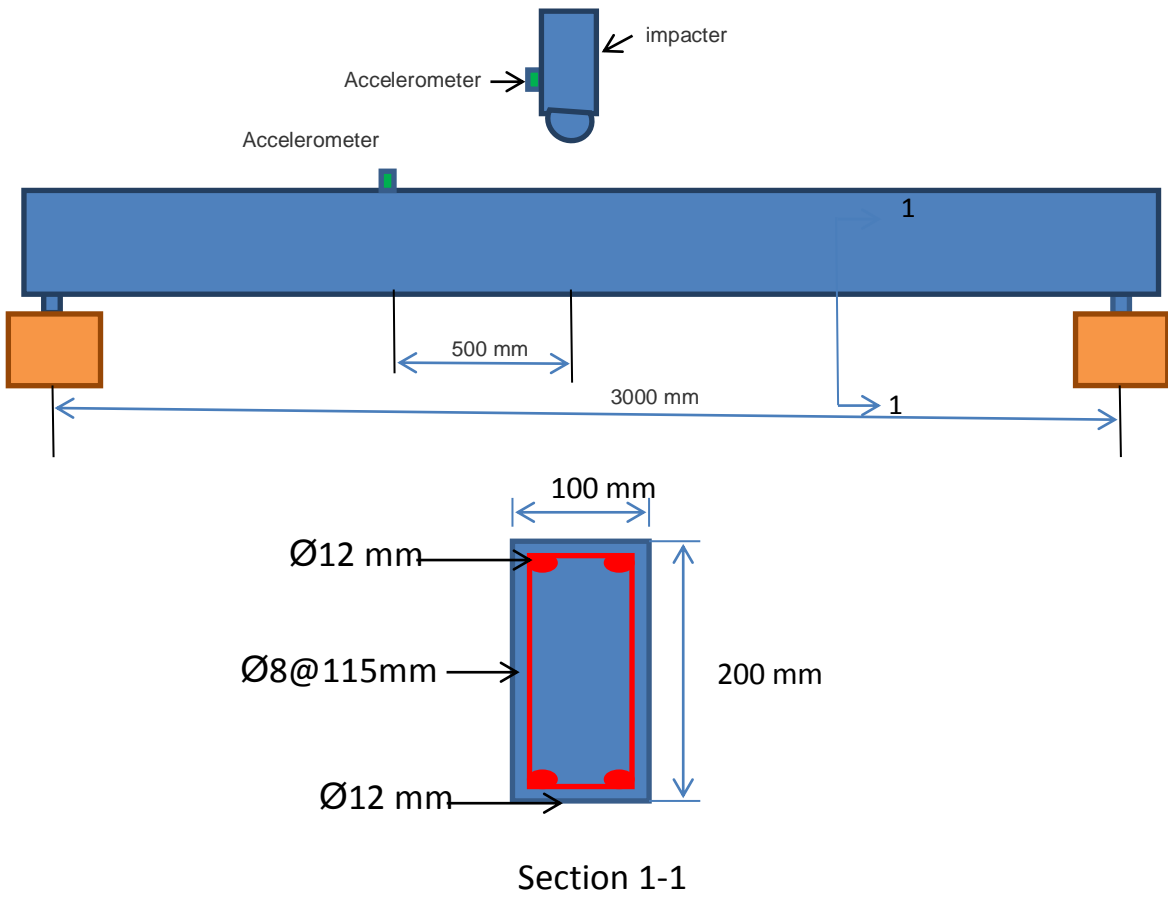
Figure 3.8 Details of the trial test beam

Accelerometer

Figure 3.9 Accelerometer at the impact hammer
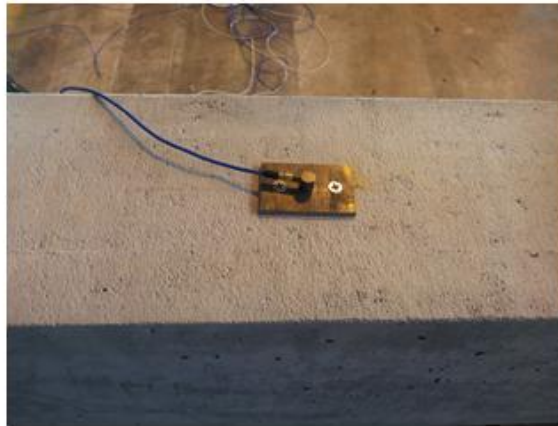
Figure 3.10 Accelerometer at the beam

3.5.1 Results from the preliminary specimen

The results of the trial test (see Figure 3.11) showed that the accelerometer at the impactor exceeded the maximum capacity of the accelerometer (500 g). The test showed that more than one accelerometer was required at the impactor to obtain reliable result in terms of impact force. Also, to find the deflection at the mid span and the inertia force of the beam due to impact, the preliminary test showed that one accelerometer at the beam was not sufficient (and may have given a wrong result). Three or more accelerometers were required to obtain accurate results and to ensure partial results if one of the accelerometers failed during the test.

The assessment of the beam after the impact test showed that local damage occurred at the top face of the beam (see Figure 3.12). This occurred because of the shape of the steel head initially used, which was too sharp, causing damage at the point of impact and spalling of pieces of concrete at the top face of the concrete. This also may have contributed to incorrect results.

When the mass was released and dropped during the test, it was observed that the guide bars were vibrating. This caused vibration at the datum which may have led to a wrong reading of the beam deflection during the impact.

The trial test also showed a good performance of the yoke support. During the impact, the steel yoke prevented the beam end vertical movement and allowed rotation.
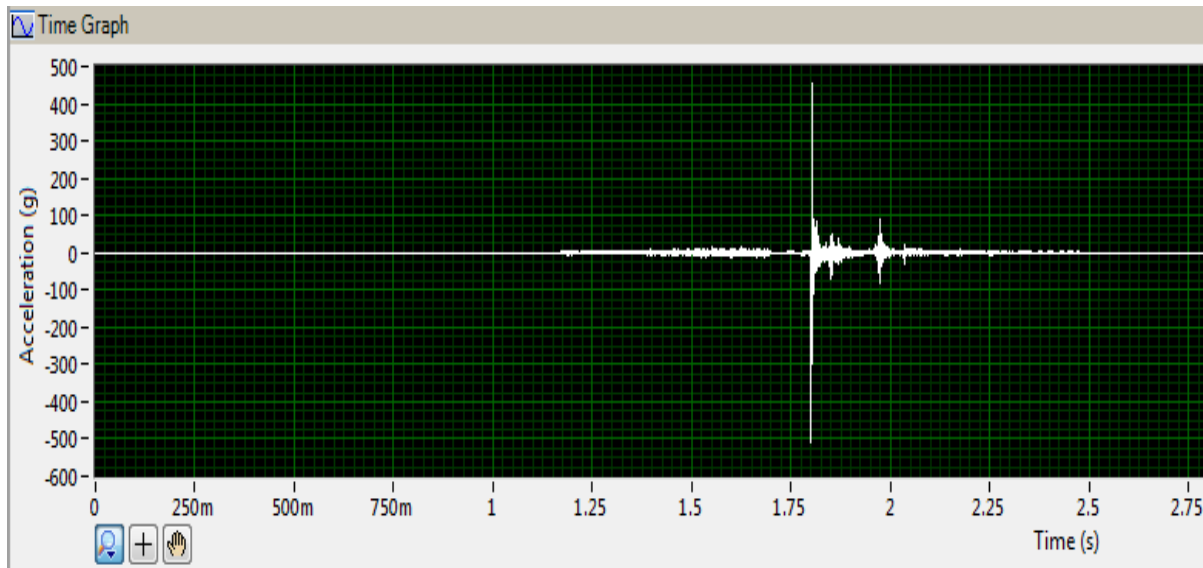
Figure 3.11 Accelerometer reading during trial test

Figure 3.12 Local damage to the beam due to impact loading

3.5.2 Lessons learned from preliminary tests

The trial test assessed the impact test machine and the test-setup. The main lessons of the tests informed further development of the impact machine. The main conclusions from the trial test were:

- The sharp steel head of the hammer caused local damage and should be flatter.
- The accelerometer capacity was too low and needs to be increased.
- More accelerometers were required to measure the beam deflection and impact force for higher accuracy.
- It is necessary to Increase the recording rate and to increase the number of frames per second
- The maximum capacity of the impactor needed to be increased so that heavier mass can be used, especially when the beams were strengthened with the CFRP strip.

3.6 Impact test machine updating

Based on the results of the trial test, the impact test machine was updated and developed. The following changes were applied to the impact machine: -

- **Impact hammer**
  The trial test showed that the convex steel impact head caused a lot of local damage to the concrete surface. To avoid this damage, avoid, the steel head was changed, so as to be flatter with a larger radius spherical section, as shown Figure 3.13. In addition, the maximum capacity of the impactor was increased to 300 kg capacity by increasing the height of the container to hold more steel plates.

Figure 3.13 Modified steel head

- **Deflection measurement**

To measure the mid-span deflection, a plastic ruler was used instead of the measurement indicated at the face of the beam. The plastic ruler was attached to the front face of the beam at the mid-span, so that the maximum deflection could be measured using the high speed camera. The datum position also was also transferred to a separate stand. The datum was adjusted before each test to be at the level of the lower surface of the concrete beam. Figure 3.14 shows the plastic rule and the datum used to measure the deflection.
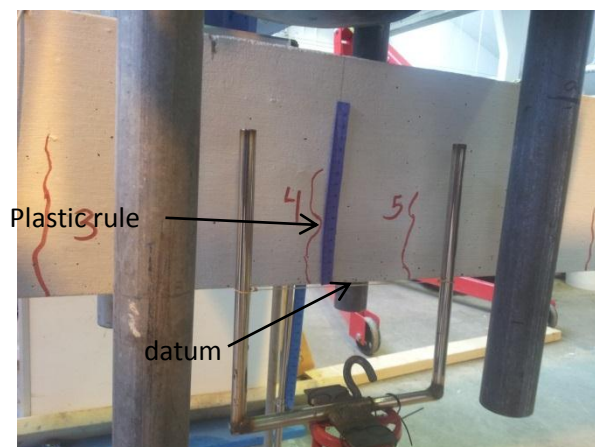
Figure 3.14 Mid-span deflection measurements

- **Instrumentation**

To obtain reliable results, six accelerometers were used to acquire the correct data in the impact test. In addition, the acceleration capacity of the accelerometers used to measure the impact force was increased from 500 g to 1000 g. Three accelerometers were installed at the top face of the steel head, with 120 degrees between them, as shown in Figure 3.15.

To measure the acceleration, velocity and deflection of the beam at any time, three accelerometers were installed on the top face of the beam at specified distances from the beam support. Figure 3.16 illustrates the distribution of the sensors along the beam length.
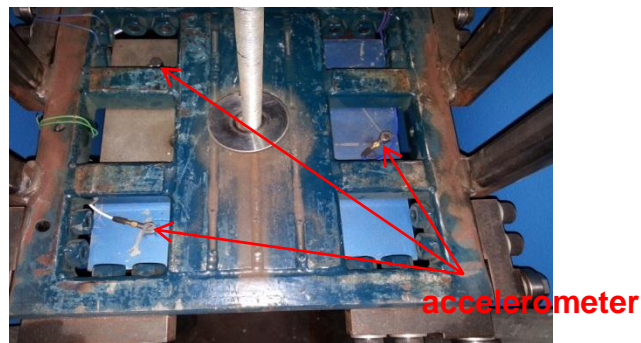
Figure 3.15 Distribution of the accelerometers in impact hammer
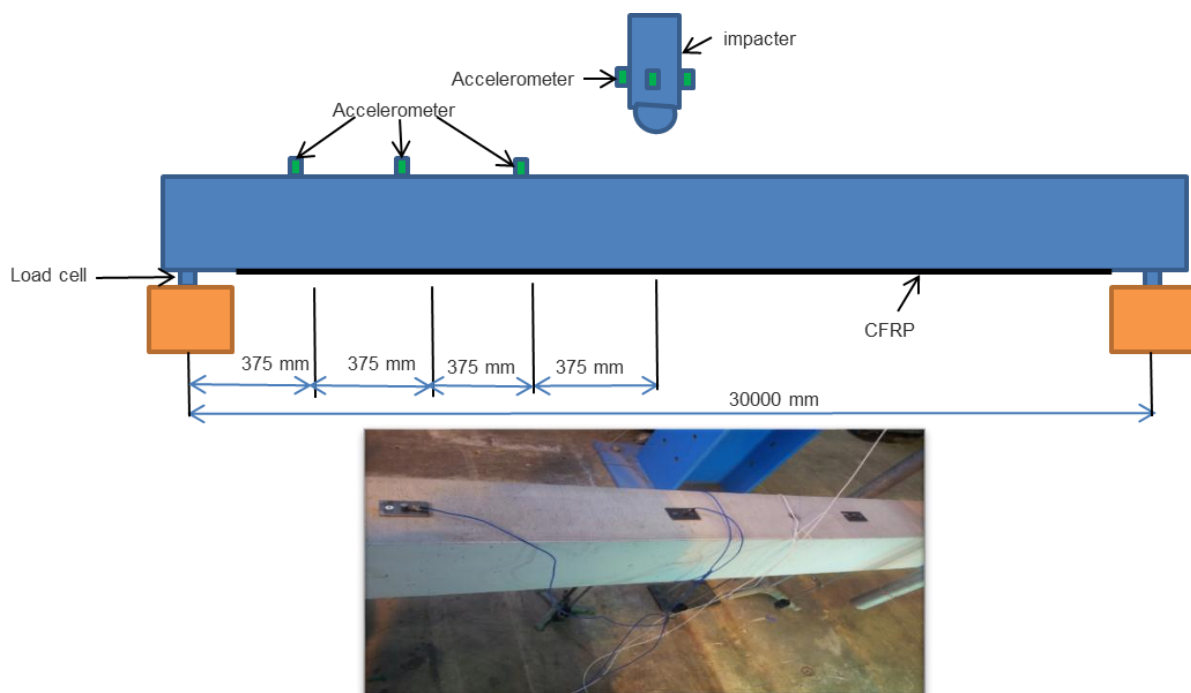
Figure 3.16 Distribution of the sensors along the RC beam length

3.7 Concluding remarks

In order to study the behaviour of the RC beams strengthened or repaired using CFRP, a heavy impact test machine was designed and manufactured. A steel yoke used in support prevented the beam end from rebounding during impact, while allowing the end to rotate. However, the top steel plate in the support and the fraction between the steel parts of the support and the beam ends may be restrained partially the rotation of the beam ends.

The shape of the steel head used to impact the beams affected the test results. Using a sharp steel head damaged the tested RC beams locally. After the trail test, therefore, the steel head was changed so as to be flatter, and this prevented local damage during the tests. Steel plate can be used on the top of the beam at the impact point to prevent any local damage, but this may affect the results, as this steel plate can absorb some of the impact energy imparted to the tested RC beam.

In terms of the instrumentation used in the impact tests, the number of sensors employed to measure the required date was increased, thus increasing the accuracy of the results. Using extra sensors to measure the same type of data ensures that, should one of the sensors break down, others will still record data. Three accelerometers were therefore used to measure the impact force and another three used to measure the beam acceleration during the impact. Due to resource limitations, one force sensor was used to measure the reaction force, and beam symmetry was assumed to measure another reaction support. However, it is more accurate to use two force sensors to measure the reaction forces in the beam supports as the beam is not perfectly symmetrical in practice.

A high speed camera was used to capture the impact moment to study the cracks and failure mechanism. The high speed camera was also used to measure the mid-span deflection history during the impact. The camera recording rate (frames per second) was important to obtain accurate results. As the impact happens within milliseconds, using a low recording rate may result in in loss of the peak deflection point, which will be not recorded by the camera. For that reason, a high recording rate (1000/s) was used to measure the beam deflection.

4. Experimental Work

4.1 Introduction

Previous studies of the impact behaviour of reinforced concrete (RC) beams strengthened with CFRP reported in literature are little. To increase the understanding of the effect of using CFRP on the impact resistance of RC beams, experimental work was conducted using a drop weight impact test machine designed for this purpose, as described in Chapter 3. The parameters monitored from the impact tests included damage pattern of the beam, crack propagation and failure mode. The data obtained from the instruments included acceleration, displacement, and reaction force as a function of time. A parametric study was conducted to assess the effect of parameters such as drop height, drop weight mass, strengthening technique types and degree of damage. These data were analysed to determine the response of strengthened reinforced concrete beams to the imposed impact loads. The following sections describe the experimental work.

4.2 Test Beam Samples

A single beam was tested before starting the main experimental work in order to examine the suitability of the manufactured impact test machine (see Section 3.5 for beam details).

The accuracy and reliability of the experimental results depended on the requirement that all test programme beams should have the same properties. The same materials, formwork, reinforcement bar mesh, mixing and vibrating equipment and laboratory environment were used for manufacturing of the RC beam samples, so as to ensure that all beams were of identical geometry, materials properties and bar details.

The experimental test programme utilised 12 reinforced concrete beams. The beam dimensions were 150 mm width, 200 mm depth and 3150mm long with clear span of 3000 mm (see Figure 4.1b). All beams were reinforced with two 10 mm diameter longitudinal reinforcement steel bottom bars and two 8 mm top bars. The shear reinforcement was an 8 mm bar with 70 mm spacing. Small spacing was necessary to avoid shear failure. Figure 4.1 shows the cross section of beam and reinforcement details.
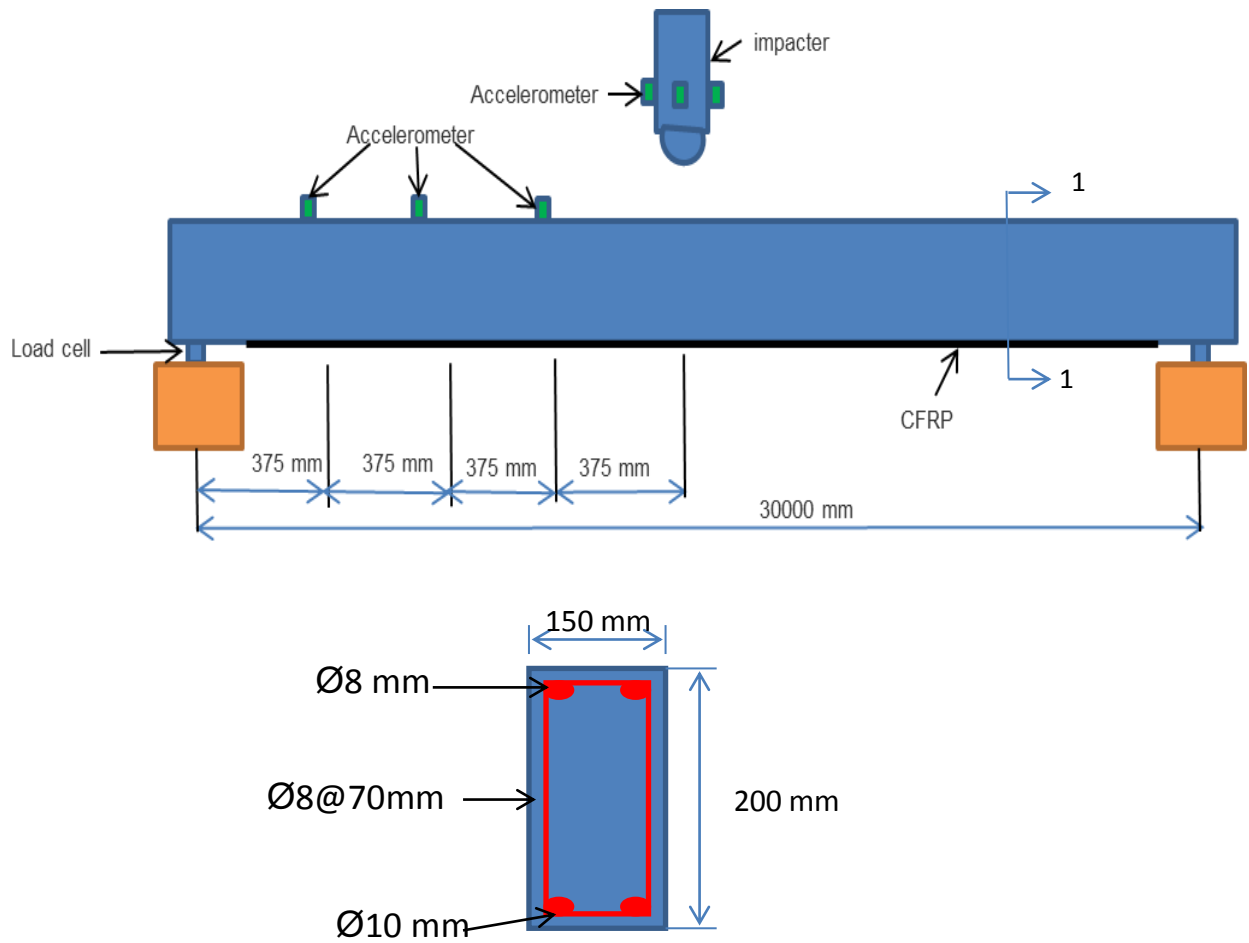
Section 1-1b Beam tested in experimental work

Figure 4.1 Tested beams details

4.3 Material properties

To find the material properties of the tested beams, concrete cubes, samples of steel bars and a CFRP strip were tested using compressive and tensile tests. Figure 4.2 shows the machines used to test the components of the tested beams.

4.3.1 Concrete

All samples used a concrete mixture designed to have a 28 day average cube compressive strength of 32 MPa. A pair of beams and nine cubes of 150 mm edge were cast from each batch of concrete. Cured cast concrete cubes were subjected later to the quality control compressive strength test to determine their compressive strength.

4.3.2 Steel reinforcement bars

Different steel bars (D8 and D10) were used to reinforce the concrete beams. Five samples were tested in tension to find the mechanical properties of the steel reinforcement. Table 4.1shows the average steel reinforcement properties tested at the lab using tensile testing machine.

Table 4.1 Material properties (tested at the laboratory)

Material	Properties		Standard deviation
Concrete	Cubic Compressive strength(MPa)	32	1.41
Steel Reinforcement(D10)	Yield strength (MPa)	577	10.7
	Ultimate tensile strength (MPa)	673	9.5
Steel Reinforcement(D8)	Yield strength (MPa)	378	4.5
	Ultimate tensile strength (MPa)	456	2.4
CFRP strip	Elastic modulus (GPa)	153	3.3
	Tensile strength (MPa)	3214	190

Concrete   **steel bar**   **CFRP strip**

Figure 4.2 Concrete cube, steel bar and CFRP strip testing machines

4.3.3 Casting and curing of concrete

Two aluminium formworks with wood faces were used to cast the RC beam samples. The wood faces gave the cast beams a smooth surface. Additional bracings were provided along the mould length to add additional support to the formwork face during casting. This also prevented bowing of the faces of the formwork during the casting process.

Before casting the beams, the moulds were coated with a thin film of oil. Spacers were added between the steel cage and the mould faces of the cage to ensure 25 mm concrete cover to the reinforcement. The sand, gravel, water and cement were mixed using a concrete mixer. Then the concrete mixture was transferred and poured into the mould and uniformly distributed along the mould length. The concrete mixture was placed in layers until the required depth was reached. A 25 mm diameter poker vibrator was used to vibrate the concrete. From each batch of concrete, nine standard cubes were cast for subsequent compressive strength tests. After casting, the concrete beams and cubes were covered, using plastic film to minimise dehydration. The mould was removed from the beams and cubes after three days. All beams and cubes were then labelled. Finally, the beams were safely stored in the lab and the cubes were placed in the curing tank in a 20°C water bath. The same casting process was used to manufacture all the samples to minimise any discrepancy between results.

4.3.4 CFRP

One unidirectional carbon fibre reinforced polymer strip was used to strengthen each reinforced concrete beam. The CFRP strip was installed at the bottom face of the beam and two techniques were used for installation, the external bonded technique, EBR, and near surface mounted technique, NSM. The CFRP strips used had the following dimensions: 1.4mm thick, 17mm depth and 2.7 m long. Five samples of CFRP with 300 mm lengths were tested to measure the tensile strength and elastic modulus for the CFRP. Table 4.1 shows the mechanical properties of the CFRP strip tested in the lab. Appendix C.1 shows the technical properties of the CFRP strip provided by manufacturer.

4.3.5 Epoxy

The MBRACE epoxy adhesive consisted of primary base resin and hardener. Appendix C.2 shows the manufacture and technical properties of the epoxy.

A layer of epoxy was applied to the concrete surface and another applied to the CFRP strip. The setting time for epoxy was about 16 hours, but to ensure good bonding, the samples were left for two days before testing to ensure that the epoxy had enough time to set and that a good bonding between the CFRP and the concrete surface was established.

4.4 Experimental work stages

The behaviour of RC beams strengthened or repaired using CFRP was investigated in this study. Twelve RC beams were tested under dynamic impact load. Two strengthening techniques were used in the experimental work, the externally bonded reinforced FRP (EBR) technique and near surface mounted technique (NSM). The experimental work was divided into two stages: Stage 1 (strengthening) and Stage 2 (repair).

At Stage 1 (strengthening), EBR and NSM strengthening techniques were used to strengthen the RC beams. Three pairs of beams were tested in stage 2 (repair). Different degrees of damage were induced using different impact energies. CFRP strips were then used to repair the damaged beams using NSM technique.

Table 4.2 shows the classification of tested beams classification. They were classified according to the type of strengthening technique, damage type and repair. More details about experimental work stages are explained in detail in subsequent sections.

Table 4.2 Tested beams classification

1-Strengthening	Group	Beam No.	Strengthening	Damage	Repairing
1-Strengthening	1	BR-1	Reference	-	-
		BR-2	Reference	-	-
	2	B-EBR-1	EBR	-	-
		B-EBR-2	EBR	-	-
	3	B-NSM-1	NSM	-	-
		B-NSM-2	NSM	-	-
2-Repair	1	B1-1	-	Heavy	-
		B1-2	-	Heavy	NSM
	2	B-2-1	-	Intermediate	-
		B-2-2	-	Intermediate	NSM
	3	B-3-1	-	Low	-
		B-3-2	-	Low	NSM

4.5 Experimental stage 1 (Strengthening)

To evaluate the EBR and NSM techniques, the behaviour of strengthened beams was investigated and a comparison between the results was made in terms of impact resistance, impact energy, reaction force, deflection, cracking and mode of failure. The experimental programme included testing six reinforced concrete beams. The beams were tested under impact loading and divided into three groups. The first pair of beams was considered to constitute the reference beams (BR-1, BR-2) without strengthening. The second pair of beams (B-EBR-1, B-EBR-2) was externally strengthened with CFRP strips using external bonded technique EBR. Third pair of beams (B-NSM-1, B-NSM-2) used the near surface mounted technique NSM. Figure 4.2 provides an overview of tested conditions for each specimen.
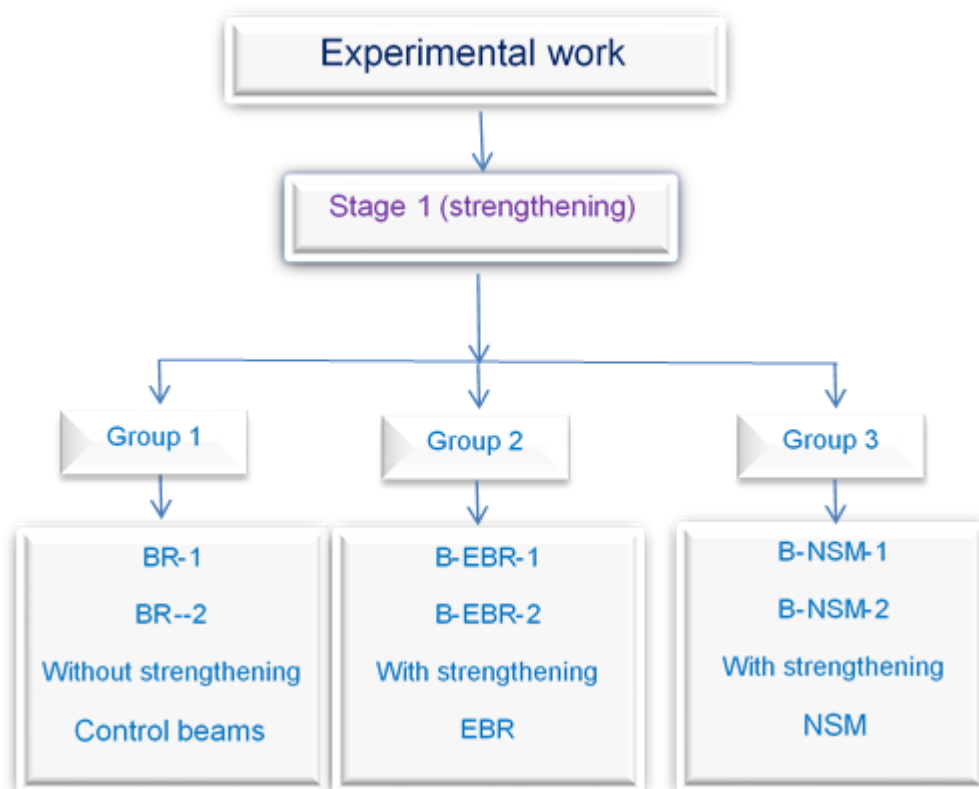
Figure 4.2 Tested specimens (strengthening stage)

4.5.1 Eternal bonding renforcement technique (EBR)

For beams strengthened using EBR technique, the following steps were followed to bond the CFRP strip at the bottom face of the concrete:

- Increasing the roughness of the concrete surface using steel brush.
- Cleaning the concrete surface using compressed air.
- Mixing the two components of the epoxy using a hand mixer.
- Applying the epoxy paste on the CFRP strip surface.
- Applying the epoxy paste on the concrete surface with thickness of 2 mm.
- Bonding the CFRP strip on the concrete surface.
- Applying pressure to the CFRP strip using steel plate.
- After two days, removing the weights and allowing the adhesive to reach its design strength.

Figure 4.3 shows the beam after installation of the CFRP strip using EBR technique.

Figure 4.3 Beam strengthened using EBR technique

4.5.2 Near surface mounted technique NSM

For the NSM technique, a small groove, formed using dense foam attached at the bottom of concrete mould, was made in the base of the beam to allow insertion of the CFRP within the concrete cover. The groove size was 3 mm width and 25 mm depth. The following steps were conducted to install the CFRP strip using NSM technique:

- Removing the dense foam from the groove.
- Cleaning the groove using compressed air.
- Mixing the two components of the epoxy resin system using a mobile mixer.
- Applying the epoxy paste inside groove.
- Inserting the CFRP strip inside the groove.
- Levelling the strip top surface.

After installing the CFRP strip, the beams were tested after at least 2 days for epoxy setting.

Figure 4.4 shows the beam after installation of the CFRP strip.

Embedded CFRP strip
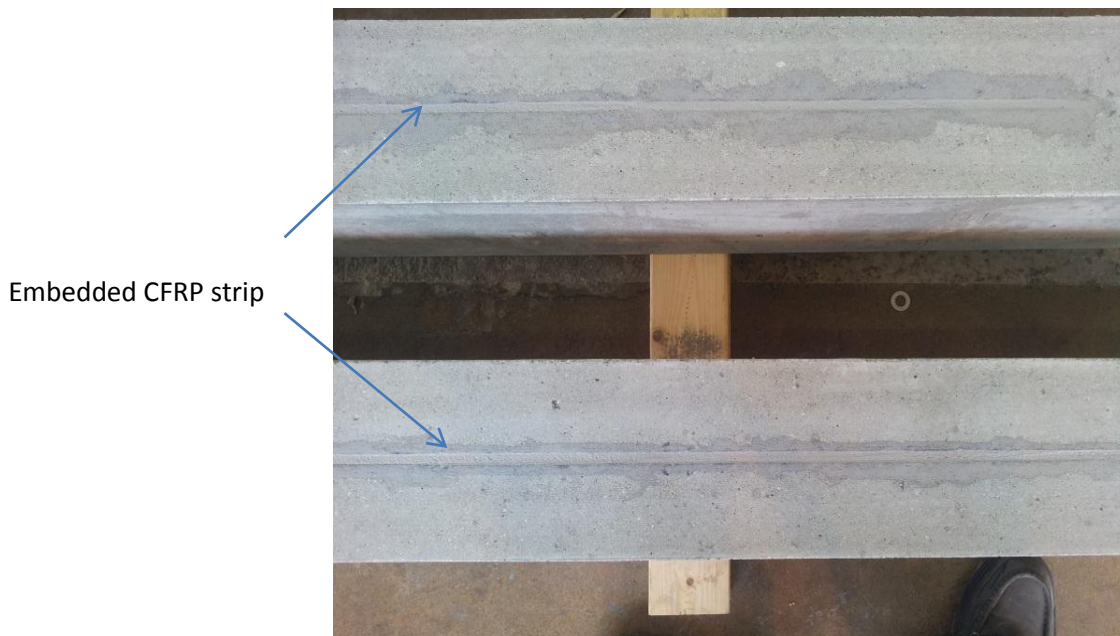
Figure 4.4 Beam strengthened using NSM technique

4.5.3 Test procedure

The testing was started by applying low impact energy. Then the impact energy was gradually increased. At Group 1 (control beams), the impact energy was increased by increasing the drop height. Table 2 shows the impact testing scheme applied to the Group 1 beams. The beams failed by concrete crushing at drop height 0.46 m and at a mass of 198 kg. Group 2 beams strengthened by EBR CFRP failed by debonding of the CFRP strip. Table 4 shows the impact testing scheme applied on the EBR strengthened beams. At Group 3, NSM technique was used to strengthen the beam using CFRP strip. To increase the impact energy, the drop height was first increased up to 0.46 m as in Groups 1 and 2. The NSM-strengthened beams resisted high impact energy and did not fail at the same drop height (0.46 m) as for the control and the EBR strengthened beams. At this height (0.46m), the accelerometers were close to their maximum capacity (1000g). To increase the impact energy and to ensure the acceleration did not exceed the maximum capacity of accelerometers, the drop weight was increased gradually up to 300 kg and mass was dropped from same reduced drop height of 0.35 m. Table 4 shows the impact testing scheme applied on the Group 3 beams. Each Group of beams had two identical beams. The average results from each pair of beams were calculated. The result comparisons were made between the three groups based on the average testing results at each group. The results of the tested beams were compared for each single impact test and for the sum of all impact loads applied on the beams.

Table 4.3 experimental work scheme (control beams)

Impact No.	Velocity m/s	Height m	Mass kg	Energy (J)
1	1	0.05	198	99
2	1	0.05	198	99
3	2	0.20	198	396
4	2.3	0.32	198	633
5	3	0.46	198	891

Table 4.4 Experimental work scheme (NSM strengthened beams)

Impact No.	Velocity m/s	Height m	Mass kg	Energy (J)
1	1	0.05	198	99
2	1	0.05	198	99
3	2	0.20	198	396
4	2.3	0.32	198	633
5	3	0.46	198	891
6	3	0.46	220	990

Table 4.5 Experimental work scheme (EBR strengthened beams)

Impact No.	Velocity m/s	Height m	Mass kg	Energy (J)
1	1	0.05	198	99
2	1	0.05	198	99
3	2	0.20	198	396
4	2.3	0.32	198	633
5	3	0.46	198	891
6	3	0.46	220	990
7	3	0.35	260	892
8	3	0.35	280	961
9	3	0.35	300	1030

After completing the tests, the results from the strengthening stage were analysed and discussed. Chapter 5 shows the discussion at this stage of the experimental results.

4.6 Experimental Stage 1 (Repair)

This stage of the experimental work was conducted to investigate the effect of using CFRP on the impact resistance of damaged RC beam in terms of stiffness, impact force, reaction force, deflection and cracking. This stage of the experimental programme included testing undamaged, damaged and CFRP repaired beams. Three groups of two RC beams were tested experimentally, using impact and static test. The beams were subjected to different degree of damage, using heavy, intermediate and low impact energies on beams of Groups 1, 2 and 3 respectively.

The first beams of each group were subjected to impact load to obtain the impact force required to induce the targeted degree of damage. Then the same impact force was used to damage the second beams of each group. NSM CFRP was then used to repair these damaged beams. The damaged and repaired beams were retested under static and impact loading to investigate the restored impact resistance and the behaviour of the beams under impact load.

The impact response of repaired RC beams was compared with that of undamaged and damaged beams in terms of stiffness, impact resistance, bending force, crack distribution and failure modes.

4.6.1 Test procedure

Each group consisted of two similar beams but with different conditions (i) the damaged beam and (ii) the repaired beam. Figure 4.10 shows the testing procedure flow chart of experimental work. Table 4.5 shows the testing procedure applied to each group.

The following steps were carried out in testing a damaged beam In each group:

1. The beam faces were painted white, so that the location and length of cracks could be more accurately assessed. The beam was inspected visually to check its overall condition in terms of cracks, alignment and dimensions. Static tests were carried out to these damaged beams for a small deformation to evaluate the beam stiffness (see Section 4.6.2).
2. The beam was then further damaged using a single impact to induce the specified degree of damage (see Table 4.5).

3. A careful visual inspection and static test was conducted on these beams. Damages like cracks, deformation, spalling and crushing of concrete were recorded by marker pen and photographs. A direct measurement microscope (Elcometer 900 with x50 magnification, www.elcometer.com) was used to measure the width of the cracks.

4. A partial static test was conducted on the damaged beam as in Step 2.

5. Finally; the damaged beam was retested using multi-impact loading up to failure (see Table 4.5).

6. Static tests were carried out after each impact for a small deformation to evaluate the beam stiffness.

The impact resistances of the damaged beams obtained from step 5 were compared with those of the reference beams (BR-1, BR2) tested in the strengthening stage. Comparison was made between the stiffness of the beams before and after damage to find the reduction in beam stiffness due to damage.

After testing the initial damaged beam from each group, the second beam from that group (the repaired beam) was damaged using impact loading and then repaired using NSM technique. The following steps were conducted on the repaired beam from each group:

1. The general condition of the cast beam was carefully inspected visually as conducted on the first (damaged) beam.

2. The beam was damaged using single impact. To induce the same damage, the same amount of impact energy applied on the damaged beam was used to damage the beam to be repaired (see Table 4.5).

3. The beam was subjected to visual inspection and static test.

4. CFRP strip was used to repair the damaged beam using NSM technique.

5. Visual inspection and static test was applied to the repaired beam.

6. Finally, the repaired beam was tested using multi-impact loading up to failure to evaluate its ultimate impact strength (see Table 4.5).

To find the enhancement of impact resistance for the CFRP repaired damaged beam, comparison was made between the impact resistance of the repaired damaged beam obtained from step 6 and those of the reference beams (BR-1, BR-2).

Stiffness of the beam before and after repair was compared to determine the degree of increase in the beam stiffness after the damaged beams was repaired using CFRP.

Chapter 6 shows the results and comparison of the repairing stage of the experimental work.
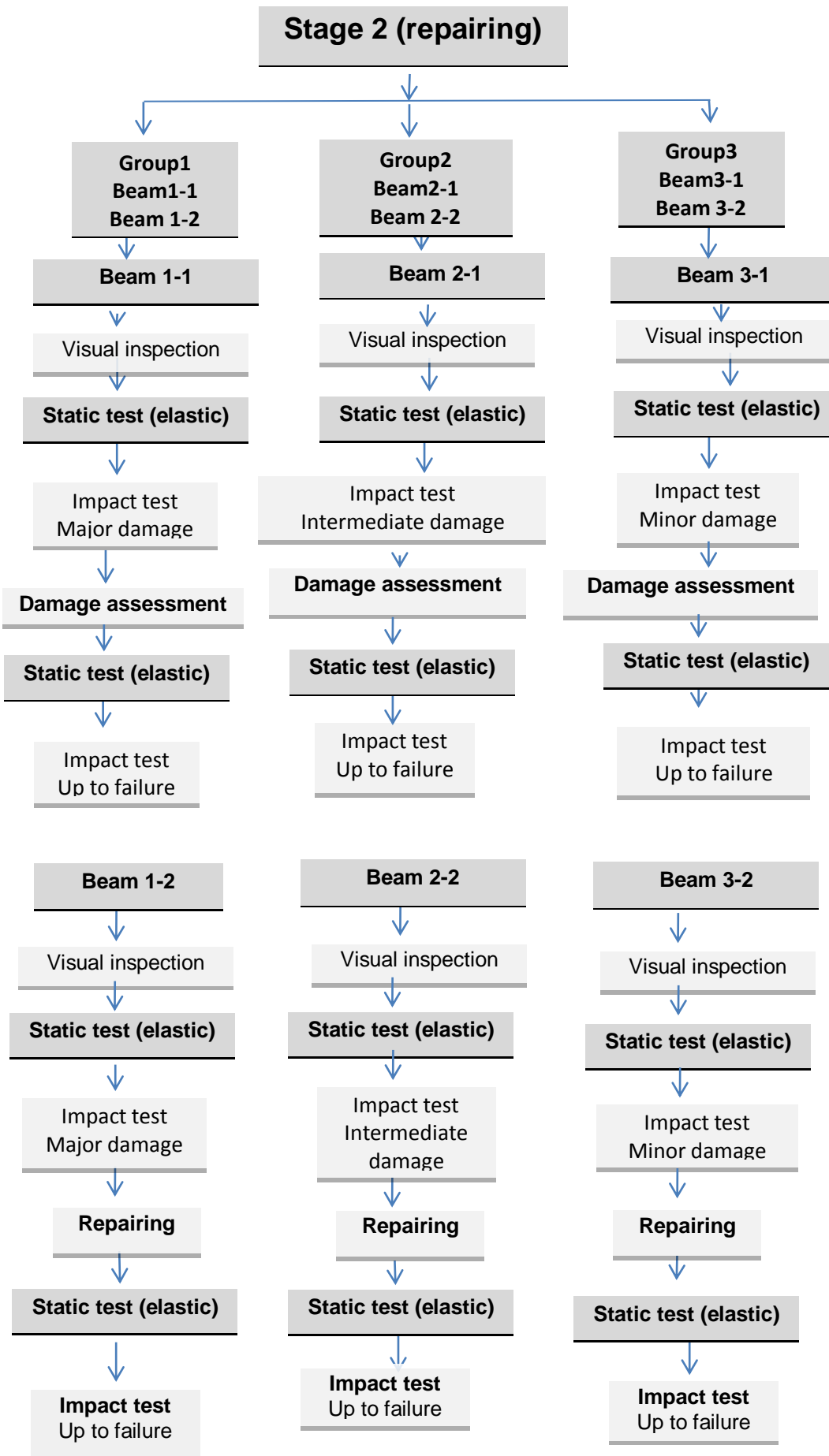
Figure 4.5 Experimental work (repairing)

Table 4.5 Impact test scheme applied on each group

Group 1	impact no.	Energy(J)	Tested beam
Single Impact(damage)	**1**	891	B1-1
			B1-2
Multi-impact	**1**	99	B1-1
			B1-2
	2	99	B1-1
			B1-2
	3	396	B1-1
			B1-2
	4	622	B1-2

Group 2	impact no.	Energy(J)	Tested beam
Single Impact(damage)	**1**	622	B2-1
			B2-2
Multi-impact	**1**	99	B2-1
			B2-2
	2	99	B2-1
			B2-2
	3	396	B2-1
			B2-2
	4	622	B2-1
			B2-2
	5	891	B2-2

Group 3	impact no.	Energy(J)	Tested beam
Single Impact(damage)	**1**	396	B3-1
			B3-2
Multi-impact	**1**	99	B3-1
			B3-2
	2	99	B3-1
			B3-2
	3	396	B3-1
			B3-2
	4	622	B3-1
			B3-2
	5	891	B3-2
	6	990	B3-2
	7	892	B3-2
	8	961	B3-2
	9	1030	B3-2

4.6.2 Static test

To find the reduction in beam stiffness, a partial static test was conducted on the beam after each single impact load test. The partial static test was conducted using a hydraulic jack and pump placed above the beam and located in the impact test rig. The static test was controlled either by load increment or by displacement increment. To measure the displacement during the static test, two dial gauges were used. To avoid any additional residual deflection, the loading was applied gradually in displacement increment of 0.2 mm. The loading was increased up to 5 mm at mid-span deflection (or less, depending on the degree of damage). The static test was stopped if any residual deflection was observed. Figure 4.8 shows the static test procedure.

Figure 4.7 Static test using hydraulic jack and pump

5. Experimental Results –Strengthening

5.1 Introduction

The behaviour of three groups of two CFRP strengthened RC beams was investigated experimentally under impact load. Comparisons between the results from the three groups was made to determine the enhancement of the beam behaviour and to compare the EBR and NSM techniques using the reaction force, impact force and impact energy, beam deflection, crack distribution and mode of failure. The conclusions from this stage of the experimental work informed the final stage of the experimental work (repair stage).

5.2.1 Types of forces affecting the RC beam under impact loading

When the impactor hits the beam, the recorded response is not the true bending load, because part of impact force is used to accelerate the beam from rest. This beam reaction is called the inertia force (P_i). The inertia force acts in a direction opposite to that of the impact force. The beam is considered to be in a state of equilibrium when the inertia force is included each time. The free-body diagram for the beam under impact loading is shown in Figure 5.1. Three forces affect the beam under impact loading: impact force, bending force and inertia force

$$P_t(t)$$

R (t)   R (t)

$$P_i(t)$$
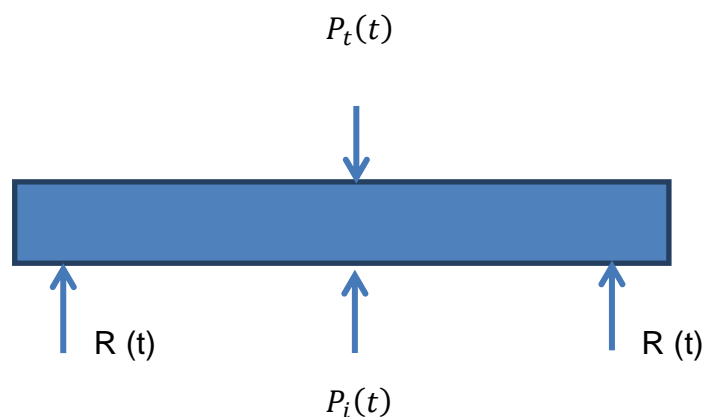
Figure 5.1 Free-body diagram of the beam under impact loading

5.2.1 Impact force (P_t)

The new instrumented heavy impact test machine, described in Chapter 2, was used to conduct this experimental work. A mass was dropped freely to induce impact. Steel tubes were used to guide the weight to the point of impact. Before testing, the guide bars were cleaned and oiled to minimise the friction between the bars and the dropped mass. Neglecting the energy losses due to friction, the mass velocity during dropping was calculated as follows:

Potential energy= mgh   (5.1)

Kinetic energy = ½ mV^2 (5.2)

Potential energy= Kinetic energy

mgh=½ mV^2 (5.3)

$$V_h = \sqrt{2gh}$$ (5.4)

$$V_h = 4.43\sqrt{h}$$ (5.5)

Where:

m= mass (kg)

V_h= mass velocity (m/s)

g = acceleration due to gravity (m/s^2)

h = dropping height (m)

By applying Newton's Second Law, the impact force can be found:-:

P_t=m.a   (5.6)

Where:

P_t= the applied impact force (N)

m= mass (kg)

a= mass acceleration (m/s^2)

The acceleration at different locations along the beam length was recorded using three accelerometers. The velocity at any time can be found by integrating the acceleration ($\ddot{u}_{(t)}$) :

$$u_{(t)} = \int \ddot{u}_{(t)} \, dt \qquad\qquad (5.7)$$

Displacement at any time can be found by integrating the velocity ($\dot{u}_{(t)}$):

$$u_{(t)} = \int \dot{u}_{(t)} \, dt \qquad\qquad (5.8)$$

Where:

$\ddot{u}_{(t)}$: Acceleration at time (t)

$\dot{u}_{(t)}$: Velocity at time (t)

$u_{(t)}$: Displacement at time (t)

5.2.2 Inertia force (P_i)and bending load (P_b)

The inertia force is a distributed load (body force) and acts along the length of the beam, while the impactor load is a concentrated load acting at the mid span of the beam.

Two methods were used to find the inertia force at any time (t):

Method 1: In the first method, the beam acceleration due to impact is used to find the inertia force. According to Bantia (1987), to find the inertia force developed in the beam under impact, two assumptions can be used for acceleration distribution along the beam length: linear and sinusoidal distribution.

1) **Linear distribution**

The distribution of inertia forces at any time t can be assumed to be linear, as shown in Figure (5.2). The overhanging part of the beam after the support is small compared to the beam length and it was neglected in the interests of simplification. The acceleration in the linear assumption in any position can be expressed as function of the centre acceleration: -

$$u_{(x,t)}'' = \frac{2u_o''(t)}{l}x \tag{5.9}$$

$$\delta u_{(x,t)} = \frac{2\delta u_{o(t)}}{l}x \tag{5.10}$$

If central load $P_i(t)$ is equivalent to the distributed inertia force, then the virtual work done will be equal for the distributed inertia force and its load equivalent central load. The inertia force at any time (t), $P_i(t)$ can be found by multiplying the beam mass by the beam acceleration.

virtual work done= $P_i(t)\delta u_{o(t)}$

inertia equivalent central load= m.a= $2\,\rho A \int u_{(x.t)}''\, \delta u_{(x,t)} d_x$

$$P_i(t)\delta u_{o(t)} = 2\,\rho A \int u_{(x.t)}''\, \delta u_x d_x \tag{5.11}$$

Where:

$M = beam\; mass = \rho A l$

a= beam acceleration

$u_{(t)}''$= beam acceleration at any time (t)

ρ= mass density of the beam material kg/m^3

A= cross-sectional area of the beam

By substitution Eq.5.9 and Eq. 5.10 in Eq. 5.11, we have

$$P_i(t)\delta u_{o(t)} = 2\,\rho A \int (\frac{2u_{o(t)}''}{l}x)(\frac{2\delta u_{o(t)}}{l}x\,)d_x$$

$$P_i(t)\delta u_{o(t)} = \frac{8\rho A u_{o(t)}''\delta u_{o(t)}}{l^2} \int_0^{l/2} x^2 d_x$$

By deleting $\delta u_{o(t)}$ form both side of equation, Eq. 5.12 can be written as:

$$P_i(t) = \frac{8\rho A u_{o(t)}''}{l^2} \int_0^{l/2} x^2 d_x \tag{5.12}$$

$$\boldsymbol{P_i(t)} = \frac{\rho A u_{o(t)}'' l}{3} \tag{5.13}$$
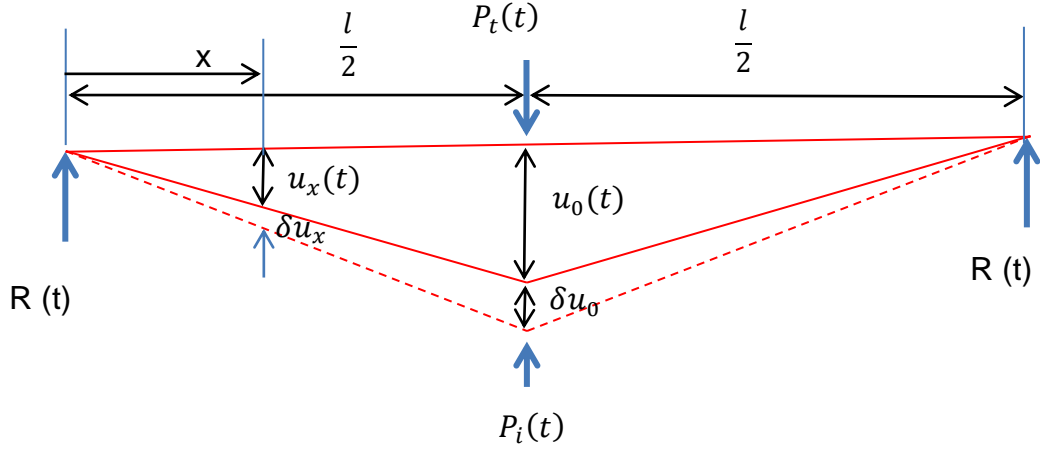
Figure 5.2 Beam acceleration distribution (linear assumption)

2) Sinusoidal distribution

In this assumption, the beam acceleration is assumed to be sinusoidal as illustrated in Figure (5.3).

$$\ddot{u}_{(x,t)} = \ddot{u}_{o(t)} \sin \pi \frac{x}{l} \tag{5.14}$$

$$\delta u_{(x,t)} = \delta u_{0(t)} \sin \pi \frac{x}{l} \tag{5.15}$$

By substitution Eq.5.14 and Eq. 5.15 in Eq. 5. 11, we have

$$P_i(t)\delta u_{o(t)} = 2 \rho A \int (\ddot{u}_{o(t)} \sin \pi \frac{x}{l})(\delta u_{0(t)} \sin \pi \frac{x}{l}) dx$$

$$P_i(t)\delta u_{o(t)} = 2 \rho A \delta u_{0(t)} \ddot{u}_{o(t)} \int_0^{l/2} \sin^2 \pi \frac{x}{l} dx$$

By deleting $\delta u_{o(t)}$ form both side of equation, the Eq. 5.16 can be written as:

$$P_i(t) = 2\rho A \ddot{u}_{o(t)} \int_0^{l/2} \sin^2 \pi \frac{x}{l} dx \tag{5.16}$$

$$\boldsymbol{P_i(t)} = \frac{\rho A \ddot{u}_{o(t)} l}{2} \tag{5.17}$$

The solution to Eq. 5.16 Integration is shown in Appendix D
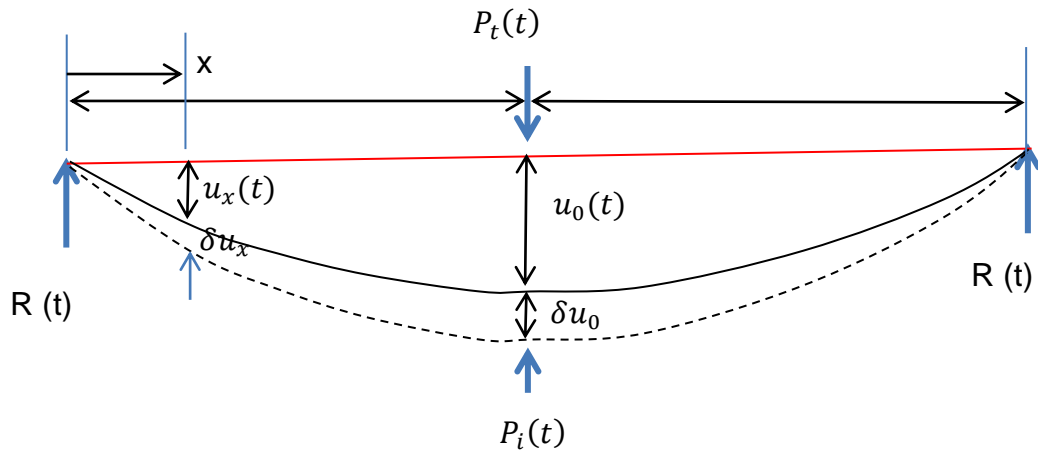
Figure 5.3 Beam acceleration distribution (Sinusoidal assumption)

Method 2: In the second method, the inertia force can be found by applying the equation of equilibrium. By subtracting the bending force from the impactor load, the inertia force can be found at any time:

$$\boldsymbol{P_i(t) = P_t(t) - P_b(t)} \tag{5.18}$$

Where:

$P_b(t)$= The actual bending load at time (t)

$P_t(t)$= impactor load at time (t)

$P_i(t)$=Inertia force at time (t)

The true bending load $P_b(t)$ was found experimentally, using load cell to record the reaction force at each time R (t). By assuming the symmetry of the beam, the bending load at any time will be equal to:

$$P_b(t)\text{=2R (t)} \tag{5.19}$$

In this project, both methods were used to determine the inertia force.

5.3 Results and discussion

Three groups of beams were tested under impact loading. Two RC beams were tested in each group. Group 1 beams represented the control beams without any strengthening. Group 2 beams were EBR strengthened beams. Group 3 beams were strengthened by CFRP strip using NSM Technique. See Section 3.5.3 for more details about the impact testing scheme of each group.

The tested beams from each group were cast and cured under the same laboratory conditions and had the same dimensional and material properties. The beams from each group were subjected to the same testing scheme. The results of the impact testing were similar for the two beams in each pair (Group) of beams. The impact results for each group of beams are presented in Appendix E.

Average results for both identical beams in each group were calculated and then used for comparisons between the three Group results. The impact force, impact energy, bending load, deflection and cracking are discussed further in the following sections.

5.3.1 Impact force P_t

The impact force applied on beams was calculated by multiplying the dropped mass by its acceleration at impact, Eq. 5.6. Three accelerometers mounted around the striker head at 120 degrees measured the mass acceleration. Figure 5.4 shows the comparison of the impact force between the reference and strengthened beams for each single impact test. Table 5.1 shows the impact force for both control and strengthened beams. It also shows the percentage of the impact force for the strengthened beams relative to the control beams.

Figure 5.4 shows that the impact force of the control beams increased rapidly at the early stage of testing. However, when the beam was close to failure there was a smaller increase in the impact force with increasing impact energy. This arises from damage occurring in the control beam due to the previous impacts, which causes damage and cracks in the beam.

The results comparison shows that the control beams impact force is greater than that of strengthened beams. The strengthened beams are much stiffer than the

control beams. It is clear that increasing beam stiffness resulted in reduction in impact force. The impact force of the strengthened beams is less than that of the control beam.
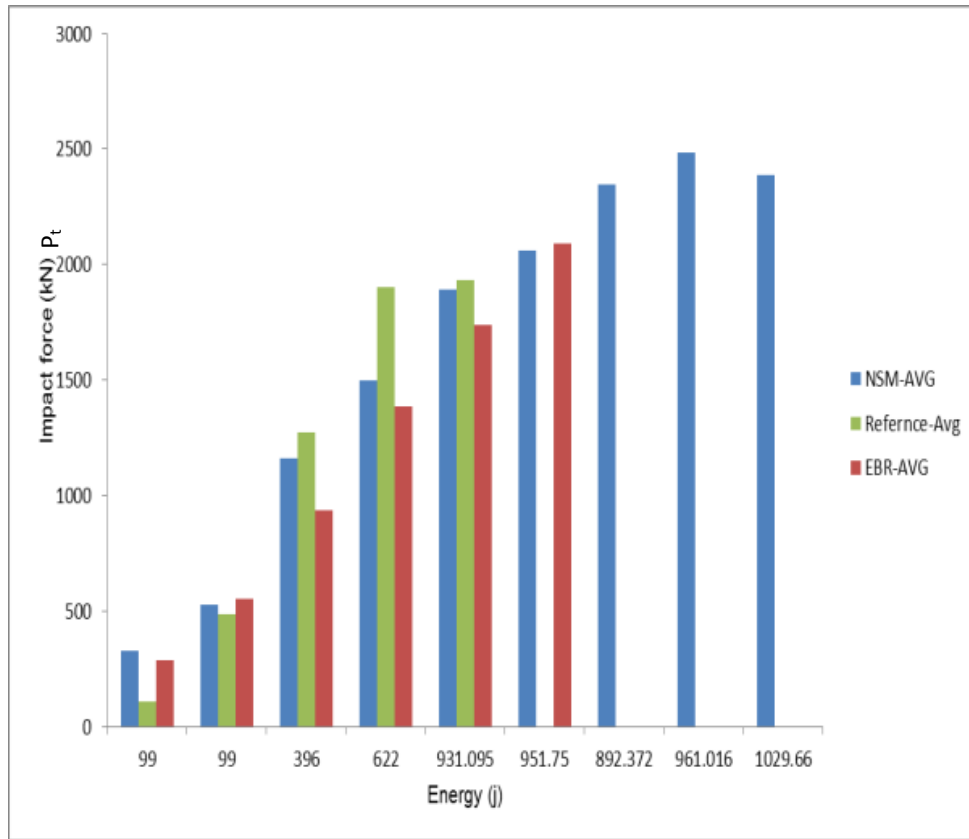
Figure 5.4 Beam impact force under different single impact energy

Table 5.1 impact force for the tested beam

impact No.	Energy (J)	beam type	impact force(kN)	% B-ST/B-R
1	99	*Reference-Avg	107	
		**EBR-Avg	284.58	266
		***NSM-Avg	327.2	306
2	99	Reference -Avg	485.4	
		EBR-Avg	550.39	113
		NSM-Avg	524.65	108
3	396	Reference -Avg	1275.65	
		EBR-Avg	933.61	73
		NSM-Avg	1163.35	91
4	622	Reference -Avg	1900.65	
		EBR-Avg	1387.13	73
		NSM-Avg	1500	79
5	891	Reference -Avg	1930.4	
		EBR-Avg	1737.84	90
		NSM-Avg	1894	98
6	990	EBR-Avg	2091.98	-
		NSM-Avg	2062.5	-
7	892.372	NSM-Avg	2347	-
8	961.016	NSM-Avg	2485.5	-
9	1029.66	NSM-Avg	2385.5	-

*reference beam (average results of beams BR-1 and BR-2)

**strengthened beam using EBR technique (average results of beams B-EBR-1 and B-EBR-2)

*** Strengthened beam using NSM technique (average results of beams B-NSM-1 and B-NSM-2)

In an impact test, the mass applies a force over a given period of time. The beam experiences an impact force for a specific duration that results in a change in momentum of the mass. Impulse is simply the product of the force being applied multiplied by the time over which that force is being applied. The result of the impact is that the momentum changes and the mass slows down and moves upwards.

When Newton's second law (Eq. 5.6) is combined with the definition of acceleration (Eq.5.20) it can be concluded that, during the impact, the impulse (F • t) experienced by the mass equals the change in momentum (m • Δv) of the mass.

a = change in velocity / time=Δv / t   (5.20)

P_t = m • Δv / t   (5.21)

Multiply both sides by the time t, and a new equation results.

P_t • t = m • Δv   (5.22)

Impulse = Change in momentum

Figure 5.4 and Table 5.1 shows that the impact force for reference and strengthened beams was different. In the strengthened beam, the mass slows down over a short period of time with less change in momentum, applying less impact force. For the EBR strengthened beam (B-EBR-1) under impact energy (931 J), the change in velocity after first impact was (0.891 m/s) and the impact time was (0.118 ms). In reference beam (BR-1), the mass applied large impact force over a long period of time with high change in momentum. Under impact energy (931 J), change in mass velocity after first impact was (1.213 m/s) and the time of the first impact was (0.1284 ms).

The impact force depends mainly on the stiffness of the beam. The NSM-strengthened beam has a high impact force compared with the EBR beams stiffness as the EBR is stiffer than NSM beam. CFRP strip in EBR beams is a greater distance from the natural axis compared with the NSM beam.

5.3.2 Bending load P_b

The force sensor mounted at the beam support was used to measure the reaction force. The true bending load should be equal to the summation of the support reaction forces. Figure 5.5 shows the bending load for different impact energies applied to the beams. It is clear from the figure that, at the beginning of the test with low impact energy (99 J), the increase in the bending force is low because most of the impact energy is absorbed by the inertia force of the beam. For each single impact, there was no large difference between the bending loads for the control and strengthened beams as they behave elasiticlly and they had less deformation and fewer cracks.

By increasing the impact energy (396 J), a high percentage of impact energy in the reference beam was absorbed and dissipated as fracture energy, and therefore the reference bending load was less than that of the strengthened beams. Under high impact energy (622 J, 981 J), less impact energy was released to crack and deform the reference beam because it was already had a large amount of cracking and a high residual deflection. High impact energy was therefore transferred to the support in the reference beam, resulting in a high degree of bending force.

For strengthened beams with increasing the impact energy, (396 J), the CFRP decreased the deformation and deflection of the beam. The strengthened beams had low crack width and length. Thus, less impact energy dissipated as fracture energy and high percentage transfer to the support, which caused high bending force compared with control beam. When the impact energy was increased, the difference between the bending force of the reference and strengthened beams became less, because the cracks width and length of the strengthened beams began to increase.

 Figure 5.5 clearly shows that EBR- strengthened beams had a high bending load compared with the NSM- strengthened beams. The reason for this is that the EBR - strengthened beams are stiffer than NSM beams, as the CFRP strip in EBR technique had high distance from the neutral axis than in the NSM technique. The EBR beams showed less cracks and deformation compared with NSM beams. In EBR beams, low impact energy was absorbed and dissipated as fracture energy and a high percentage of impact energy was transferred to the support, compared with

NSM beams. Table 5.2 shows the reaction and bending load for each single impact load and also the cumulative reaction and bending load.
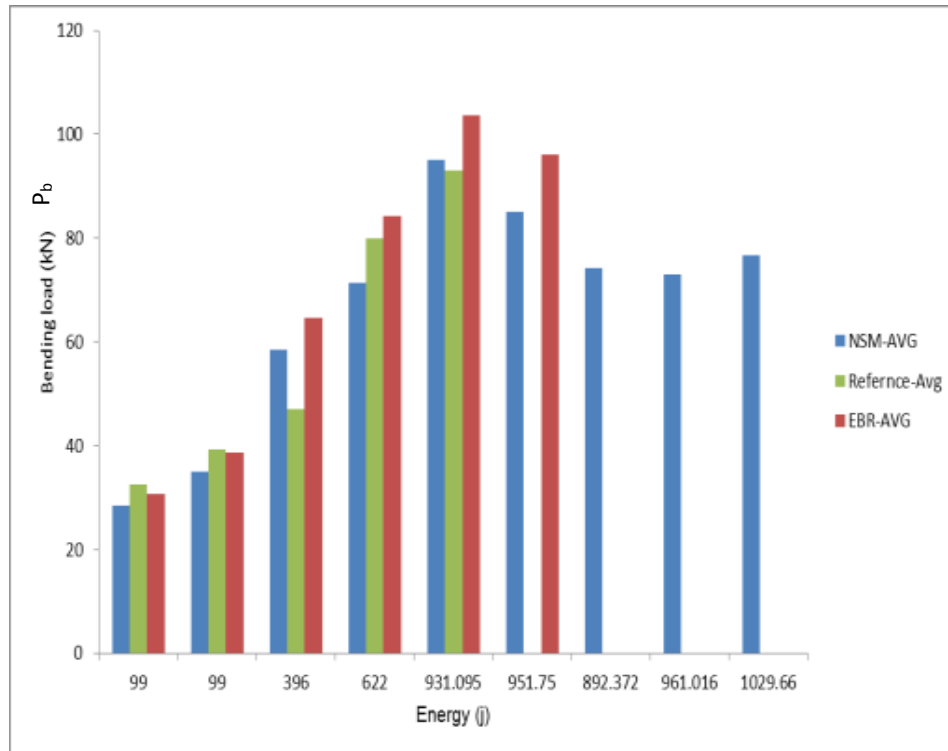
Figure 5.5 Beam bending force under different single impacts

Table 5.2 Reaction and bending load for each single impact load

impact No.	Energy (J)	beam type	reaction force(kN)	bendng load(kN)	% (EBR or NSM) /B-R
1	99	*Reference-Avg	16.3	32.6	
		**EBR-Avg	15.36	30.72	94
		***NSM-Avg	14.25	28.5	88
2	99	Reference-Avg	19.6	39.2	
		EBR-Avg	19.31	38.62	99
		NSM-Avg	17.5	35	89
3	396	Reference-Avg	23.5	47	
		EBR-Avg	32.35	64.7	138
		NSM-Avg	29.25	58.5	124
4	622	Reference-Avg	40	80	
		EBR-Avg	42.17	84.34	105
		NSM-Avg	35.7	71.4	89
5	891	Reference-Avg	46.5	93	
		EBR-Avg	51.84	103.69	111
		NSM-Avg	47.5	95	102
6	990	EBR-Avg	48.02	96.05	
		NSM-Avg	42.5	85	88
7	892.372	NSM-Avg	37.15	74.3	
8	961.016	NSM-Avg	36.5	73	
9	1029.66	NSM-Avg	38.35	76.7	

*reference beam (average results of beams BR-1 and BR-2)

**strengthened beam using EBR technique (average results of beams B-EBR-1 and B-EBR-2)

*** Strengthened beam using NSM technique (average results of beams B-NSM-1 and B-NSM-2)

5.3.3 Inertia force P_i

During the impact test, when the impactor hits the beam, the recorded impact force is not the true bending load because part of impact force is used to accelerate the beam downwards from the rest. This beam reaction is called the inertia force

To find the inertia force, two methods were used. The first method was to calculate the inertia force using beam acceleration developed at the beam due to impact. Two assumptions were used in the second method. In the first assumption, linear distribution was used and inertia force was calculated using Eq. 5.13. In the second assumption, sinusoidal distribution was used and Eq. 5.17 was used to find the inertia force.

The second method was to record the experimental reaction force using load cell and then subtracting the bending load (Eq. 5.19) from the impact force to find the inertia force, using Eq. 5.18.

The standard error of estimate (SEE) was used to evaluate the two assumptions of linear and sinusoidal distribution. The standard error measured the error in the prediction of inertia force. Table 5.3-5.5 shows a comparison between the two methods for the control, EBR -strengthened and NSM- strengthened beams respectively.

Table 5.3 shows a good correlation between the linear and sinusoidal distribution assumptions for control beams with the inertia force measured experimentally (using method 1). The standard error of the sinusoidal distribution assumption is less than that of the linear distribution assumption, because the control beam was highly cracked and deformed due to impact, which reduced the beam stiffness and made the beam deflection and acceleration come closer to being sinusoidal.

It can be seen from Tables 5.4 and 5.5, which display comparisons of control and strengthened beams, that the SEE for the linear distribution is lower than with the sinusoidal distribution. In strengthened beams, the CFRP increased the stiffness of the beams and reduced both the beam deformation and cracks. That made the deflection and acceleration of the beam approximately linear along the beam length. Thus, the linear inertia force distribution assumption gave better agreement when compared to the sinusoidal assumption as shown in Tables 5.4 and 5.5.

Table 5.3   Inertia force for the control beam

Energy J	Impact force P_t kN	Bending force P_b Eq.5.19 kN	Inertia force P_i Eq.5.18= $C2 - C3$ kN	Inertia force P_i Eq.5.13 kN linear distribution	Inertia force P_i Eq.5.17 kN sinusoidal distribution	$\dfrac{C5 - C4}{C4}$ $*100$	$\dfrac{C6 - C4}{C4}$ $*100$
99	464	37	427	366	465	14	9
99	495	40	455	353	449	22	1
396	998	52	946	834	1061	12	12
396	1515	42	1473	1030	1310	30	11
622	1843	70	1773	1610	2047	9	16
622	1900	90	1810	1427	1814	21	0
891	1897	108	1789	1704	2166	5	21
The standard error (SEE)				285	227		

Table 5.4 Inertia force for the EBR strengthened beam

Energy J	Impact force P_t kN	Bending force P_b Eq.5.19 kN	Inertia force P_i Eq.4.18= $C2 - C3$ kN	Inertia force P_i Eq.5.13 kN linear	Inertia force P_i Eq.5.17 kN sinusoidal	$\dfrac{C5 - C4}{C4}$ $*100$	$\dfrac{C6 - C4}{C4}$ $*100$
99	250	30	220	176	225	20	2
99	318	31	287	222	283	23	1
99	564	41	523	429	546	18	4
99	536	36	500	417	532	17	6
396	933	61	872	764	973	12	12
396	933	67	866	705	898	19	4
622	1451	85	1366	1238	1576	9	15
622	1322	83	1239	1082	1377	13	11
891	1799	92	1707	1918	2440	12	43
891	1676	115	1561	1619	2059	4	32
990	2084	87	1997	2079	2644	4	32
990	2099	104	1995	1909	2428	4	22
The standard error (SEE)				127	386		

Table 5.5 Inertia force for the NSM strengthened beam

Energy J	Impact force P_t kN	Bending force P_b Eq.5.19 kN	Inertia force P_i Eq.5.18= $C2 - C3$ kN	Inertia force P_i Eq.5.13 kN linear distribution	Inertia force P_i Eq.5.17 kN sinusoidal distribution	$\dfrac{C5 - C4}{C4}$ $* 100$	$\dfrac{C6 - C4}{C4}$ $* 100$
99	346	17	329	259	331	21	1
99	307	11	296	195	250	34	16
99	568	20	548	421	537	23	2
99	481	14	467	426	542	9	16
396	1200	30	1170	996	1268	15	8
396	1126	28	1098	873	1111	20	1
622	1500	34	1466	1733	2205	18	50
622	1500	37	1463	1341	1707	8	17
990	1975	42	1933	1831	2330	5	21
891	2275	37	2238	1997	2541	11	14
1030	2335	41	2294	2513	3196	10	39
The standard error (SEE)				177	410		

5.3.4 Deflection

The deflection at different positions on the beams was measured using three methods, accelerometers, dial gauges and a high speed camera. Figure 5.6 compares the mid-span maximum deflection of one sample, using all three methods as an example. It is clear from the figure that the deflections recorded by all three methods are comparable.

Figures 5.7 and 5.8 show the mid-span maximum and residual deflections for each single impact test. Many factors such as stiffness, the properties of the material, the impact energy and the crack distribution and widths affect the deflection. The deflection of the beams mainly depends on their stiffness. After increasing the height of the drop-weight, the beam stiffness is decreased due to increased deformation and the formation of cracks by the previous impact. This in turn resulted in an increase in maximum and residual deflection values. The impact loading

causes damage and cracks to the beam. In reference beams, even with small impact, the beams show a small residual deflection due to the yielding of steel bars.

From Figures 5.7 and 5.8, it is clear that residual deflection and the maximum deflection for strengthened beam are much reduced compared with the unstrengthened beams. This is due to the high stiffness of the strengthened beam. With an increase in the impact energy, most of tensile stresses are resisted by the CFRP strip and the beam becomes very stiff, due to high stiffness of the CFRP until the CFRP was debonded. There was a large difference between the residual deflection of the control beam and that of the strengthened beam, as shown in Table 5.6. However, there was small difference in terms of the maximum deflection. It can be noted from Figure 5.7 that the EBR beam under impact loading (931 J) shows high residual deflection and that is due the debonding of the CFRP.
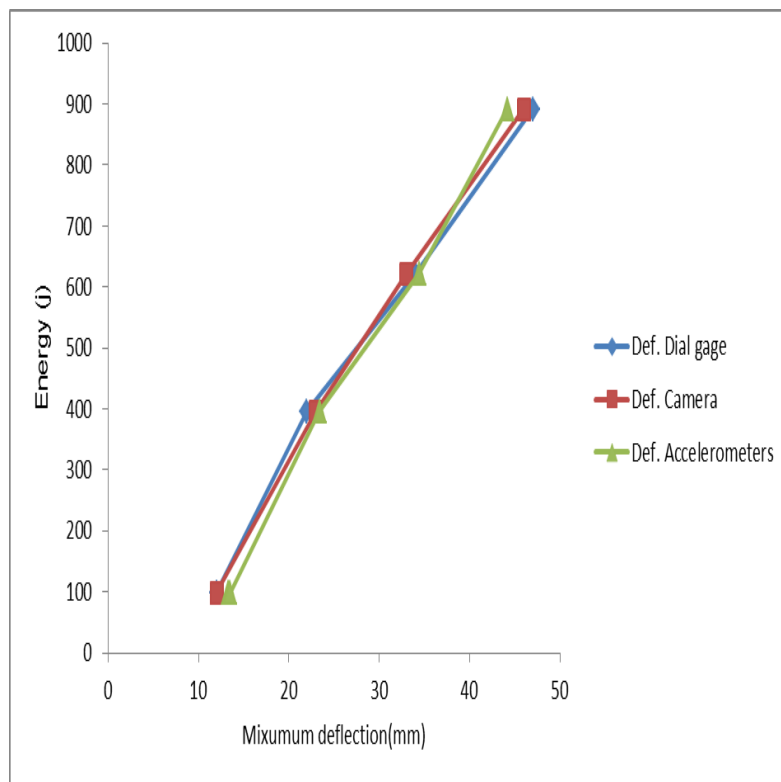
Figure 5.6 Maximum deflection recorded by different methods
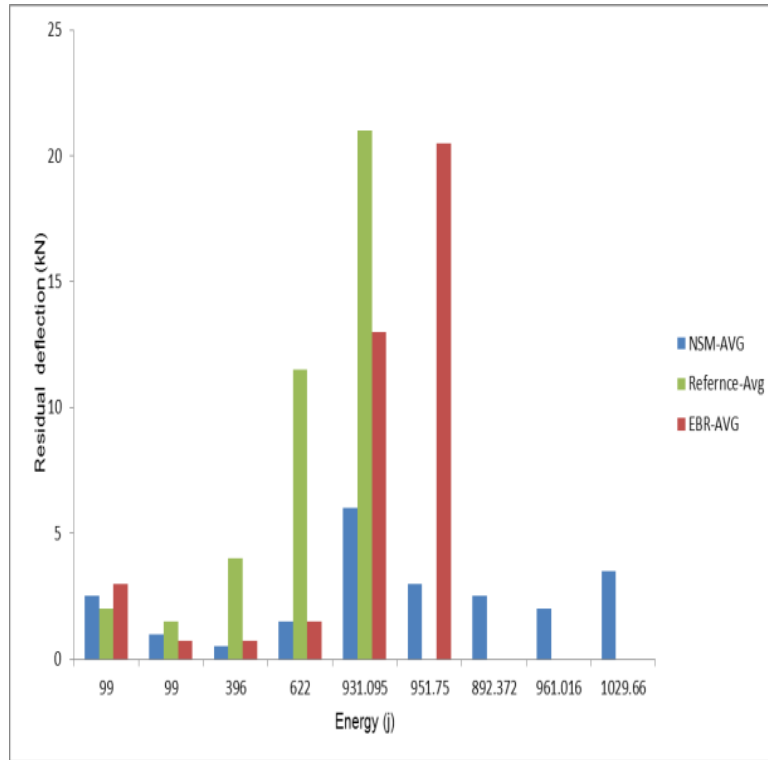
Figure 5.7 Residual deflections under each single impact
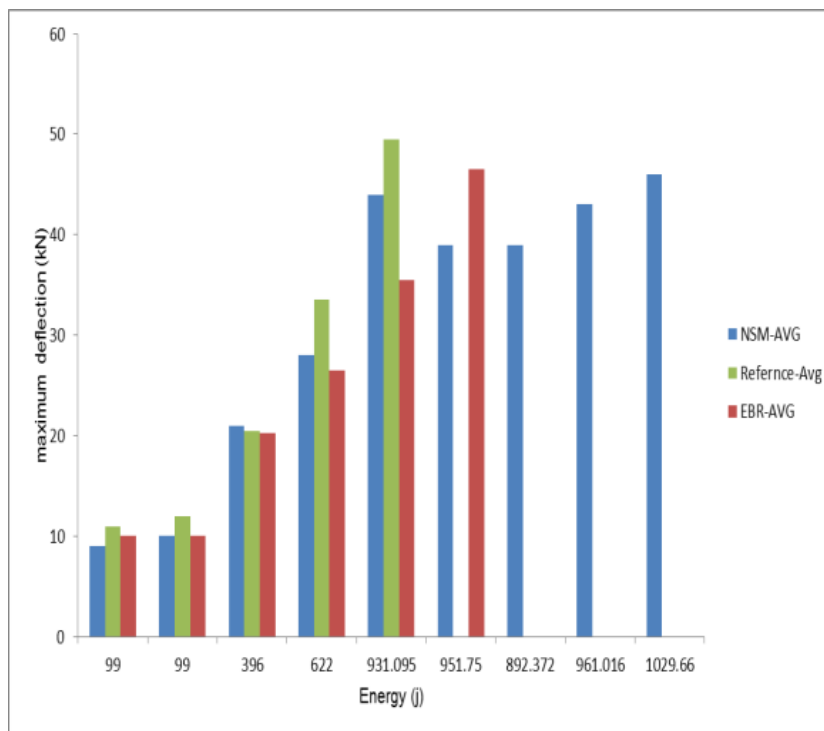
Figure 5.8 Maximum deflections under each single impact

Table 5.6 Tested beams deflection under different impact energies

impact No.	Energy J	beam type	deflection maximum(mm)	deflection residual(m	Notes
1	99	*Refernace-Avg	11	2	
		**EBR-Avg	10	3	
		***NSM-Avg	9	2.5	
2	99	Refernace-Avg	12	1.5	
		EBR-Avg	10	0.75	
		NSM-Avg	10	1	
3	396	Refernace-Avg	20.5	4	
		EBR-Avg	20.25	0.75	
		NSM-Avg	21	0.5	
4	622	Refernace-Avg	33.5	11.5	
		EBR-Avg	26.5	1.5	
		NSM-Avg	28	1.5	
5	891	Refernace-Avg	49.5	21	Beam failed
		EBR-Avg	35.5	13	CFRP debonding
		NSM-Avg	44	6	
6	990	EBR-Avg	46.5	20.5	Beam failed
		NSM-Avg	39	2	
7	892.372	NSM-Avg	39	2.5	
8	961.016	NSM-Avg	43	2	
9	1029.66	NSM-Avg	46	3.5	

*reference beam (average results of beams BR-1 and BR-2)

**strengthened beam using EBR technique (average results of beams B-EBR-1 and B-EBR-2)

*** Strengthened beam using NSM technique (average results of beams B-NSM-1 and B-NSM-2)

5.3.5 Cracking and failure

The impact test was started by applying low impact energy. At first impact, amass of 198 kg was dropped from a height of 0.05 m. As a result, fine cracks initiated at the bottom face of the control beam with a small residual deflection. All tested beams showed a central crack. When the tensile stress exceeds the tensile strength of the concrete, the bottom face of the beam started to crack and the bottom steel reinforcement started to carry the tensile stress at control beam. In the strengthened beams, the CFRP strip with steel reinforcement contributed significantly to the resistance of the tensile stresses.

For the control beam, after increasing the imparted impact energy by increasing the drop height, the cracks extended vertically toward the top face of the concrete beam. With increasing impact energy, the crack lengths and widths increased and the beam showed a large residual deflection. The major crack was at the mid-span of the beam and the crack widths decreased with increasing distance of the crack from the beam mid-span. At impact 4, the beam suffered from high residual deflection, with major central cracks of 1.2 mm width. At impact 5 with mass of 198kg dropped from height of 0.48m, the cracked beam could not resist the impact loading, so it failed by concrete crushing in mid-span compression zone, as shown in Figure 5. 9.

The effect of the impact in terms of the width and length of the cracks decreased with increase in the distance from the impact point. No shear cracks were observed during the test.

For the strengthened beams, the CFRP strip decreased the number and width of the cracks. Comparing with the control beam and for the same impact loading, the crack width and length for the strengthened beam was much less than that of the control beam. The CFRP strip increased the beam stiffness and improved its confinement. For the beam strengthened with EBR technique, the crack distribution was uniform along the beam length. The major cracks developed at the mid-span of beam and the crack extended at the bottom of beam toward the top face. For the EBR strengthened beam, with increasing impact energy, the cracks were extended longitudinally along the length of the CFRP strip at the interface between the beam and the CFRP strip. The concrete cover did not resist much shear stress at the bottom face, which caused spalling of the concrete layer and debonding of the

CFRP, which caused sudden failure of the beam by concrete crushing. Figure 5.10 shows the debonding of the CFRP.

For beams strengthened using NSM technique, the crack distribution was similar to that of the EBR strengthened beam. However, the cracks started at the bottom face of the beam and stopped at the CFRP strip after the impact energy was increased, as shown in Figure 5.11. No CFRP debonding was observed in the NSM strengthened beams. No shear cracks were observed in the beams and no local damage occurred for any beams. All beams failed by concrete crushing at the mid-span. Appendix E shows the crack development during the test for the control and both strengthened beams.
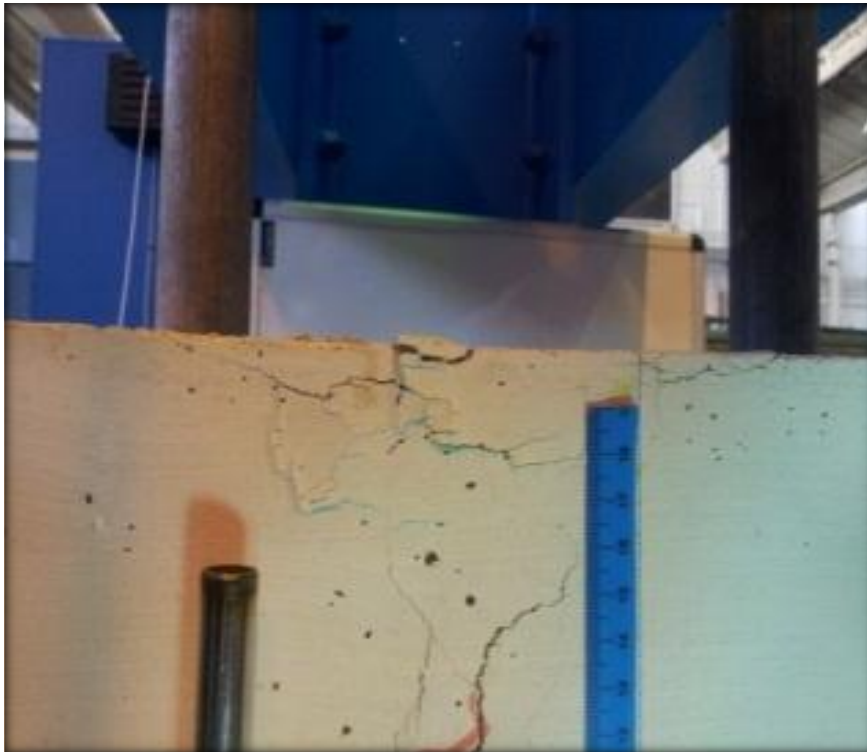
Figure 5.9 Control beam failure (concrete crushing)

Figure 5.10 CFRP debonding (EBR beam bottom face)

Figure 5.11 Beam cracks (NSM strengthened beam bottom face)

5.3.6 Impact Energy

In an impact test, a mass is raised to a certain height and falls on the test specimen. The mass has a potential energy, and when it falls, the potential energy of the mass converts to kinetic energy. The kinetic energy of the mass suddenly transfers to the specimen. When the mass hits the specimen, it develops high stress in a short time and causes deformation in the specimen.

The energy gained by the beam can be divided into two parts; (i) bending energy (ii) inertia energy. A part of the hammer energy is used to accelerate and vibrate the beam and induce the inertia force. The beam will be stressed by bending energy leading to deformation and formation of cracks and residual deflection. The bending energy comprises of elastic energy and fracture energy. The energy losses at impact test machine due to elastic deformation are assumed to be ignored, so the hammer energy is transmitted to the beam.

To find the exact impact resistance of the RC beams or the single impact that can cause the beam failure, it would be necessary to conduct individual impact tests on a large number of beams. This was not possible due to resource limitations. Thus, researchers used alternative methods to find an approximate indication of the impact resistance of the beams. Appendix (A) shows a summary of a number of studies conducted on beams under impact loading. It is clear from Appendix (A) and the literature review that researchers used an accumulative impact energy method to evaluate the impact resistance of the beams. In this method, the summation the total impact energies applied to the beam in multi-impact tests from different heights, or repeated from the same height, is used to evaluate the impact behaviour of the impacted beam. In the drop impact test recommended by the ACI Committee 544 (1982), the impact resistance of the specimens is equal to the number of drops multiplied by the impact energy (see Section 1.2). Both methods are approximate and do not show the exact impact force resisted by the beam. The effect of the single impact is not equal to that of multi -impacts because of the deformations and cracks generated by the sequence of lower energy impacts. However, these methods can give an indication of the impact resistance and behaviour of the beam.

Figure 5.12 shows the accumulative impact energy resisted by reference and strengthened beams. The cumulative impact energy is defined in this thesis simply as the sum of the impact energy imposed at each of the single impacts in multi-impact tests. As can be noted from Figure 5.12 7, the NSM-strengthened beam resisted more cumulative impact energy, impact force and bending load compared with the reference and the EBR- strengthened beams. The EBR- strengthened beams show a low increase in accumulative impact energy compared with the control beam, due to a sudden debonding of CFRP.

Figure 5.12 illustrates the cumulative impact energy versus the cumulative residual deflection. It is clear from the figure that the strengthened beams are much stiffer than the control beams. The behaviour of the EBR- strengthened beam is similar to that of the NSM -strengthened beam at the early stage of the test and with increasing impact energy. It was observed that the CFRP strip debonded from the EBR strengthened beams, which then made the beam behave in a manner similar to that of the control beam. Because the CFRP strip did not debond, the NSM-strengthened beam resisted more impact energy than the control beam and the EBR- strengthened beam.

Figure 5.12 shows that the reference beams were more ductile and had a high residual deflection compared with the strengthened beams. This demonstrates that the reference beams absorbed more impact energy as fracture and bending energy.

CFRP are elastic materials with a high tensile modulus, so they increased the elasticity and stiffness of the beams. The strengthened beams showed a low residual deflection compared with the unstrengthened beams, as shown in Figure 5.13. When the strengthened beams are impacted by the mass, most of the imparted energy is released by the beam vibration rather than as fracture energy and plastic deformation. The number, width and length of the cracks in the strengthened beams were fewer than those in the reference beams.
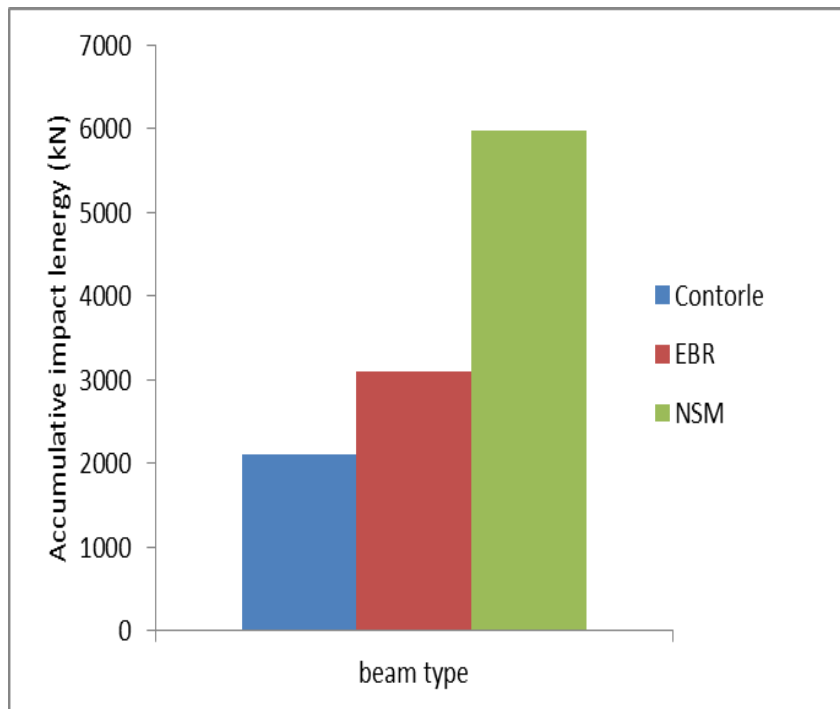
Figure 5.12 Accumulative impact energy of reference and strengthened beams
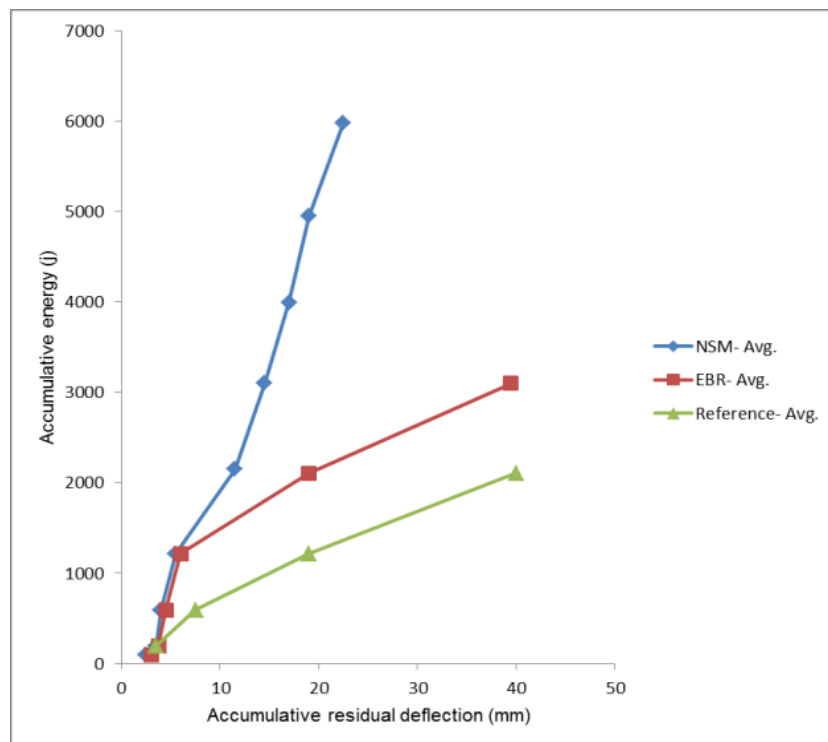
Figure 5.13 Accumulative impact energy vs accumulative residual deflection

5.3.7 Beam behaviour analysis

A high speed camera and accelerometers were used to study the beam behaviour during impact. The high speed camera captured the moment of the impact to allow study of the behaviour of the beam under impact. For greater understanding of the moment of impact, three accelerometers were used to study the beam behaviour during impact. The acceleration was measured at three positions: 375 mm, 750 mm and 1125 mm from the beam supports. Figure 5.14 shows the acceleration against time for beam BR-1. To find the velocity at these points, Eq. 5.7 was used. The integration is equal to the area under the curve. The velocity at any time is equal to the area under the acceleration–time curve. The sampling rate for the accelerometers was 10 kHz. The area between two points was calculated numerically using the trapezoidal method, and MatLab software was used to conduct the integration process. Figure 5.15 shows the mid-span velocity compared to the mass velocity at the moment of impact. Using the same method, the deflection was equal to area under velocity–time curve (Eq. 5.8). Figure 5.16 shows the deflection at the moment of impact for different points along the length of the control beam BR-1 (impact energy= 622 J).

The behaviour of the beam during impact can be understood by examining Figures 5.14 to 5.16. The impact test began by dropping a mass from a certain height. When the mass contacted the beam at point A, the impact energy was transferred from the mass to the beam and both the mass and beam moved downwards. This collision resulted in a rapid increase in beam velocity and decrease in mass velocity. The beam reached maximum velocity at point B, and the, the beam velocity decreased rapidly due to beam stiffness. The beam continued to move down with a reduction in velocity until it reached zero velocity at point C. After that, the beam started moving upwards until it reached a velocity of 0.16 m/s at point D. Meanwhile, the mass velocity was 0.36 m/s downwards. At point D, the mass hit the beam again and pushed it downward, meanwhile, the mass rebounded upward. The same situation occurred at the time interval from point D to E. The beam continued deflecting downwards until reaching maximum deflection at point E. The beam velocity at point E (maximum deflection point) became zero. Then the beam rebounded upward due to its elasticity, as shown in Figure 5.16.
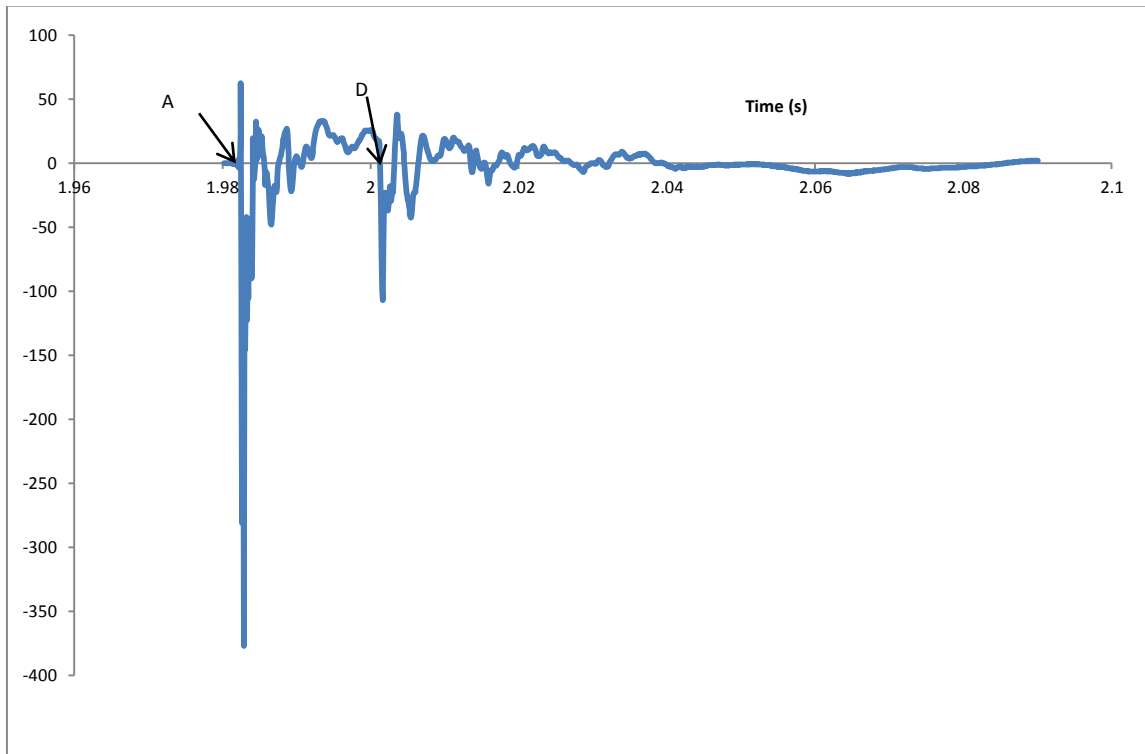
Figure 5.14 Beam acceleration vs time of control beam BR-1, Impact NO.4, energy=622 J
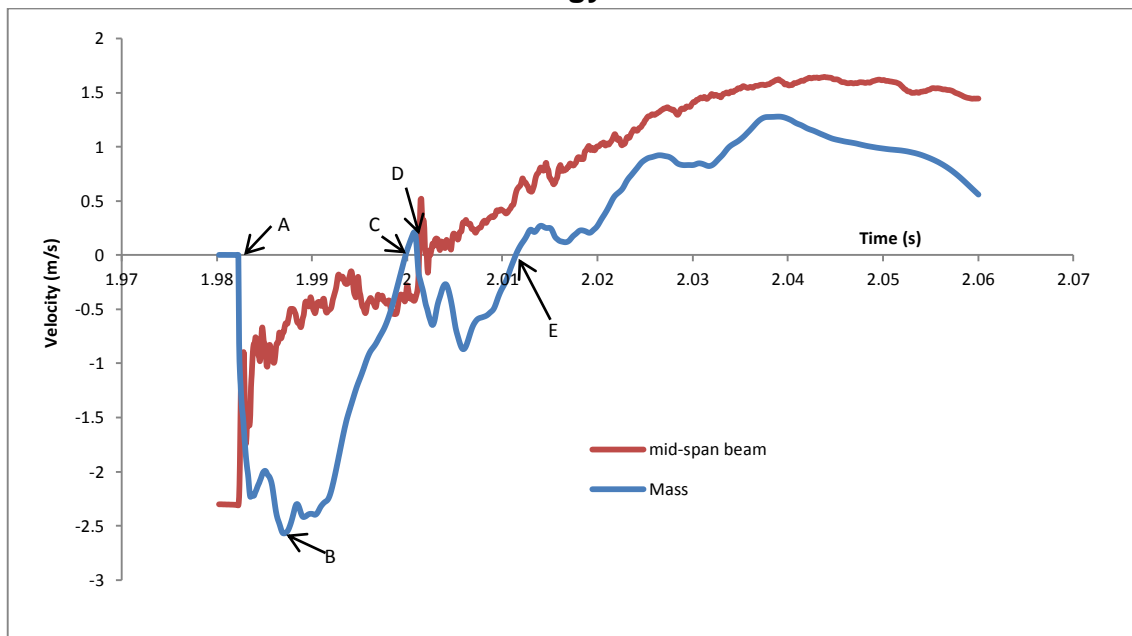
Figure 5.15 Beam and mass velocity vs time of control beam BR-1, Impact NO.4, energy=622 J
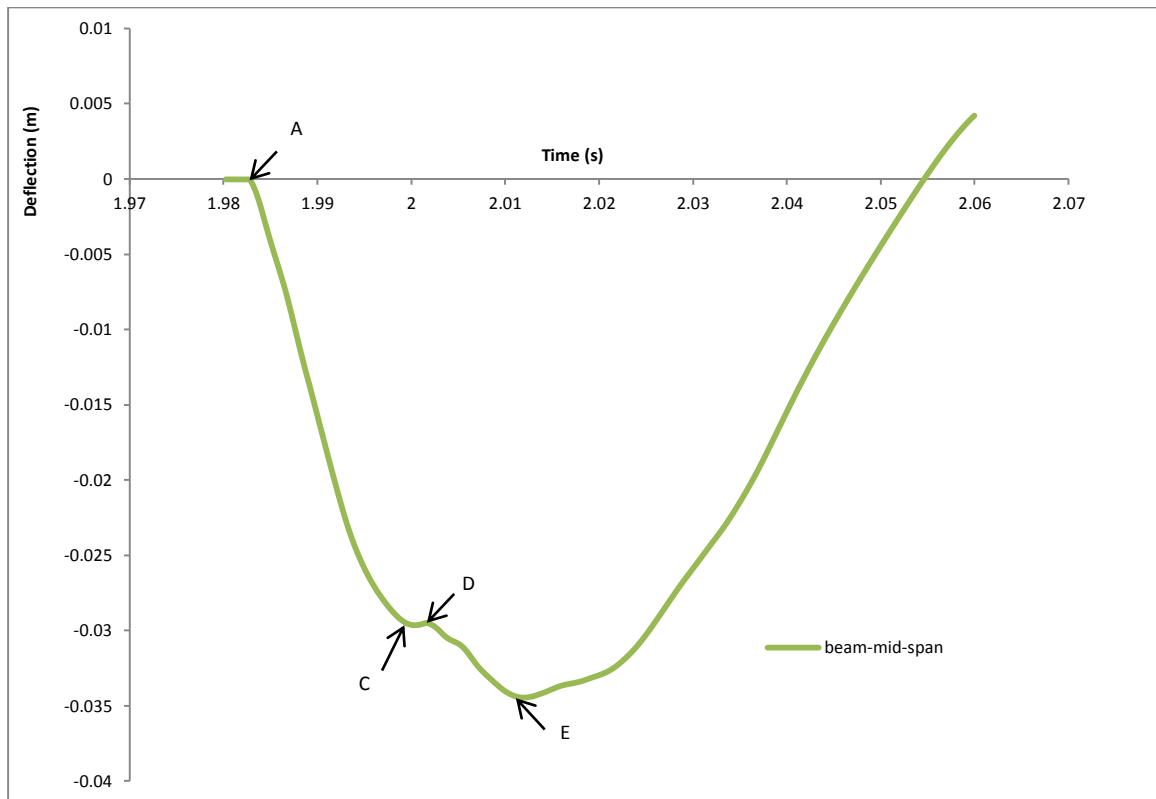
Figure 5.16 Deflection vs time of control beam BR-1, Impact NO.4, energy=622 J

5.3.8 Beam deflection distribution

Figures 5.17- 5.19 show the deflection distribution along the control beam BR-1 length at any time (t) for different impact energies. As can be noted from Figures 5.17 and 5.18, in low and intermediate impact energy the beam deflection was approximately linear at any time, due to high beam stiffness as the cracks length and width were less under low impact. Under high impact energy and when the beam came close to failure, the beam deflection become nonlinear and exceeded the maximum deflection capacity of the beam, as in Figure 5.19.

It can be noted from Figure 5.19, that at the beginning of the impact (t=2.155 s), the beam deflection was linear: thereafter, the beam deflection increased due to mass momentum. The latter increased the length and width of the cracks, which caused the beam to lose its stiffness and also the beam deflection became nonlinear, as can be seen from the Figure 5.19 (t= 2.1851 s).
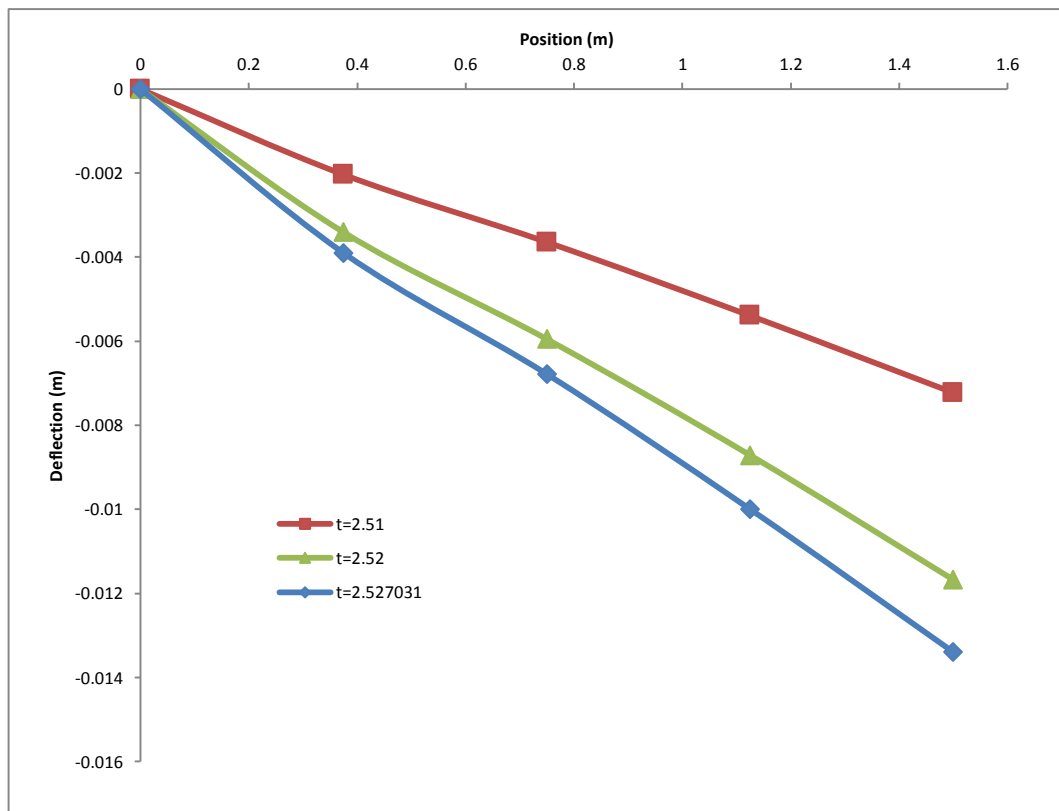
Figure 5.17 Deflection vs position of control beam BR-1, Impact NO.4, energy=99J
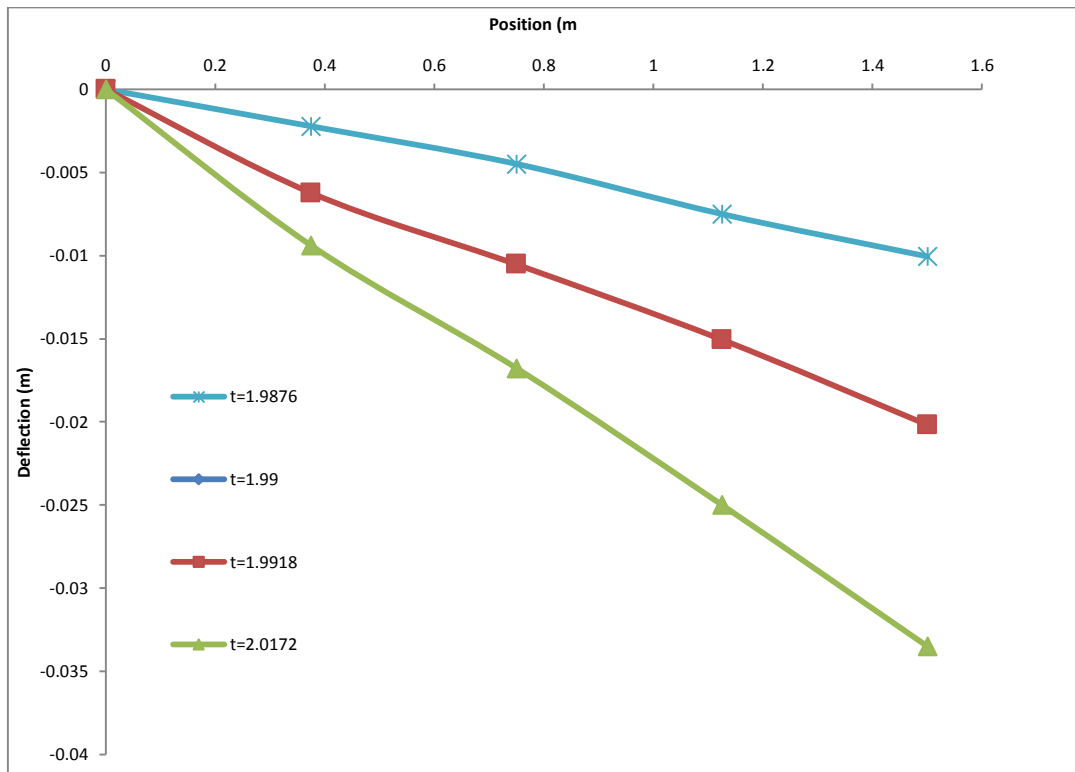
Figure 5.18 Deflection vs position of control beam BR-1, Impact NO.4, energy=622 J
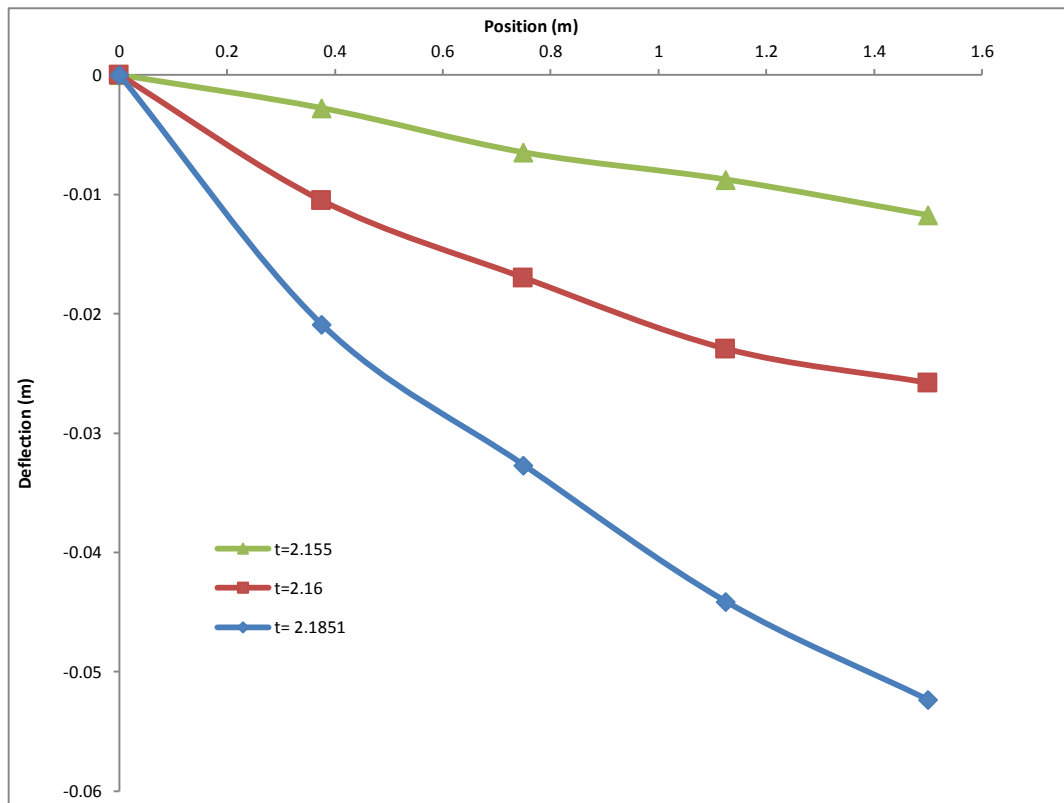
Figure 5.19 Deflection vs position of control beam BR-1, Impact NO.5, energy=890 J

Figure 5.20 shows the comparison between the measured maximum deflection and the calculated maximum deflection using Eq.5.8. As can be seen from the figure, there was good agreement between the calculated and measured maximum deflection under different impact energies. Figure 5.20 shows, that with increasing impact energy, the beam deflection became nonlinear due to deformations and cracks.
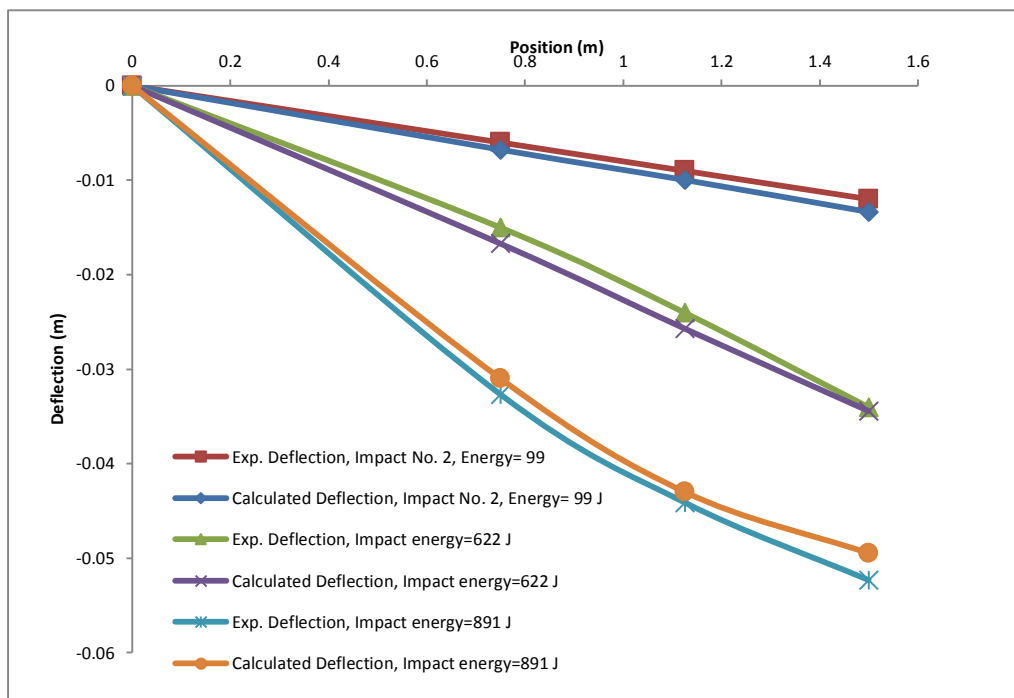
Figure 5.20 Comparison between measured and calculated maximum deflection vs position of control beam BR-1 under different impact energies

Figure 5.21 shows the EBR strengthened beam deflection at different positions during Impact no.5 (energy=890 J). Under this impact, the CFRP strip was debonded from the concrete bottom face. It is clear from the figure that, at the early stage of the impact, the beam deflection was linear due to high beam stiffness gain by CFRP. When the beam deflection was increased due to mass momentum, a high shear stress developed in concrete cover which caused CFRP debonding due to the concrete cover delamination undergoing high tensile stresses concentrated at the concrete cover. After CFRP debonding, the beam lost its stiffness suddenly and rapidly, which made the beam deflection nonlinear due to high deformation. There was also an increase in the cracks length and width of the cracks, as can be seen in Figure 5.21(t=0.564375 s). Figure 5.22 shows a good correlation between the recorded mid-span maximum deflection and that calculated using Eq. 5.8.
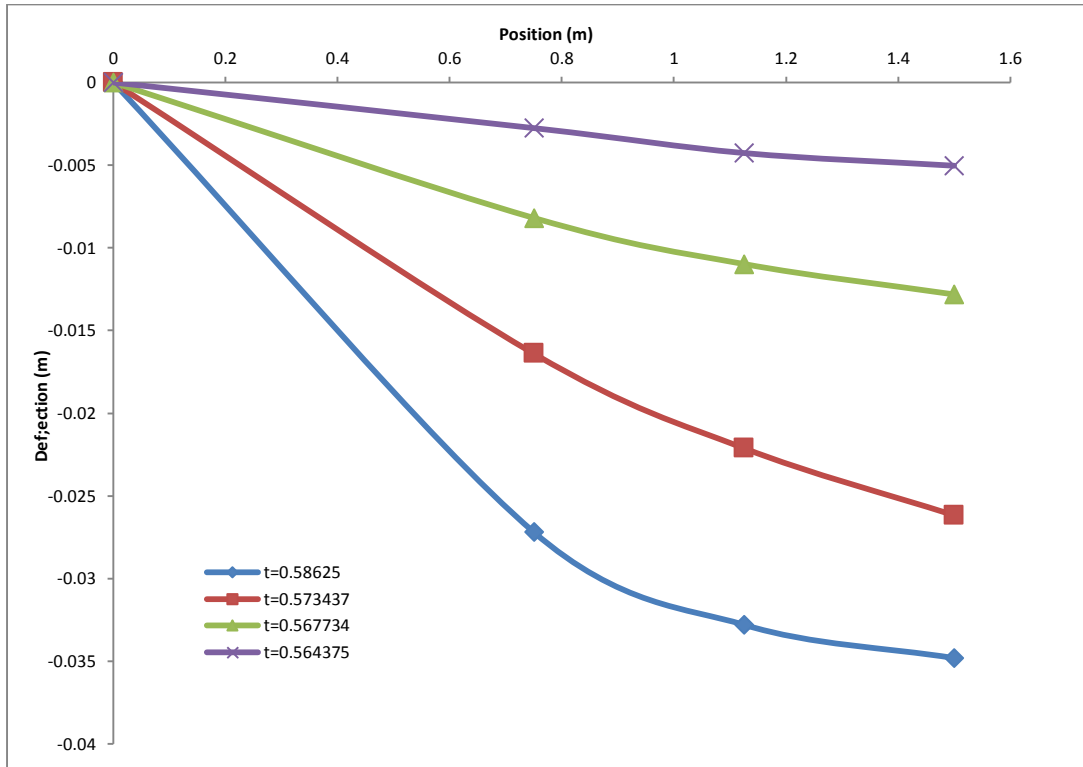
Figure 5.21 Deflection vs position of control beam B-EBR-1, Impact NO.5, energy=890 J
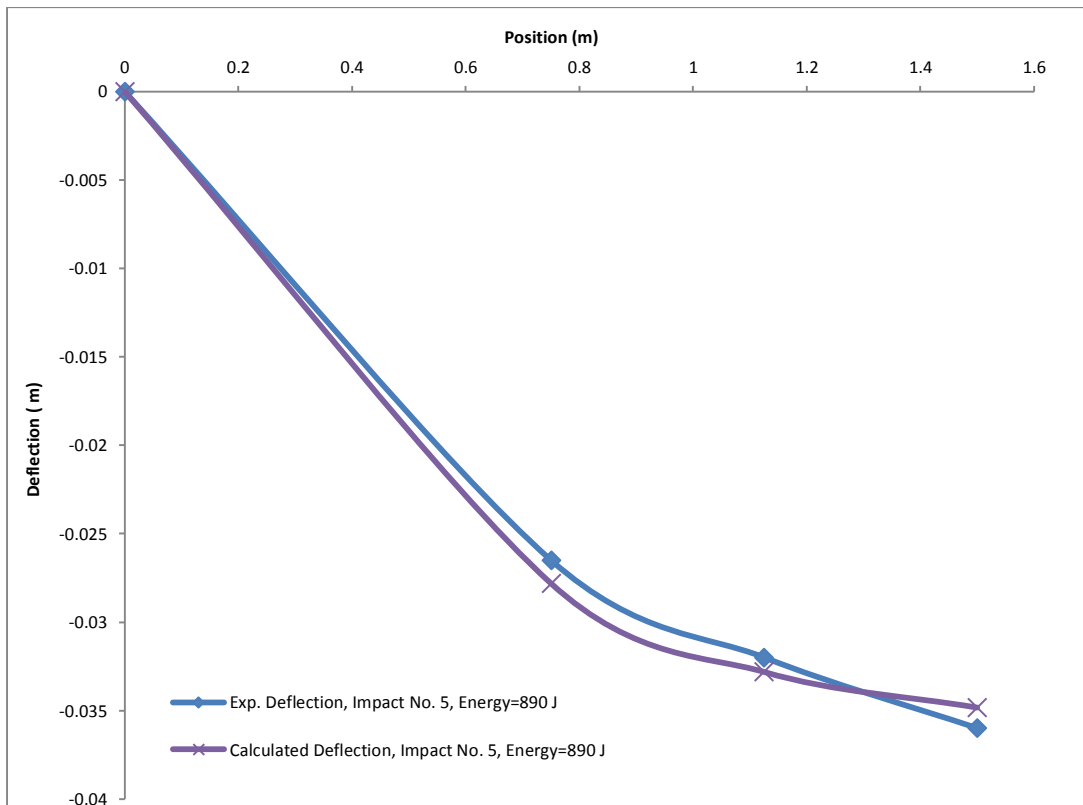
Figure 5.22 Comparison between measured and calculated maximum deflection vs position of control beam B-EBR-1

Figures 5.23 and 5.24 show the maximum deflection of the NSM- strengthened beam under last two impacts (961 J and 1029 J). Under the heavy impact energy of 1029 J, the beam failed due to concrete crushing. However, the beam deflection was approximately linear because the CFRP strip did not debond, as happened in the EBR -strengthened beams, which made the beam stiffer and reduced the maximum deflection of the beam compared with control and the EBR -strengthened beam.

A good agreement was found between the beam's measured maximum deflections and the calculated maximum deflection, as can be seen in Figure 5.25.
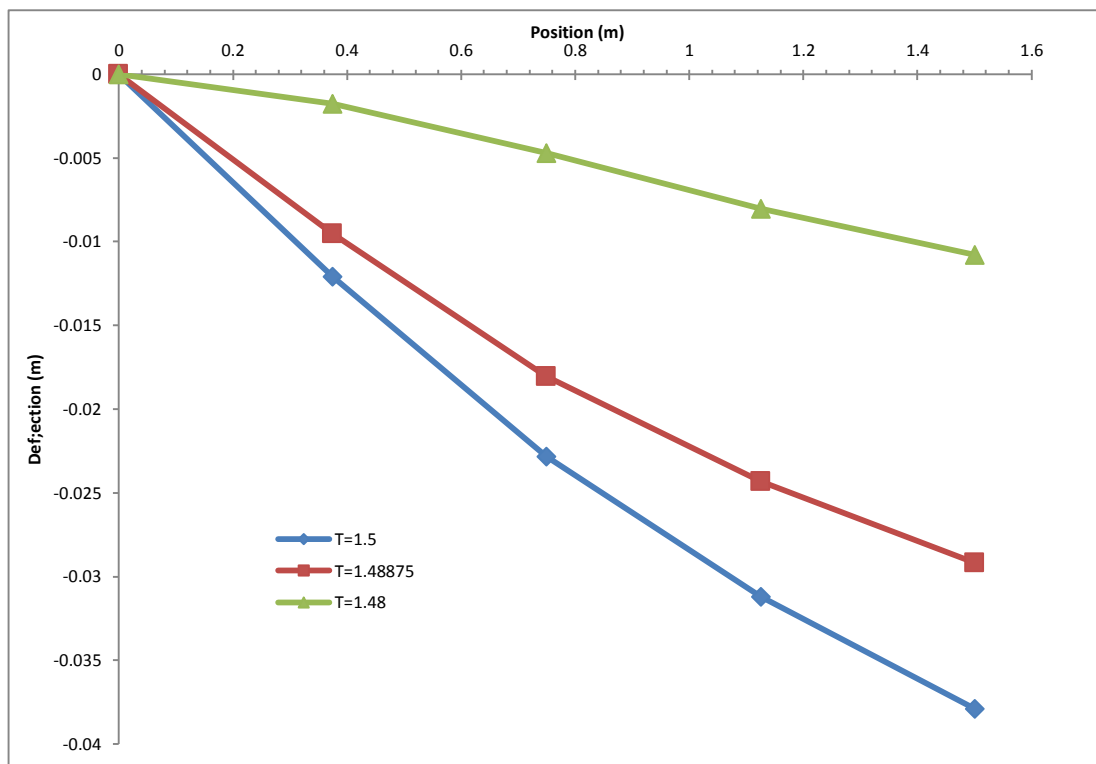
Figure 5.23 Deflection vs position of control beam B-NSM-1, Impact NO.8, energy=961 J
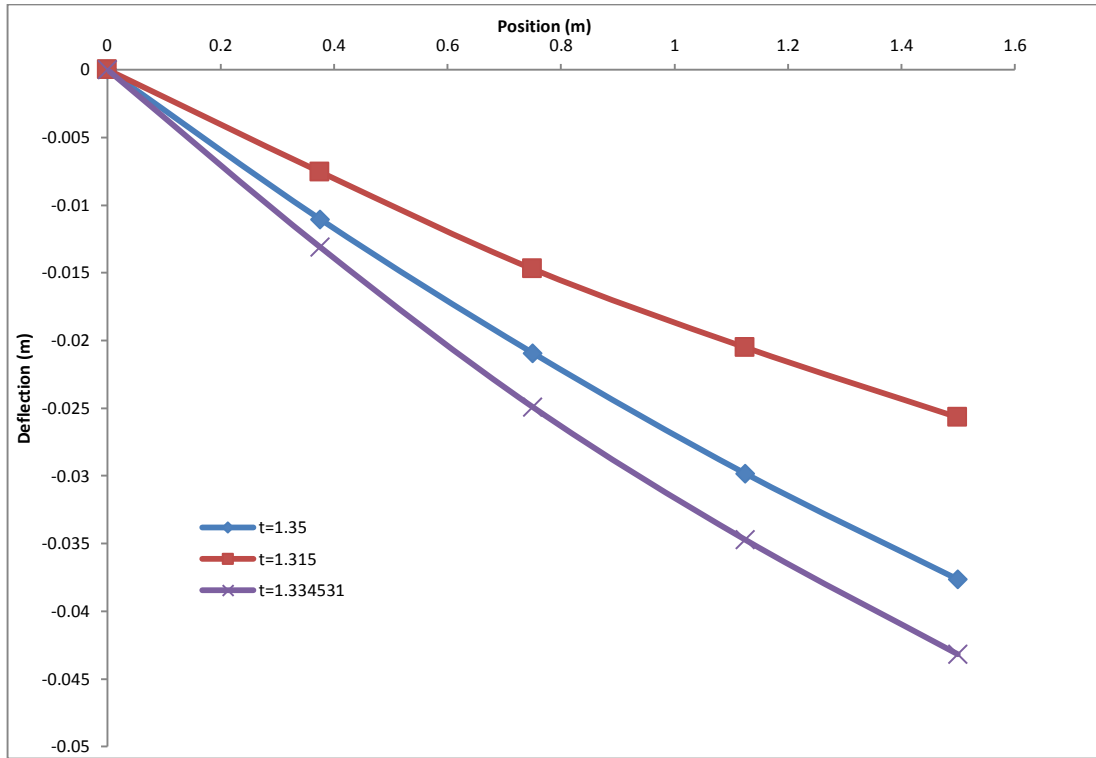
Figure 5.24 Deflection vs position of control beam B-NSM-1, Impact NO.9, energy=1029 J
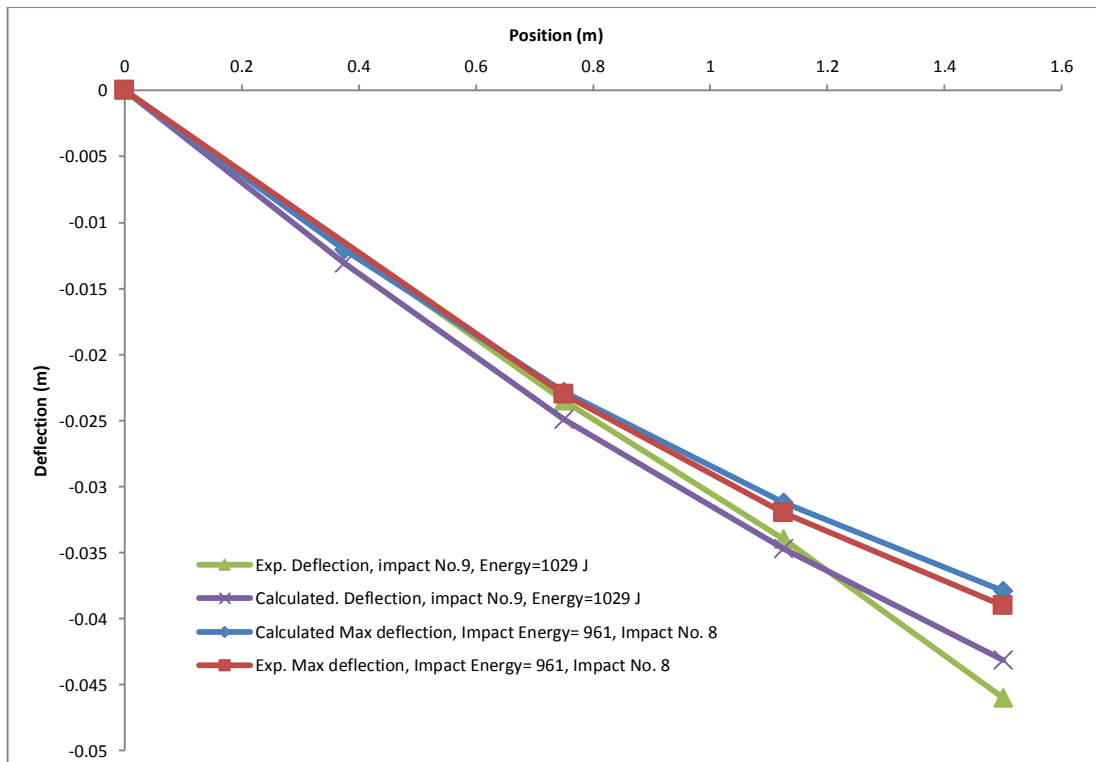
Figure 5.25 Comparison between measured and calculated maximum deflection vs position of control beam B-NSM-1under different impact energies

5.4 Concluding remarks

The impact tests result analyses showed that the unstrengthened beam absorbed more impact energy. The width and length of the cracks and the residual and maximum deflection of the strengthened beam were much higher than that of the unsrengthened beam. A high percentage of bending impact energy was absorbed and dispatched as fracture energy (cracks and deformations) rather than as elastic energy. That resulted in low impact energy transferred to the support, so, the reaction force of the reference beams was lower than that of the strengthened beams. In strengthened beams, CFRP strip increased the stiffness and elasticity. The impact energy was released by beam vibration rather than by fracture energy. The impact force of the strengthened beams was less than that of the reference beams. The change in momentum and the time of impact of the strengthened beams were different than that of the reference beams.

Under impact loading, the reference beam deflection shape was sinusoidal than lines because the reference beams were heavily cracked and deformed under impact loading. The high stiffness of the CFRP- strengthened beams made the deflection along the beam length more linear. In strengthened beams, the inertia force calculated using a linear assumption produced good agreement with the experimental inertia force, while a sinusoidal assumption gave good inertia force predation in the reference beam.

In EBR strengthened beams, the CFRP strip was debonded, due to concrete cover delamination followed by beam failure due to concrete crushing. Therefore, when the EBR technique is used to strengthen the RC beams under impact loading, the use of an anchor system is recommended in order to reduce the probability of CFRP debonding. In NSM CFRP beams, The CFRP strip did not debond, as the CFRP was mounted in the concrete cover, which increased the bonding between the CFRP strip and concrete. NSM beams resisted more accumulative impact energy compared with EBR and reference beams. All tested beam were failed by mid-span concrete crushing. The reference beams were more ductile and the cracks and residual deflection were evident before failure. In the strengthening beam, the beam was stiff and showed low residual deflection and cracks, and suddenly failed by concrete crushing.

6. Experimental results –Repairing

6.1 Introduction

Three groups of beams with different degrees of damage were tested under impact loading. Group 1 beams (B1-1, B1-2) were damaged using a single impact to induce heavy damage. To produce intermediate damage, Group 2 (B2-1, B2-1) beams were damaged using single impact loading lower than that used to damage Group 1 beams. Low impact energy was used to induce the lowest damage to Group 3 beams (B3-1, B3-2). The main conclusion from the strengthening stage of the experiments was that the NSM technique was more effective compared with the EBR technique. Thus, only the NSM technique was used to repair the damaged beams in the repair stage of the experimental work. The behaviour of the damaged and repaired beams was investigated in terms of beam stiffness, impact energy, bending load, impact force, deflection and crack distribution. The same testing procedure was applied to each group of beams. The only difference between groups was the degree of damage induced in the beams. Each group of beams included two identical beams. The first beam was initially damaged using single impact load. The damaged beam was retested again under multi-impact, loading up to failure to find the remaining impact resistance after damage. The second beam from each group was damaged using the same initial impact energy as was used to damage the first beam in order to induce the same degree of damage. Thereafter, the damaged beam was repaired using NSM- CFRP strip. The repaired beam was tested again under multi-impact test up to failure to find its impact resistance. The testing procedure was described in Section 3.6.

This chapter includes three main sections. In Section 6.2, the stiffness of the damaged and repaired beam and stiffness variation under impact loading are discussed. Section 6.3 discusses impact resistance and behaviour of the damaged and repaired beam under impact loading. In Section 6.4, the proposed equations are discussed.

6.2 Beam stiffness under impact loading

6.2.1 Stiffness of undamaged and damaged beam

Figure 6.1 shows the rigidity (EI) of the reinforced beam. Before damage, the beam stiffness is about constant and the rigidity equal to EI_g. This means that the stiffness of the beam is constant before the first crack and the beam behaves elastically. When the beam starts cracking, the beam stiffness starts decreasing due to the formulation of the cracks. When the applied moment is close to the ultimate load, the concrete is about fully cracked and the beam stiffness becomes very low. In the ultimate stage, the beam rigidity is about constant and equal to EI_{cr} as shown in Figure 6.1. The moment of inertia of the beam varies between the moment of inertia of gross area I_g and moment of inertia of cracked section I_{cr}.
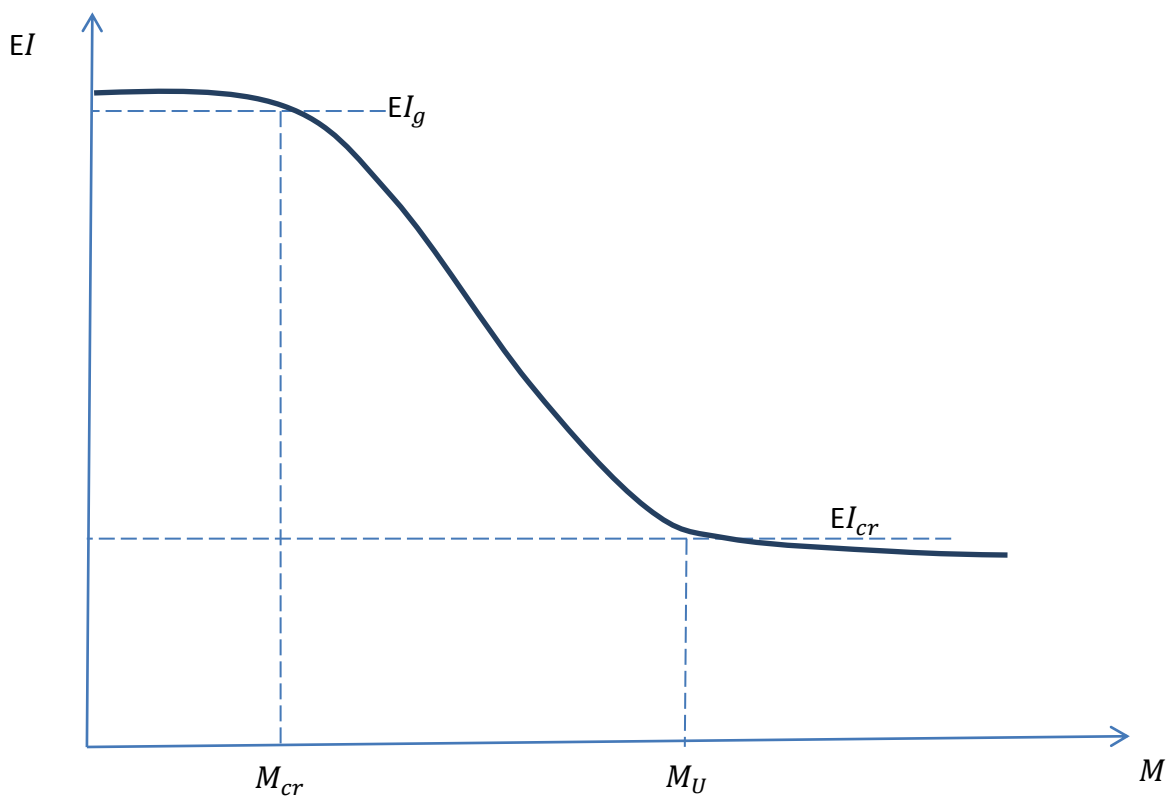
Figure 6.1 Variation of bending rigidity with bending moment

In experimental work conducted, the beam stiffness was found for the tested beams (undamaged, damaged and repaired beams) experimentally (see Section 4.6.2).

In addition to the experimental method, the elastic beam stiffness can be found theoretically as following:

Figure 6.2(a) show the cross-section of the tested beams.
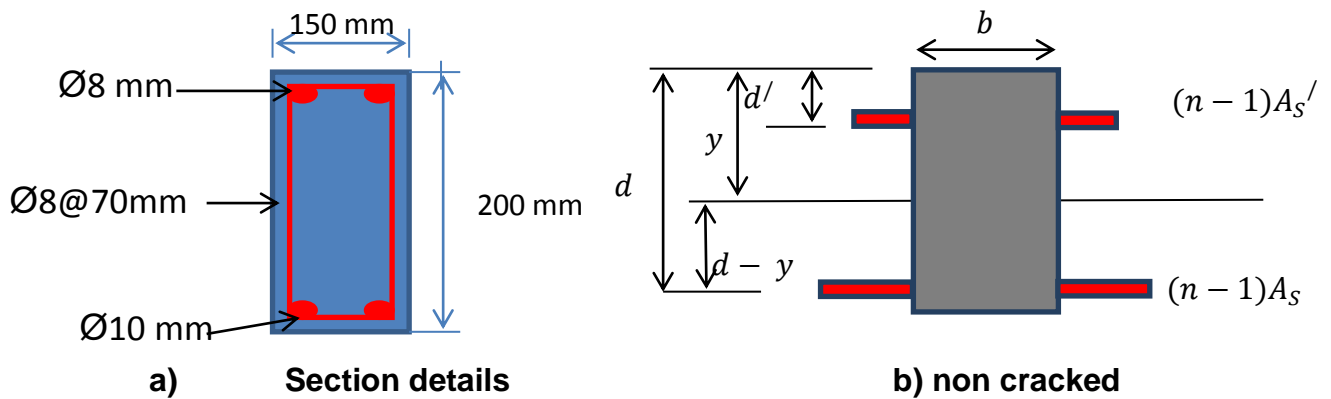
Figure 6.2 Section of tested beam cross section

For simple supported beam under point load at the centre

$$\delta = \frac{P\,l^3}{48EI}$$
6.1

$$stiffness\ (K) = \frac{P}{\delta} = \frac{48EI}{l^3}$$

$$E_c = 4700\sqrt{f_c^{/}} \qquad (\text{ACI-318 Code})$$
6.2

Where:

δ: Mid-span deflection

I : Beam moment of inertia

Ec: Concrete modulus of elasticity

$f_c^{/}$: Cylinder concrete compressive strength

Figure 6.2(b) show the cross-section of the tested beams.

The theoretical cracked section stiffness can be found as following

$d \quad = 147 \ mm$

b= 150 mm

$A_S = 157 \ mm^2$

$A_S{}' = 100 \ mm^2$

$(f_c')_{cylider} = 0.8 \ (f_c')_{cubic} = 0.8 * 32 = 25.6 \ N/mm^2$

$n = \dfrac{E_S}{E_c} = 8.4$

7.4*100*(y-53)-7.4*157(147-y) =0

y=110 mm

$$I_{uncr} = \frac{150 \times 110^3}{3} + \frac{150 \times 90^3}{3} + 7.5 * 100 * (110 - 53)^2 + 7.5 * 157 * (147 - 110)^2$$

$I_{uncr} = 107048747.5 mm^4$

$E_c = 4700\sqrt{f_c'} = 23.8 * 10^3 \ N/mm^2$

uncracked section stiffness $= K_e = \frac{48EI_{uncr}}{l^3} = 4.53 \ kN/mm$

Figure 6.3 shows the stiffness of all beams before the impact test. As the beams were notionally identical (the same dimensions, bar details and material properties), the stiffness of the beams was very similar, as can be seen in Figure 6.3.

The initial elastic beam stiffness before first crack was considered as stiffness of the undamaged beam, by comparison with the damaged beams discussed in the following sections.

The theoretical elastic load deflection curve was drawn, based on the calculated elastic stiffness ($K_e = 4.53 \ kN/mm$) as illustrated in Figure 6.3. The comparison shows a good agreement between the theoretical and experimental elastic load-deflection curve.
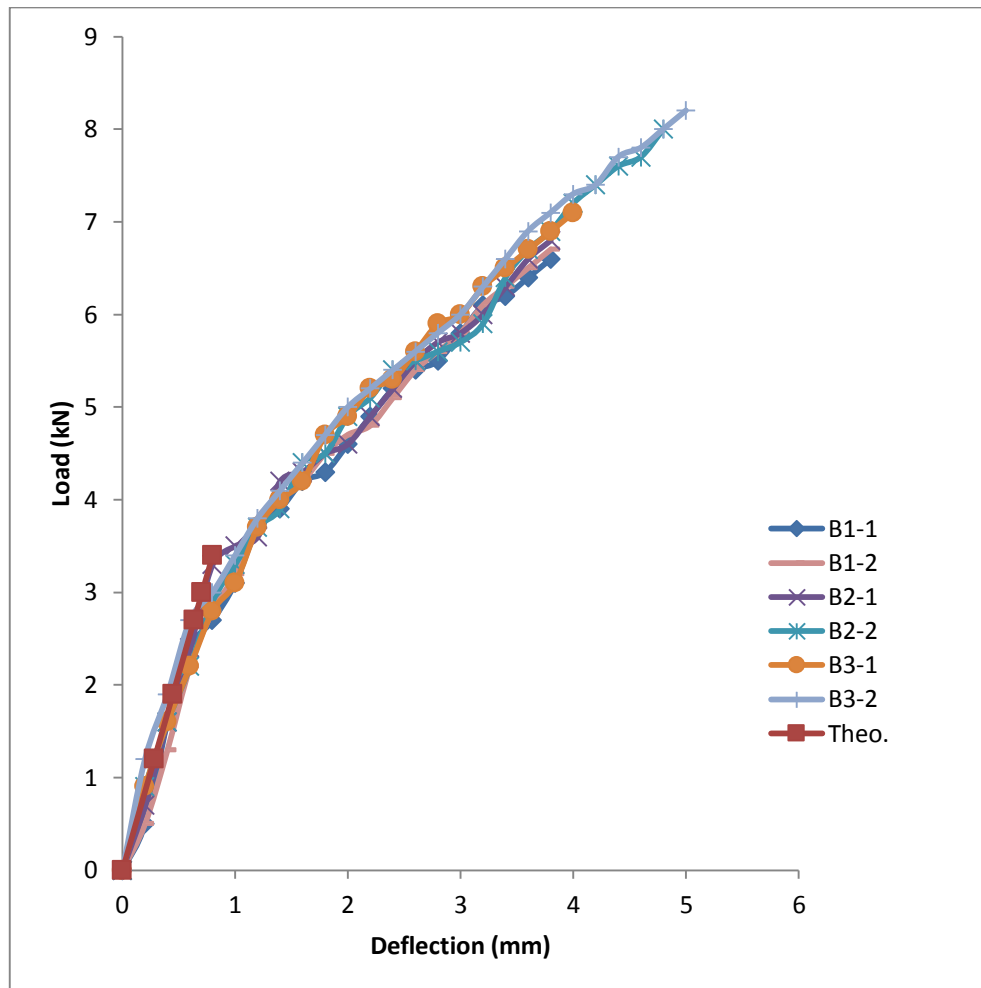
Figure 6.3 Load- deflection curves for casted beams before testing

The beam stiffness was obtained using static tests before and after each impact test (see Section 4.6.2). The beam stiffness reduction percentage was determined by referencing the stiffness of the damaged beam to that of the undamaged beam.

Figures 6.4- 6.6 show the stiffness of the beams before and after damage for Group 1, 2 and 3 respectively. The figures show that beam stiffness decreased considerably when the beams were damaged by impact loading. As the beams were identical, both beams had a similar response before and after impact. The same behaviour was observed in all tested beams.
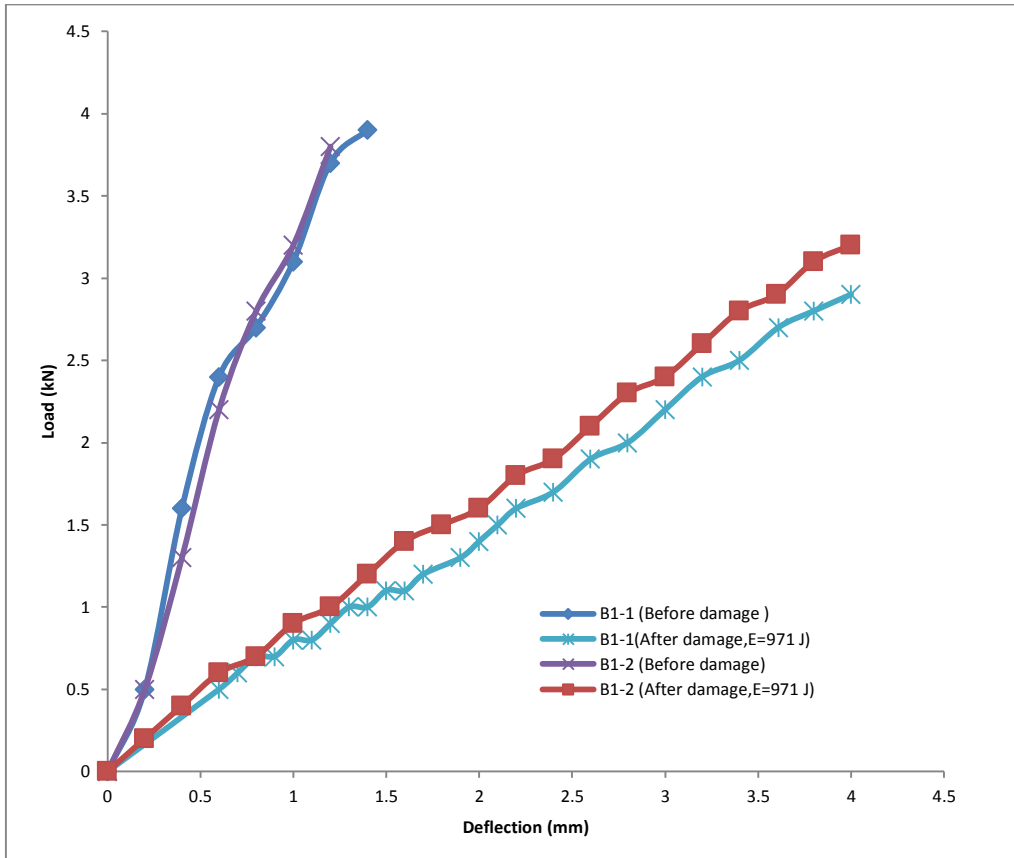
Figure 6.4 Load- deflection curves for Group 1 beams
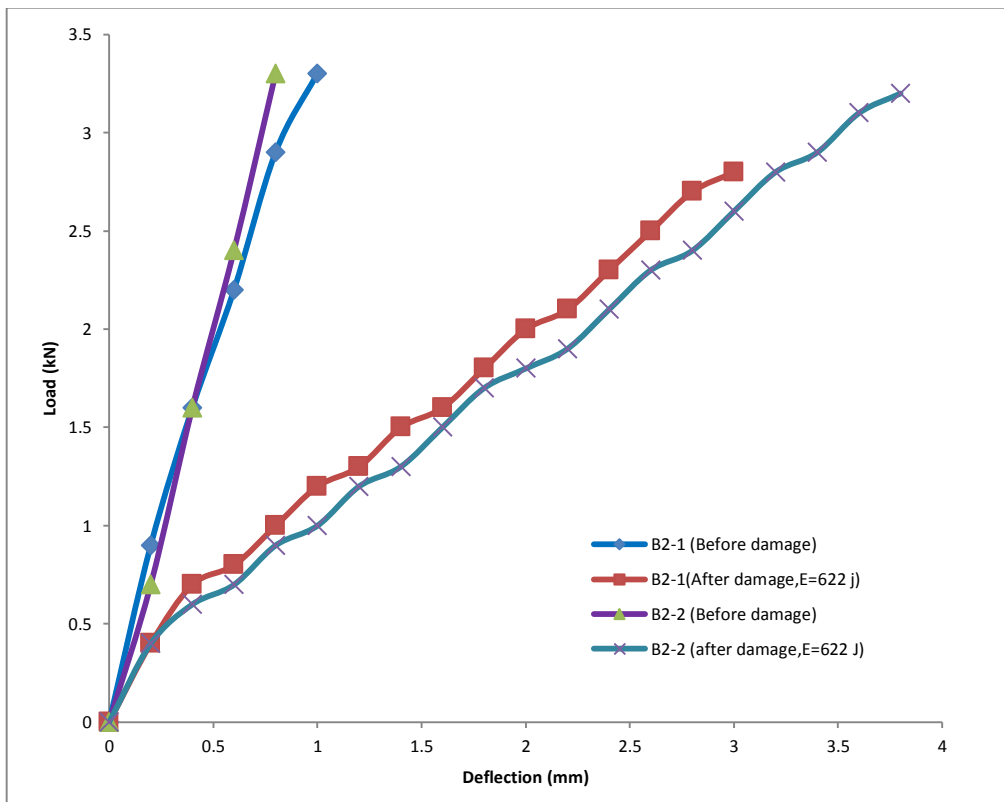
Figure 6.5 Load- deflection curves for Group 2 beams

123
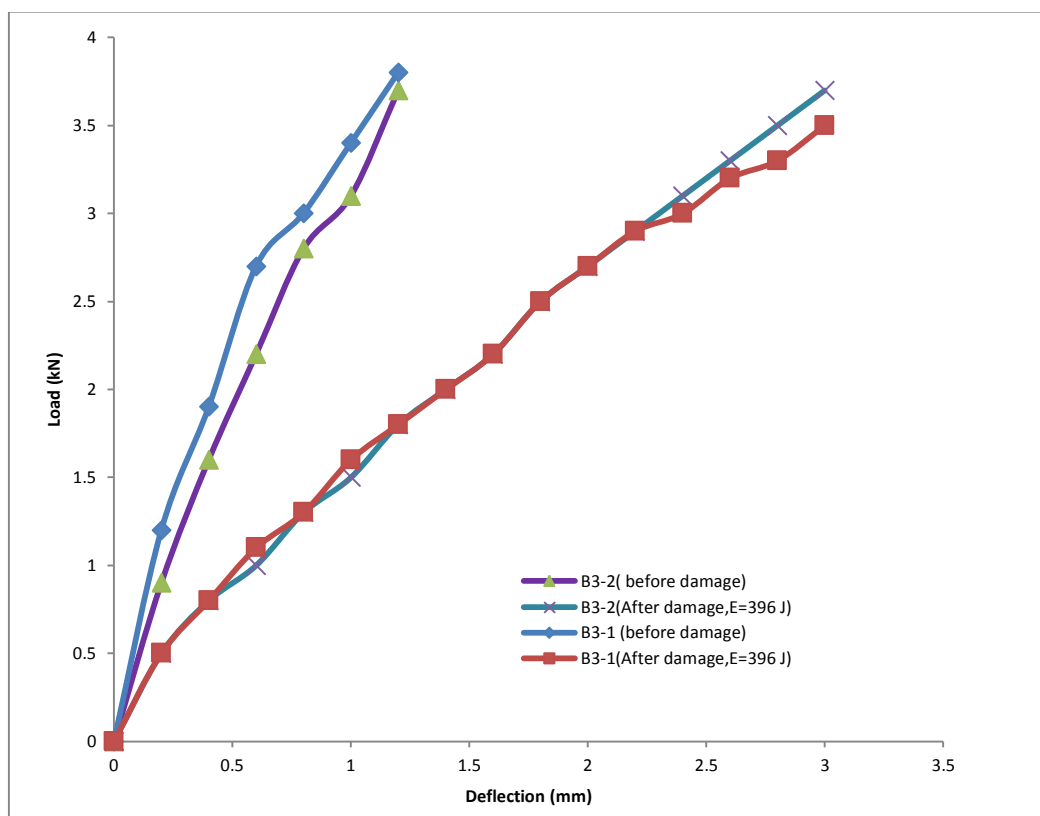
Figure 6.6 Load- deflection curves for Group 3 beams

Table 6.1 shows the stiffness of the beams for each group and the corresponding stiffness reduction. The stiffness of each beam was obtained before and after damage (see Section 4.6.2). The stiffness reduction of each beam was calculated and then the average reduction of each Group was obtained. Figure 6.7 shows a comparison between the damaged beam stiffness and that of undamaged beams. As can be seen from that figure, that beam lost a high percentage of its stiffness even under low impact energy.

The average stiffness reduction for the Group 1 (heavy damaged) and Group 2 beams (intermediately damaged); was estimated to be 76 %. For Group 3, the mass was dropped from low height (0.2 m) to induce low damage. However, high reduction of beam stiffness was indicated. The average stiffness reduction of Group 3 beams was 67 %.

Table 6.1 Stiffness of the damaged and undamaged beams

Group	beam	type	K Stiffness kN/mm	% stiffness reduction	% stiffness reduction avg.
1	B1-1	Reference	3.26	-	76.5
	B1-1	after damage	0.73	78	
	B1-2	Reference	3.28	-	
	B1-2	After damage	0.81	75	
2	B2-1	Reference	3.55	-	76.5
	B2-1	after damage	0.87	75	
	B2-2	Reference	4.05	-	
	B2-2	after damage	0.88	78	
3	B3-1	Reference	3.75	-	67
	B3-1	after damage	1.18	69	
	B3-2	Reference	3.45	-	
	B3-2	after damage	1.24	64	

% stiffness reduction =100*(1- (Kdamage/Kref.))
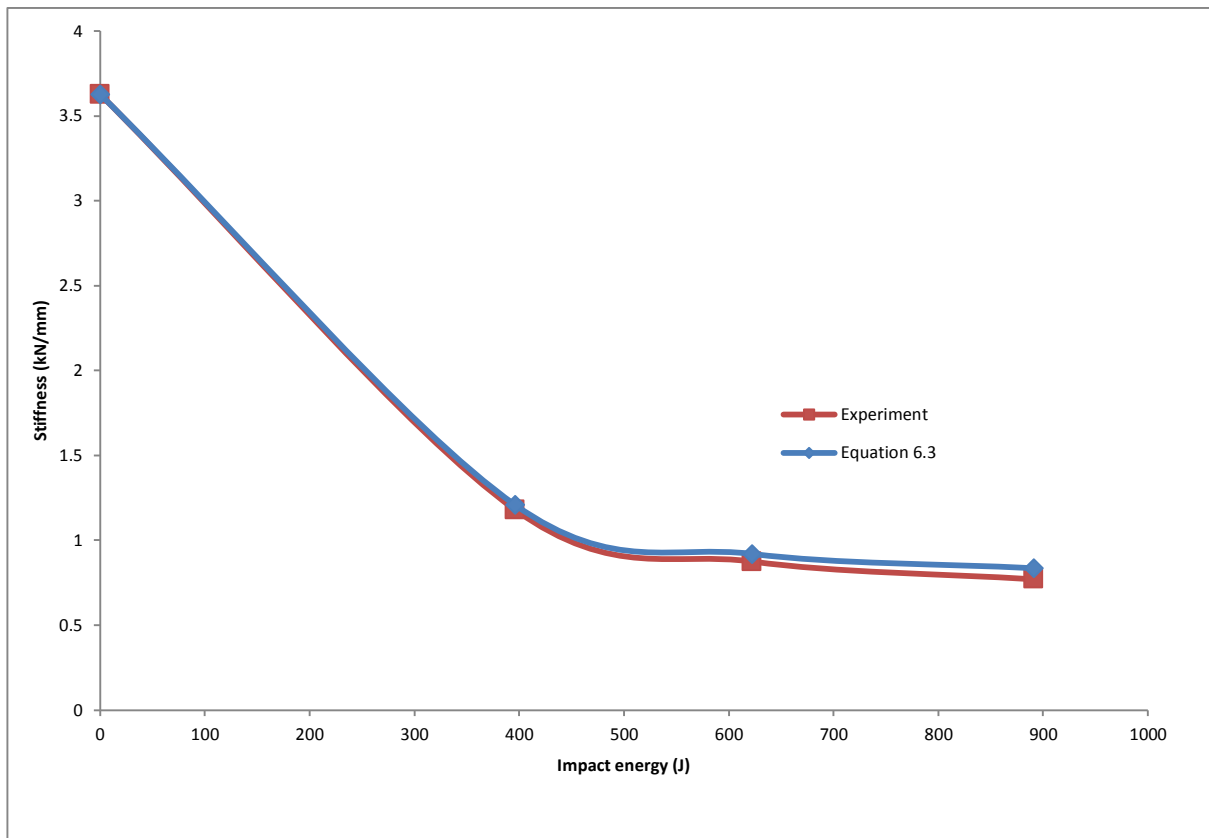
Figure 6.7 Reduction in beam stiffness under single impact loading

From Figure 6.7, the following equation was proposed to predict the stiffness of the beams under different impact energies.

$$K\ damaged = K\ undamged - 6.54*10^{-9}EN^3 + 1.443*10^{-5}EN^2 - 0.0108EN \qquad 6.3$$

Where:

K: beam stiffness (kN/mm)

EN: Impact energy (J)

For a greater understanding of the damage to the beams due to impact loading, the beam stiffness before and after damage was compared to the fully cracked beam stiffness. Figure 6.8 shows a typical cracked section.
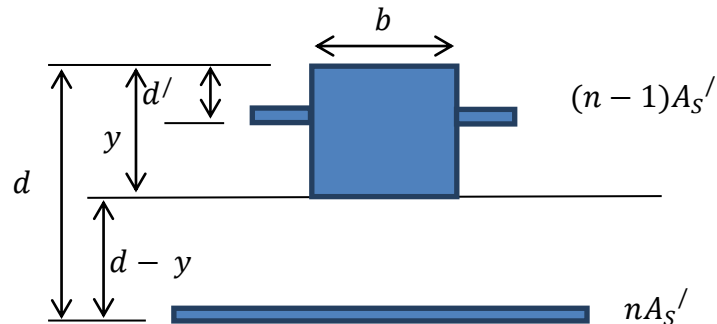
Figure 6.8 Cracked section

The theoretical cracked section stiffness can be found as follows:

$\frac{150y^2}{2}$+7.5*100*(y-53)-8.5*157(147-y) =0

$y = 41.8\ mm$

$$I_{cr} = \frac{150y^3}{3} + 7.5 * 100 * (53 - 41.8)^2 + 8.5 * 157 * (147 - y)^2$$

$I_{cr} = 18076590\ mm^4$

$\text{cracked section stiffness} = K_{cr} = \frac{48EI_{cr}}{l^3}$= 0.76 kN/mm

Figure 6.9 shows the percentage differences of experimental damaged beam stiffness (k) to theoretical cracked beam stiffness (K_{cr}= 0.76 kN/mm) under different impact energies. It is clear from Figure 6.10 that the beams under low and high impact energy were severely cracked under impact loading and lost a high percentage of stiffness. The stiffness of the beam is dependent on the elastic modulus and cross section dimensions EI. When the beam was impacted by mass, the beam deflected down with a high maximum deflection. For group 3 under low impact, the maximum deflection was 23 mm. The maximum deflections were 33 mm and 45 mm for Group2 (intermediate impact) and group 1 (heavy impact) respectively. The high deflection due to the high bending load caused high tensile stresses, which cracked beams severely and led to a reduced effective cross section

and a reduced value of EI. The reduction in EI resulted in a high percentage reduction of the initial elastic stiffness of the beams.
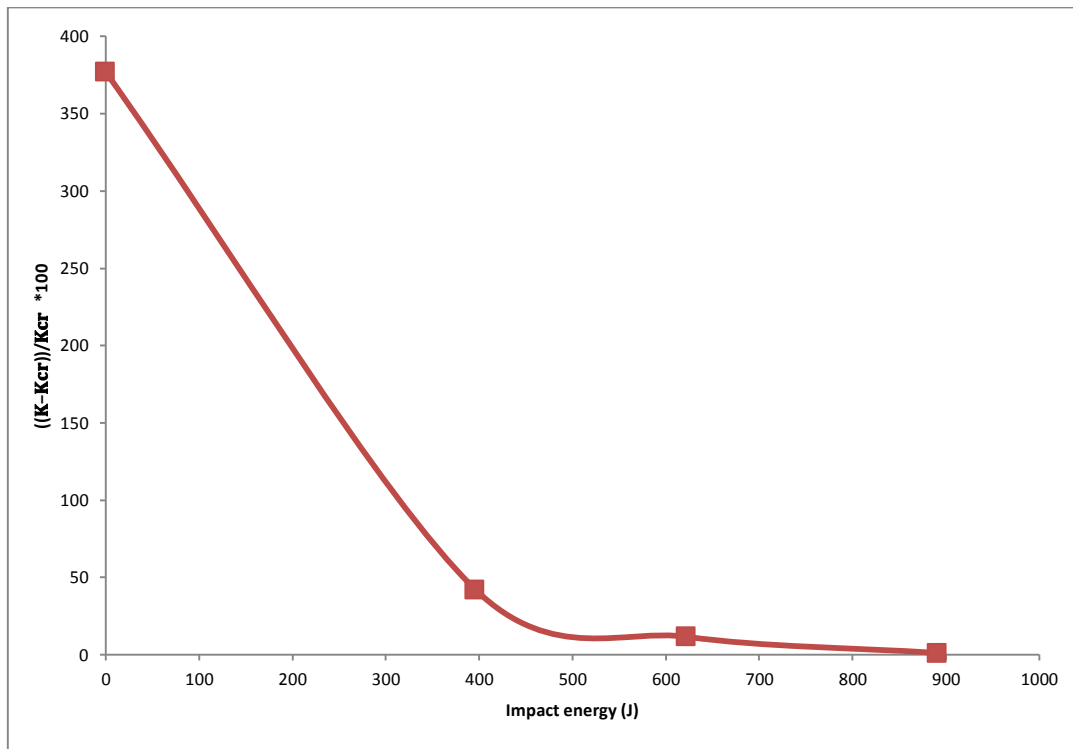
Figure 6.9 Damaged beam stiffness under single impact loading

6.2.2 Effect of NSM-CFRP repair on stiffness of beams

The damaged beams were repaired using CFRP. To find the effect of CFRP repair on beam stiffness, a comparison was made between the stiffness of the repaired and damaged beams.

Figures 6.10-6.12 compare the stiffness of the damaged and repaired beams for Group 1, 2 and 3 respectively. The figures show that CFRP strip used to repair the damaged beam increased and improved the beam stiffness. In repaired beams, CFRP strip decreased the width and length of, which increased the beam stiffness.
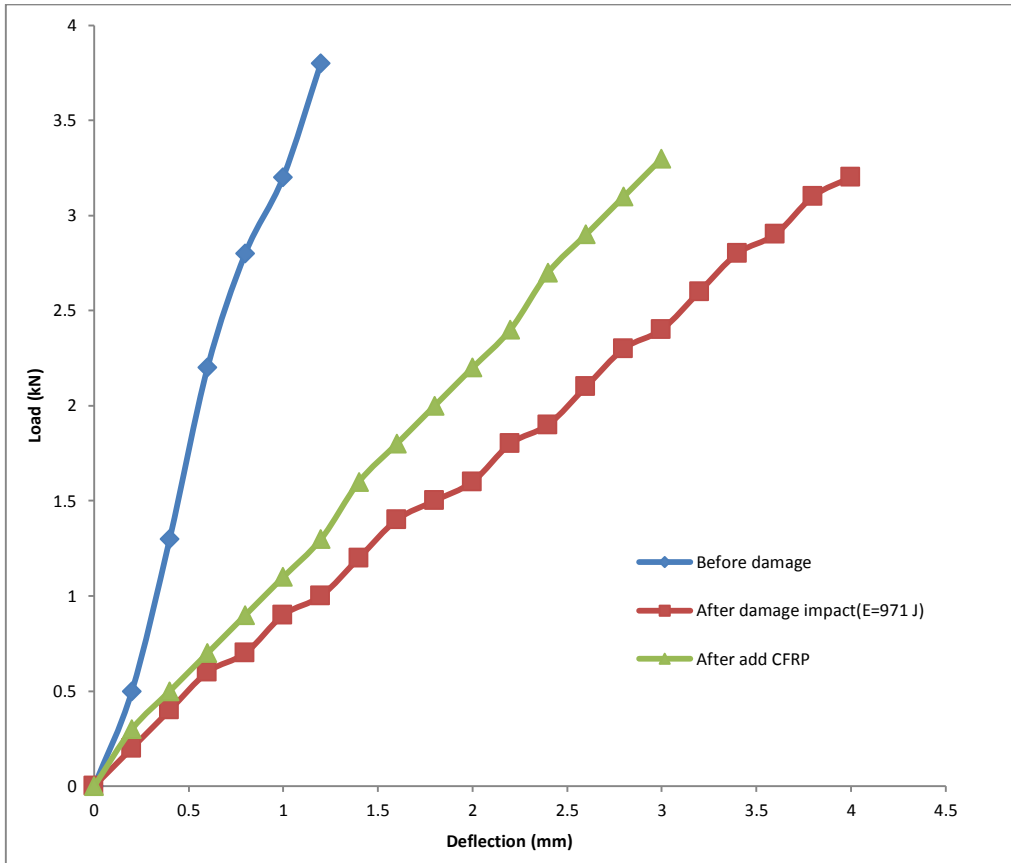
Figure 6.10 Load- deflection curves for B1-2
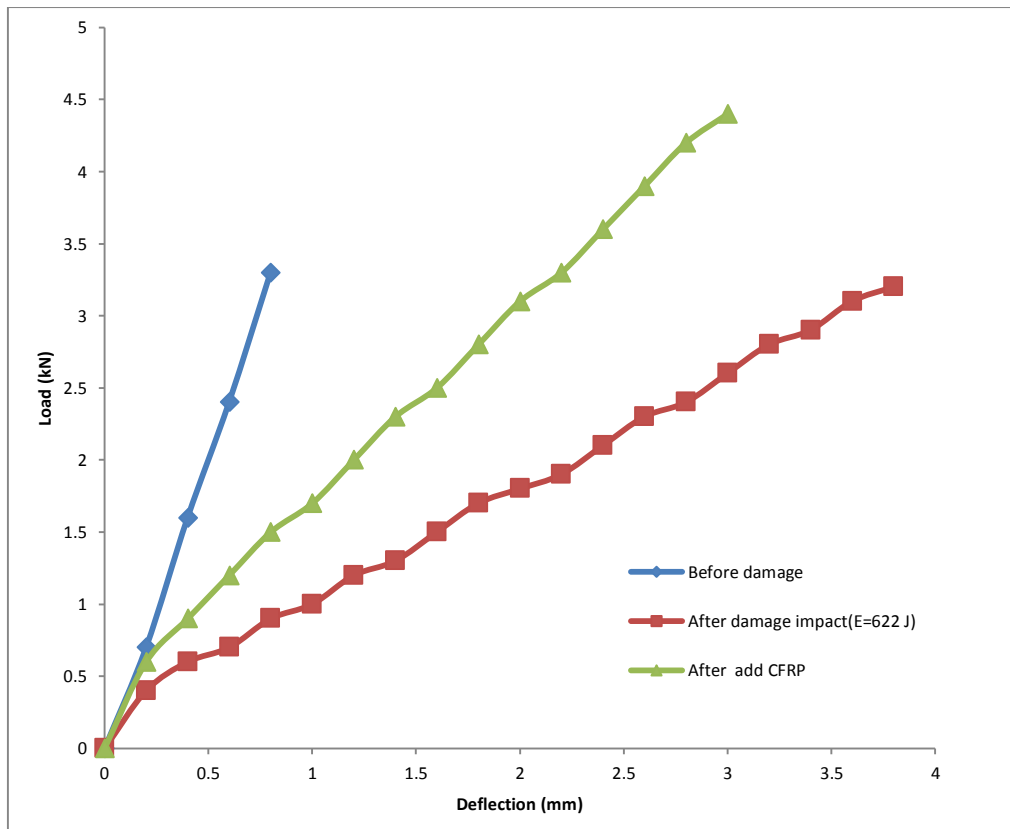
Figure 6.11 Load- deflection curves for B2-2

129
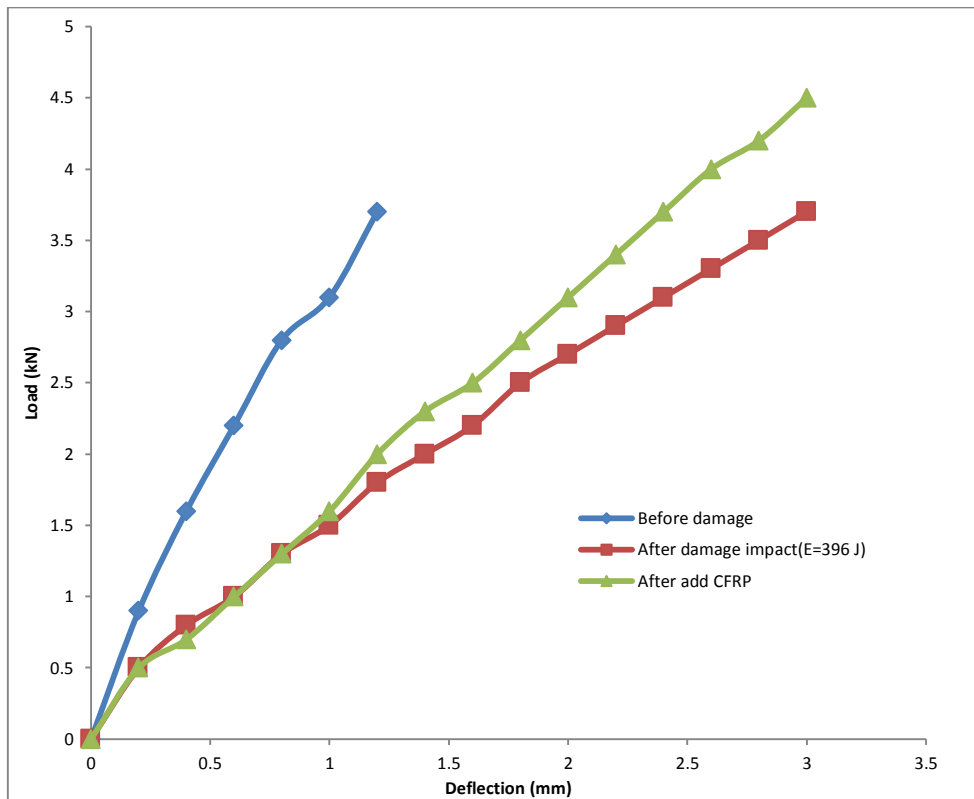
Figure 6.12 Load- deflection curves for B3-2

Figure 6.13 shows the stiffness percentage increase of damaged beams for Groups 1, 2 and 3 under different single impact energies. It is clear from Table 6.2 and Figure 6.3 that there was low enhancement in Group 1 beams (damaged heavily) and Group 3 beams (low damage) compared with Group 2 beams (intermediate damage).

Table 6.2 shows the percentage enhancement of the beam stiffness when CFRP strip was used to repair the damaged beams. When the beam was heavily damaged, as were the Group 1 beams, CFRP strip increased the beam stiffness of the damaged beam by 38%. The highest increase in damaged beam stiffness (74%) was for Group 2 damaged beams (intermediate damage). For Group 3 beams, with low damage, the CFRP strip increased the damaged beam stiffness by 19% in the Group 3 beam, a small amount compared to Group 1 and 2 damaged beams.

Under heavy damage, the Group 1 damaged beam had a high residual deflection, and a high crack length and crack width, which resulted in high stiffness reduction. Thus, the CFRP did not greatly increase the beam damage of Group 1 compared with the Group 2 damaged beam, as shown in Figure 6.13.

Despite the fact that Group 3 repaired beams had a high stiffness (1.48) compared with Group 2 repaired beams (1.39), the Group 3 stiffness increase was less than that of the Group 2 beams. This was because the damaged beam of Group 3 had lower damage and had high stiffness (1.24) compared with Group 2 damage beam stiffness (0.88), as shown in Table 6.2.

For high damage (Group 1) and intermediate damage (Group 2), the repaired beams stiffness was about a third of the undamaged beam stiffness, while with low damage (Group 3), the stiffness of the repaired beams was 43% of the stiffness of the undamaged beams, as can be seen in Table 6.2.

CFRP strip increased the damaged beam stiffness; however, the stiffness of the repaired beams was still lower than that of the undamaged beams. CFRP did not recover all the stiffness lost due to damage by impact. This was because the damaged beams already had cracks and residual deflection and these remained in the CFRP- repaired beams. CFRP decreased any further damage (increase in width and length of cracks and deformation) when the repaired damaged beams were exposed to impact load again by increasing the damaged beams stiffness, as can be seen in Figure 6.13 and Table 6.2.
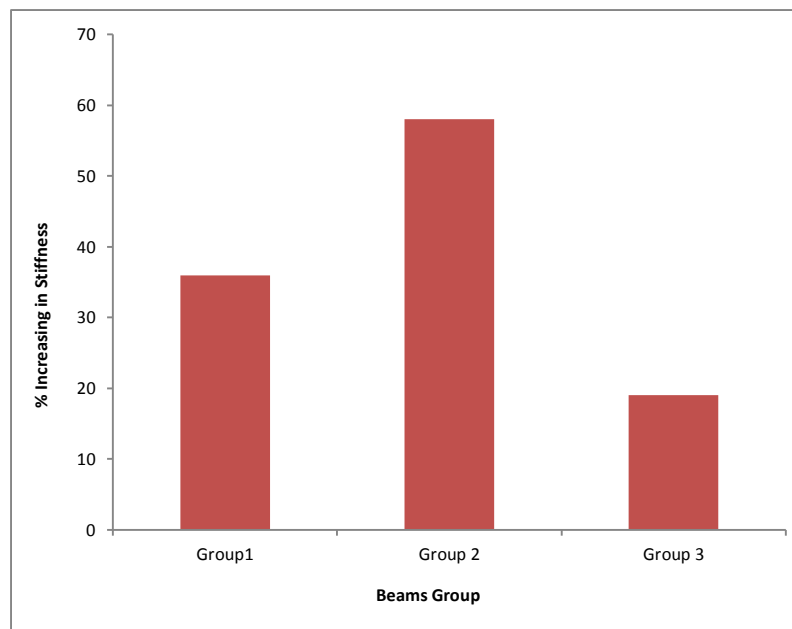
Figure 6.13 Percentage increases of the stiffness of the damaged beams under different damage impact energies

Table 6.2 Stiffness of the damaged and repaired beams

Group	beam	type	k	Damage degree	$\left(\dfrac{\text{K repaired}-\text{K damaged}}{\text{K damaged}}\right)$ %	$\left(\dfrac{\text{K}}{\text{K undamaged}}\right)$ %
1	B1-2	undamaged	3.28	-	-	-
	B1-2	damaged	0.8	heavy	-	24.4
	B1-2	repaired	1.09	-	36	33.2
2	B2-2	undamaged	4.05			-
	B2-2	damaged	0.88	intermediate	-	21.7
	B2-2	repaired	1.39	-	58	34.3
3	B3-2	undamaged	3.45	-	-	-
	B3-2	damaged	1.24	low	-	35.9
	B3-2	repaired	1.48	-	19	42.9

6.2.3 Stiffness variation of damaged and repaired beam under multi-impact loading

The first beam of each group was damaged using single impact loading. Thereafter, the damaged beams were retested under multi-impact loading up to their failure. The stiffness of the beam was measured before and after each impact test

Figure 6.14 shows the stiffness variation of Groups 1, 2 and 3 damaged beams (B1-1, B2-1, and B3-1) under different single impact loading. It was concluded that even under low impact energy, the beam lost a high percentage of its stiffness due to damage. The beam also lost a high percentage of its stiffness due to formation of cracks induced by its impact.

After damaging the beams by single impact, the damaged beams were retested under multi-impact loading up to failure. The subsequent impacts reduced the stiffness of the damaged beams. It is clear from Figure 6.15 that the multi-impacts decreased the beams stiffness by a small percentage, because the beams stiffness was already greatly decreased due to single impact used to damage the beam.
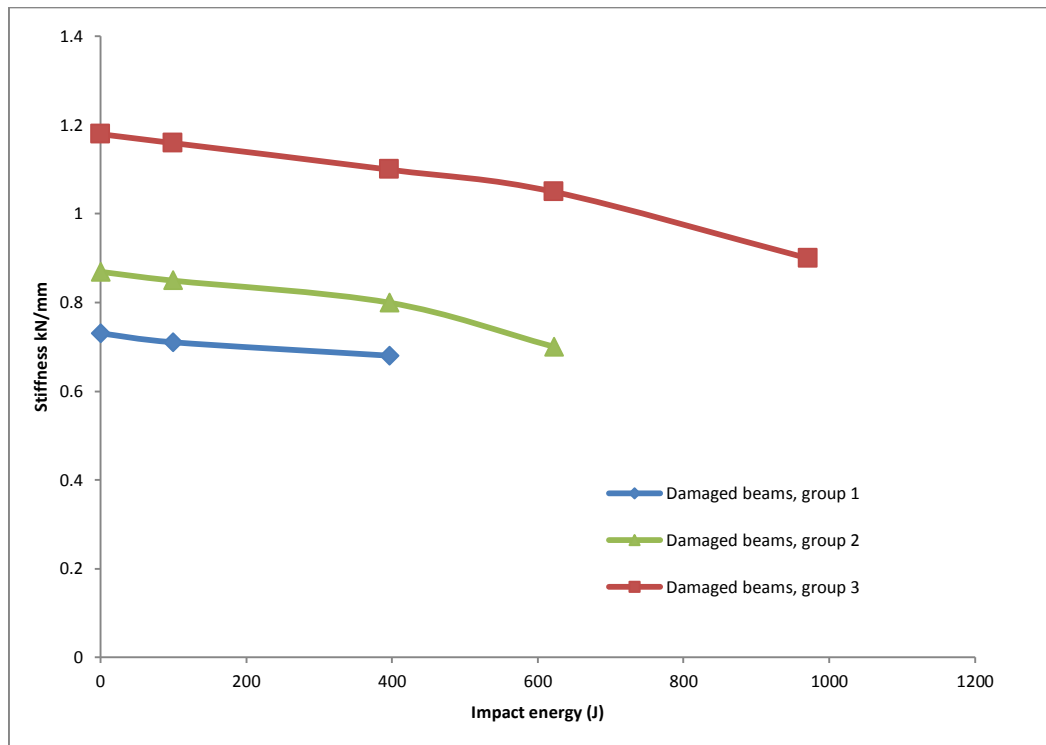
Figure 6.14 Stiffness variation of damaged beams under different impact energies

The second beams of each Group were first heavily damaged by single impact and then repaired using CFRP strip. The repaired beams were then tested under multi-impact loading and after each impact test. The CFRP strip increased the stiffness of the damaged beam. Figures 6.16 show the repaired beams stiffness of groups 1, 2 and 3 under different impact energies.

CFRP is an elastic material and that causes the CFRP- repaired beam to behave elastically. Also it did not show a high residual deflection and did not lose a high percentage of stiffness when it was multi impacted. Therefore, the beam stiffness of the repaired beam was slightly decreased under repeated impact loadings, as shown in Figure 6.15.

The high tensile modulus of the CFRP allowed the beam to resist higher impact energy. With increasing impact energy, most of tensile stresses were resisted by the CFRP strip and the beams became stiffer. Meanwhile, high impact energy caused high compressive stress at the top face of the beam in addition to the high tensile stresses at the tension zone. When the stress at the compression zone at the top face of the beam exceeded the concrete compressive strength, the beam failed by concrete crushing at the top face. This type of failure appeared in all the NSM CFRP

repaired beams. After visual inspection the failed beams, no debonding failure was indicated when the NSM technique was used to repair the damaged beam. The NSM technique increased the bonding surface between the concrete and the CFRP strip, as demonstrated at the strengthening stage of the experimental work
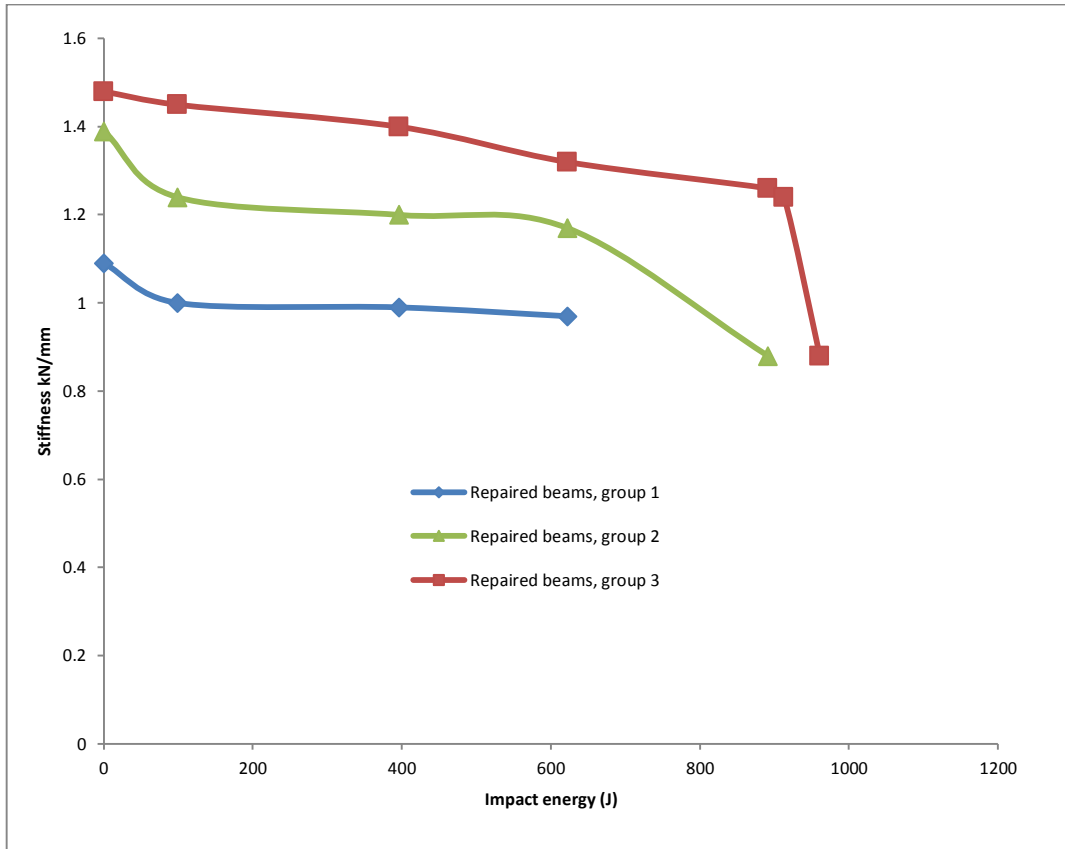
Figure 6.15 Stiffness variation of repaired beams under different impact energies

6.3 Impact energy of the damaged and repaired beams

As discussed in Section 5.3.6, the accumulative impact energy of the beam is not equal to the exact impact resistance of the beam. In this study, comparisons of accumulative impact energies were used to qualify but not quantify the performance of the repaired beams under impact loading.

The accumulative impact energy was found by summing the total impact energies applied on the beam. A comparison was made between the results of the accumulative impact energy of control, damaged and repaired beams as shown in Figure 6.16. It was clear that, with an increasing degree of damage, the accumulative impact energy of the damaged beams was decreased proportionately. Accumulative impact energy was ranked Group 1 (heavy damage) < Group 2 < Group 3 (low damage) = control beam. The highest reduction in the accumulative impact energy was for the Group 1 beams, which were heavily damaged compared with the control beam. For the Group 2 beams, the drop height of mass was reduced to decrease the degree of damage. The reduction of the accumulative impact energy of Group 2 was intermediate. For the Group 3 beams, the beams were damaged by low impact energy to induce a low degree of damage. The low damage had no effect on the accumulative impact energy of the beam compared with control beam.

Figure 6.16 shows that the CFRP strip increased the accumulative impact energy of the damaged beams. For Group 2, with intermediate damage, the CFRP strip increased the impact energy of the damaged beam to a level equal to that of the control beam. With the low damage, the impact energy resisted by Group 3 repaired beams was greater than for the control beam. Group 3 beams were heavily damaged, thus the CFRP increased the accumulative impact energy of damaged beams by a low amount. The accumulative impact energy of the Group 3 repaired beam was less than that of the control beam and higher than that of the damaged beam.

The comparisons of control, damaged and repaired beams showed that CFRP increased the damaged beams capacity to resist more impact energy. The damaged beams were already cracked and had residual deflection. The CFRP decreased the width of these cracks and their propagation due to impact force. The CFRP

decreased maximum deflection and any additional increase in the residual deflection of the damaged beam.
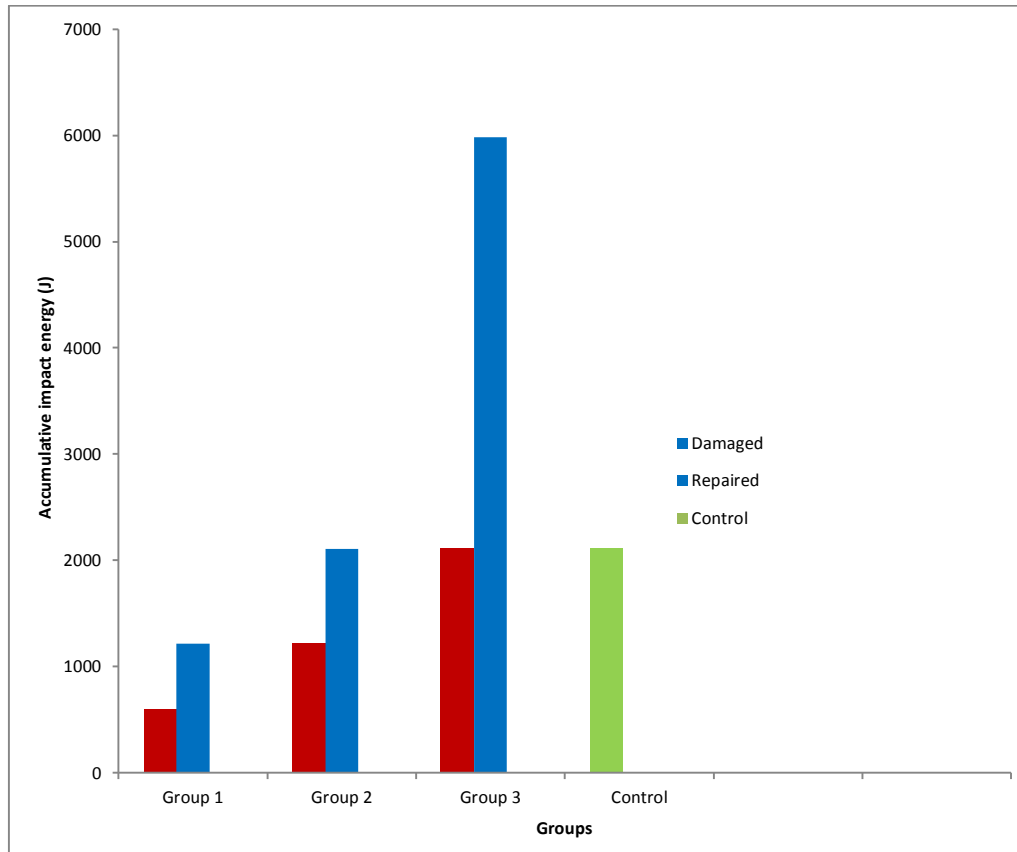
Figure 6.16 Accumulative impact energy of the of the reference, damaged and repaired beams

6.4 Behaviour of damaged and repaired beams under impact loading

In this section, comparisons between the damaged and repaired beam for each single impact test were made in terms of bending load, impact force and maximum and residual deflection

6.4.1 Bending load P_b

For this experimental work, the bending load at any time will be equal to the sum of the supports' reactions. The reaction force at each time was recorded using a force sensor mounted on the support. By assuming symmetry in the beam, the bending load at any time will be equal to the summation of the reaction forces of the supports.

Figures 6.17-6.19 shows the bending load for different impact energies applied on the Group 1-3 beams respectively. From these figures, it is clear that the bending load of the damaged beams is higher than that of the repaired beams. The damaged beams were already cracked and hid residual deflection. These cracks and deformations reduced the damaged beam's elasticity and inertia force. This in turnreduced the impact energy absorbed by the damaged beams and increased the energy transferred to the beam support ,which resulted in a high bending load compared with the repaired beam.

The CFRP increased the inertia force elasticity of the damaged beam. Hence, most of the impact energy is absorbed by the repaired beam vibration and the balance transferred to the beam support.

Figures 6.17-6.19 show that the bending force increases with an increasing percentage of damage. The damaged and repaired beams of Group 1, which are heavily damaged, have a high bending force compared to those of Group 2 (intermediate damage) and Group 3 (low damage).
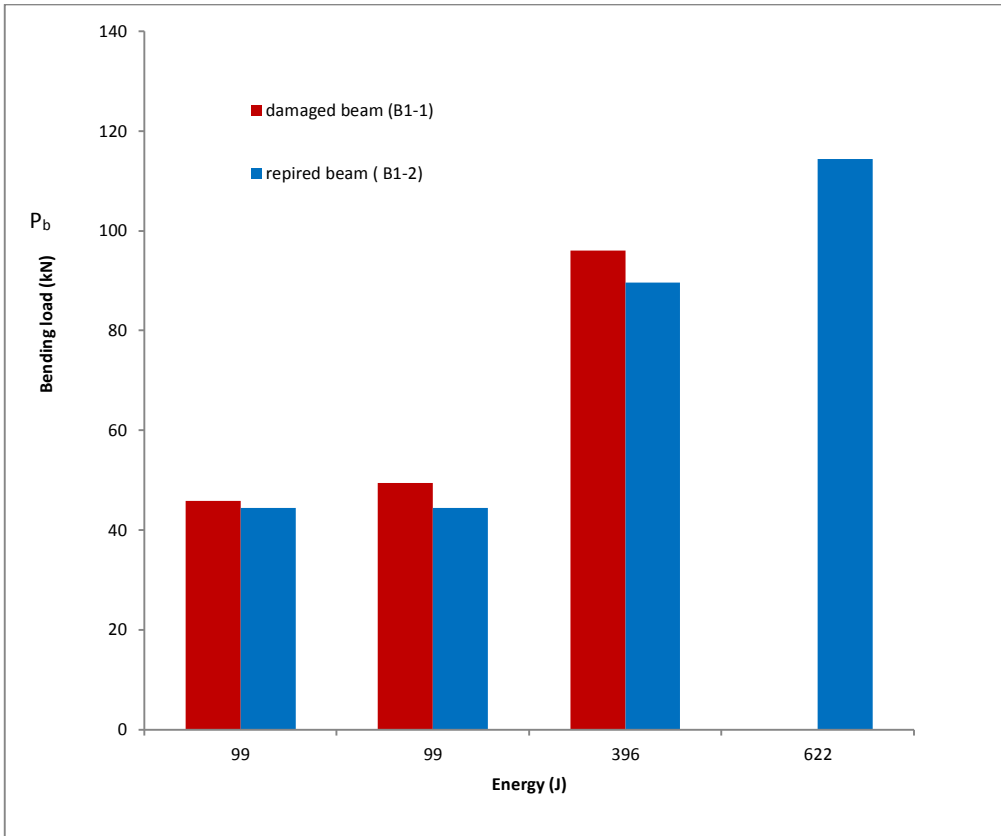
Figure 6.17 Bending load of Group 1 beams at different impact energies
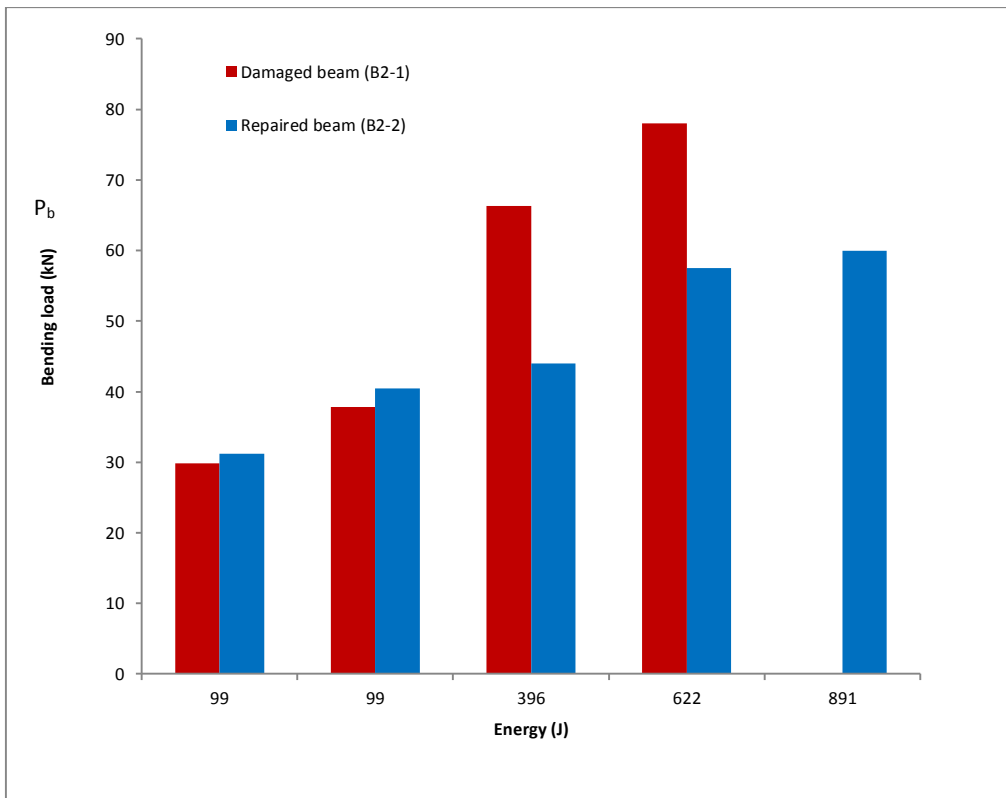
Figure 6.18 Bending load of Group 2 beams at different impact energies
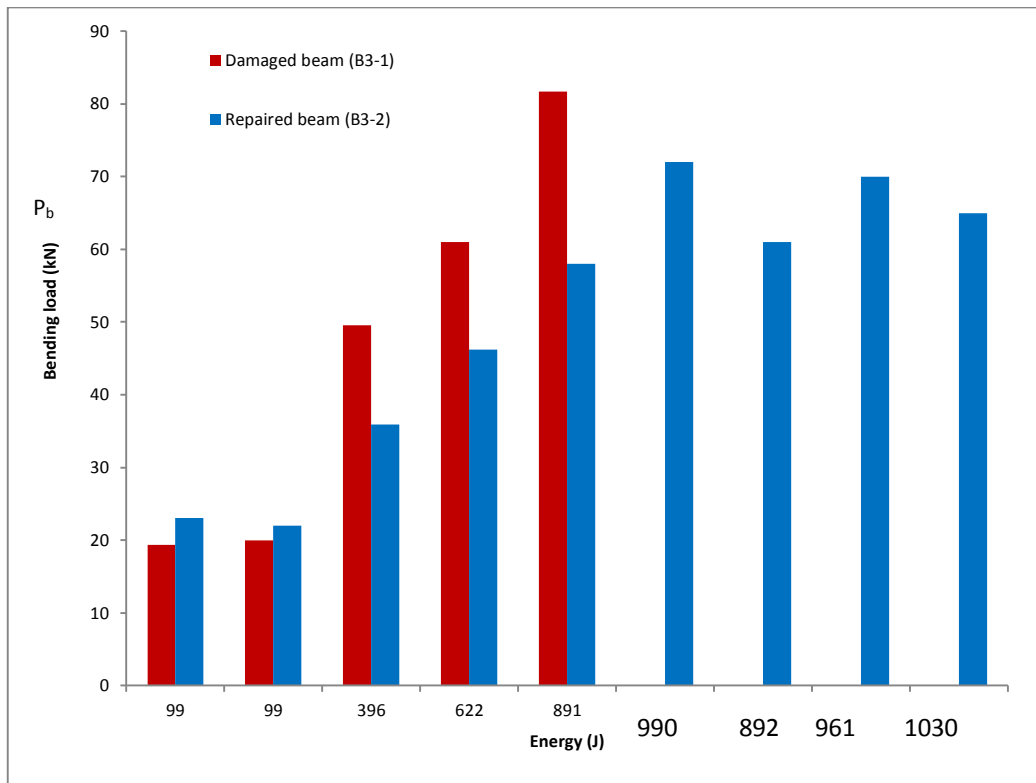
Figure 6.19 Bending load of Group 3 beams at different impact energies

6.4.2 Impact force P_t

Figures 6.20-6.22 shows the impact force of the tested beams for each single impact loading for Group 1-3 respectively. The difference between the impact force t of the damaged and repaired beams is proportional to the degree of damage. As the percentage damage is decreased, the impact force is increased.

For Group 1 and 2, the impact force for the damaged beam was slightly less than that of the repaired beam. This is because the damaged beam was already damaged and cracked. The cracks and deformations reduce the beam stiffness and this decreases the impact resistance of the beam. CFRP increased the stiffness of the damaged beam; however, the heavy damage will still affect beam behaviour.

In Group 3, with low damage, the impact force for the damaged beam is higher than that of the repaired beam. CFRP increased the stiffness of the damaged beam and that decreased the impact force of the repaired beam. Increase in beam stiffness decreased the impact force induced, as discussed in section 5.3.1.
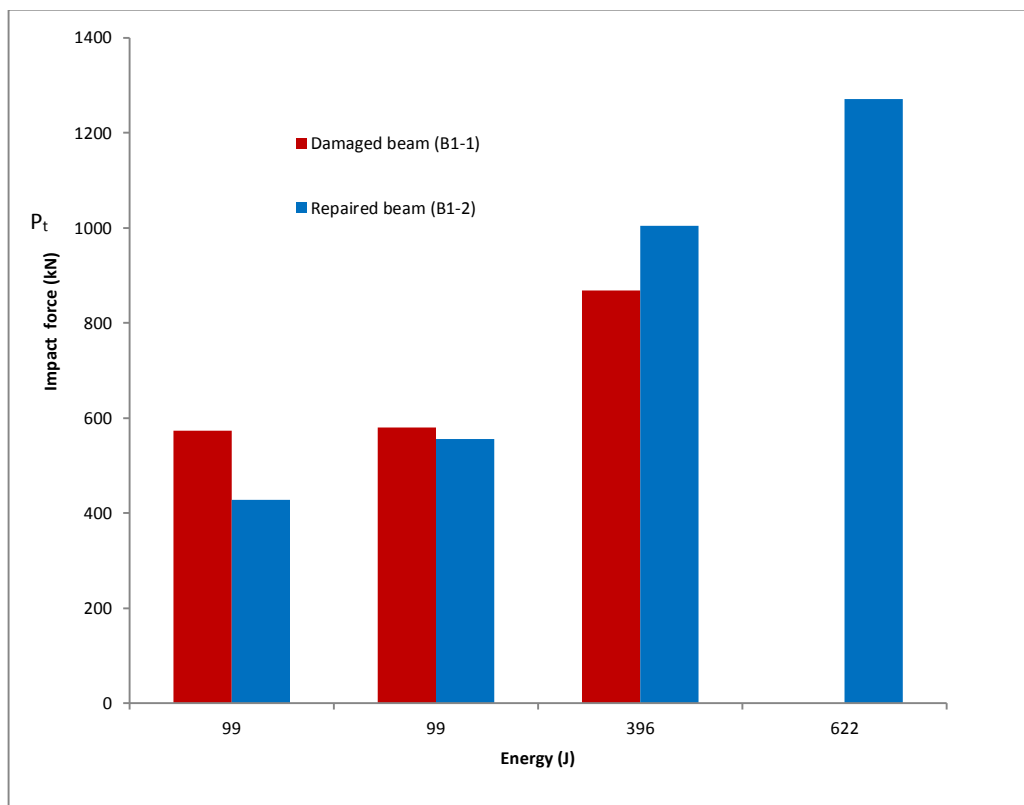
Figure 6.20 Impact forces of Group 1 beams at different impact energies
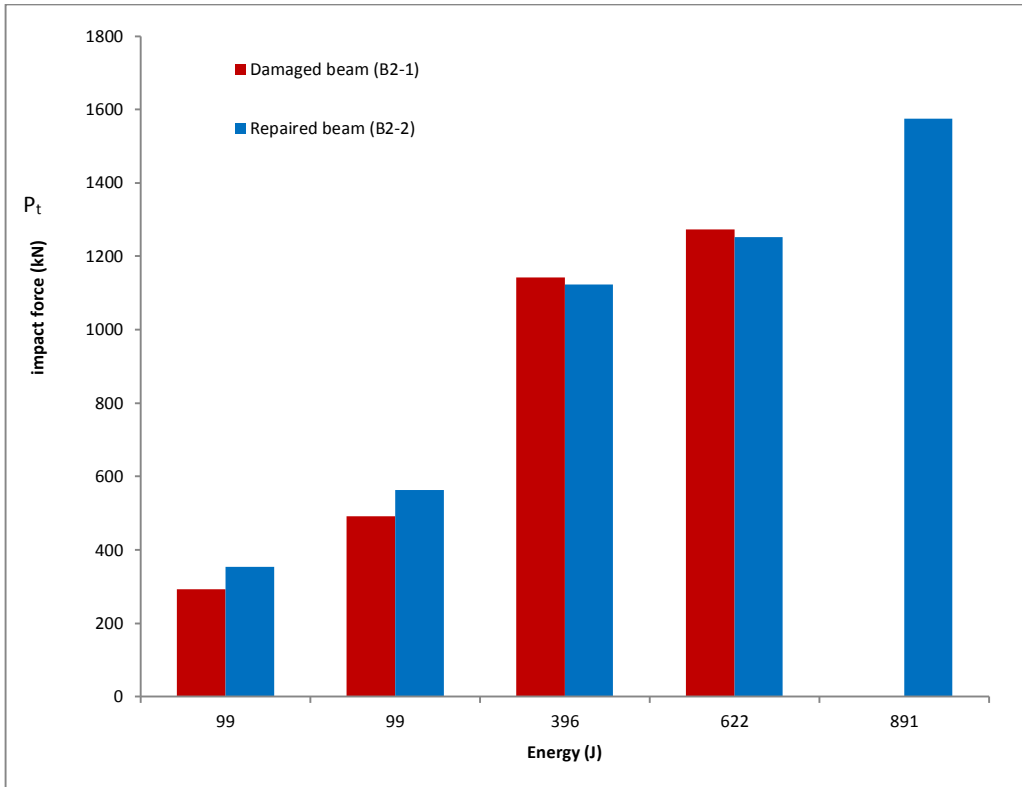
Figure 6.21 Impact forces of Group 2 beams at different impact energies
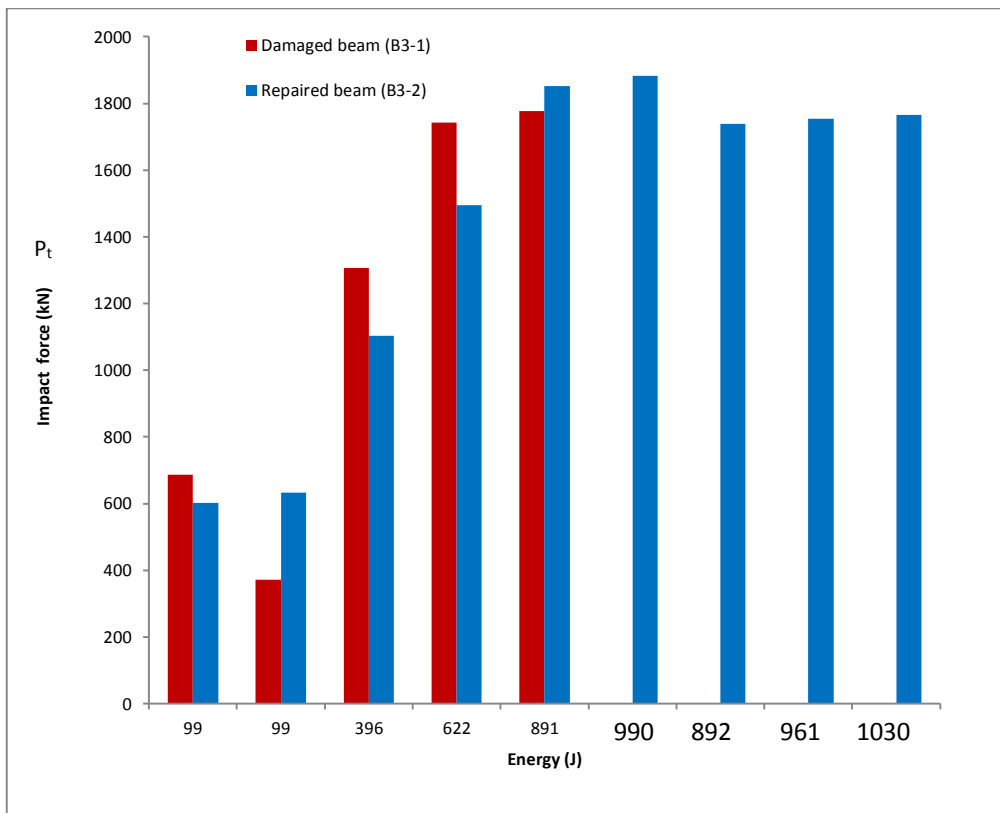
Figure 6.22 Impact forces of Group 3 beams at different impact energies

141

6.4.3 Maximum and Residual deflection of damaged and repaired beams

Figure 6.23 shows the mid-span maximum deflection of Group 1 damaged and repaired beams (B1-1, B1-2) for different impacts. This figure shows that the maximum deflection of the damaged beam is greater than that of the repaired beam. The damaged beam had many cracks due to damage by impact load. The damage reduced the beam stiffness and increased the beam's maximum deflection. The CFRP increased the beam stiffness, which reduced maximum deflection of the repaired beams compared with that of the damaged beam.

The same trend was indicated in Group 2 and Group 3 beams as shown in Figures 6.24 and 6.25 respectively.
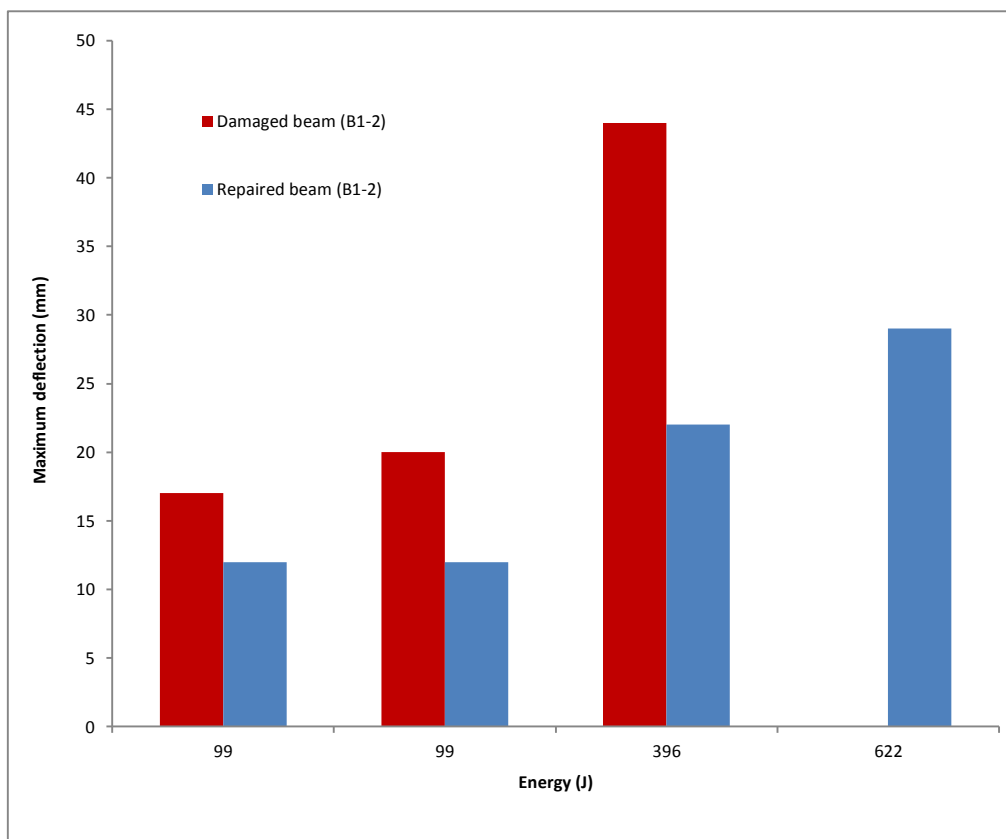
Figure 6.23 Maximum deflection of Group 1 beams at different impact energies
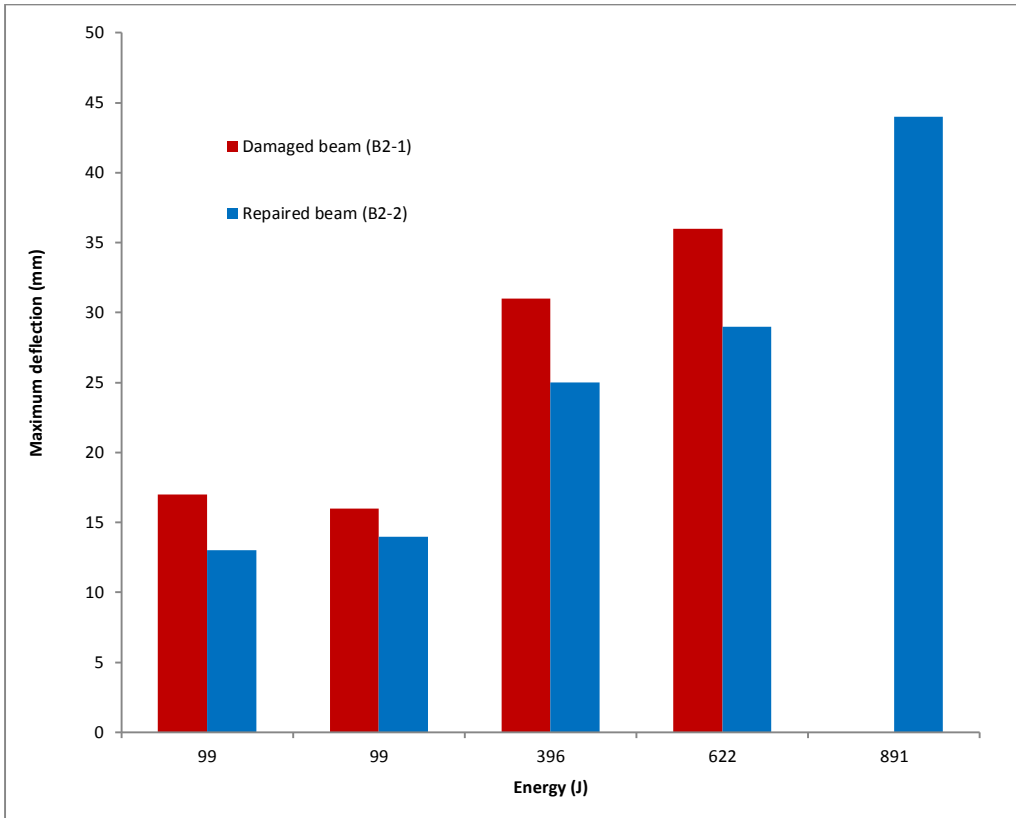
Figure 6.24 Maximum deflection of Group 2 beams at different impact energies
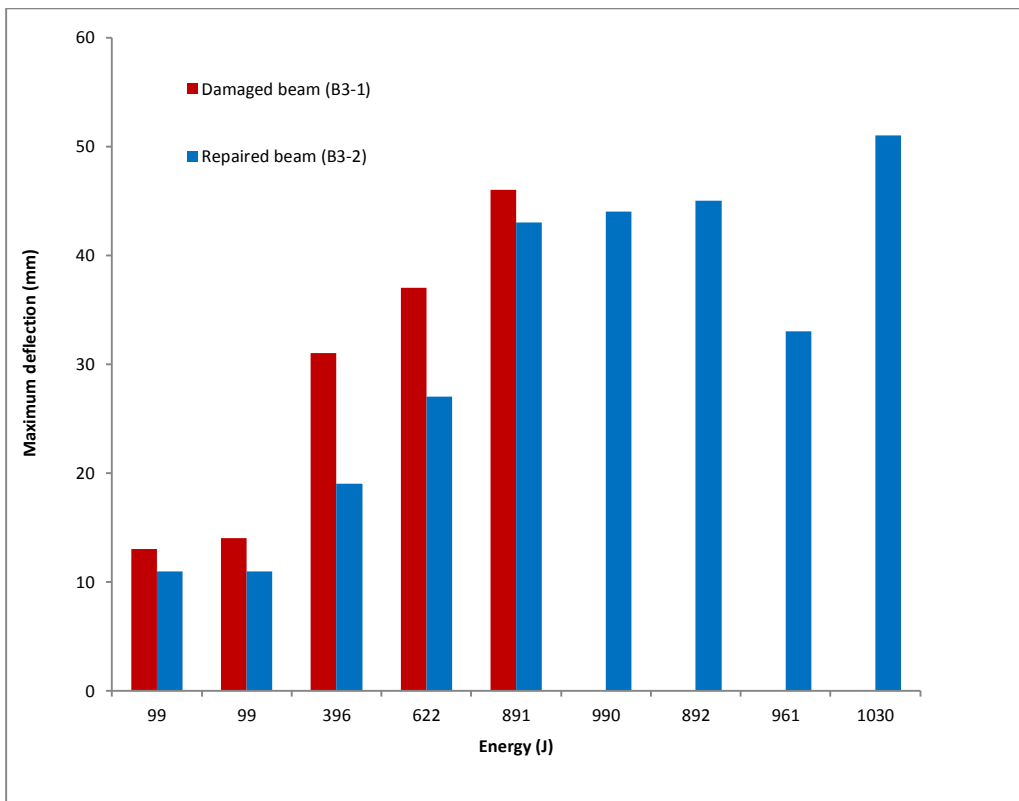
Figure 6.25 Maximum deflection of Group 3 beams at different impact energies

Figure 6.26 shows the residual deflection of the Group 1 beams after each single impact loading. The CFRP strip increased the stiffness of the repaired beam and reduced residual deflection. The repaired beams were so stiff that they had a minimal residual deflection, which disappears from the graph when scaled for the control beam. The damaged and repaired beams of Group2 and 3 show the same behaviour as Group 1 beams. Figure 6.27 and Figure 6.28 show the residual deflection for each single impact for Group 2 and Group 3 beams respectively. In repaired beams, CFRP strip decreased the length and width of the cracks, which increased the beam stiffness. The high stiffness of the repaired beams decreased the maximum and residual deflections. It is clear from the figures that the damage degree is inversely proportional to the stiffness of the beam.
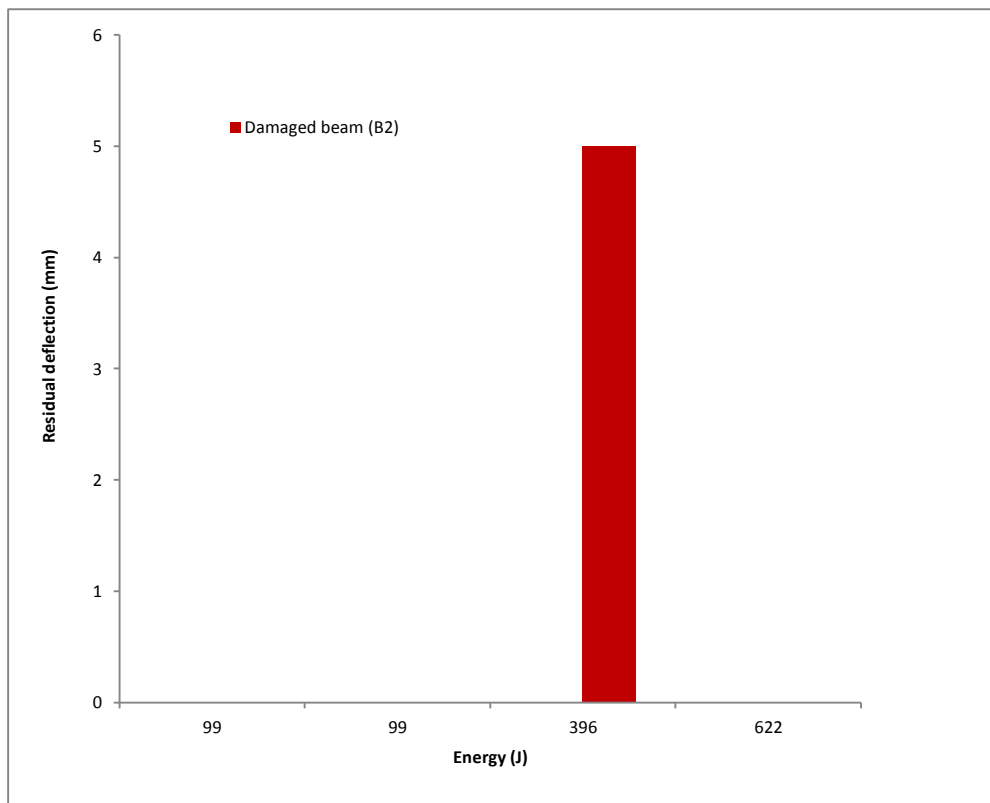
Figure 6.26 Residual deflection of Group 1 beams at different impact energies

144
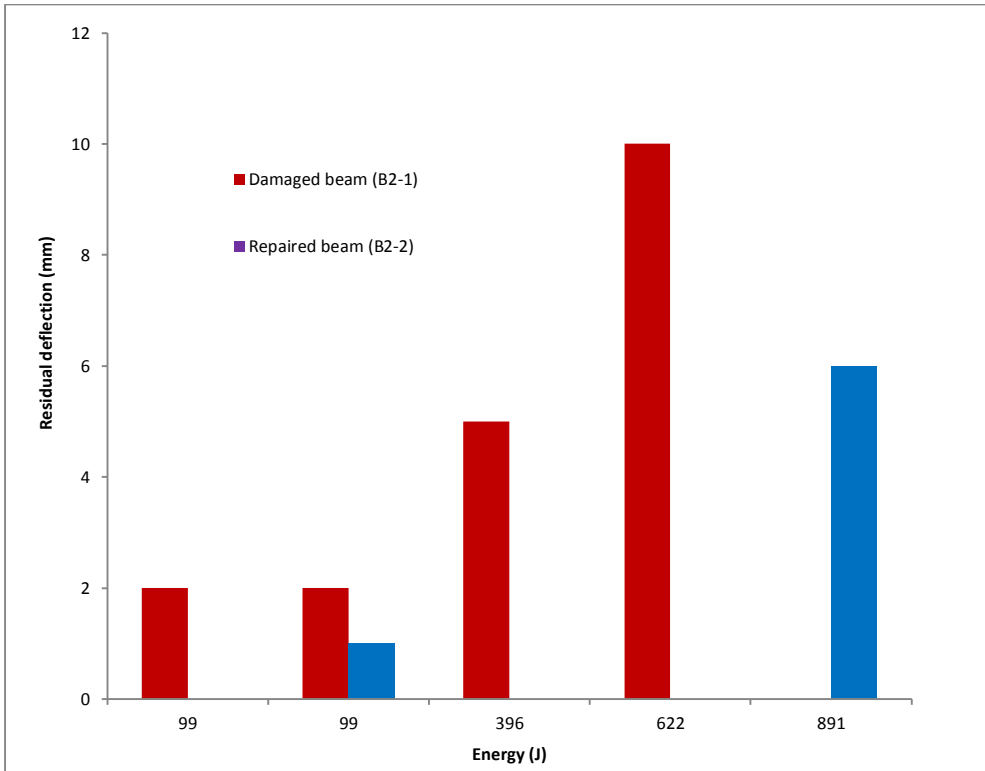
Figure 6.27 Residual deflection of Group 2 beams at different impacts energies
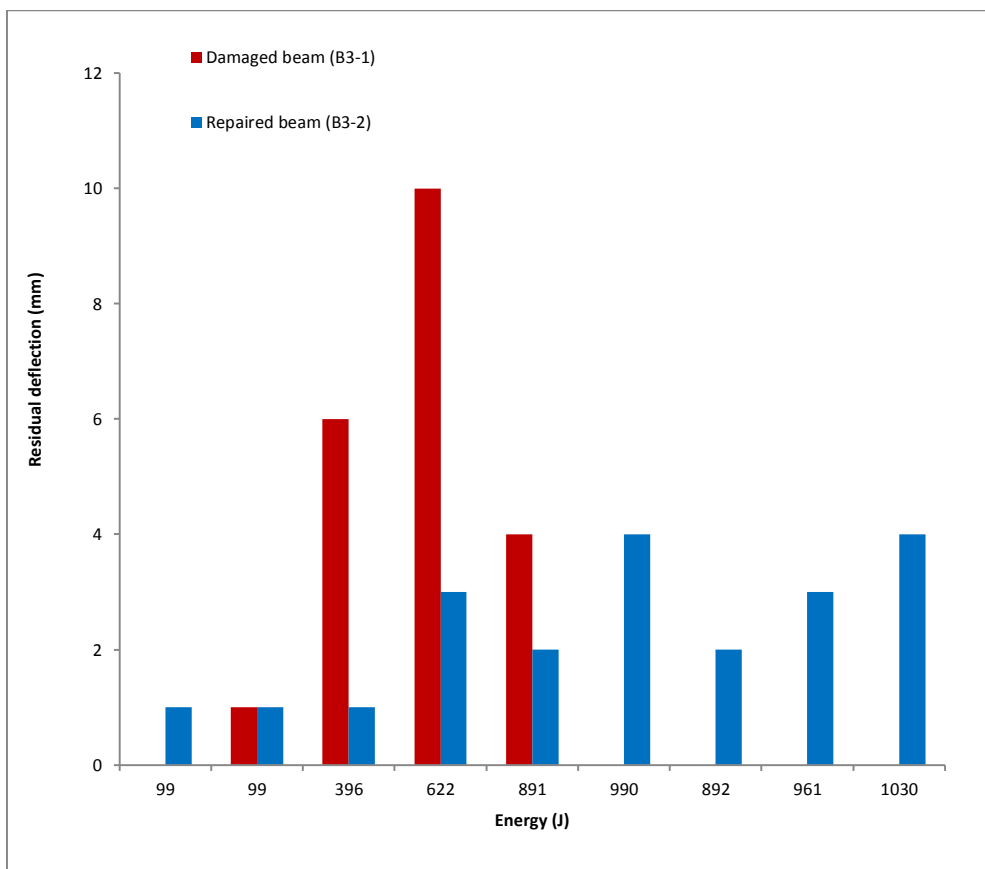
Figure 6.28 Residual deflection of Group 3 beams at different impact energies

145

6.5 Crack distribution in the beams under impact loading

The impact load induced many cracks in the beams, which reduced their stiffness. Figure 6.7 illustrates the crack distribution along the beam length of the damaged beams (B1-1, B2-1, B3-1). Table 6.3 shows the length, width and position of the cracks in the damaged beams. It can be seen from Figure 6.7 that the beam was cracked and deformed due to impact load. Increased damage decreases the beam stiffness due to an increase in beam cracks numbers, width and length. Due to heavy damage, the length and width of cracks in the beam 1-1 of Group 1 were more than that of Group 2 and 3. As can be seen from Table 6.3, the cracks in beam B3-1 were minor, with a width of 0.01-0.02 mm. This was because the mass dropped from a low height of 0.2 m. The width and length of mid-span cracks increased with increasing drop height and impact energy in beams 2-2 and beam 2-1.

It is clear from Figure 6.7, B1-1, that under high impact loading (891 J), cracks appeared at the top face of the beam. When the damaged beams were retested under impact loading, more top cracks were appeared. This indicates that beam vibration due to impact is another source of cracking, in addition to tensile stresses.

Table 6.3 Crack length, width and location in damaged beams

B1-1, Damage impact , H=0.46 m													
Crack No	7L	6L	5L	4L	3L	2L	1L	1R	2R	3R	4R	5R	6R	7R
Length mm	200	214	200	130	132	160	138	180	85	120	147	85	117	140
Width mm	0.02	0.02	0.1	0.1	0.1	1.35	0.74	1.4	0.06	0.12	0.1	0.2	0.02	0.01
Distance From Centre mm	1011	846	672	456	304	133	75	50	235	321	506	679	846	1001

B2-1, Damage impact , H=0.318 m													
Crack No	6L	5L	4L	3L	2L	1L	1R	2R	3R	4R	5R	6R	7R	8R
Length mm	78	100	115	140	98	150	180	60	100	110	128	95	200	40
Width mm	0.2	0.04	0.2	0.1	o.1	0.4	1.6	0.1	0.06	0.12	0.1	0.04	0.08	0.08
Distance From Centre mm	758	558	418	293	148	50	20	168	208	330	502	626	793	971

B3-1, Damage impact , H=0.2 m													
Crack No	6L	5L	4L	3L	2L	1L	1R	2R	3R	4R	5R	6R	7R	
Length mm	50	50	72	121	112	108	158	145	115	93	112	115	70	
Width mm	0.02	0.02	0.02	0.02	0.02	0.02	0.2	0.1	0.02	0.02	0.02	0.02	0.01	
Distance From Centre mm	844	612	420	283	149	95	37	229	345	490	650	793	903	
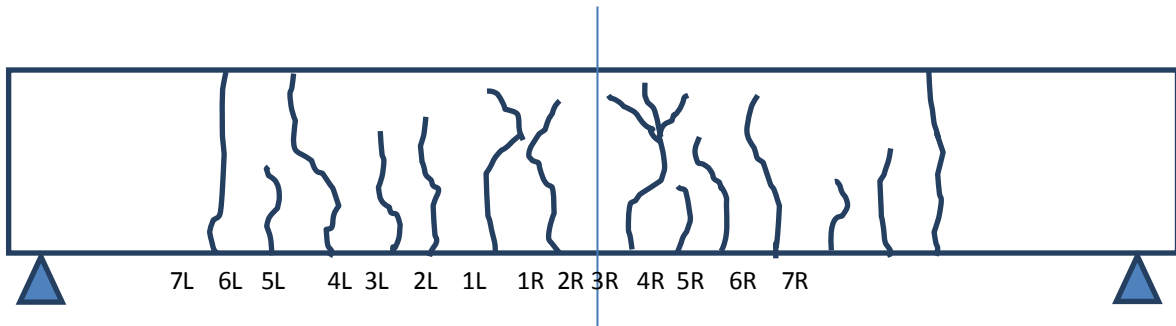
B1-1 Damage impact, impact energy (891 J)
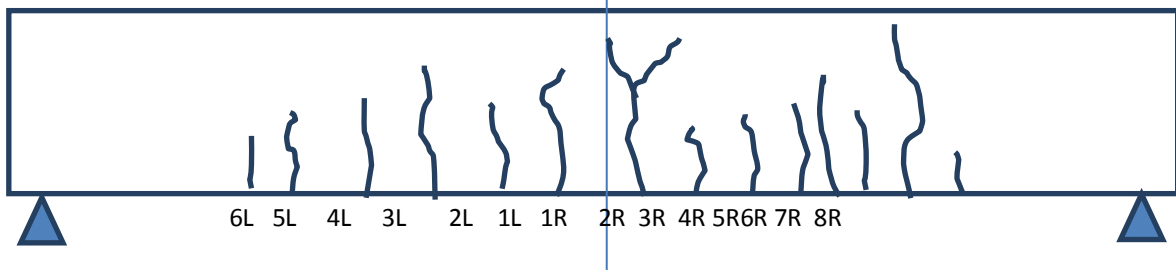
B2-1   Damage impact, impact energy (622 J)
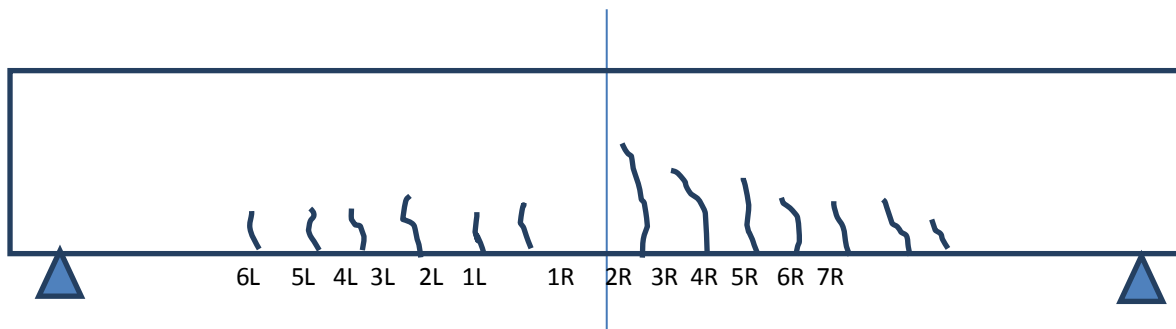
B3-1   Damage impact, impact energy (396 J)

Figure 6.7 Crack distribution of damaged beams

It can be seen from Figure 6.7 and Table 6.3 that about two-thirds of the beam length was damaged. The damages were distributed between cracks 7L to 7R, located about 1 m from the beam centre. This means that not all beam lengths was affected and damaged by the impact. Only 2/3 of beam length was damage by impact and that is consistent with the choice of 2/3 for proportion of damaged beam in FE modelling.

6.6 Proposed equations

Empirical equations were proposed to predict the bending load and the maximum deflection of the damaged and repaired beams. The main variables were the impact energy and the beam stiffness. Regression analysis of the experimental data was used to find the proposed equations. Two variables were used in the equations, impact energy and beam stiffness. The experimental results showed that the bending load mainly depends on the impact energy. The beam stiffness reflects the damage in the beam due to cracks and deformation. The standard error (SEE) was used to evaluate the proposed equations. The standard error measured the amount of error in the prediction of the bending load and the maximum deflection.

$$SEE = \sqrt{\frac{\sum_{i=1}^{n} \varepsilon_i^2}{n-2}}$$ 6.4

6.6.1 Bending load of the damaged and repaired beams under impact loading

By using regression analysis, the following equations were proposed to predict the bending load of the damaged and repaired beams under impact loading. For the damaged beams, the following equation can be used to predict the beam bending load.

$$P_b = \frac{3.27 EN^{0.48}}{K^{0.06}}.$$ 6.5

Where:

P_b:- Damaged beam bending load under impact loading (kN)

EN:- impact energy (J)

K:- elastic beam stiffness (kN/mm)

The results of the regression analysis show that the bending load for the damaged beams depends mainly on the applied impact energy ($EN^{0.48}$). The stiffness of the damage beam slightly affected the bending load ($K^{0.06}$). The experimental results show the damaged beams lost the majority of its stiffness even under low impact energy. For verification, the bending load calculated from the Eq. 6.5 was compared with experimental results as shown in Table 6.4. A good agreement was found between the calculated and experimental results with SEE= 6.8 as shown on Table 6.5.

Table 6.4 experimental and theoretical bending load comparison of the damaged beams

Energy J	Stiffness, K kN/mm	Bending force P_b, Experimental kN,	Bending force P_b, Equation 6.5 kN	$\frac{C4 - C3}{C3} * 100$
971	3.26	85.3	80.5	6
622	0.71	66.3	71.7	8
622	3.55	68.0	64.8	5
99	0.88	33.8	29.5	13
396	0.9	66.3	57.0	14
622	0.8	78.0	71.2	9
396	3.45	45.2	52.3	16
396	1.25	49.5	55.8	13
622	1.23	61.0	69.3	14
891	1.2	81.7	82.3	1
SEE		6.8		

For the repaired beams, the bending load of the damaged beams can be found from the following proposed equation.

$$P_b = \frac{2.38EN^{0.48}}{K^{0.15}}. \hspace{3cm} 6.6$$

The beam stiffness affected the bending load of the repaired beams more than that of the unrepaired damaged beams, as the CFRP strip increased the beam stiffness.

The results of the proposed equation were compared with that of experimental results for verification purposes, as shown in table 6.5. The comparison shows a good correlation between the experimental and calculated bending load. The SEE was equal to 4.37.

Table 6.5 Experimental and theoretical bending load comparison of the repaired beams

Energy J	Stiffness, K kN/mm	Bending force P_b, Experimental kN,	Bending force P_b, Equation 6.6 kN	$\dfrac{C4 - C3}{C3} * 100$
99	1.11	22.2	21.8	2
396	0.9	44.8	44.0	2
622	0.97	57.2	54.2	5
622	1.2	57.5	52.4	9
891	1.17	60.0	62.7	4
99	1.48	22.5	20.8	7
396	1.45	35.9	40.9	14
622	1.4	46.2	51.2	11
891	1.32	58.0	61.5	6
990	1.26	72.0	65.2	9
892	1.24	61.0	62.2	2
961	1.2	70.0	64.8	7
1030	0.88	65.0	70.2	8
SEE		4.37		

6.6.2 Maximum deflection of the damaged and repaired beams under impact loading

The following equation can be used to find the maximum deflection of the damaged beams under impact loading.

$$MaxDef = \frac{1.52EN^{0.51}}{K^{0.27}}. \hspace{3cm} 6.7$$

Where:

Max Def: maximum deflection (mm)

EN: Impact energy (J)

K: beam stiffness (kN /mm)

According to Eq. 6.7, the beam stiffness affects the damaged beam maximum deflection ($K^{0.27}$). The cracks and deformation reduce the beam stiffness and that increases the deflection of beam under impact loading. Table 6.6 shows the comparison between the experimental maximum deflection and that obtained from the proposed equation (Eq. 6.7). A good agreement was found between the experimental and calculated maximum deflection.

Table 6.6 Experimental and theoretical maximum deflection comparison of the damaged beams

Energy J	Stiffness, K kN/mm	Max. deflection, Experimental kN,	Max. deflection, Equation 6.7 kN	$\frac{C4 - C3}{C3} * 100$
99	0.81	18	17	6
396	0.71	44	36	19
99	0.88	14	16	18
396	0.9	31	33	7
622	0.8	36	43	20
99	1.28	12	15	24
396	1.25	31	30	2
622	1.23	43	39	10
891	1.2	46	47	1
	SEE	4.87		

For the repaired beams under impact loading, the following equation was proposed:

$$MaxDef = \frac{0.5EN^{0.65}}{K^{0.026}}.$$ 6.8

Under different impact energies, the repaired beam stiffness was slightly reduced, as CFRP is very stiff, and the repaired beam showed approximately elastic behaviour. The predicted maximum deflection was close to that of the experimental tests and the SEE was equal to 2.83, as shown in Table 6.7

Table 6.7 Experimental and theoretical maximum deflection comparison of the repaired beams

Energy J	Stiffness, K kN/mm	Max. deflection, Experimental kN,	Max. deflection, Equation 6.8 kN	$\frac{C4-C3}{C3} * 100$
99	1.11	12	10	16
396	0.99	22	25	14
622	0.97	29	34	16
99	1.53	13	10	21
396	1.24	25	25	1
622	1.2	29	34	16
891	1.17	44	43	3
99	1.48	13	10	22
396	1.45	26	25	3
622	1.4	35	34	3
891	1.32	43	43	1
990	1.26	44	46	4
892	1.24	44	43	3
SEE		2.83		

In practice, the stiffness (k) of damaged or CRP- repaired beams can be discovered by using partial static tests, as used in this experimental work (see Section 4.6.2). When the stiffness has been determined, the bending loading and maximum deflection of damaged or CFRP- repaired beams under different impact energies can be calculated using the proposed equations (6.5, 6.6, 6.7 and 6.8).

6.7 Concluding remarks

RC beams were damaged in this experimental work by using different impact energies. The impact load considerably reduced the stiffness of the beams. The initial beam stiffness was reduced by 76% under high and intermediate impact energy. The beam stiffness was decreased by a high percentage (67%), even under low impact energy. The impact force applied to the beam caused high bending force on the beam, which cracked and deformed the beam heavily. An equation (6.3) was proposed to predicate the beam stiffness after damage by the impact load.

CFRP strips were used to repair the damaged beams using the NSM technique. CFRP increased the stiffness of the damaged beams. The CFRP increased stiffness by 38%, 74% and 19 % for heavy, intermediate and low damaged beams respectively. CFRP strip decreased the propagation and the increasing in the length and width of cracks in damaged beams when impacted. Thus the repaired damaged beams resisted more accumulative impact energy and showed low residual and maximum deflection.

The empirical equations (6.5, 6.6, 6.7, and 6.8) that were proposed in order to find the bending force and maximum deflection of the damaged and repaired beams gave a good agreement with the experimental results. The bending force and maximum deflection depend mainly on impact energy. The beam stiffness had a slight effect on the bending force and maximum deflection of the damaged beams. This was because the damaged beams had already lost high percentages of their stiffness due to damage; whereas the stiffness of the repaired beams had a strong effect on the bending force and maximum deflection when compared to the damaged beams. The reason for this was that the CFRP increased the stiffness of the damaged beams.

7. Finite Element Analysis (FEA) of CFRP strengthened beams under static loading

7.1 Introduction

Experimental work is costly and time consuming, especially with large-scale components. A reliable analytical model that closely predicts the true behaviour of RC structural elements can dramatically reduce the number of expensive laboratory tests. In this chapter, FEA are used to closely predict the behaviour of the RC beam under impact loading with and without CFRP.

The beams tested experimentally in this project were modelled and analysed using FEM. The LUSAS-FEA software was used in the analysis. A model-updating technique was used to model the strengthened RC beams. The Genetic Algorithm (GA) was used as the model-updating tool to tune some of the parameters within the analytical model. The behaviour of the RC beams without CFRP was initially investigated using the FEA. Then the CFRP- strengthened beams were analysed using the model-updating technique. The bond between the reinforcement bars and the surrounding concrete was modelled using joint elements that connect the steel reinforcements and concrete through "springs". The damage to the beams was modelled by reducing the bonding between the steel bars and the concrete and reducing the elastic modulus of the concrete.

For validation purposes, the analytical results were compared with the experimental load-deflection curves and ultimate failure load.

7.2 Case study

Prior to the modelling the beams tested experimental in this research, RC beams (with and without CFRP) that had been tested elsewhere and reported in the literature were used in the analytical study. Esfahani et al. (2007) investigated the behaviour of RC beams strengthened with CFRP under static four-point flexural loading. The EBR technique was used to strengthen the RC beams using CFRP sheets. The effect of the steel reinforcement ratio and the length, number and width of CFRP sheets were examined. Twelve RC beams were tested up to failure. The dimensions of the tested beams were 150 mm width, 200 mm depth and 2000 mm length. Figure 7.1 shows the beam dimensions and details. Three of the RC beams without CFRP were considered as reference beams. The other nine beams were externally strengthened with CFRP using different reinforcement ratios. Table 7.1 illustrates the details of the tested beams. Test specimens are named as Ba-bD-cLd. The letters a, b, c, and d refer respectively to beam numbers, tensile bar diameter, the number of layers and the width of CFRP sheet. The RC beams were divided into three groups of four beams with 12 mm, 16 mm or 20 mm longitudinal bottom reinforcement bars. The experimental results of the RC beams strengthened with CFRP were compared with those of control beams in terms of the load-deflection curve, the mode of failure and the ultimate load. The results show a considerable increase in flexural strength using CFRP to strengthen the RC beam relative to the control beam.

Figure has been removed due to Copyright restrictions.
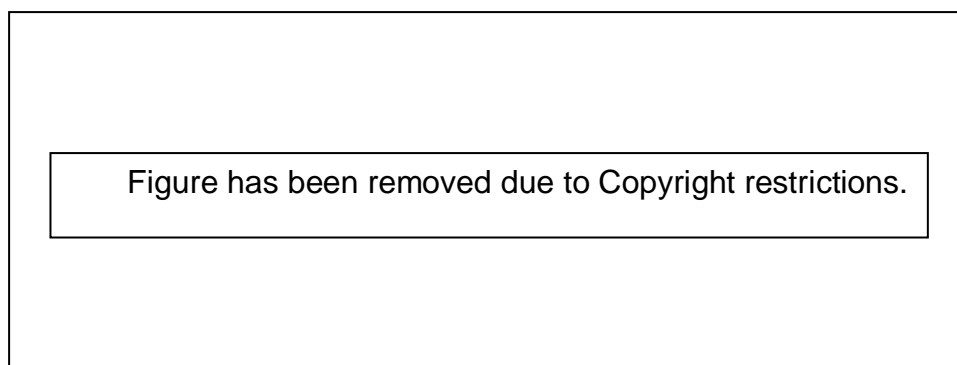
Figure 7.1 Beam details. Esfahani et al. (2007)

Table 7.1 Details of the tested beams Esfahani et al. (2007)

Table has been removed due to Copyright restrictions.

7.3 CFRP debonding modelling

Debonding of the CFRP is the most common failure observed for strengthened concrete structural members. Thus, it is important to pay extra attention to this kind of failure and to find ways of preventing it in order to take full advantage of the CFRP- strengthened members. Finite element method (FEM) has been used in many studies to investigate the behaviour of structural members strengthened with CFRP. However, the debonding failure mode, adhesive layer modelling and concrete-CFRP interface modelling have not been fully studied. Two models were used to simulate the interface layer between concrete and the CFRP to predict the behaviour of the strengthened beam under flexure. The multi-crack concrete model (Jefferson, 1999) was used to model the concrete and the Drucker-Prager (Yu et al. 2010) model was used to model the interface between the concrete and CFRP strip. Both models were implemented into the commercial FE software LUSAS. For validation purposes, the finite element results were compared with the experimental load deflection curves and the ultimate failure load.

7.3.1 RC beam modelling

In modelling RC beams, two different mesh divisions were used. A fine mesh was used at support and point load locations and a coarser mesh was used for the rest of the beam. The concrete was modelled using a multi-crack 2D plane stress element.

A 2-D bar element was used to model the reinforcement bars and CFRP. This type of element can resist only an axial force, and contact nodes with two degrees of freedom were used. The same element was used to model the CFRP sheet and an isotropic elastic material was used to represent the CFRP sheet. The yield criterion for steel rebar was the widely used Von Mises criterion. A pin support at one end and roller support at other end of the RC beam were used in the analysis. Point loads were used to model the applied loads. Figure 7.2 shows the finite element beam model. A quadratic interpolation was adopted in all cases and the nonlinear and transient analyses were used to analyse the beam.
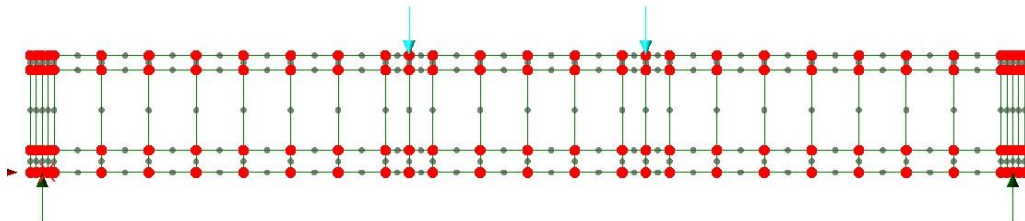
Figure 7.2 Beam two- dimensional F.E model

7.3.2 Concrete – CFRP interface layer

Two models were used for the CFRP-concrete interface layer. In the first model, the multi-crack concrete model was used and a perfect bond between the concrete and CFRP was assumed. In the second model, the Drucker-Prager cohesive element was used for the concrete–CFRP interface layer and the multi-crack concrete model for the rest of the beam. At the interface between the concrete and CFRP, and to simulate the debonding failure, cohesive elements were used. Debonding occurs when the cohesive element is degraded and damaged due to the high tension and/or shear stresses.

The cohesive element was modelled using a Drucker and Prager model. In 1952, Drucker and Prager proposed a model to describe pressure-sensitive materials, such as rock, soil and concrete, which exhibit volumetric plastic strain (Yu *et al*, 2010). In the Drucker and Prager model, the parameters related to friction angle and cohesion governed the yielding and hardening criteria, which are material properties of granular materials. The Drucker-Prager model is a simple model that has the capability to capture shear strength increases. The Drucker-Prager plasticity model can accurately investigate the behaviour of concrete structural members (Karabinis et al. 2002). Figure 7.3 shows a graphic interpretation of the cohesion and friction angle definition for the Drucker-Prager Yield Model. The model is included in the commercial software LUSAS. More details about the model are available in the LUSAS material library (LUSAS. 2012)
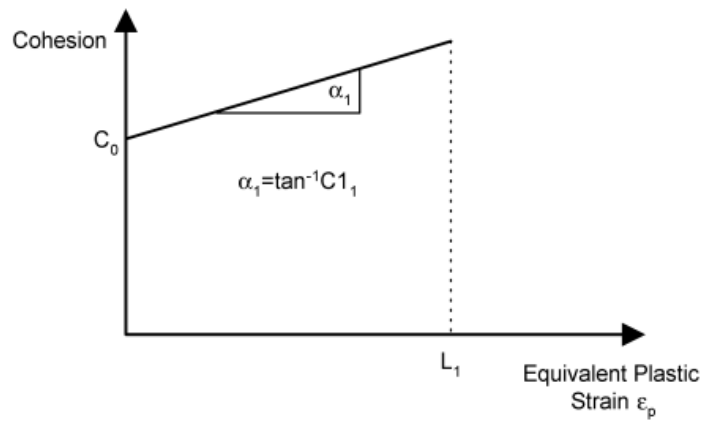
Cohesion Definition for the Drucker-Prager Yield Model (Model 64)

$\alpha_1 = \tan^{-1} C1_1$

Friction Angle Definition for the Drucker-Prager Yield Model (Model 64)

$\alpha_2 = \tan^{-1} C2_1$
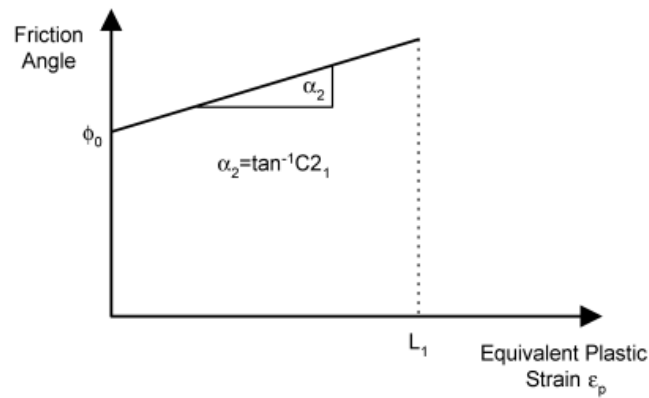
Figure 7.3 Drucker-Prager yield models (LUSAS. 2012).

7.3.3 Results and discussion

Table 7.2 shows the comparison between the experimental and numerical results in terms of ultimate load and mode of failure for three groups of RC beams. The comparison shows a close agreement between the experimental and numerical results for both control and strengthened beams.

The ultimate loads from numerical results were less than those for the experimental failure load using model one (multi-crack concrete) and slightly higher using model two (Drucker-Prager model). The results show that the ultimate load using multi-crack concrete model is higher than that using the Drucker-Prager model.

Table 7.2 Comparison of results between the experimental and numerical work

	Experimental results		Numerical results				Ultimate Load Comparison Num. / Exp%	
Specimen	Ultimate Load kN	Mode Of failure	Ultimate Load		Mode of failure		Model 1	Model 2
			Model 1*	Model 2**	Model 1	Model 2		
B1-12D-0L	50	Flexure	44		Flexure	Flexure	88	
B2-12D-IL15	61.3	Debonding	62.4	66.4	Flexure	Debonding	101.8	108.3
B3-12D-2L15	70.8	Debonding	72.1	72	Flexure	Debonding	102	102
B4-12D-3L15	75.1	Debonding	72	80.6	Flexure	Debonding	95.8	107.3
B5-16D-0L	72.5	Flexure	74.7		Flexure	Flexure	103	
B6-16D-1L10	83	Debonding	92.6	84.8	Flexure	Debonding	111.5	102.1
B7-16D-1L15	90.9	Debonding	89.6	99.6	Flexure	Debonding	98.5	109.57
B8-16D-2L15	102	Debonding	97	111	Flexure	Debonding	95.09	108.8
B5-20D-0L	97	Flexure	95.8		Flexure	Flexure	95	
B6-20D-1L10	107	Debonding	96.8	111	Flexure	Debonding	90.4	103.7
B7-20D-1L15	108	Debonding	97.5	111	Flexure	Debonding	90.2	102.77
B8-20D-2L15	112	Debonding	100	104	Flexure	Debonding	89.2	92.85

 * Multi-crack concrete model

** Drucker-Prager model

Figures 7.3 - 7.14 show the load deflection curves for numerical and experimental tests. All curves include linear-elastic behaviour at the first stage followed by nonlinear perfect plastic at the second stage, up to failure. These figures show a close agreement for the load-deflection curves of the control beam between numerical and experimental results, while for strengthened beams, the numerical load-deflection curves were stiffer than experimental load-deflection curves. For Model One, when a high percentage of longitudinal steel reinforcement was used in an RC beam of Group three (20 mm bars), the load deflection curves of numerical results were stiffer than those in the experimental results. This is because the model assumes perfect bonds between the concrete and reinforcement steel and between the concrete and CFRP sheet as modelled in FEA. The numerical results showed that the load-deflection curves using the Drucker-Prager model were slightly stiffer than when using the multi-crack concrete model.

The results show that the mode of failure for the control beams was a flexural failure in both experimental and numerical results. The debonding failure was noted in the EBR beams tested experimentally. All strengthened RC beams in the FEA using the multi-crack concrete model failed in flexure. By contrast, the results showed debonding failure when the Drucker-Prager model was used.

The perfect bond model was unable to model the debonding fracture mode because the fracture of the bond is not included in this model. After the appearance of the cracks, the shear strain increases with increasing applied load and becomes concentrated at the concrete cover a few millimetres from the CFRP layer, leading to debonding failure. This high shear stress concentration is not taken into account in the perfect bond model. When the Drucker-Prager cohesive model was used to represent the debonding, the bond between the concrete and the CFRP failed due to high shear stress concentration at the interface layer between the concrete and the CFRP, which resulted in debonding failure, similar to the failure in the experiment. Generally, the load-deflection curves of the FE results are stiffer than those of the experiment results. This increasing bottom reinforcement bar size, the FEA predicted load-deflection curves become stiffer when compared with the experimental results. To address this problem, a model updating technique was used, and this will be described in the sections that follow.
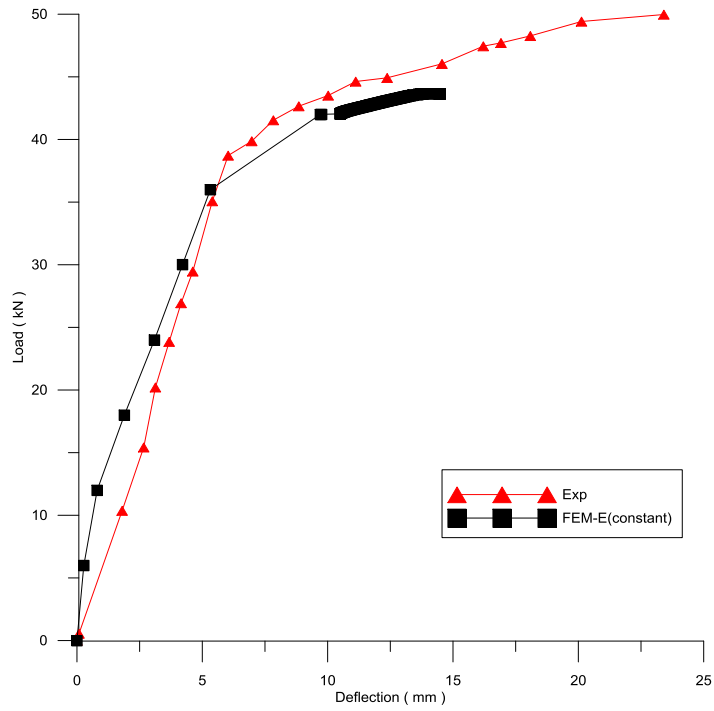
Figure 7.3   **Load-Deflection curve for beam B1-12D-0L**
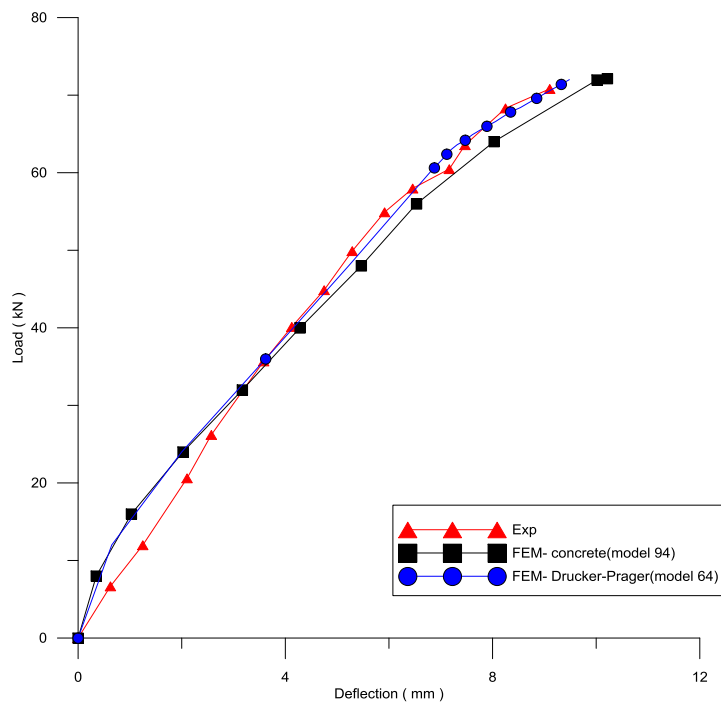
Figure 7. 4   **Load-Deflection curve for beam B3-12D-2L15**

163
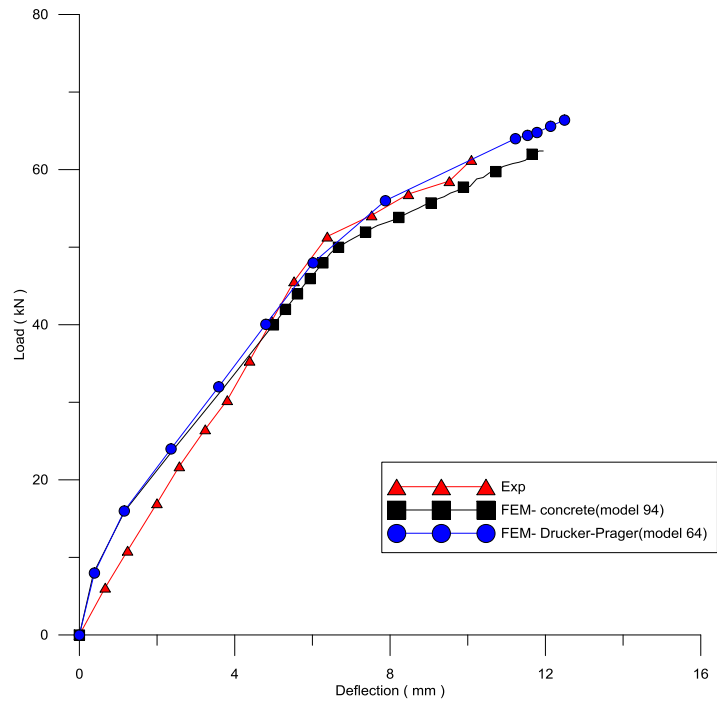
Figure 7.5   Load-Deflection curve for beam B2-12D-1L15
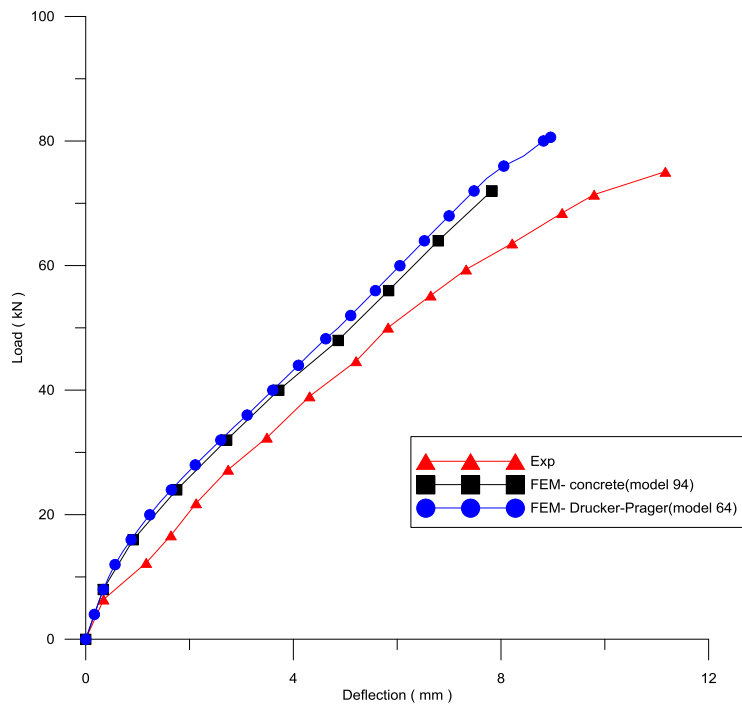
Figure 7.6   Load-Deflection curve for beam B4-12D-3L15
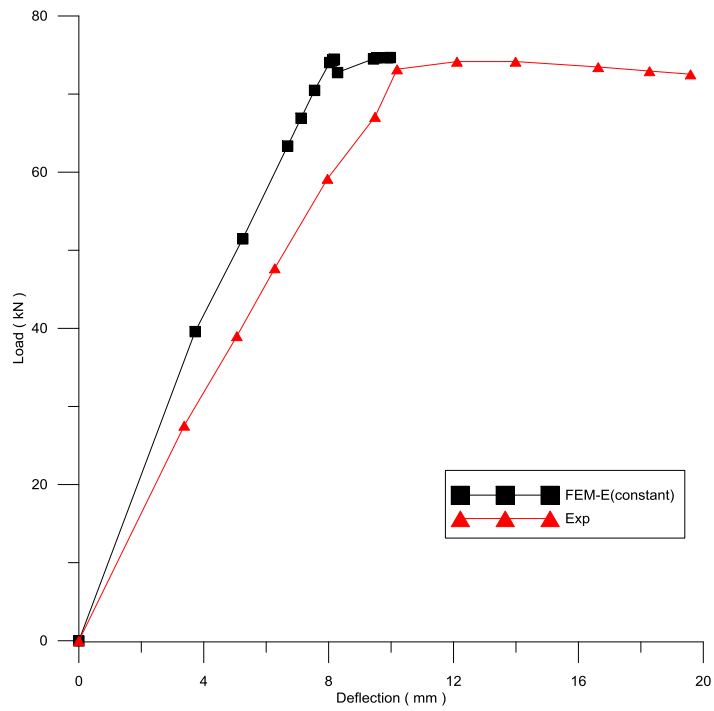
Figure 7.7   Load-Deflection curve for beam B5-16D-0L
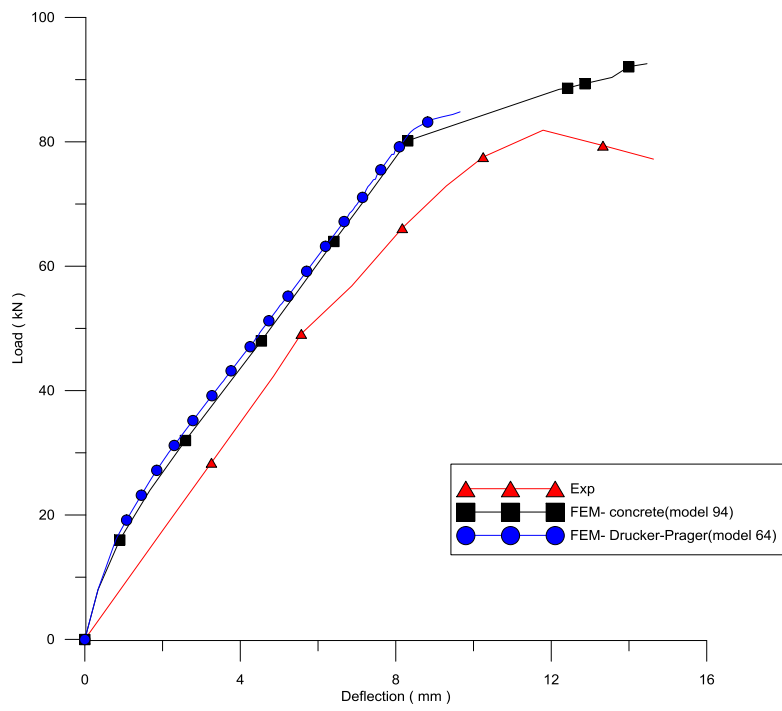
Figure 7.8   Load-Deflection curve for beam B6-16D-1L10
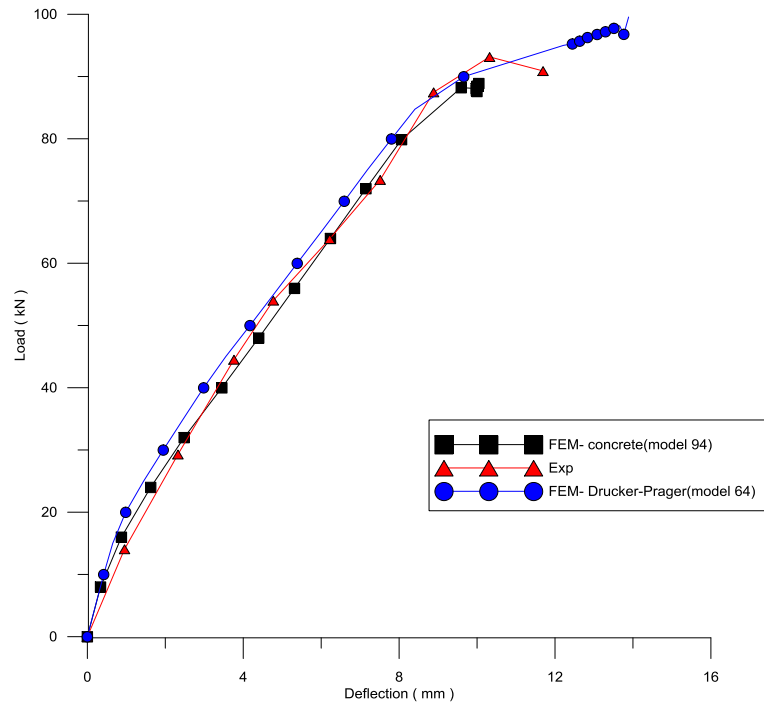
Figure 7.9   Load-Deflection curve for beam B7-16D-1L15
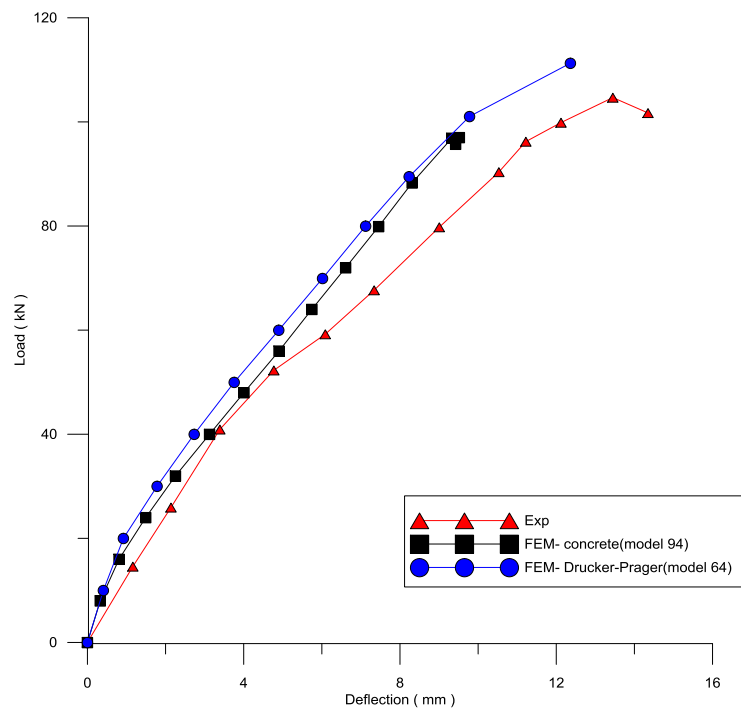
Figure 7.10   Load-Deflection curve for beam B8-16D-2L15
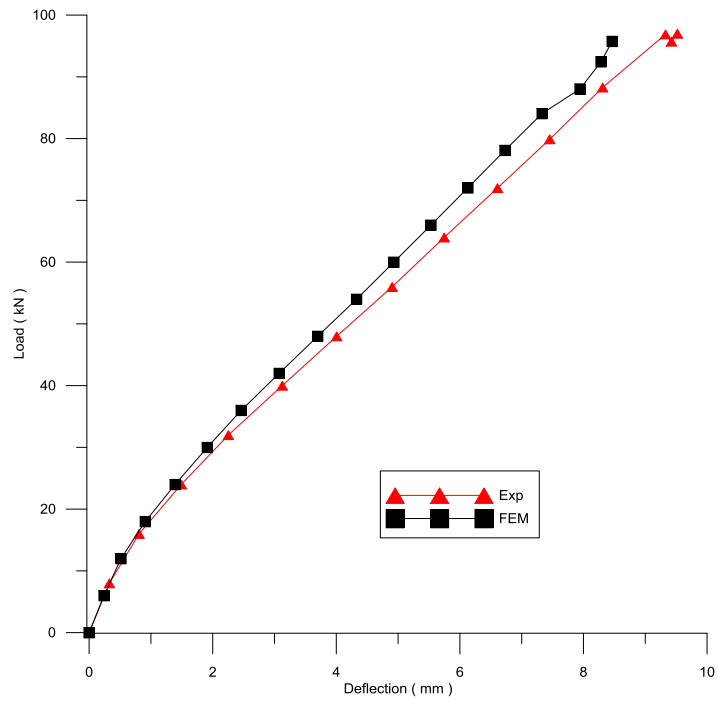
Figure 7.11   Load-Deflection curve for beam B1-20D-0L
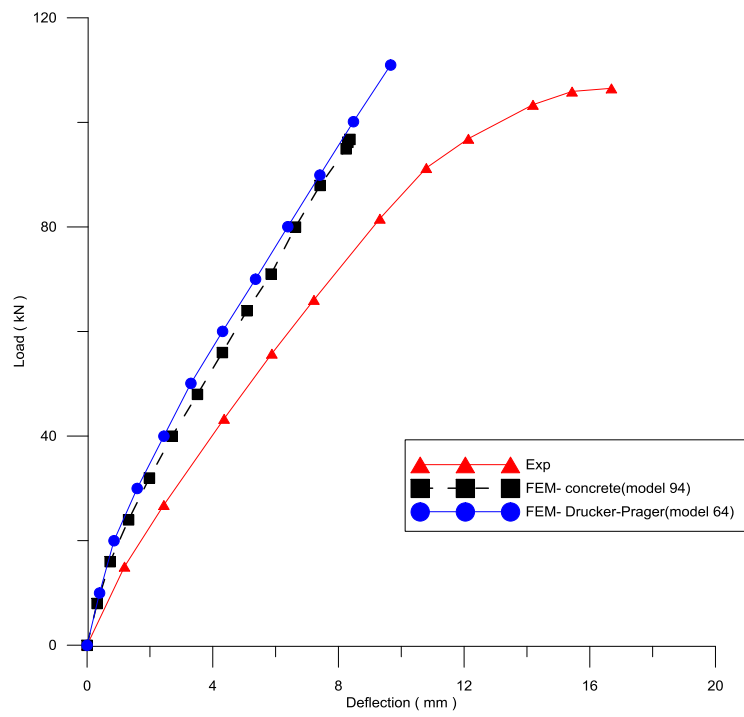
Figure 7.12   Load-Deflection curve for beam B10-20D-1L10

167
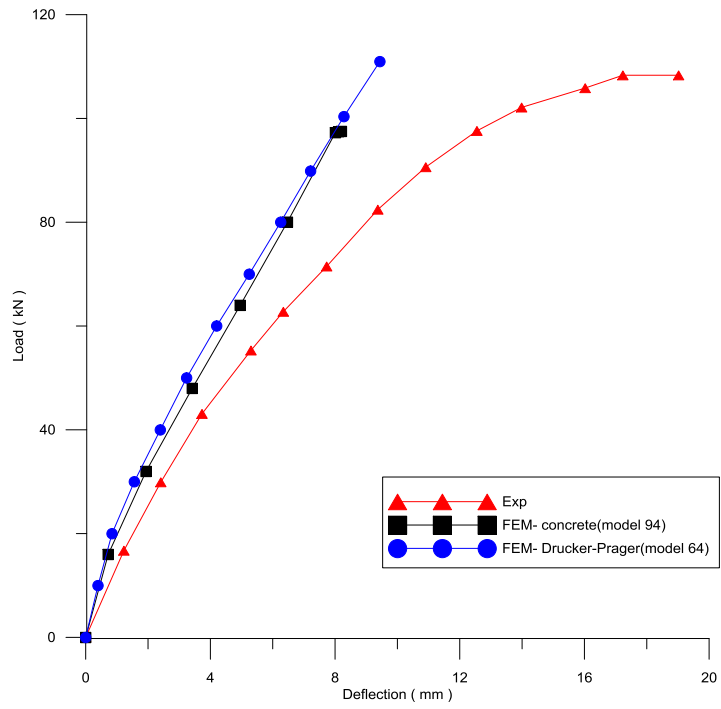
Figure 7.13   **Load-Deflection curve for beam B11-20D-1L15**
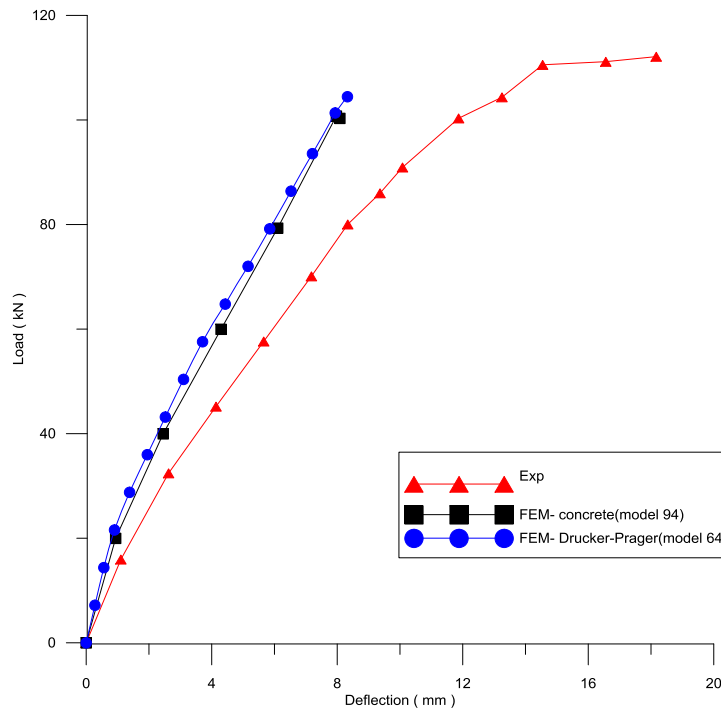
Figure 7.14   **Load-Deflection curve for beam B12-20D-2L15**

168

7.4 Bond-slip assessment in reinforced concrete beams externally strengthened with CFRP

The results of the study (section 7.2 3) showed that the FEA results are stiffer than the experimental results, especially with using large bar size to reinforce the RC beams. Rafiq and Al-Farttoosi (2013) demonstrated that the model updating techniques could successfully address some of the modelling issues with RC beams. A model updating technique was used to closely assess the behaviour of the RC beam without CFRP under static loading. Three RC beams (B1-12-0L, B5-16-0L, and B9-20-0 L), tested by Esfahani et al. (2007), were used for validation of the GA optimisation process. The elastic modulus (E-values) values of concrete along the length of the beam were tuned using modelling updating techniques. Comparison of experimental results and finite element results gave good agreement. It was possible to find more reliable analytical models for these beams when using modelling updating techniques.

Rafiq and Al-Farttoosi (2014) extended the findings from unstrengthened RC beams, using the same concrete E-values at different regions of the beam, in order to investigate the behaviour to CFRP strengthened beams. Three CFRP strengthened RC beams (B2-12D-IL15, B7-16D-1L15, B11-20D-1L15), tested experimentally by Esfahani et al. (2007), were used in the validation process. Although the models showed good correlation between the FEA and experimental results, the correlation was not as good as that for the same beam without the CFRP. The difference between the analytical and experimental load deflection curves was more pronounced with reinforcement bars of larger diameter (20mm rather than 16mm or 12mm) bars. A closer look at these models revealed that the main cause for this difference was the effect of bond slip between the concrete and the reinforcing bars. In reality, there is no perfect bond between concrete and either steel bars or CFRP under high transfer shear stresses, and hence the bond-slip.

Al-Farttoosi et al. (2014) extended the research on the implementation of the model updating techniques on RC beams strengthened with CFRP by modelling the bond slip between the reinforcement bars and the concrete. In these FEA models, the bonding between the concrete and the CFRP was modelled using a Drucker-Prager model. To simulate the bonding between steel and concrete, a joint element was

used with spring constants to model bond resistance between steel bars and the surrounding concrete. A model updating technique was used to tune the values of spring constants at different locations along the length of the beam. A comparison was conducted between the FEA analytical load deflection results and those of the experimental results. Figure 7.15 shows details of the analytical model.
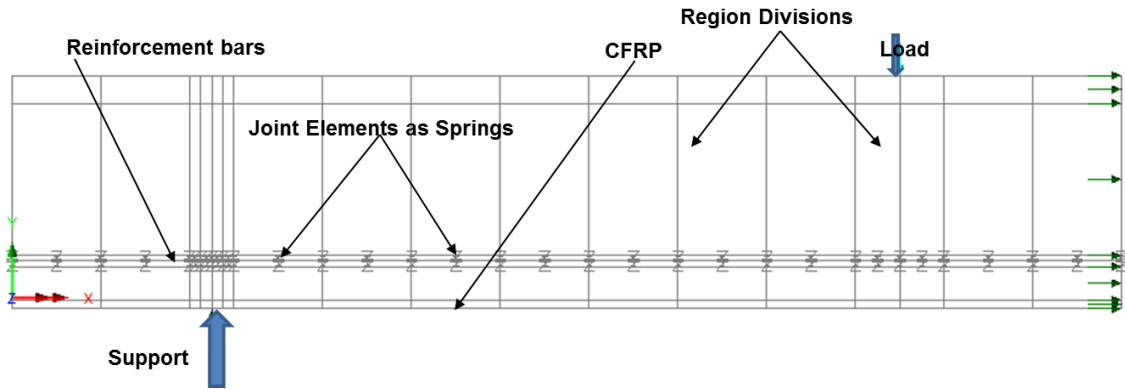
Figure 7.15 Spring modelling bond-slip at various regions of the beam

(Al-Farttoosi et al. 2014)

A very good agreement was found between the analytical and experimental load-deflection curves, as can be seen in the Figure 7.16.
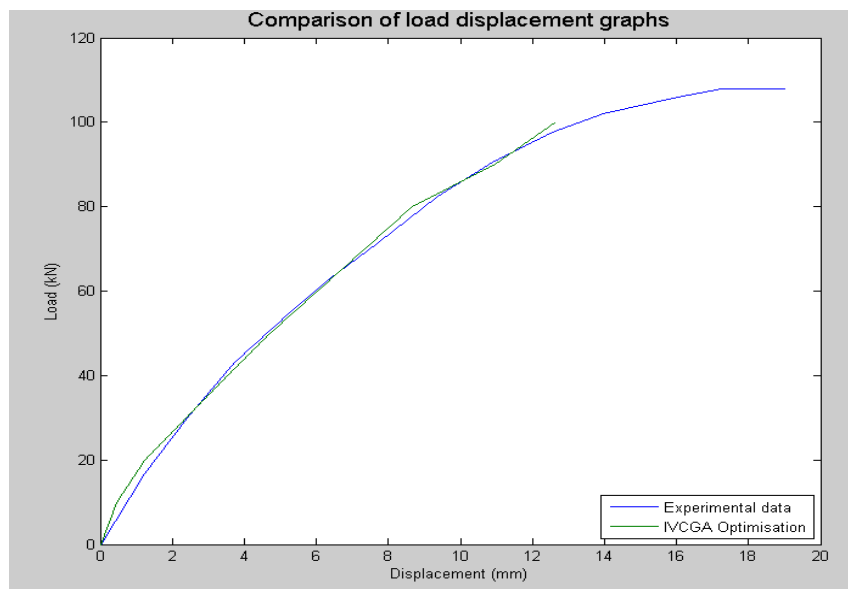
Figure 7.16 Comparison of the FEA and experimental results for beam with 20mm bar (Al-Farttoosi et al, 2014)

170

The main finding of the work of Al-Farttoosi et al. (2014) was that using the Joint Elements to model the bond between the concrete and the reinforcement bars was a sensible model that gave close matches between the analytical and experimental load-deflection curves.

In this research, joint elements were used in the 3-D FE model to model the bond-slip between the steel bars and concrete. The 3-D FE model was used to simulate the behaviour of CFRP -strengthened or repaired RC beams under impact loading as tested in the conducted experimental work. Chapter 8 describes the 3-D FE model and damage modelling of the beams under impact loading with results comparison between the FE and the experimental work. The results of the CFRP repaired beams are discussed in Chapter 9.

7.5 Concluding remarks

RC beams tested experimentally under static loading by Esfahani et al. (2007) were simulated using FEM. Using a perfect bond between the steel bars and concrete resulted in stiff behaviour of the beam tested by FEM compared with that tested experimentally, while spring elements used to model the bond-slip gave a good agreement with experimental results.

Model updating technique was used to find the values of the spring elements stiffness to give a good match with the experimental results. The GA gave a very good agreement with experimental load deflection curves. This is because GA changed the spring stiffness tens of times in order to find a better agreement with the experimental results. In GA, 2-D FE model was run thousands of times to find the optimum results and that needed days to finish the analysis (about 5 days). In addition, the required time to finish the GA analyses will be greater in 3-D FE model. Therefore, empirical model based on experimental data was required to predicate the bond stiffness in the 3-D FE model. GA is a good tool to investigate the effect of parameters on the FE analysis. However, it is time and cost effective.

In Chapter 8 and 9, GA tool was not used and instead, Harajli et al. (2002) bond slip relationship was used to find the spring stiffness in 3-D model used to simulate the experimental work conducted in this study.

8. Finite Element Modelling of CFRP strengthened and repaired beams under impact loading

8.1 Introduction

Once the experimental results were available, a nonlinear finite element method was used to model the experimentally tested beams. Comparisons were made between the experimental and numerical analysis results. In this study, the RC beams strengthened or repaired using CFRP were analysed using 3D FEM. A spring element was used to model the bonding between the steel bars and the concrete. The main challenge in the analysis was modelling the damage in the beam caused by impact loading. The damage was modelled by (a) reducing the mechanical properties of the concrete and (b) bonding between steel bars and concrete. The following sections show the beams modelling and comparison between the FEA strengthened beams results and the experimental tests.

8.2 Three- dimensional FE model
8.2.1 RC beam modelling

In modelling RC beams, a quadratic brick element was used to model the concrete. A 3-D bar element was used to model the reinforcement bars and the CFRP strip. An isotropic elastic material was used to represent the CFRP strip. The yield criterion for the steel rebar was the widely used Von Mises criterion. Due to symmetry, half of the beam was modelled to reduce the computation time of the analysis. The single CFRP strip ($24 \mathrm{~mm}^2$) used in experimental test was modelled by two single CFRP strips with equivalent cross-sectional area ($12 \mathrm{~mm}^2$each). The impact load was applied by dropping a mass at a specific velocity to hit the beam. A quadratic interpolation was adopted in all cases and the nonlinear and transient implicit dynamic analysis was used to analyse the beams. Figure 8.1 shows the 3-D FE model used to simulate the CFRP- strengthened or repaired beams.
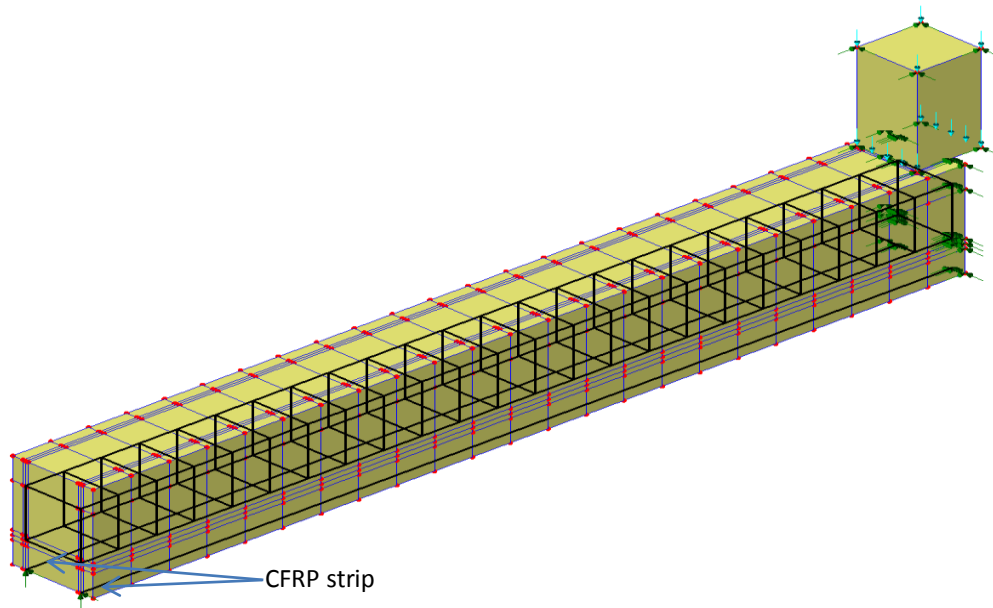
Figure 8.1 Three-dimensional FE beam model for CFRP Strengthened/repaired beams under impact loading

8.2.2 Bond modelling

To simulate the bonding between the concrete and the steel bars, a bond slip was assumed between the concrete and steel bars.

In the bond slip model, a joint element was used to model the bond between the steel bars and the surrounding concrete, using spring constants (K-Springs), as shown in Figure 8.2.
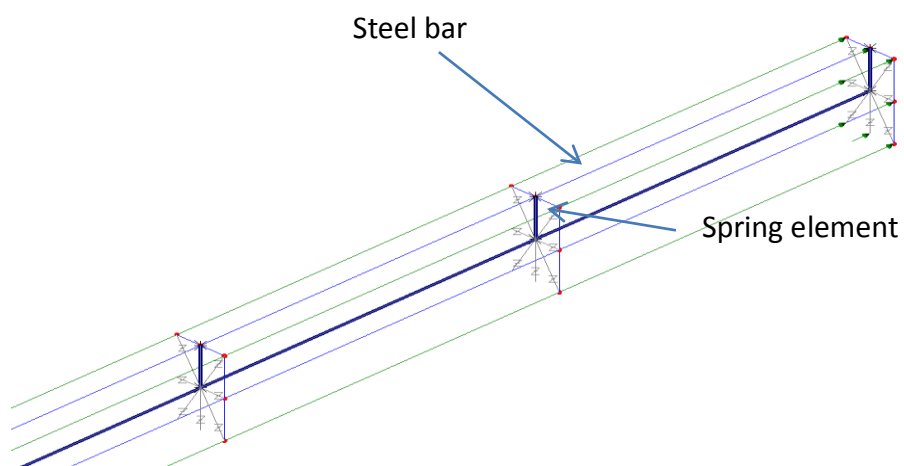
Figure 8.2 Spring element used in 3-D FEA beam model

8.2.3 Damage modelling

The experimental impact test results revealed that when the beam was impacted, the beam stiffness was decreased due to damages. This stiffness reduction results from reduction in both the mechanical properties of concrete and of the bonding between the steel bars and concrete. The compressive strength and elastic modulus of concrete and the steel bars-concrete bonding were considered as damage parameters in the 3-D FE model. These damage parameters were decreased to simulate the reduction in the beam stiffness due to impact damage.

The cracks distribution, indicated from the experimental impact tests, shows that 2/3 of the beam length was damaged by the impact loading (see section 6.4). Thus, In the FE model, the beam was divided into two unequal parts, damaged and undamaged, as shown in Figure 8.3.
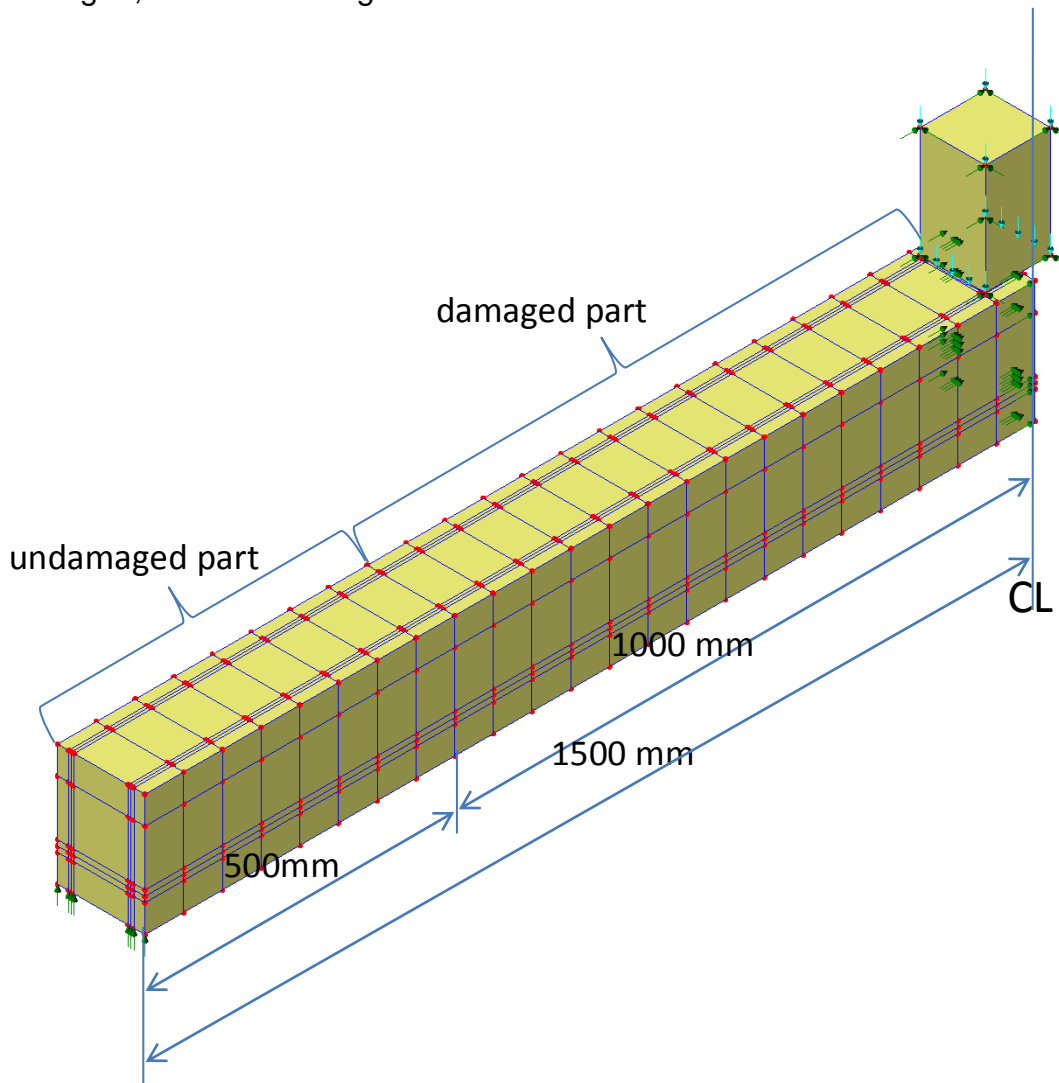
Figure 8.3 beam damage in FEA beam model

The damage parameters (compressive strength, elastic modulus and bond stress) were reduced only to the damaged part of the beam. For the undamaged beam part, the damage parameters were kept same without any reduction after impact.

In the FE model, the impact affected and reduced the damage parameters as following: -

1- Concrete compressive strength $(f_c^/)$

The concrete compressive strength of the reference (undamaged) beam was reduced, based on reduction in beam stiffness obtained from the experimental tests.

$$(f_c^/)damaged = (1- R) * (f_c^/) \; refernce \qquad\qquad \text{Eq.8.1}$$

$$R= \text{beam stiffness reduction} = \frac{(K)reference - (K)damaged}{(K)refernce} \qquad \text{Eq. 8.2}$$

2- Concrete modulus of elasticity (E_c)

The modulus of elasticity of concrete E_c used in FE model was calculated using the ACI-318 Code formula given below:

$$E_c = 4700 \sqrt{f_c^/} \qquad\qquad \text{Eq.8.3}$$

It should be noted from the formula that the concrete elastic modulus is proportional with the concrete compressive strength. Thus, in the FE model, when the concrete compressive strength was decreased using Eq. 8, the elastic modulus was reduced proportionally.

3- The bond stress

The bond stress slip relationship proposed by Harajli et al. (2002) (see Section 2.7) was used to determine the stiffness for spring elements used to model the bond slip between the steel bars and concrete.

$$\text{The maximum bond stress} = 31\sqrt{f_c^/} \ldots\ldots psi$$

$$= 2.574\sqrt{f_c^/} \ldots\ldots \frac{N}{mm^2} \qquad\qquad \text{Eq. 8.4}$$

8.3 FE results and comparisons (Strengthening stage)

FE method was used to analyse the control and CFRP strengthened beams under impact loading. Comparisons were conducted between FE results and experimental tests in terms of reaction force and maximum deflection. Two assumptions were used in FE modelling; in the first assumption, a perfect bond was assumed and no slipping was allowed between the concrete and steel bars. In the second assumption, a spring element was used to simulate the steel bar-concrete bond slip.

8.3.1 Reference beams (Unstrengthened)

Figures 8.4 and 8.5 show the comparison between the experimental and FE results of control beam in terms of maximum reaction force and maximum deflection. The comparison showed a very good agreement between the reaction force of the experimental results with that of the numerical results for the bond-slip model. In terms of the maximum deflection, the bond-slip between the steel bar and concrete affected the finite element results. The maximum deflection of the finite element results using the bond-slip were much closer to the experimental results compared with analysis using a perfect bond between the steel bar and concrete. With increasing impact energy, the bond between the steel bars and concrete was reduced due to damage and cracking. The FEA maximum deflection using bond slip was very close to the experimental maximum deflection with increasing impact energy, as shown in Figure 8.5. Table 8.1 shows the percentages of the FEA results compared with the experimental results. The table shows the reduction in the concrete compressive strength, elastic modulus and K-spring values for each impact due to beam damage, using equations 8.2, 8.3 and 8.4 respectively. The comparison between the FE and experimental results illustrated in Table 8.1 showed that the FEA model using the spring element is more representative than the FEA model using a perfect bond model.
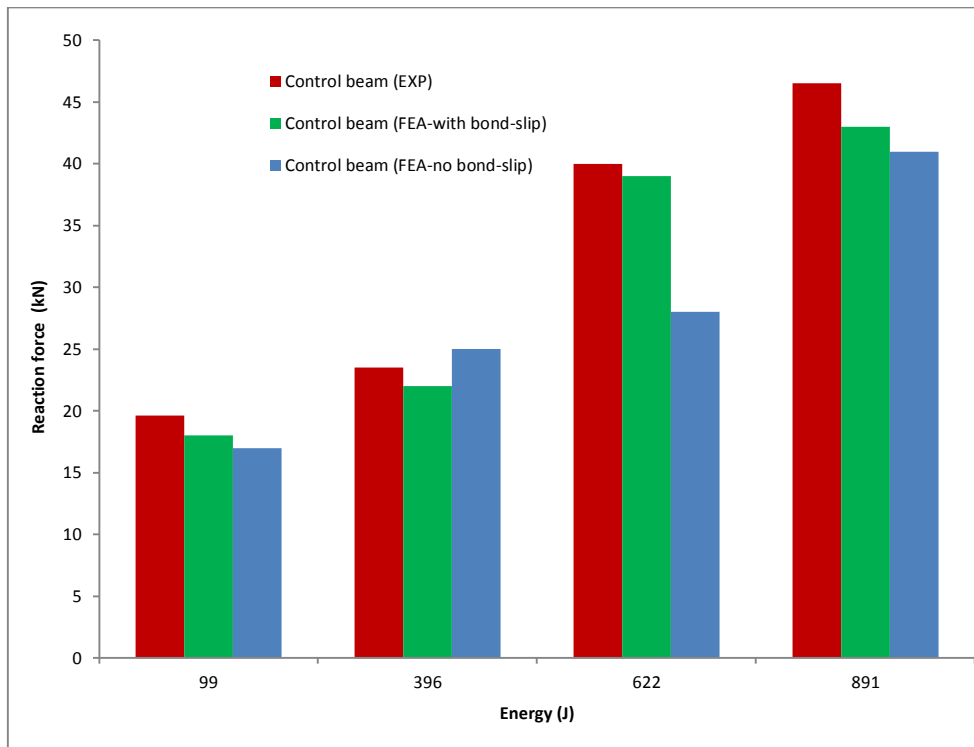
Figure 8.4 Reaction force comparison between experimental and FEM of control beam under different impact energies
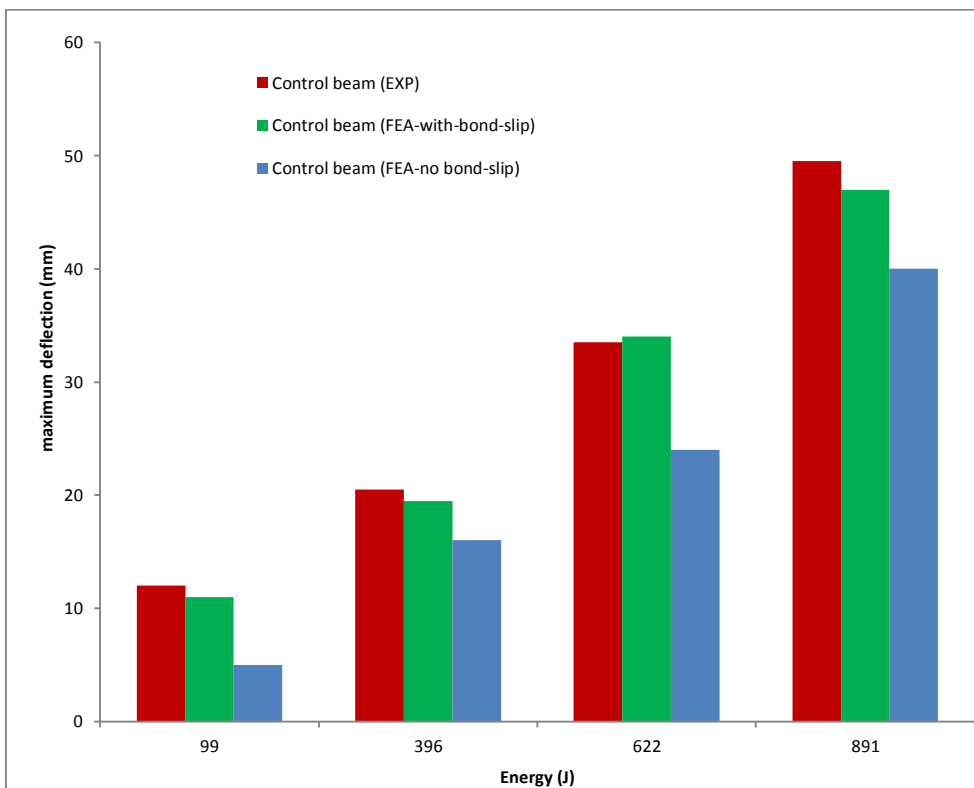
Figure 8.5 Maximum deflection comparison between experimental and FEM of control beam under different impact energies

178

Table 8.1 Comparison between experimental and FEM results of control beam

Impact energy (J)	Beam stiffness kN/mm^2	Beam stiffness reduction % Eq. 8.1 *100	$f_c^{/}$ N/mm^2 Eq.8.2	K Spring N/mm^2 Eq.8.4	E_c N/mm^2 *10³ Eq.8.3	Reaction force (R) (kN) EXP	Reaction force (R) (kN) FEA1*	Reaction force (R) (kN) **FEA2	$\frac{R_{FEA1}}{R_{EXP}}$ %	$\frac{R_{FEA2}}{R_{EXP}}$ %	Max. Deflection (D) (mm) EXP	Max. Deflection (D) (mm) FEA1	Max. Deflection (D) (mm) FEA2	$\frac{D_{FEA1}}{D_{EXP}}$ %	$\frac{D_{FEA2}}{D_{EXP}}$ %
99	3.63	-	25.6	13.02	23.8	19.6	17	18	87	92	12	5	11	42	92
396	2.69	① 25.8	② 18.99	③ 11.22	④ 20.48	23.5	25	22	106	94	20.5	16	19.5	78	95
622	1.21	66.7	8.52	7.51	13.71	40	28	39	70	98	33.5	24	34	72	101
891	0.92	74.7	6.48	6.55	11.96	46.5	41	43	88	92	49.5	40	47	87	95

*FEA1: no bond-slip, **FEA2: with bond-slip

① Beam stiffness reduction% = R = $\frac{(K)reference-(K)damaged}{(K)refernce}$ = $\frac{3.63-2.69}{3.63}*100 = 25.8\%$

② $(f_c^{/})damaged = (1-R)*(f_c^{/})\,refernce = (1-\frac{25.8}{100})*25.6 = 18.99 N/_{mm^2}$

③ $K_{spring} = 2.574\sqrt{f_c^{/}} = 2.574\sqrt{18.99} = 11.22\frac{N}{mm^2}$

④ $E_c = 4700\sqrt{f_c^{/}} = 4700\sqrt{18.99} = 20480\ N/_{mm^2}$

8.3.2 CFRP Strengthened beams

The experimentally tested beams strengthened using NSM CFRP strip were analysed using the FE method. The results of the FE model are compared with the experimental results in Figures 8.6 and 8.7 in terms of the reaction force and maximum deflection. Compared with the experimental results, the FE model results using bond slip were closer than the model using perfect bond between the steel bars and the concrete. Table 8.2 shows the comparison off the FEA and experiments. The comparison showed a good agreement between the FEA and that of the experimental data using a bond-slip model.
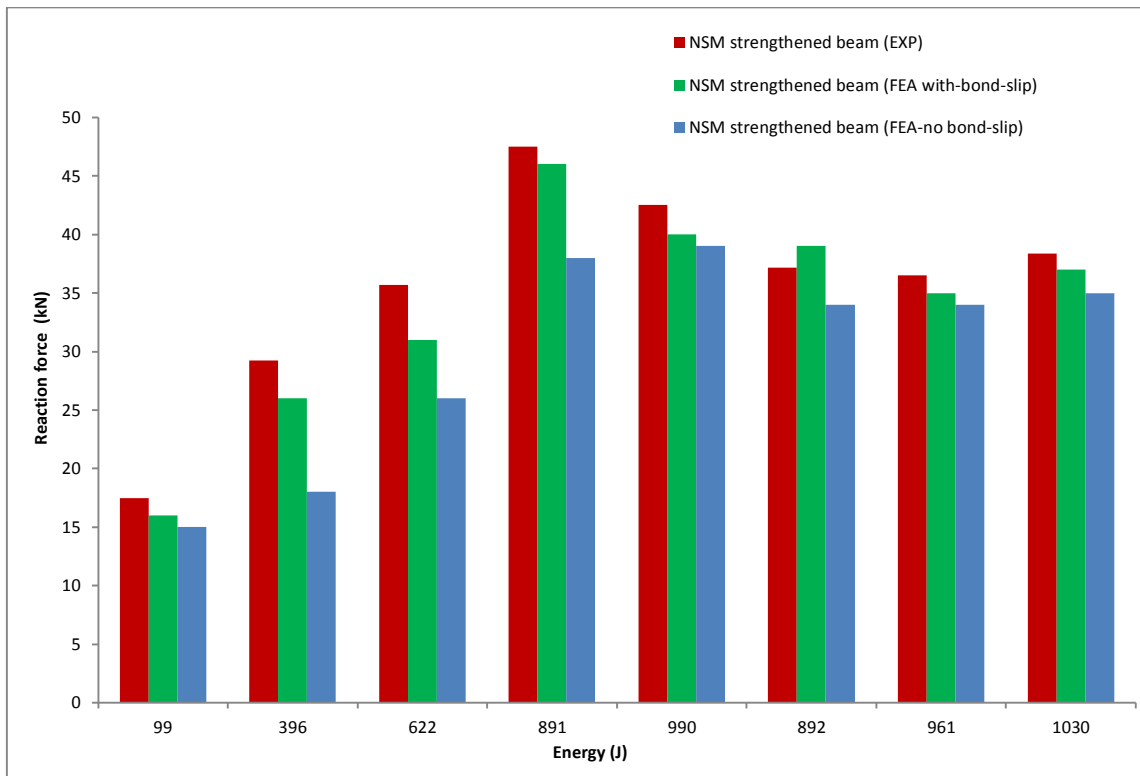
Figure 8.6 Reaction force comparison between experimental and FEM of strengthened beam under different impact energies
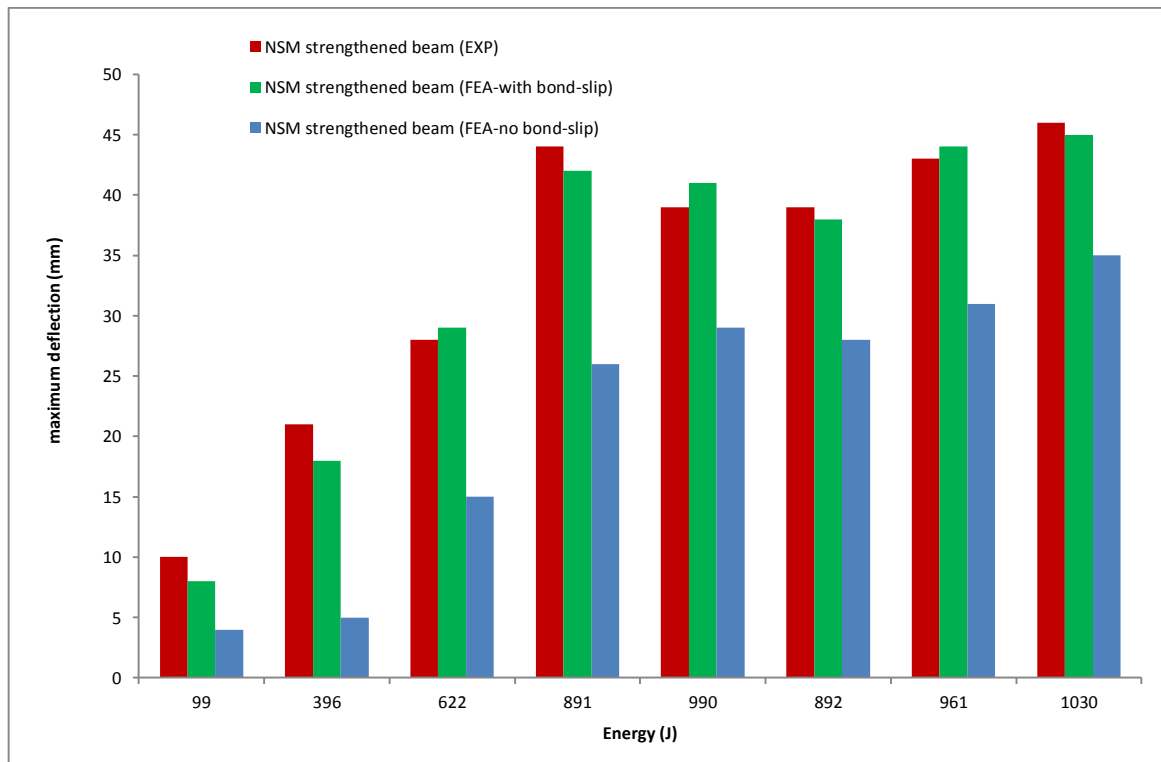
Figure 8.7 Maximum deflection comparison between experimental and FEM of strengthened beam under different impact energies

Table 8.2 Comparison between experimental and FEM results of strengthened beams

Impact energy (J)	Beam stiffness kN/mm^2	Beam stiffness reduction % Eq. 8.1 *100	$f_c^/$ N/mm^2 Eq.8.2	K Spring N/mm^2 Eq.8.4	E_c N/mm^2 *10^3 Eq.8.3	Reaction force (R) (kN) EXP	Reaction force (R) (kN) FEA1*	Reaction force (R) (kN) **FEA2	$\frac{R_{FEA1}}{R_{EXP}}$ %	$\frac{R_{FEA2}}{R_{EXP}}$ %	Max. Deflection (D) (mm) EXP	Max. Deflection (D) (mm) FEA1	Max. Deflection (D) (mm) FEA2	$\frac{D_{FEA1}}{D_{EXP}}$ %	$\frac{D_{FEA2}}{D_{EXP}}$ %
99	3.63	-	25.6	13.02	23.8	17.5	15	16	86	91	10	4	8	40	80
396	2.69	25.9	19	11.2	20.5	29.25	18	26	62	89	21	5	18	24	86
622	1.48	59.2	10.44	8.32	15.18	35.7	26	31	73	87	28	15	29	54	104
891	1.46	59.8	10.30	8.26	15.08	47.5	38	46	80	97	44	26	42	59	95
990	1.38	62.0	9.73	8.03	14.66	42.5	39	40	92	94	39	29	41	74	105
892	1.33	63.4	9.38	7.88	14.39	37.15	34	39	92	105	39	28	38	72	97
961	1.26	65.3	8.89	7.67	14.01	36.5	34	35	93	96	43	31	44	72	102
1030	1.24	65.8	8.74	7.61	13.90	38.35	35	37	91	96	46	35	45	76	98

*FEA 1: no bond-slip, **FEA 2: with bond-slip

8.4 Beam behaviour under impact loading

For better understanding of the beam behaviour under impact loading, the FE model was used to investigate the deflection history and stress, and the strain distribution in the steel bars and CFRP strip.

8.4.1 Deflection history of the beams under impact loading

Figure 8.8 shows the deflection history of the experimental and FE results compared to the control beam BR-1 (impact energy= 622 J). It can be noted that the FE model predicted the experimental impact time and the maximum deflection of the beam. The comparison showed good agreement between the deflection-time curves of the FEA and the experimental results. The beam behaviour in FEA and the experimental test was similar. The experimental beam behaviour was discussed in section 5.3.7. The impacted beam, after the first impact (point A), loses the contact with the mass and moves downward. Then, when the beam slowed down due to beam stiffness, the mass re-impacted the beam (point B) and deflected it down to reach the

maximum deflection (point C). The same behaviour was found in the FEA, as can be seen in Figure 8.8. The same behaviour was found in the other tested beams.
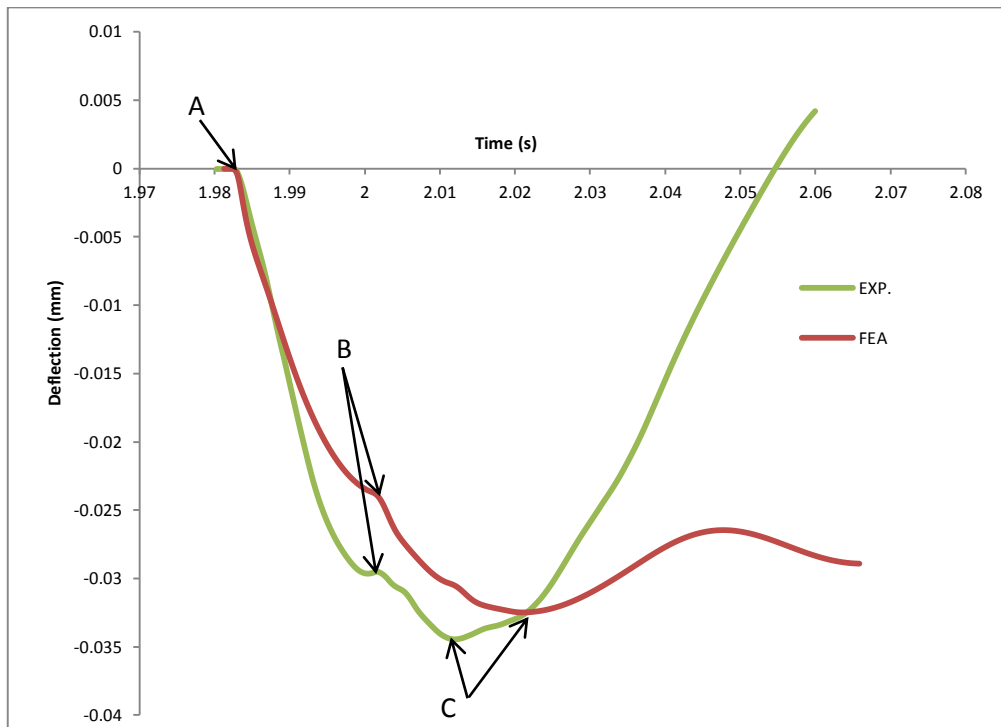
Figure 8.8 Experimental and FEA Deflection vs time of control beam BR-1, Impact energy=622 J

8.4.2 Stresses and Strains distribution in CFRP strengthened beam

FE method was used to study the distribution of stresses and strains in steel bars and an CFRP strip. The maximum tensile forces, stresses and strains developed in steel bars and the CFRP strip in strengthened beam due to (396 J) impact energy are shown in Figures 8.9 - 8.11 respectively. Figure 8.9 shows that tensile forces in steel bars (two 10-mm bottom steel bars) are slightly higher than in CFRP strips. However, the tensile stresses in CFRP were much higher than in the steel bar, as shown in Figure 8.10, because the cross-section area of CFRP strips ($24 \ \mathrm{mm}^2$) is about a third of the steel cross-section area ($79 \ \mathrm{mm}^2$). The tensile stresses in steel bars and the CFRP strip during the impact increased rapidly with time, owing to the sudden transfer of the impact force to the beam. When the mass hit the beam, the beam deflected down, which produced high tensile stress in the bottom face of the beam, due to bending force. High percentages of these stresses were resisted by the CFRP strip. Table 8.3 shows

the maximum tensile forces, stresses and strains in the CFRP for strengthened beams under different impact energies. When the beam reached the maximum deflection, the maximum stress in CFRP (1278 N/mm^2) is about 5.8 times the steel bar' maximum stress (221 N/mm^2). Figure 8.10 and Table 8.3 show that the steel bars' maximum stress (221N/mm^2) did not exceeded the yield stress (570 N/mm^2). That is because a high percentage of the tensile stresses was resisted by the CFRP strip, and also the steel bars-concrete bond slip affected the stresses transferred between the concrete and steel bars. The high CFRP stresses resulted in high CFRP strain compared with the steel bars, as shown in Figure 8.11. The maximum strain in the steel bars (0.0011) did not exceed the yield strain (0.00275), due to low tensile stress in the steel bars.

The stress distribution is proportional to the reinforcement stiffness, bonding with the concrete and distance from the neutral axis. The CFRP strip resisted high bending stresses due to high stiffness of the CFRP, high bonding between the CFRP and concrete and high distance from the neutral axis compared with steel

bars.

Figure 8.9 Maximum tensile forces in steel bars and CFRP strip vs time of strengthened beam. Impact energy=396 J
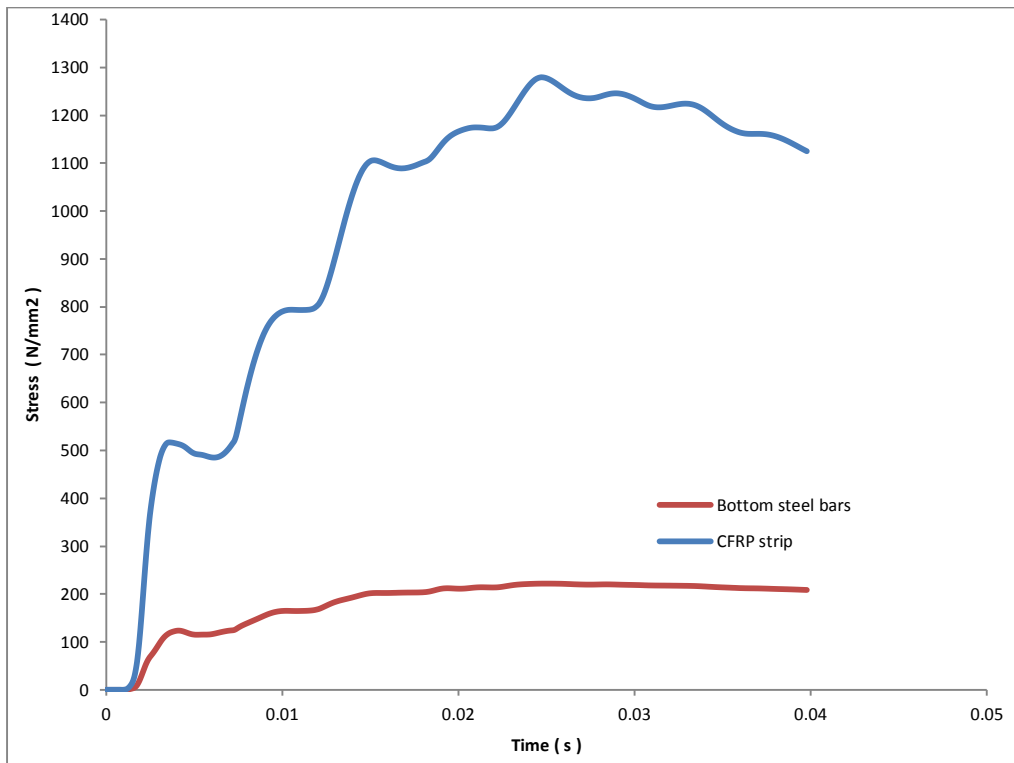
Figure 8.10 Maximum tensile stresses in steel bars and CFRP strip vs time of strengthened beam. Impact energy=396 J
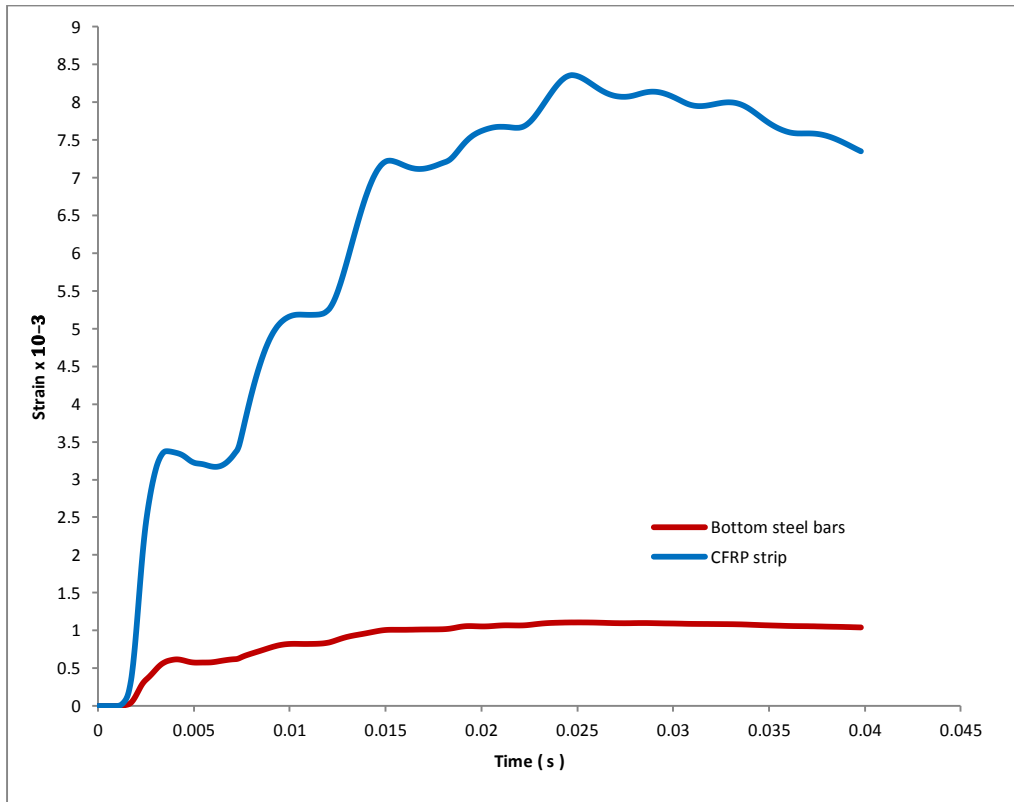
Figure 8.11 Maximum tensile strains in steel bars and CFRP strip vs time of strengthened beam. Impact energy=396 J

Figures 8.12 - 8.14 shows respectively the maximum tensile forces, stresses and strains in steel bars and CFRP strip developed in strengthened beam under (620 J) impact energy. It can be noted from Figure 8.12 and Table 8.3that the tensile force in the CFRP (39.6 kN) is slightly higher than that in steel bars (38.8). With increasing impact energy (from 396 J to 620 J), the stresses in steel bars were increased slightly and did not exceed the steel yield stress because a high percentage of the tensile stresses was resisted by the CFRP strip. The CFRP stresses (2113 N/mm^2) were about 8.5 times than that of the steel bars (247 N/mm^2), as shown in Figure 8.13. The CFRP strain was increased with increasing impact force, as shown in Figure 8.14. Table 8.3 shows that the CFRP strain is much higher than that in the steel bars because of high stress developed in the CFRP strip.
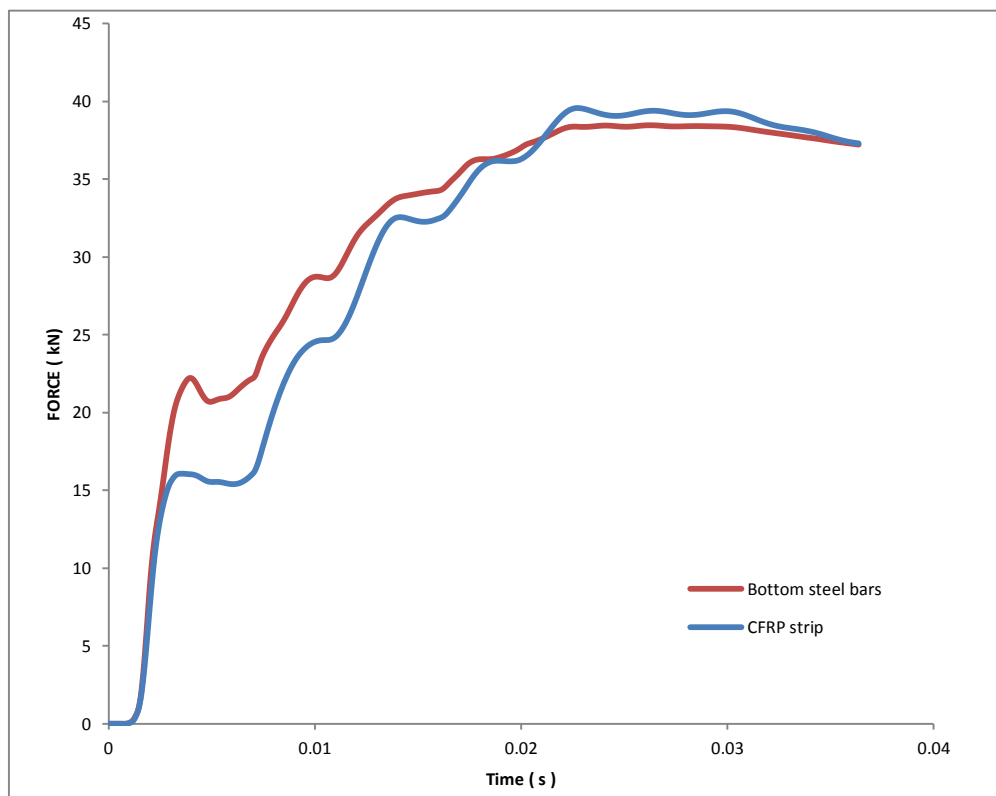
Figure 8.12 Maximum tensile forces in steel bars and CFRP strip vs time of strengthened beam. Impact energy=622 J
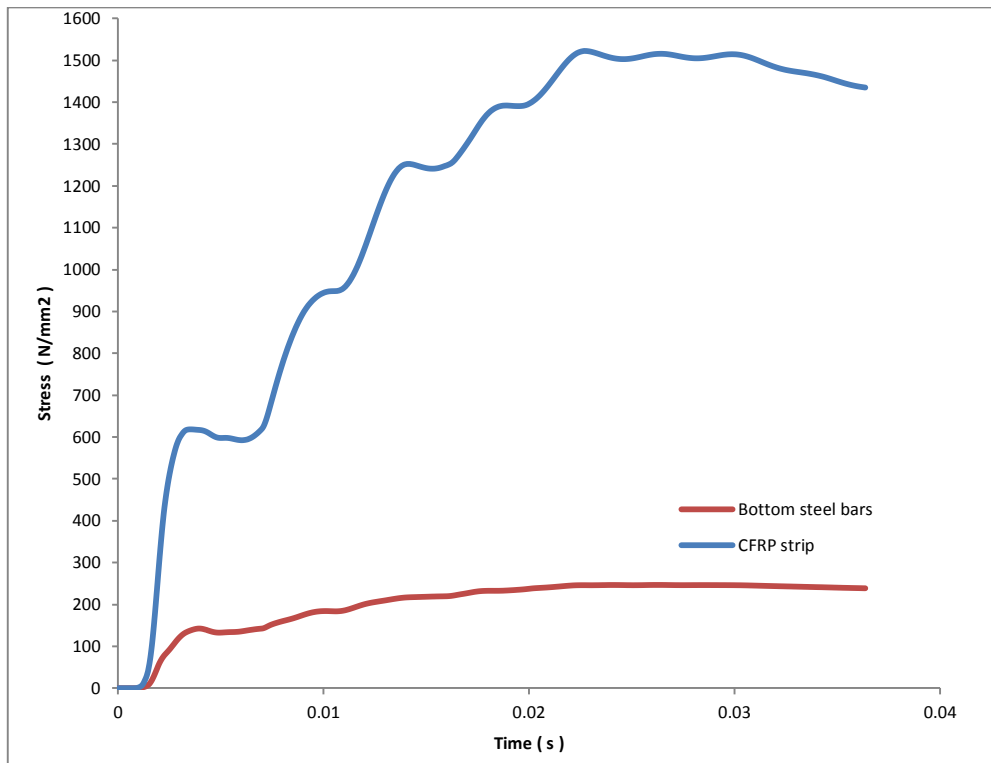
Figure 8.13 Maximum tensile stresses in steel bars and CFRP strip vs time of strengthened beam. Impact energy=622 J
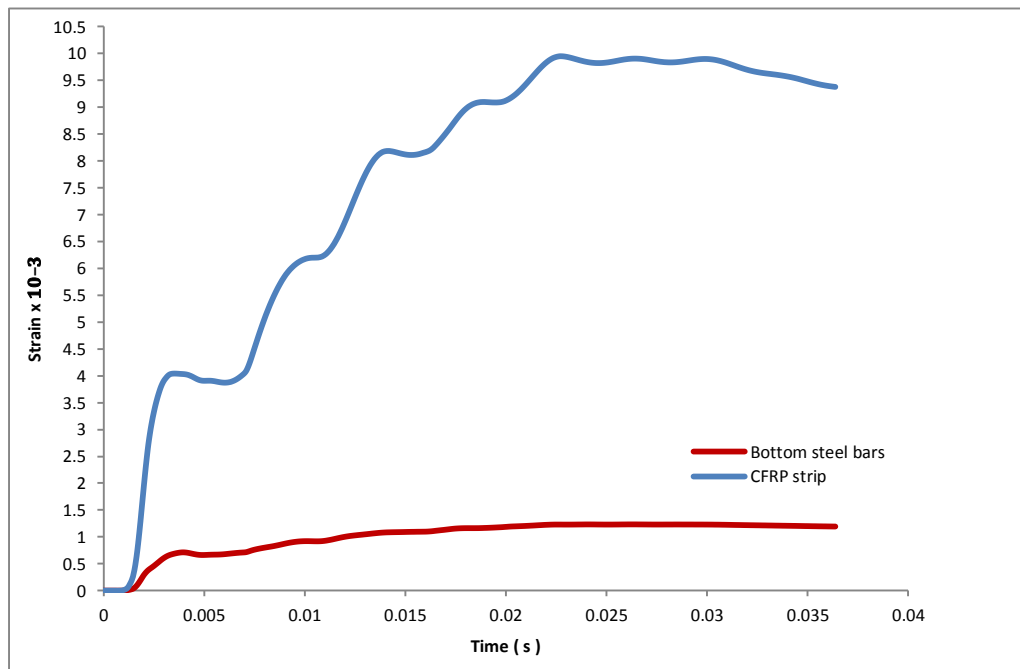
Figure 8.14 Maximum tensile strains in steel bars and CFRP strip vs time of strengthened beam Impact energy=622 J

The tensile stresses were increased in steel bars under high impact energy (891 J). However, the maximum steel tensile stress was less than the yield stress, as shown in Figures 8.16 and Table 8.3. This is because the contribution of the CFRP strip in resisting the bending stresses became higher with the increasing impact energy. CFRP has high stiffness compared to the steel bars and the effective depth of the CFRP strip is greater than that of the steel bars.

Under high impact force (891 J); the tensile stress in the CFRP was much higher than in steel bars as shown in Figure 8.15. However, The CFRP strip did not rupture, as the CFRP stress was less than the CFRP ultimate tensile strength (3214 N/mm^2). A considerable increase in CFRP strain was noted for beam under high impact loading, as shown in Table 8.3 and Figure 8.17: this was due to the high tensile stress developed in the CFRP strip.
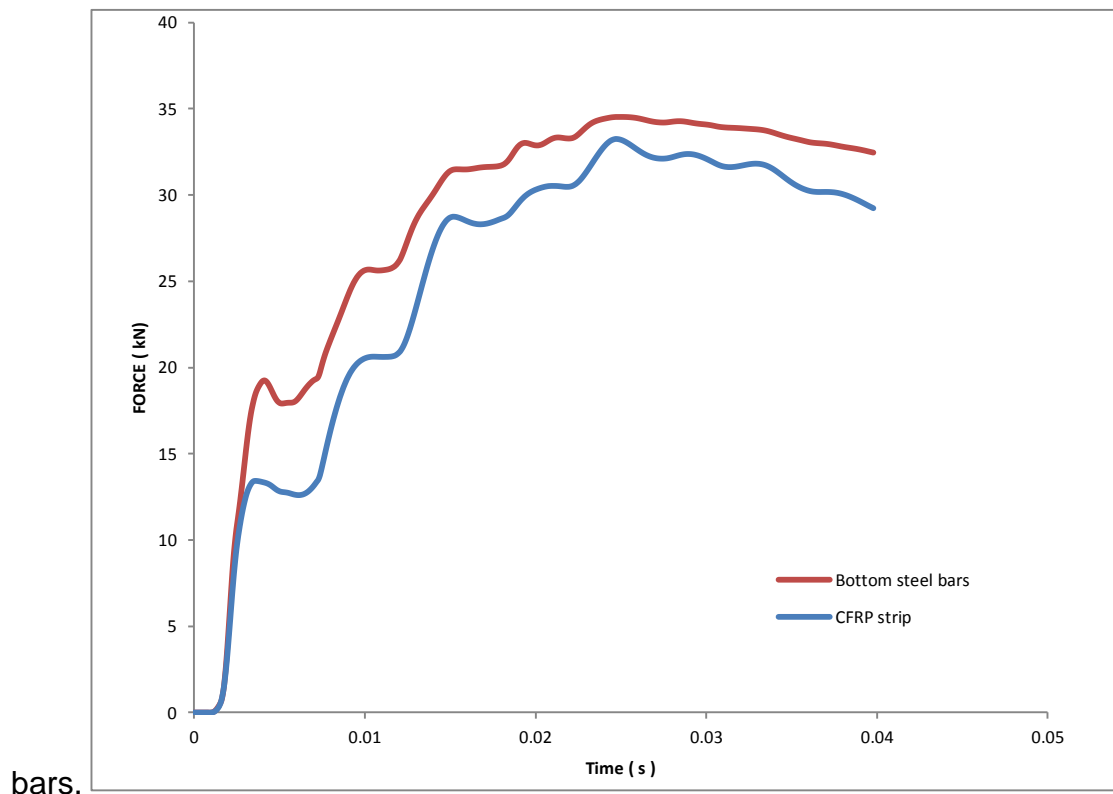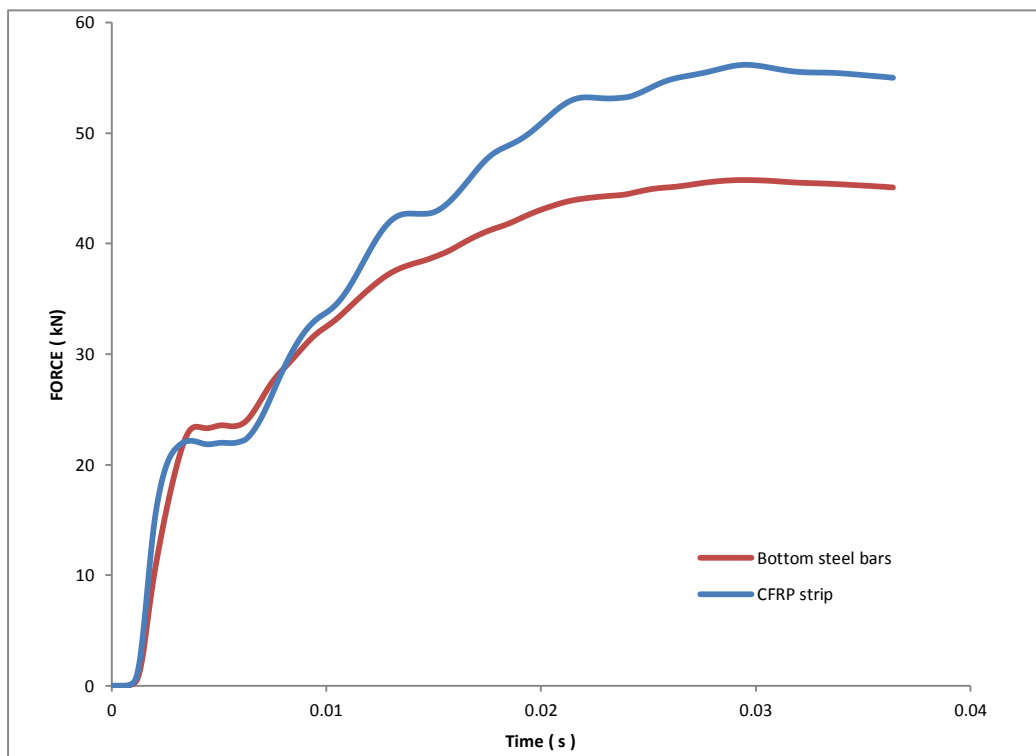

Figure 8.15 Maximum tensile forces in steel bars and CFRP strip vs time of strengthened beam. Impact energy=891 J
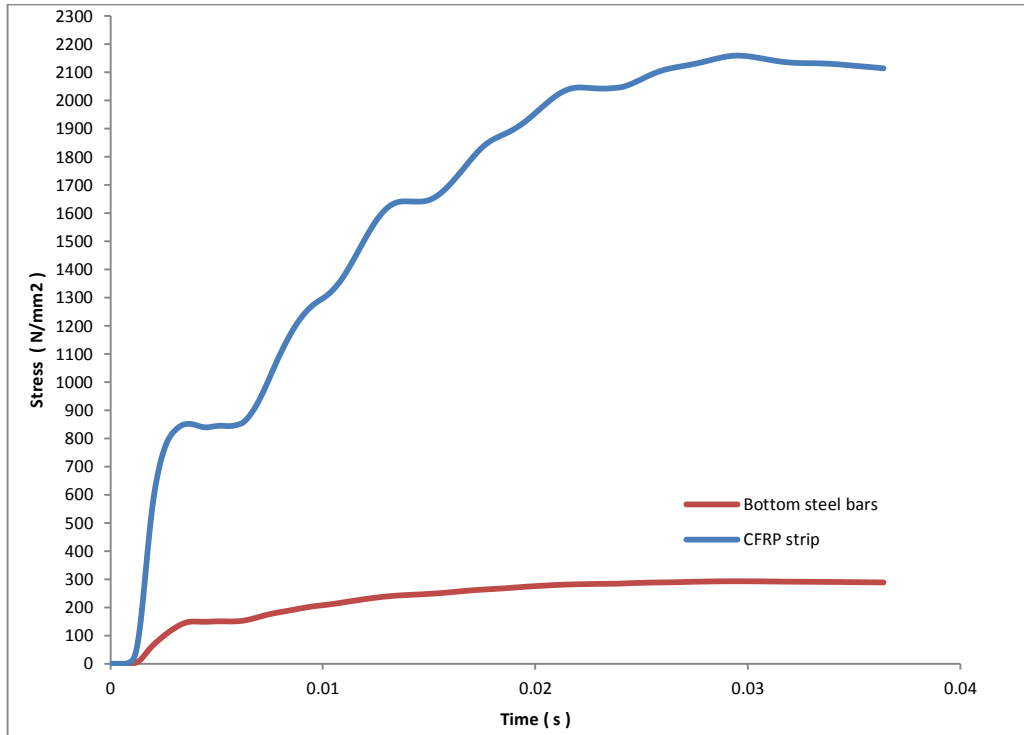
Figure 8.16 Maximum tensile stresses in steel bars and CFRP strip vs time of strengthened beam. Impact energy=891 J
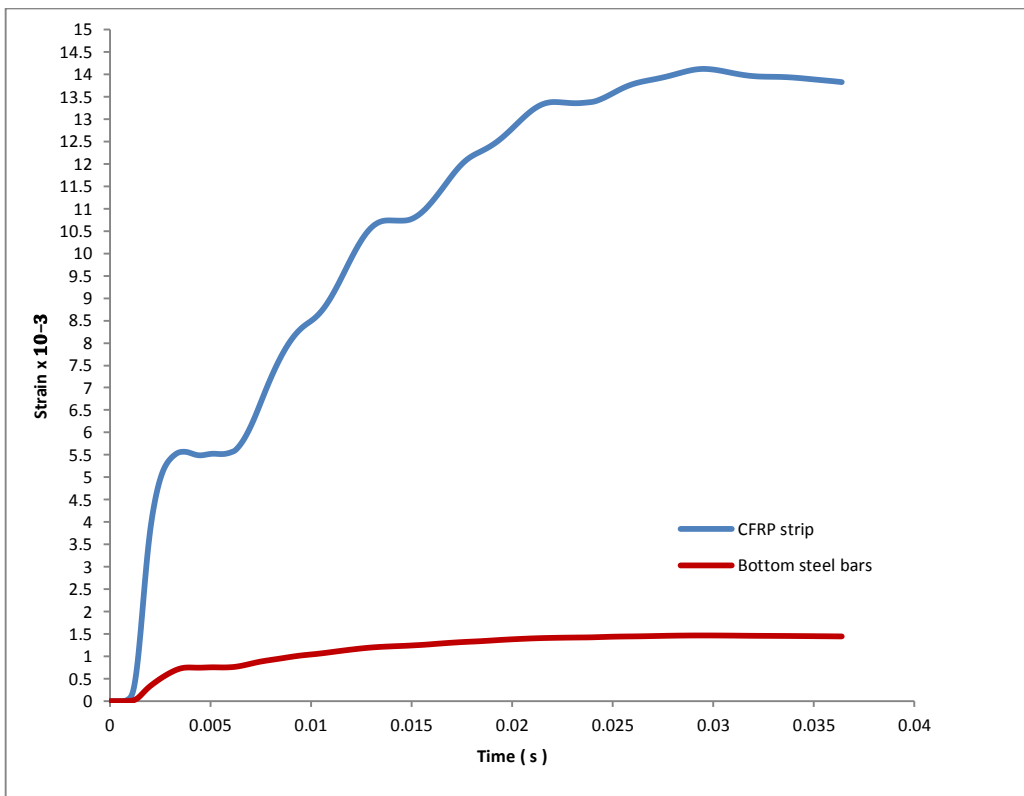
Figure 8.17 Maximum tensile strain in steel bars and CFRP strip vs time of strengthened beam. Impact energy=891 J

Table 8.3 Maximum tensile stresses and strains in steel bars and CFRP strip of strengthened beam under different impact energies

Impact energy (J)	Max. Force (F) (kN) Steel bars	Max. Force (kN) CFRP strip	$\dfrac{F_{CFRP}}{F_{steel}}$	Max. Stress (S) (N/mm^2) Steel bar	Max. Stress (N/mm^2) CFRP strip	$\dfrac{S_{CFRP}}{S_{steel}}$	Max. Strain Steel bar $m\varepsilon$	Max. Strain CFRP strip $m\varepsilon$
396	34.5	33.2	0.95	221	1278	5.8	1.1	8.4
622	38.8	39.6	1	247	2113	8.5	1.2	10
891	45.7	56.2	1.2	293	2160	7.4	1.5	14

8.5 Concluding remarks

A 3-D FE model was used to model and analyse the experimental work conducted in this study. A perfect and bond slip assumption were used to model the bonding between steel bars and concrete. The FE model, including perfect bond between steel bars and concrete, gave good agreement in experimental results in terms of reaction force and maximum deflection compared with the perfect bond.

Good agreement was found between FE results and that of the experimental work in terms of the reaction force, maximum deflection. The FE beam deflection history using FEA was similar to that found experimentally. However, the beam in FEA was damped at a higher rate than in the experimental test.

The FEA of the strengthened beams showed that the stresses and strain in CFRP were much higher than that in steel bars. That revealed that CFRP is a very effective material to use in retrofitting structural members. The FE results showed that the stresses in steel bars did not exceed the yield stresses in early and intimidate stage of impact test. This could explain the very low residual deflection recorded in experimental tests. More FE analysis are required to investigate the stress and strain in steel bars and CFRP strip in failure stage, when the beam was failed by heavy impact loading.

9. Finite Element Analysis (FEA) results of damaged and CFRP repaired beams (repairing stage)

9.1 Introduction

The experimental programme included testing damaged then repaired beams. using CFRP under impact loading. The results of the FEA of strengthened beams showed that FE with bond slip assumption is more reliable than perfect bond. The bond slip assumption using spring element in the 3-D finite element model was used to analyse the damaged and repaired beams. The damage in the beams was modelled by reducing the K-values of the spring element between steel bars and the concrete. The elastic modulus and compressive strength of the concrete were also reduced to simulate the beam damage under impact loading (see section 8.2).

9.2 Damaged and repaired beams, Group 1

Group1 beams were heavily damaged using single impact (891 J). Figure 9.1 shows the experimental and the FEA reaction force of Group 1 damaged beam (B1-1). Figure 9.2 compares the Group 1 damaged beam (B1-1) experimental and FE maximum deflection. A good agreement was found between the experimental and FE results.

The experimental reaction force and the maximum deflection of the repaired beam (B1-2) were compared with the FEA in Figures 9.3 and 9.4 respectively. The comparison showed that FEA results were similar to the experimental results. Table 9.1 compares experimental and FEA results of damaged and repaired beams. The stiffness of the damaged beam was much decreased due to heavy damage. Table 9.1 shows the reduction in bond-slip between the steel bars (k-spring values) and the concrete properties (elastic modulus and compressive strength) due to damage. Equation 8.1 was used to find the stiffness of beams after impact damage, while Equation 8.2 was used to calculate the reduced concrete compressive strength. The concrete elastic modulus was found using Equation 8.3 and spring element stiffness was obtained using Equation 8.4 (see section 8.2.3). Table 9.1 shows the close agreement between the percentages of the FE results and those of the experimental results.

Figure 9.1 Reaction force comparison between experimental and FEM of Group 1 damaged beam under different impact energies

Figure 9.2   Maximum deflection comparison between experimental and FEM of Group 1 damaged beam under different impact energies

Figure 9.3 Reaction force comparison between experimental and FEM of Group 1 repaired beam under different impact energies

Figure 9.4 Maximum deflection comparison between experimental and FEM of Group 1 repaired beam under different impact energies

Table 9.1 Comparison between experimental and FEM results of Group 1 damaged and repaired beams

Impact energy (J)	Beam stiffness $kN/_{mm^2}$	Beam stiffness reduction % Eq. 8.1 *100	$f_c^/$ $N/_{mm^2}$ Eq.8.2	K Spring $N/_{mm^2}$ Eq.8.4	E_c $N/_{mm^2}$ *10^3 Eq.8.3	Reaction force (R) (kN) EXP	Reaction force (R) (kN) FEA	$\frac{R_{FEA}}{R_{EXP}}$ %	Max. Deflection (D) (mm) EXP	Max. Deflection (D) (mm) FEA	$\frac{D_{FEA}}{D_{EXP}}$ %
Damaged beam B1-1											
891	3.63	-	25.6	13.02	23.8	40	41	103	46	45	98
99	0.73	80	5.12	5.82	10.6	20	20	100	17	15	88
396	0.71	80.5	5	5.7	10.3	45	47	104	44	41	93
Repaired beam B1-2											
99	1.09	-	5.12	5.82	10.6	19	17	89	9	7	78
396	1	8.2	4.7	5.58	10.2	41	39	95	16	15	94
622	0.99	9.2	4.65	5.55	10.1	59	50	85	28	25	89

9.3 Damaged and repaired beams, Group 2

A single impact (622 J) was used to induce intermediate damage in Group 2 beams. The FEA was used to model the experimental results of these beams. Figures 9.5 and 9.6 show a comparison between the reaction force and maximum deflection for the experimental and FE results of the damaged beam (B2-1) respectively. Figures 9.7 and 9.8 show the FEA and the experimental reaction force and maximum deflection of the repaired beam (B2-2) respectively. The comparisons show a good correlation between the experimental and FE results for damaged and repaired beams. Table 9.2 shows the percentage of the FEA results relative to the experimental results. The reduction in K-values of the spring element and the reduction in the concrete elastic modulus and compressive strength are also shown in Table 9.2. The results showed that with increasing the impact energy, the damage was increased, which reduced the beam stiffness, which in turn resulted in reduction of the elastic modulus and compressive strength of the concrete.
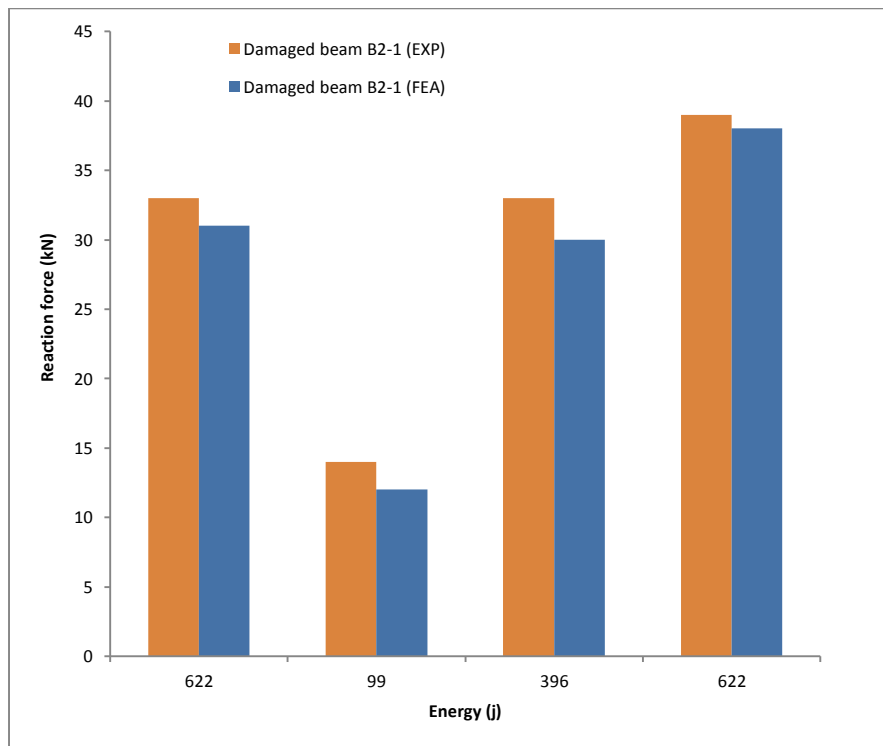
Figure 9.5 Reaction force comparison between experimental and FEM of Group 2 damaged beam under different impact energies
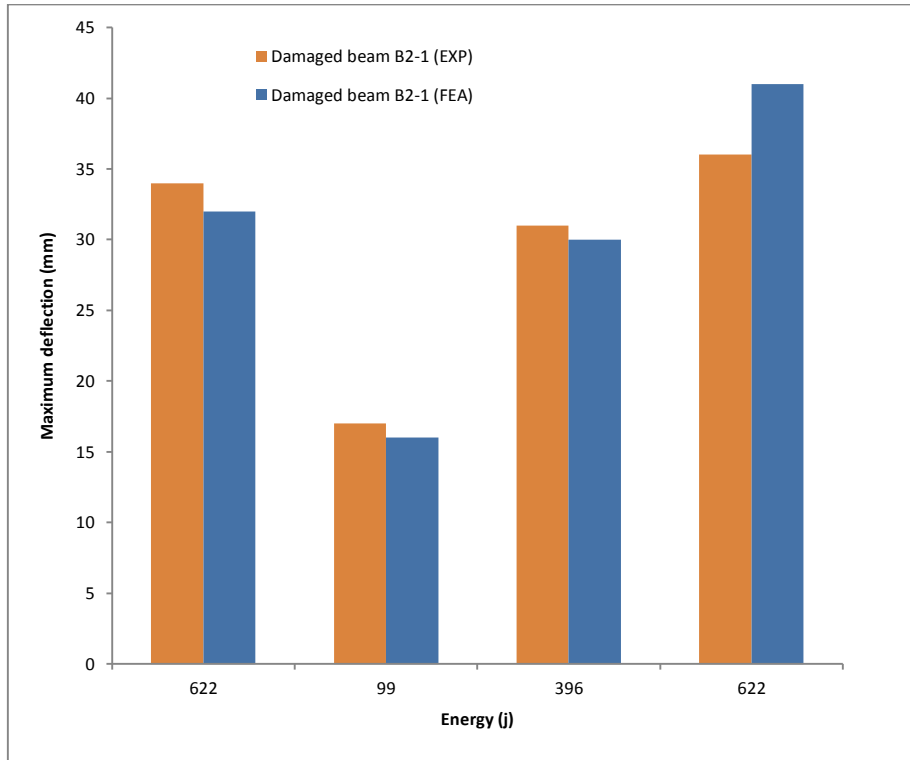
Figure 9.6 Maximum deflection comparison between experimental and FEM of Group 2 damaged beam under different impact energies
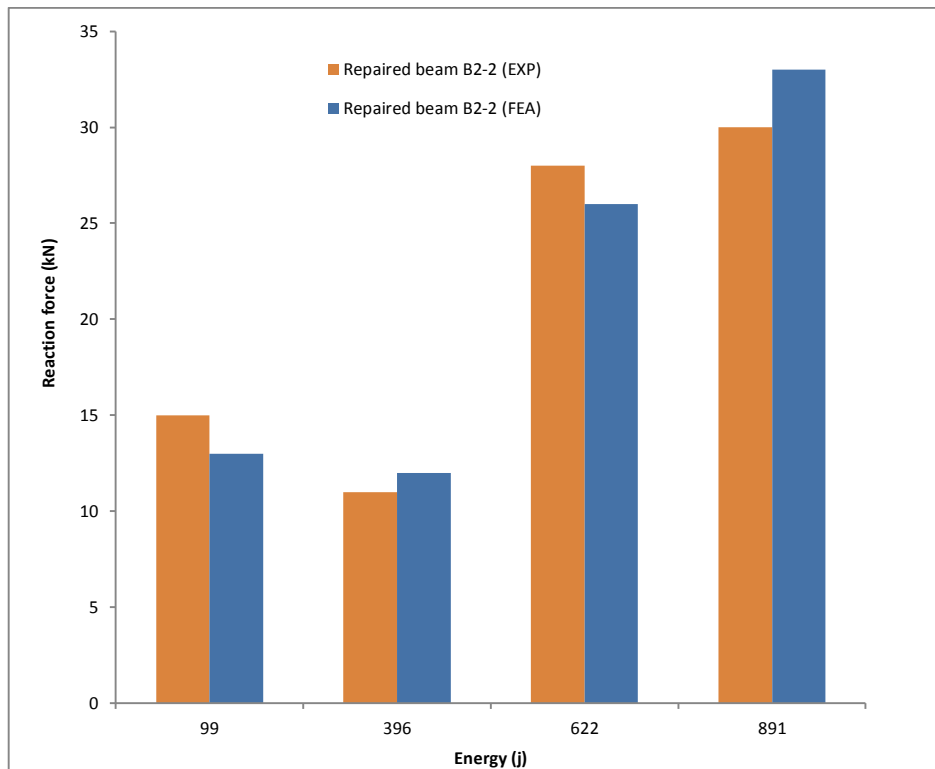
Figure 9.7 Reaction force comparison between experimental and FEM of Group 2 repaired beam under different impact energies
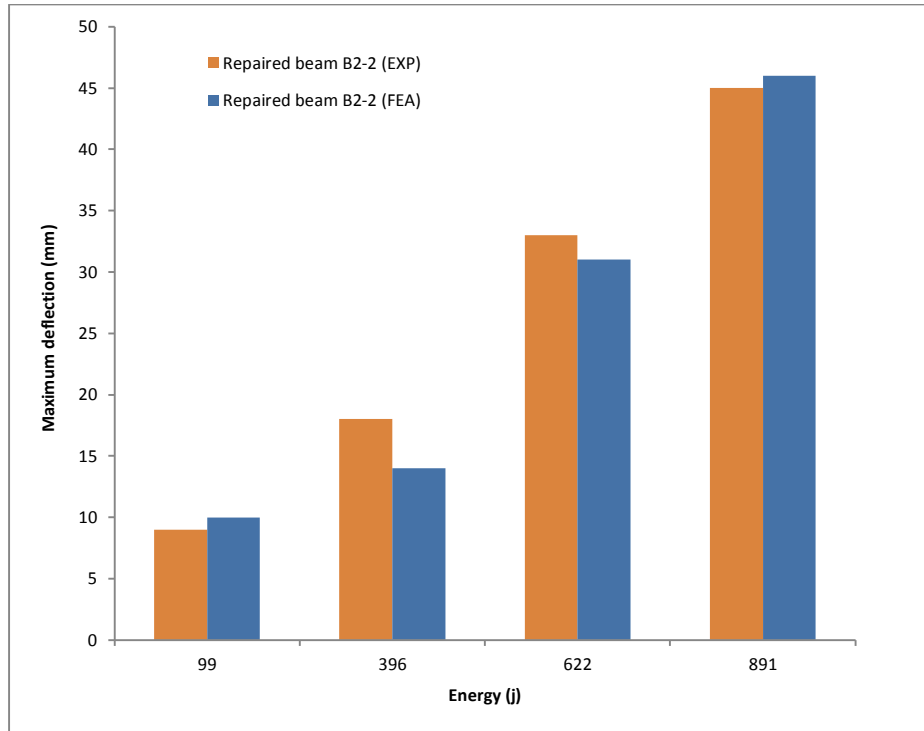
Figure 9.8 Maximum deflection comparison between experimental and FEM of Group 2 repaired beam under different impact energies

Table 9.2 Comparison between experimental and FEA results of Group 2 damaged and repaired beams

Impact energy (J)	Beam stiffness $kN/_{mm^2}$	Beam stiffness reduction % Eq. 8.1 *100	$f_c^/$ $N/_{mm^2}$ Eq.8.2	K Spring $N/_{mm^2}$ Eq.8.4	E_c $N/_{mm^2}$ *10^3 Eq.8.3	Reaction force (R) (kN) EXP	Reaction force (R) (kN) FEA	$\dfrac{R_{FEA}}{R_{EXP}}$ %	Max. Deflection (D) (mm) EXP	Max. Deflection (D) (mm) FEA	$\dfrac{D_{FEA}}{D_{EXP}}$ %
Damaged beam B2-1											
622	3.63	-	25.6	13.02	23.8	33	31	94	34	32	94
99	0.87	76	6.13	6.37	11.6	14	12	86	17	16	94
396	0.85	76.5	6	6.3	11.5	33	30	91	31	30	97
622	0.8	78	5.64	6.11	11.1	39	38	97	36	41	114
Repaired beam B2-2											
99	1.39	-	6.13	6.37	11.6	15	13	87	9	10	111
396	1.24	10.8	5.47	6.02	11	11	12	109	18	14	78
622	1.2	13.7	5.29	5.92	10.8	28	26	93	33	31	94
891	1.17	15.8	5.16	5.85	10.7	30	33	110	45	46	102

9.4 Damaged and repaired beams, Group 3

Group 3 beams were damaged using low impact energy (396 J). Figures 9.9 and 9.10 show a comparison between the reaction force and maximum deflection of the experimental method and the FEM of the damaged beam (B3-1) respectively. Figures 9.11 and 9.12 display a comparison between the reaction force and the maximum deflection of FEA and the experimental method respectively. A good agreement was found between the numerical and experimental results in terms of reaction force and maximum deflection for damaged and repaired beams. Table 9.3 shows good match percentages between the FEA and experimental results.
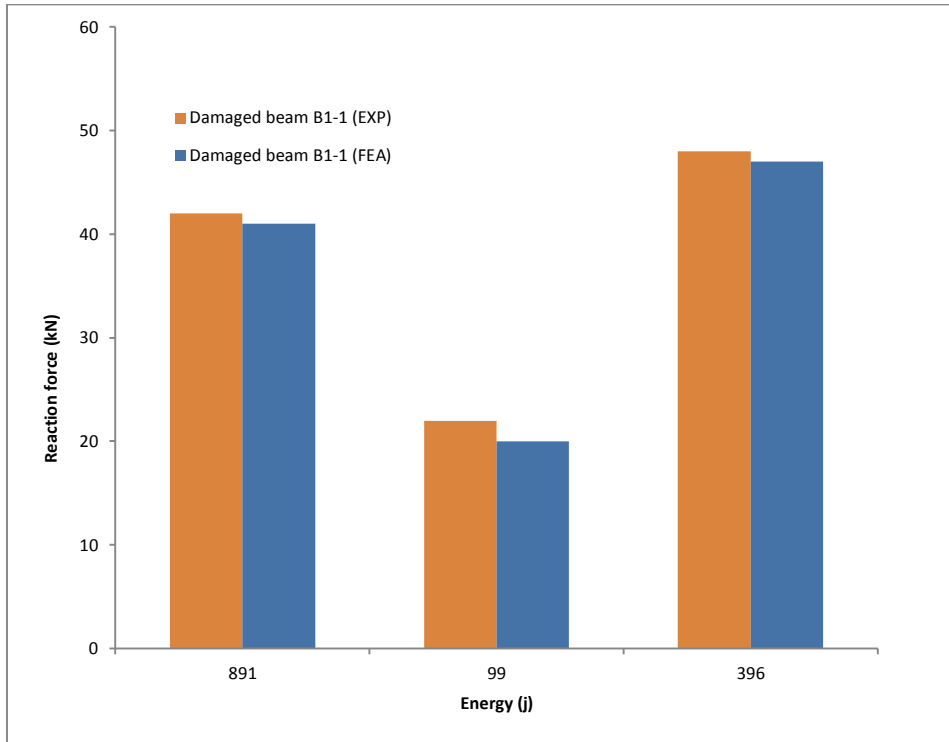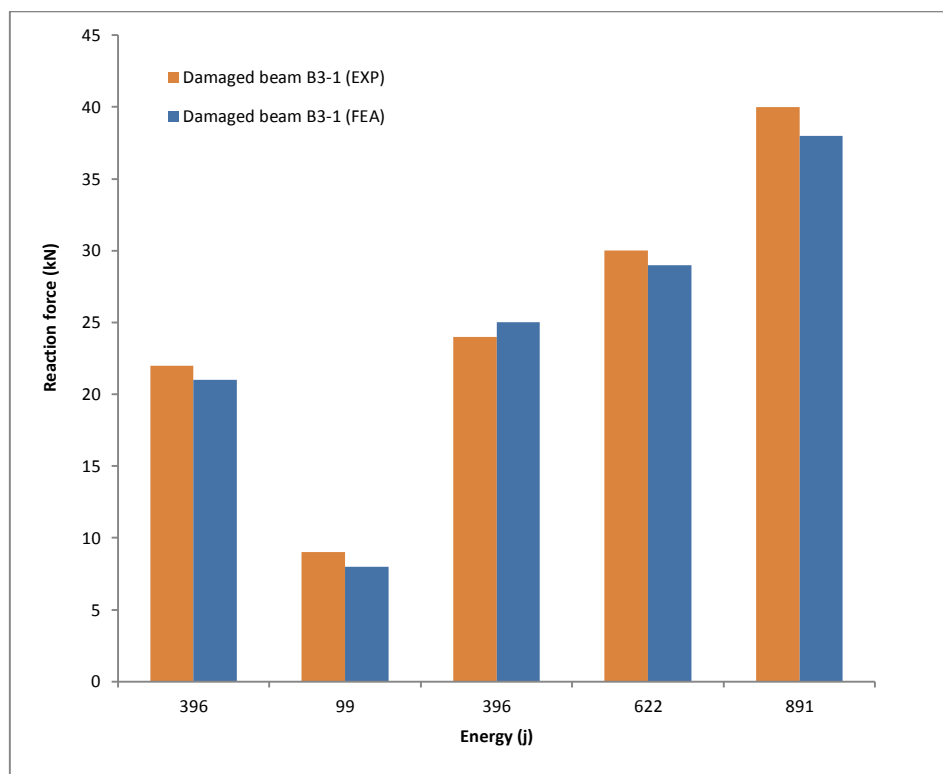

Figure 9.9 Reaction force comparison between experimental and FEM of Group 3 damaged beam under different impact energies
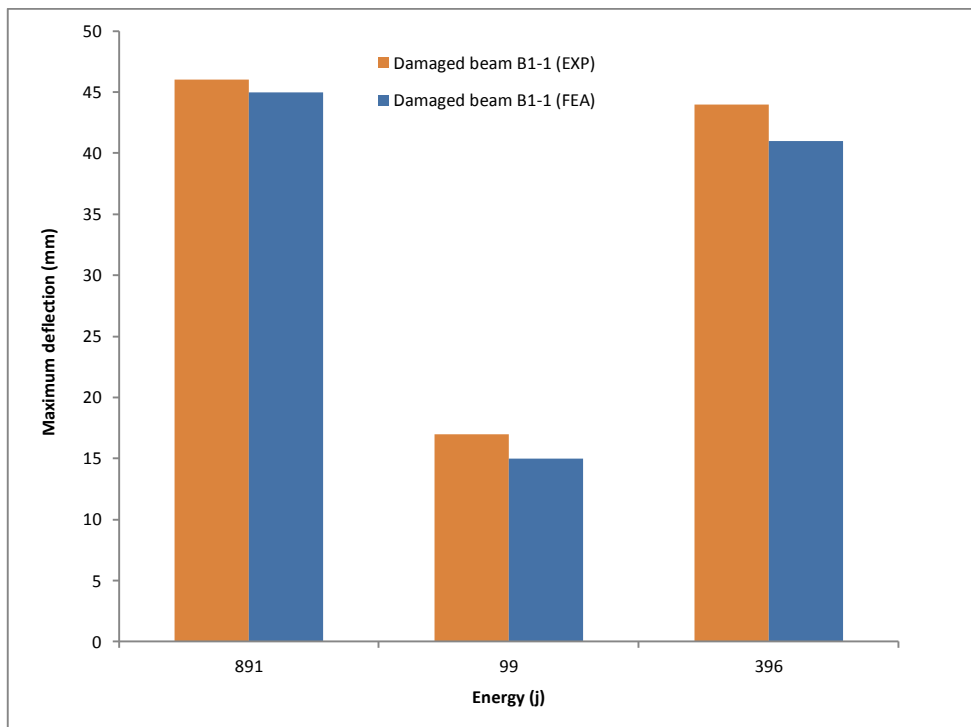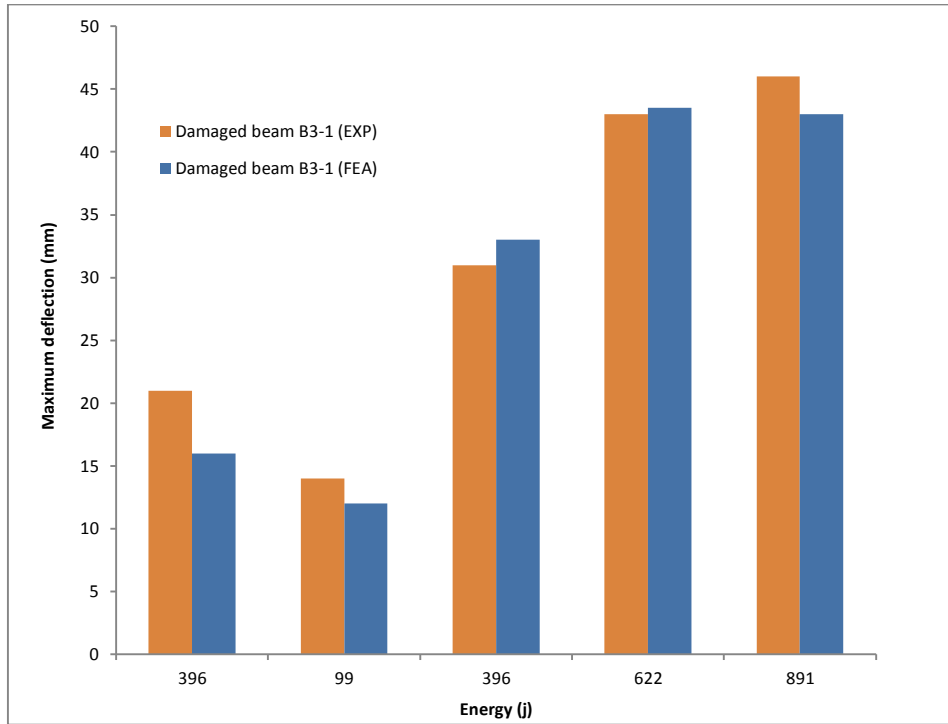
Figure 9.10 Maximum deflection comparison between experimental and FEM of Group 2 damaged beam under different impact energies
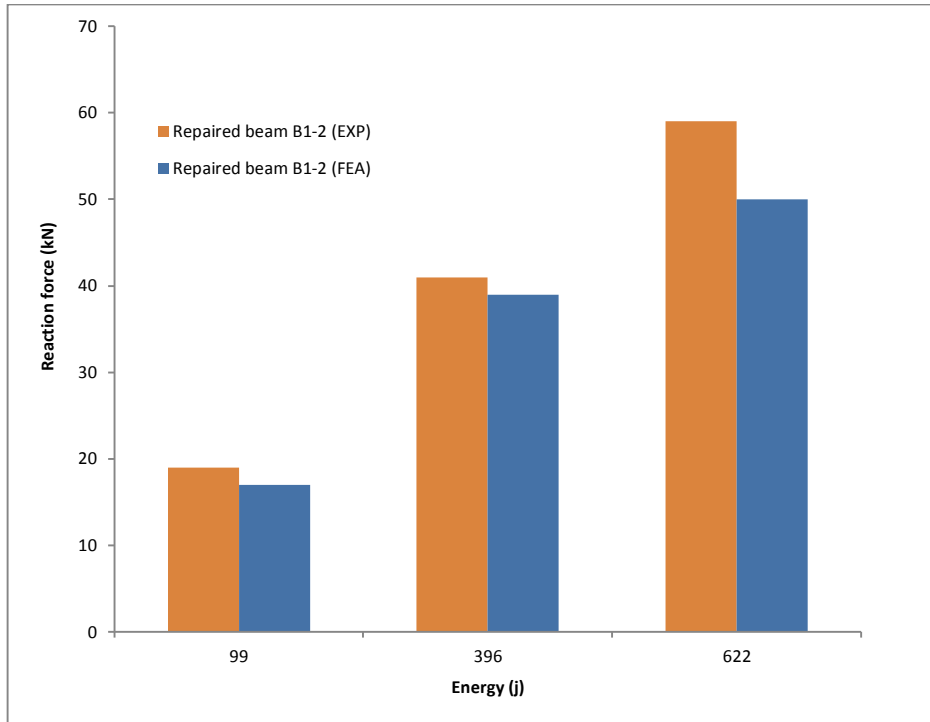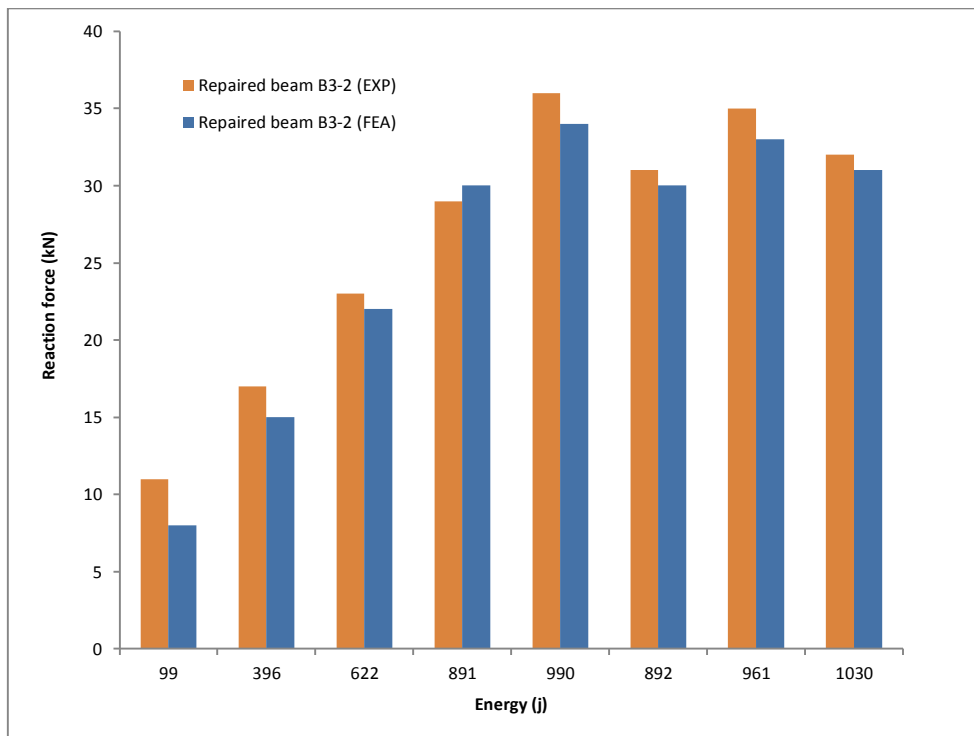

Figure 9.11 Reaction force comparison between experimental and FEM of Group 3 repaired beam under different impact energies
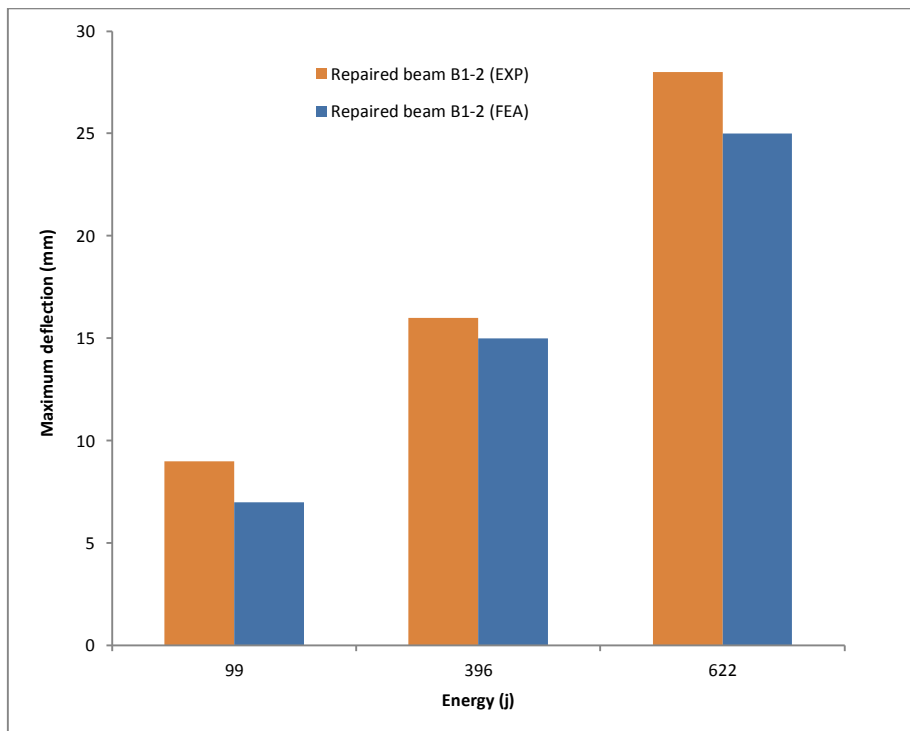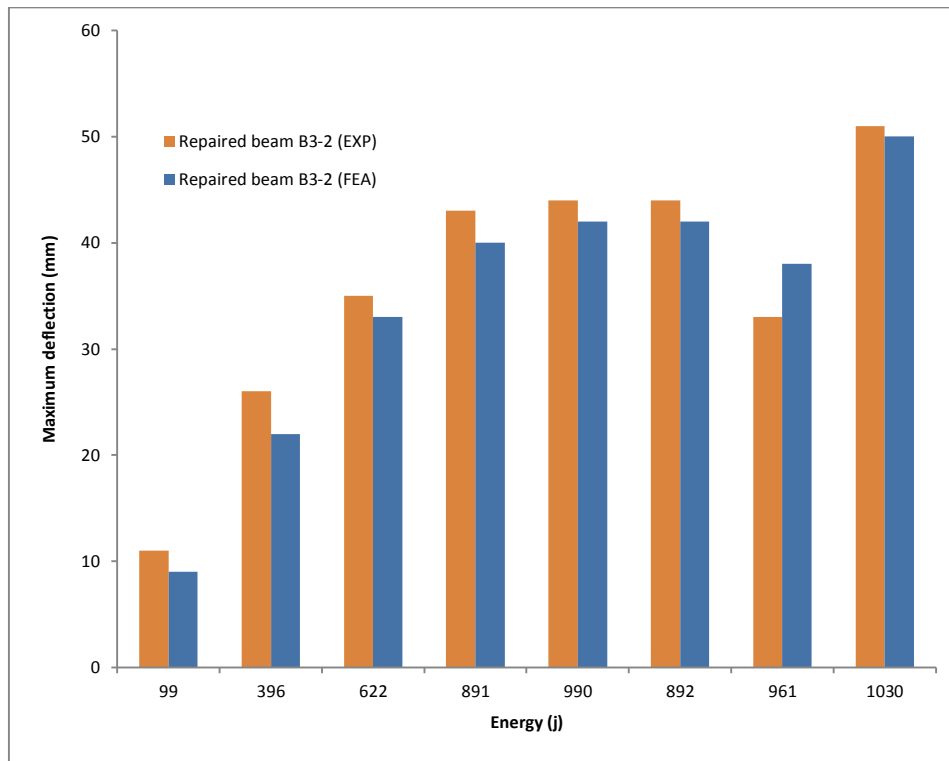
Figure 9.12 Maximum deflection comparison between experimental and FEM of Group 3 repaired beam under different impact energies

Table 9.3 Comparison between experimental and FEM results of Group 3 damaged and repaired beams

Impact energy (J)	Beam stiffness $kN/_{mm^2}$	Beam stiffness reduction % Eq. 8.1 *100	$f_c^/$ $N/_{mm^2}$ Eq.8.2	K Spring $N/_{mm^2}$ Eq.8.4	E_c $N/_{mm^2}$ *10^3 Eq.8.3	Reaction force (R) (kN) EXP	Reaction force (R) (kN) FEA	$\dfrac{R_{FEA}}{R_{EXP}}$ %	Max. Deflection (D) (mm) EXP	Max. Deflection (D) (mm) FEA	$\dfrac{D_{FEA}}{D_{EXP}}$ %
Damaged beam B3-1											
396	3.63	-	25.6	13.02	23.8	22	21	95	21	16	76
99	1.18	67.5	8.32	7.42	13.56	9	8	89	14	12	86
396	1.16	68	8.18	7.36	13.44	24	25	104	31	33	106
622	1.1	69.7	7.75	7.17	13.09	30	29	97	43	43.5	101
891	1.05	71.1	7.4	7	12.8	40	38	95	46	43	93
Repaired beam B3-2											
99	1.48	-	8.32	7.42	13.56	11	8	73	11	9	82
396	1.45	2.0	8.15	7.35	13.42	17	15	88	26	22	85
622	1.4	5.4	7.87	7.22	13.19	23	22	96	35	33	94
891	1.32	10.8	7.42	7.01	12.80	29	30	103	43	40	93
990	1.26	14.9	7.08	6.85	12.51	36	34	94	44	42	95
892	1.24	16.2	6.97	6.80	12.41	31	30	97	44	42	95
961	1.2	18.9	6.75	6.69	12.21	35	33	94	33	38	115
1030	0.88	40.5	4.95	5.73	10.45	32	31	97	51	50	98

9.5 Sensitive analysis

A series of impact tests was conducted on the reference beam, using the 3-D FE model. The study the effect of each damage parameter individually would have given unreliable results, because the damage parameters (compressive strength and elastic modulus of concrete and bond slip) are proportional. Thus the main variable in the parameter study was the beam stiffness. When the beam stiffness was decreased due to impact damage, the concrete compressive strength, elastic modulus and bond–slip stiffness were decreased accordingly (see section 8.2.3). The stiffness of reference beam was reduced by different percentages (10%-60%). Equations 8.2, 8.4 and 8.3 were used to calculate the concrete compressive strength, elastic modulus and bond–slip respectively, as shown in Table 9.4. Different impact energies were used to impact the beam, using FE model (300 J-800 J). Table 9.4 shows the tested beams properties and FEA results. The FEA bending force and maximum deflection were compared with data calculated using Eq. 6.5 and Eq. 6.7 respectively. Figure 9.13 and Figure 9.14 show the comparison between the FE and calculated bending force and maximum deflection respectively. The comparison shows a good agreement between the FE and calculated results.

Table 9.4 Comparison between calculated and FEM results reference beam for different degrees of damaged

Beam stiffness reduction %	Beam stiffness $kN/_{mm^2}$ Eq.8.1	$f_c^/$ $N/_{mm^2}$ Eq.8.2	K Spring $N/_{mm^2}$ Eq.8.4	E_c $N/_{mm^2}$ $*10^3$ Eq.8.3	Impact energy (J)	Bending force Pb (kN) Eq. 6.5	Bending Force Pb (kN) FEA	$\frac{Pb_{FEA}}{RPb_{Eq}}$ %	Max. Deflection D (mm) Eq.6.7	Max. Deflection (mm) FEA	$\frac{D_{FEA}}{D_{Eq}}$ %
-	3.63	25.60	13.02	23.8	-	-	-	-	-	-	-
10	3.27	23.04	12.36	22.56	800	75.10	72	95.9	33.39	35.5	1.1
20	2.90	20.48	11.65	21.27	700	70.96	68	95.8	32.20	34	1.1
30	2.54	17.92	10.90	19.90	600	66.46	60	90.3	30.86	31.5	1.0
40	2.18	15.36	10.09	18.42	500	61.48	56	91.1	29.31	31	1.1
50	1.82	12.80	9.21	16.82	400	55.88	50	89.5	27.48	29	1.1
60	1.45	10.24	8.24	15.04	300	49.36	46	93.2	25.20	26	1.0
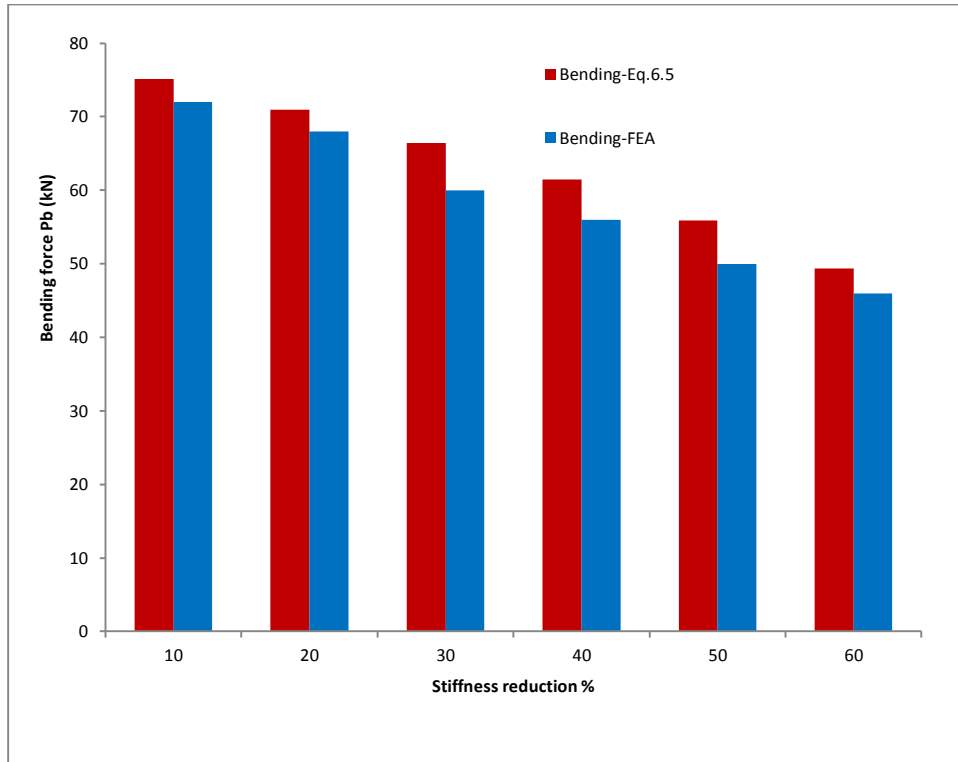
Figure 9.13 Bending force comparison between calculated and FEM for different degrees of damage
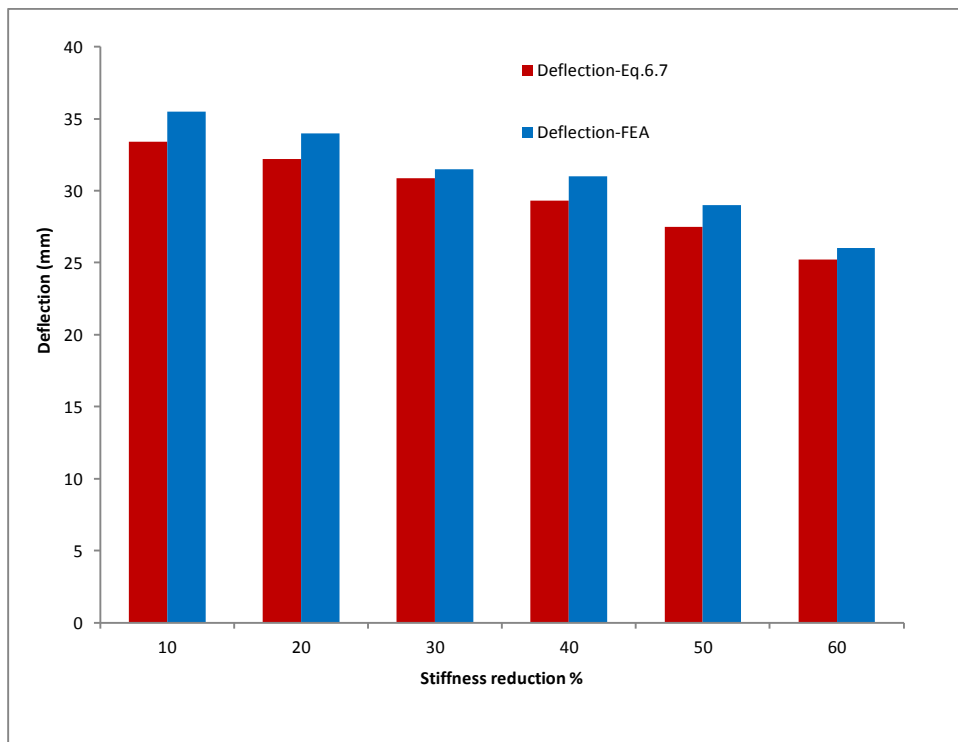
Figure 9.14 Maximum deflection comparison between calculated and FEM for different degrees of damage

Different CFRP repaired beams of different stiffness and concrete properties were tested, using FEM under different impact energies. The increase in the beams stiffness was (10-60 %) and the impact energy was increased from 200 J – 700 j as shown in Table 9.5. The FEA results were compared with those calculated from Eq. 6.6 and Eq. 6.8 in terms of bending force and maximum deflection. Figure 9.15 shows the bending force comparison between calculated and FEM of CFRP repaired beams for different stiffness and impact energies. The maximum deflection comparison between calculated and FEM of CFRP repaired beams for different stiffness and impact energies is shown in Figure 9.16. The comparisons show a very good agreement between the FEA and calculated results. The study shows that the FE model is capable of analysing RC damaged or repaired beams under different stiffness and impact energies.

Table 9.5 Comparison between calculated and FEM results reference beam of CFRP repaired beams for different stiffness and impact energies

Beam stiffness increasing %	Beam stiffness $kN/_{mm^2}$ Eq.8.1	$f_c^/$ $N/_{mm^2}$ Eq.8.2	K Spring $N/_{mm^2}$ Eq.8.4	E_c $N/_{mm^2}$ $*10^3$ Eq.8.3	Impact energy (J)	Bending force Pb (kN) Eq. 6.6	Bending Force Pb (kN) FEA	$\frac{Pb_{FEA}}{RPb_{Eq}}$ %	Max. Deflection D (mm) Eq.6.8	Max. Deflection (mm) FEA	$\frac{D_{FEA}}{D_{Eq}}$ %
Damaged beam	0.88	6.21	6.41	11.71	-	-	-	-	-	-	-
10	0.97	6.83	6.73	12.28	200	30.4	34	111.8	15.7	16.5	1.1
20	1.06	7.45	7.03	12.83	300	36.5	39	106.9	20.3	23	1.1
30	1.14	8.07	7.31	13.35	400	41.4	40	96.7	24.5	25.5	1.0
40	1.23	8.69	7.59	13.86	500	45.6	46	101.0	28.2	30	1.1
50	1.32	9.32	7.86	14.34	600	49.2	53	107.7	31.7	32.5	1.0
60	1.41	9.94	8.11	14.82	700	52.5	54	102.9	35.0	36.5	1.0
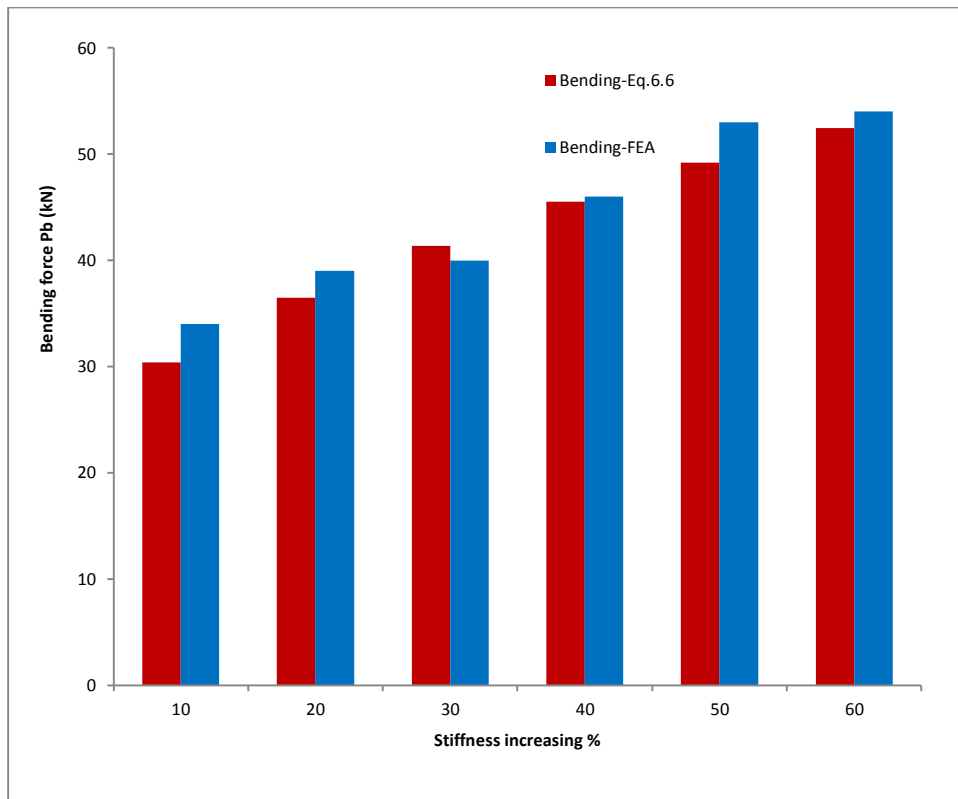
Figure 9.15 Bending force comparison between calculated and FEM of CFRP repaired beams for different stiffness and impact energies
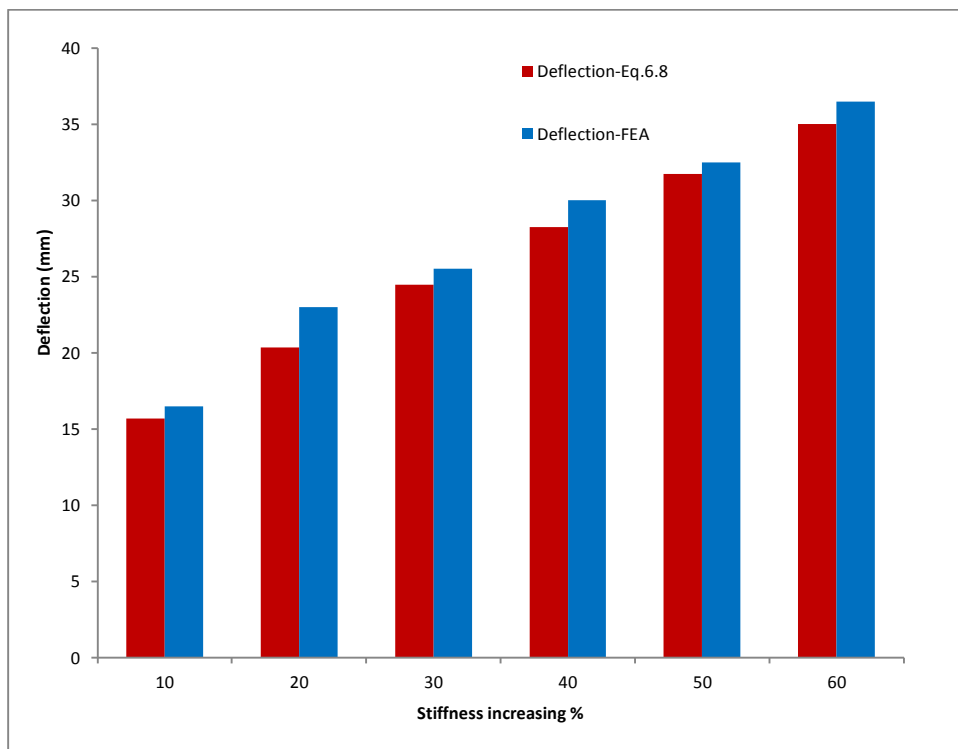
Figure 9.16 Maximum deflection comparison between calculated and FEM of CFRP- repaired beams for different stiffness and impact energies

9.6 Concluding remarks

The impact tests on the damaged and the repaired beams were simulated using a 3-D FE model. The damage to RC beams due to impact was successfully modelled by reducing beam damage parameters (concrete compressive strength, elastic modulus of concrete and bonding between steel bars and concrete). Good agreement was found between the reaction force and maximum deflection of FE results and that of experimental results.

The beam was divided in the FE model into two parts (damaged and undamaged parts) based on crack distribution observed experimentally. Due to the absence of an empirical model to predicate the varying damage along the beam length under impact loading, and also in the interest of simplification, the reduced damage parameters in the damage area were constant and not varied. However, the damage may be varied in the damage area as the damage is proportional to the distance from the impact point

The FE parametric study showed that the behaviour of the beam was affected by reduction in beam damage parameters (in damaged beams) and increase in beam stiffness (in strengthened and repairing beams). The results of the sensitive analysis were compared with that found using proposed equations in terms of the reaction force and maximum deflection and a good agreement was found.

10. Conclusions and future research

10.1 Experimental work

In this study, experimental work was conducted in order to investigate the behaviour of CFRP -strengthened or repaired RC beams under impact.

10.1.1 Impact test machine

A new test machine was designed, manufactured and successfully used to conduct a series of tests to study the behaviour of large RC beams under impact loading. The main conclusions resulting from the use of the new test machine to conduct the tests were as follows:

i.   The steel yoke used in support was successful in preventing the vertical movement and rebounding of the beam ends, while at the same time allowing the beam ends to rotate.

ii.   The flat steel head of the hammer reduced local damage to the tested beams. The sharp steel head caused damage at the point of impact and spalling of pieces of concrete at the top face of the concrete.

iii. Increasing the numbers and capacity of the accelerometers required to measure the beam deflection and impact force increased the precision of measurements. Three accelerometers were used to measure the impact force and three accelerometers used to measure the beam acceleration, velocity and deflection. Due to resource limitations, a single force transducer was used to measure the reaction force at one end of the beam support. The beam was assumed to be perfectly symmetrical and the reactions were assumed to be equal at both supports. However, in reality there is no perfect symmetry and so, for better experimental results and more accuracy, it was decided to use two force sensors, one at each support, to measure the reaction forces more realistically.

iv.   Maximum deflection was measured at different locations of the beam during impact tests, using three methods: dial-gauges, high-speed camera and accelerometers. The comparisons between the three methods gave very close results in terms of beam maximum deflection. To study the beam behaviour during impact in terms of load, acceleration, velocity and deflection time history, it was found that it was more suitable to use the accelerometers, as the dial gauges only recorded the maximum deflection, and also the high-

speed camera results were affected by the recording ratio (frames per second).

10.1.2 CFRP strengthening RC beams under impact loading

To study the impact behaviour of the RC beams strengthened with CFRP strip, three pairs of RC beams were tested under drop weight. NSM and EBR techniques were used to install the CFRP strip.

The following conclusions were drawn:

i. From the experimental results, it was clear that CFRP increased the beam stiffness, resulting in reduction of the impact force. The impact force experienced by the strengthened beams was less than that of the control beam.

ii. Bending load of beams under impact loading depends on the stiffness of the beams. For the reference beam, a high percentage of impact energy was absorbed and dissipated as fracture energy, and less impact energy was transferred to the support, which resulted in low bending force. In strengthened beams, CFRP increased the beam stiffness and reduced the width of the cracks width and their propagation. Low impact energy was released as fracture energy and high impact energy were transferred to the beam support, which increased its the bending force.

iii. In the unstrengthened beams, the impact load reduced the beam stiffness and the crack distributions become non-uniform. The beam deflection and acceleration became non-linear and close to sinusoidal. Therefore, the inertia force distribution became linear rather than sinusoidal.

iv. The CFRP increased the stiffness of the beams and reduced both the beam deformation and the number of cracks. The distribution of the cracks also became more uniform. The deflection and acceleration of the beam were approximately linear along the beam length. Therefore, the linear inertia force distribution assumption gave a higher degree of agreement than the sinusoidal assumption.

v. The CFRP considerably reduced the residual deflection and the maximum deflection of the strengthened beams under impact loading.

vi. For the strengthened beams under impact loading, the CFRP decreased the length and width of the cracks compared with the unstrengthened beams. The beam vibration was another source of cracking, and cracks were appeared at top face of the beam due to impact beam vibration.

vii. The crack distribution showed that approximately two-thirds of the beam was damaged by the impact load. The damage was proportional to the distance from the point of impact. The beam part close to the supports was not damaged, but heavy damage occurred in the middle part of the impacted beam. Therefore, for strengthening and repairing damaged beams under impact loading, the CFRP strip length might be reduced to 2/3 of beam length. In addition, when the beams were analysed theoretically, it was decided to assume that 2/3 of beam was damaged by impact loading.

viii. For the beam strengthened with EBR technique, CFRP was debonded, while no CFRP debonding was observed in the NSM- strengthened beams. The NSM- strengthened beam resisted more cumulative impact energy compared with the reference and the EBR- strengthened beams. It was clear that the NSM technique was more effective than the EBR technique, and therefore the NSM technique is highly recommended for the strengthening and repairing of RC beams under impact loading.

ix. Using CFRP in strengthening the beams decreased the ductility of the beams and increased the probability of their sudden failure. The EBR- strengthened beams failed suddenly by concrete crushing at the compression zone after the debonding of the CFRP strip. In the NSM -strengthened beams, the beams were stiff and suddenly failed by concrete crushing without CFRP debonding. The tested reference beams were under reinforcement. However, when they were strengthened using CFRP, their behaviour became close to the behaviour of the over reinforced beam and they failed suddenly. It is therefore important to pay attention to the changing mode of failure of the beams strengthened with CFRP and it is recommended that the factor of safety of CFRP- strengthened beams exposed to impact loading should be increased.

10.1.3 CFRP repaired RC beams under impact loading

Three groups of beams with different degrees of damage were tested under impact loading to investigate the behaviour of damaged beams repaired by CFRP under impact loading.

The following conclusions were drawn from the study:

(i)   The beams lost a high percentage of their stiffness and rigidity when damaged by single impact loading. This was apparent even under low impact energy. Therefore, it is very important to pay attention to impact damage, even if the beam is exposed to low impact energy. The average stiffness reduction for beams under heavy or intermediate damage was estimated to be 76 % of the initial stiffness of undamaged beam. For beams under low impact energy, a high reduction of beam stiffness was indicated (67 %). The following equation was proposed to predict the stiffness of the beams under different impact energies.

$$K\ damaged = K\ undamged - 6.54 * 10^{-9}EN^3 + 1.443 * 10^{-5}EN^2 - 0.0108EN \qquad 6.3$$

It is highly recommended to repair and strengthening of RC beams exposed to damage by impact loads using high stiffness materials such as CFRP.

(ii)   CFRP strip increased and considerably improved the stiffness of repaired beams. For beams damaged by heavy impact load, CFRP strip increased the damaged beam stiffness by 38%. The highest increase in damaged beam stiffness was 74% for beams damaged intermediately. With low damage, the CFRP strip increased the damaged beam stiffness by about 19**%.**

(iii)   When the damaged or repaired beams were tested under multi-impact loading, the subsequent impacts slightly reduced the stiffness of the beams. This is because a high percentage of beam stiffness is lost by the first single impact that damaged the beams.

(iv)   In individual impact tests, the impact force and bending force of the damaged beams and the repaired beams were similar under high and intermediate impact energies. When the impact energy was low, the impact force and the bending force of the repaired beams were lower than for damaged beams.

(v)   CFRP increased the accumulative impact energy resisted by damaged beams and it was proportional to the degree of damage. High increase in

accumulative impact energy was observed for the repaired low- damage beams, while a low increase in cumulative impact energy was indicated for the repaired beam that was heavily damaged.

(vi)   This research proposed the following equations to predict the beam bending load of the damaged and repaired beams.

$$P_b = \frac{3.27 EN^{0.48}}{K^{0.06}}.$$ 6.5

For the repaired beams,

$$P_b = \frac{2.38 EN^{0.48}}{K^{0.15}}$$ 6.6

(vii)   The following equations were proposed to find the maximum deflection of the damaged and repaired beams under impact loading.

For the damaged beams,

$$MaxDef = \frac{1.52 EN^{0.51}}{K^{0.27}}.$$ 6.7

For the repaired beams,

$$MaxDef = \frac{0.5 E^{0.65}}{K^{0.026}}.$$ 6.8

(viii)   A good agreement was found between the calculated bending load and maximum deflection using the proposed equations (6.5, 6.6, 6.7, and 6.8) and that of experimental results using the proposed equations (6.5, 6.6 and 6.8).

10.2 Finite element of RC beams strengthening or repairing using CFRP

FEM was used to study the behaviour of CFRP strengthened RC beams under static and impact loading.

10.2.1 CFRP- strengthened RC beams under static loading

FEM and the GA were used to analyse the RC beams under static loading and comparisons were made with those of the experimental results.

The following conclusions were drawn: -

i. Modelling the interface layer between the concrete and CFRP using Drucker-Prager in the FEA model resulted in a close match of the load displacement behaviour with those observed in the experimental tests. The results demonstrated that the Drucker-Prager model was more accurate than the multi-crack concrete model in predicting the ultimate failure load, load-deflection behaviour and failure mode of RC beams strengthened with CFRP.

ii. Modelling the bond-slip between the reinforcement steel bars and the concrete using joint elements resulted in a close match with the experimental results.

iii. This investigation has confirmed that model updating process using a genetic algorithm (GA) optimisation tool can lead to models that produce a good match with their physical laboratory results.

10.2.2 Strengthened or repaired RC beams under impact loading

In this study, FEM was used to predict the behaviour of the RC concrete beams strengthened/or repaired with CFRP under impact loading. The following conclusions were drawn from the FEA study:

i. The FEA model using a spring element was more accurate than an FEA model using a perfect bond model. It is therefore important to include the steel bars-concrete bond slip in theoretical modelling of the beams under impact loading.

ii. Analysing strengthened and repaired damaged beams under impact loading using a 3D FE models resulted in close agreement for both the reaction force and the maximum deflection compared with those of the experimental results. The FE model was capable of predicting the deflection-time history. Similar

beam behaviour during impact was observed in experimental tests and in the FEA results. Therefore, the proposed 3-D model can be appropriate in studying the response of more complex structures repaired or strengthened with the FRP under impact loading.

iii. The damage in beams due to impact loading was successfully modelled by reducing the beam stiffness. The beam stiffness was reduced in the FE models by decreasing the concrete elastic modulus and concrete compressive strength and by bonding the steel bars with the concrete.

iv. FEM was capable of predicating the beam deflection history during the impact, and the behaviour observed was similar that of the experiential results. The damping ratio in FEA was higher than that in the experimental tests.

v. The FEA results revealed that the stresses in steel bottom bars did not exceed their yield stress because the CFRP resisted high percentages of the tensile stresses of the beams in early and intermediate stages of impact testing. However, more FE tests are required to study the stress and strain distribution in CFRP strips and steel bars in failure stage. Experimental tests are necessary in order to investigate the stress and strain distribution in CFRP strips and steel bars and to verify the FE conclusions.

vi. The sensitivity analysis conducted in this study on stiffness degradation parameters revealed that the 3-D FE model is robust and can predicate the behaviour of strengthened or repaired beams under impact loading. The results of the sensitivity analysis were compared with that of the proposed equations. A good agreement was found between the FE bending force and maximum deflection with those calculated using the proposed equations (6.5, 6.6, 6.7, and 6.8).

10.3 Future research

The following areas of future research are recommended:

I. More experimental studies are required to investigate different parameters on the impact behaviour of the CFRP strengthened beams, such as reinforcement ratio, CFRP ratio and shear span length. In this research, a constant span length, CFRP and steel reinforcement ratios were used in the experiments.

II. Future research is required to investigate experimentally the strengthening of the compression zone of the beams under impact loading. The experimental work conducted in this research revealed that all beams failed by crushing of the concrete when strengthened with CFRP in the tension zone.

III. Due to limitations of resources for this research, the CFRP and steel stresses and strains were investigated theoretically using FEM. Therefore, further experimental work is recommended for the study of the distribution of stresses and strain in the CFRP strip and steel bars of the strengthened or repaired RC beams under impact loading.

IV. In this research, only simply supported beams were tested under impact loading. More studies are required to investigate the impact behaviour of the CFRP strengthened beams under different boundary conditions.

V. The bond slip was investigated theoretically in this project, using FEA models. Future research is recommended to experimentally investigate the mechanism of the bond-slip between the steel reinforcement bars and concrete of the strengthened or repaired RC beams under impact loads.

VI. This study is limited to RC rectangular beams. More studies are required to investigate the CFRP strengthened beams with different practical cross-sections.

VII. In the FEA model used in this research, the RC beam was divided into two zones, damaged and undamaged parts, and the damage percentage was assumed to be constant in the damaged part of the beam. However, the damage percentage could vary along the damaged part of the beam. Therefore, more experimental and analytical investigations are required to study the impact damage along the length of the beam.

Appendix A Experimental work of impact test on CFRP RC beams

Study 1	Title	Behaviour of Concrete Beams Strengthened with Fiber-Reinforced Polymer Laminates under Impact Loading.					
Authors		Taiping Tang and Hamid Saadatmanesh					
Beams properties		Dimensions	Number	Width	Height		Span
			5	203mm	95 mm		1.98 m
		Reinforcement	Longitudinal			2-9.8 mm	
			Shear			No	
		Materials Properties	Concrete Strength			27.6 MPa	
			Concrete Elastic modulus			24.9 GPa	
			Steel Yield strength			275.8 MPa	
			Steel Elastic modulus			200 GPa	
		FRP Type	Kevlar laminate, Carbon laminate				
		FRP Properties	Type			Carbon	Kevlar
			Thickness(mm)			0.67	0.43
			Weight(g/m2)			599	307
			Ultimate strain			0.014	0.017
			Ultimate strength(MPa)			1.035	460
			Elastic Modulus (GPa)			85.7	37.6
Impact machine		Impacter weight,	222 N				
		shape	Steel cylinder(127mm diameter)				
		Drop Heights (m)	0.305,0.61,0.91,1.22,1.53,1.83,2.14,2.44,2.74				
		Instruments	Accelerometer				
			LVDT				
			Load Cell				
			Dial caliper				
Beams classification		-Two beams strengthened with Kevlar laminate -Two beams were strengthened with carbon laminate -One beam without strengthening					
Brief explaining of the experimental work		Two types of impact test were performed. One was a single impact test from the same height ,the other was a repeated impact test from different heights					
Test results		- Reaction force of beams for different drop heights - Comparison of maximum reaction force with drop height for tested beams - Reaction force of beams for repeated impact load - Comparison of maximum reaction force with number of drop for beams - Deflection of beams for different drop heights. - Deflection of beams for repeated drop load. - Individual and cumulative residual deflection with drop height. - Cracking and Mode of failure					
conclusions		The impact resistance of RC beam increase with using FRP to strength the beam and its deflection reduced. -the thickness and weight of laminate affect the reaction force of beam. - The numbers and width of cracks reduced were reduced with using FRP laminate -using FRP reduce the shear increase the shear strength.					

Study 2	Title	**Resistance of CFRP strengthened RC beams under impact loadings**			
Authors		Sam Soeum, Kazunori Fujikake,Takahiro Matsui and Kenji Suzukawa			
Beams properties		Dimensions	Number	Width	Height	Span
			20	170mm	160 mm	1.7 m
		Reinforcement	Longitudinal		2-Ø10 mm	
			Shear		Ø6mm@60 mm c/c	
		Materials Properties	Concrete Strength		41.2 MPa	
			Steel yield strength		Longitudinal	382 MPa
					Shear	295 MPa
		FRP Type	Carbon			
		FRP Properties	Type	Unidirectional laminates	Unidirectional two sheets	
			Ultimate Strength MPa	2400	3400	
			Elastic Modulus GPa	156	25	

Beams classification	Control beams		Without strengthening
	TCN	Stren.	0.222 mm thick.,150 mm width CFRP sheet
		Anchor	No
	TCC	Stren.	0.222 mm thick.,150 mm width CFRP sheet
		Anchor	0.111 mm thick.,250 width CFRP sheet
	TLB	Stren.	1.0 mm thick.,50 mm width CFRP laminate
		Anchor	9mm Steel plate+16 mm anchor bolts
	TLC	Stren.	1.0mm thick.,50 mm width CFRP laminate
		Anchor	111 mm ,250 width CFRP U-wrap Sheets

Impact machine	Impacter weight,	300 kg
	shape	Hemispherical Steel (90mm diameter)
	Drop Heights mm	50,100,200,400 mm
	Instruments	Accelerometer
		Laser displacement sensor

Brief explaining of the experimental work	Two types of impact test were performed. One was a single impact test from the same height ,the other was a repeated impact test from different heights
Test results	- Maximum midspan deflections in single impact loading test. - Cracking and Mode of failure. - Relationships between maximum midspan deflection and number of blows in repeated impact loading test. - Effect of end anchorage on debonding failure.
Conclusion	- Cracks width is decreased with using FRP - Debomding failure of CFRP sheets can be prevented by using end anchorage system. - Using CFRP pultrude increase the impact resistance of RC beam.

study 3	Title	Impact Loading of Concrete Beams Externally Strengthened with CFRP Laminates				
Authors		M.A.ERKI, P.E, and U.Meier, P.E				
Beams properties		Dimensions	Number	Width	Height	Span
			4	400mm	300 mm	8.150 m
		Reinforcement	Longitudinal	Top	3-Ø10 mm	
				Bottom	4-Ø18mm	
			Shear		Ø8mm	
		Materials Properties	Concrete Strength	BF1,BF2	65.6 MPa	
				1G,2G	33 MPa	
			Concrete Elastic modulus		210 GPa	
			Steel Elastic modulus		210GPa	
		Strengthening	Steel plate , Carbon laminate			
		Properties	Type		Carbon	Steel
			Thickness mm, length mm		1 mm	3,7840
			Width, number		50,2	263,1
			Cross-sectional area (mm2)		100	789
			Yield Strength MPa		No	263
			Ultimate strain		0.014	0.017
			Elastic Modulus GPa		147.5	210
Impact machine		Heights (m)	0.5,1,1.5,2			
		Instruments	Accelerometer			
			Optical sensor			
			Load Cell			
			Strain gauge, demec gauges			
			High speed camera			
Beams classification		BF1	Strengthened with two CFRP laminate			
		BF2	Strengthened with two CFRP laminate			
		1G	Strengthened with steel plate			
		2G	Strengthened with steel plate			
Brief explaining of the experimental work		One end of the beam was lifted to specific height and then dropped. While the other end was fixed using pin connection				
Test results		- Reaction force of beams for different drop heights - Deflection of beams for different drop heights. - Influence of rate of strain - Comparison between theoretical and experimental midspan deflection - Cracking and Mode of failure				

Study 4	Title	**Nonlinear Finite Element Analysis of Impact Behaviour of Concrete Beam**			
Authors		Erkan Kantar, R.TurgulErdem and Ozgur Anil			
Beams properties		Dimensions	Number	Width	Height	Span
			10	150mm	150 mm	710 mm
		Reinforcement	No			
		Concrete Strength	Normal Strength		24.5 MPa	
			High strength		45.5 MPa	
Impact machine		Impacter weight	5.25 kg			
		shape	Hammer			
		Drop Heights mm	300 mm,350,400,450,500			
		Instruments	Accelerometer			
Beams classification		-Five normal strength concrete beams. -Five high strength concrete beams.				
Brief explaining of the experimental work		A constant weight was dropped from five different heights to induce impact force.				
Test results		- Acceleration, Velocity and Displacement Behaviours of Specimens - Absorbed energy capacity of specimens - Comparisons between experimental and theoretical results.				

Study 5	Title	Simulation of the dynamic response of concrete externally reinforced with carbon-fiber reinforced plastic.			
Authors		D. M. Jermo and C. A. Ross			
Beams properties		Dimensions	Number	Width	Height	Span
			88	76.2mm	76.2 mm	762 mm
		Reinforcement	Longitudinal		No	
			Shear		No	
		Materials Properties	Concrete Density(light)		1892.7 kg/m3	
			Nylon fiber		1.78 kg/m3	
		FRP Type	Carbon panel			
		FRP Properties	Number of panels		1,2,3	
			Thickness(mm)		0.216,0,355,0.495	
			Nylon fiber volume		60%	
			Ultimate strength(N/mm)		2206.9 MPa	
			Elastic Modulus		137.9 MPa	
Impact machine		Impacter weight	43.7 KG			
		shape	Steel cylinder(127mm diameter)			
		Drop Heights	0.61 M			
		Instruments	Electrical strain gauges			
			Non-contact linear measuring system			
			High speed camera			
			Dial caliper			
Beams classification		- beams were strengthened with 1 bottom CFRP panel - beams were strengthened with two bottom CFRP panel - beams were strengthened with three bottom CFRP panel - beams were strengthened three bottom CFRP panel with 3 lbs per cubic yards - beams were strengthened three bottom CFRP panel with both side CFRP panel				
Tests Description		Static Test	The beams were tested under central or three point loading			
		Dynamic Test	A series of 54 drop weight tests were conducted in which the beams were subjected to impulsive central loading.			
Test results		- Impact load vs Time. Displacement VS time. Velocity vs Time. Acceleration vs Time. - Impact and inertia load vs Time. Bending load vs Time. Bending energy vs Time. Bending load vs Displacement. - Strain vs Time. Strain rate vs Time. - Comparison of dynamic and static bending experiments. - Comparison of Experimental and theoretical results.				
Conclusions		- The dynamic bending is greater than static bending of beam atrengthened with CFRP - The failure modes of all beams were the same under static and impact load.All beams failed in shear. - The using CFRP ply at the sides of beam increase the shear strength and fracture energy capacity				

Study 6	Title	Effect of shear mechanisms on impact behaviour of reinforced concrete beams				
	Authors	SelcukSaatci and Frank J. Vecchio				
Beams properties	Dimensions	Number	Width	Height		Span
		12	250mm	410 mm		4.480 m
	Reinforcement	Long.	29.9 mm top,2-29.9 bot.			
		Stirrups	7 mm @100,150 and 300 mm			
	Concrete Strength		46.7,47,44.7,50.1 and 55.2 MPa			
	Yield strength	Ø29.9 bar				464 MPa
		Ø7 mm bar				605 MPa
Impact machine	Impact weight,		211 kg, 600 kg			
	shape		Square hallow section filled with concrete and steel plates			
	Drop Heights		3.26 m			
	Instruments		Accelerometer			
			Potentiometers			
			Electrical strain gauge			
Beams classification	- For Impact test, four beams pairs identical in concrete properties and differ shear reinforcement percentages. - For static test, four beams identical in concrete properties and differ shear reinforcement percentages.					
Tests Description	Static Test	The beams were tested under central or three-point loading				
	Dynamic Test	One group of beams were tested once with smaller drop-weight, followed by two tests with the larger one. Another group were tested twice with the larger drop weight, and then tested with the smaller drop-weight.				
Test results	- Crack patterns - Mid-span displacement vs static force - Mode of failure - Mid-span displacement vs Time - Support reaction vs time - Distribution of forces and dynamic equilibrium - Impact capacity of tested beams. - Displacement shape - Apparent damping - Energy imparted on specimens - Comparison between static and dynamic results.					

221

Study 7	Title	Static and dynamic response of damaged RC beams strengthened with NSM CFRP rods			
		Roberto Capozucca			
Beams properties	Dimensions	Number	Width	Height	Span
		3	150mm	250mm	3.75 m
	Reinforcement	Longitudinal	B1,B2	2-14 mm Bot., 2-10 Top.	
			B3	2-16mm Bot., 2-10 Top.	
		Shear	8@150mm		
	FRP Type	Two Near surface mounted CFRP rods			
Impact machine	Impacter type	Impact hammer			
	Frequencies	0-800 Hz			
	Resolution	0.5 Hz			
	Spring stiffness	8 N/mm			
	Instruments	Accelerometer, strain gauge			
Beams classification	-B1,B2, B3, B4 with four degrees of damageD1, D2, D3, D4				
Brief explaining of the experimental work	Static Test: Four point load test was conducted on undamaged beams to induce four degrees of damages D1…D4.After that, the beams were strengthened with NSM CFRP rods and tested with the same loading path. Dynamic test: The free vibration tests were used to obtain the experimental dynamic parameters for beams with different state of damages. The beams were hung with the flexible spring and subjected to impulsive loading using impact hammer.				
Test results	- Comparison of experimental and theoretical results at yielding phase and failure. - Comparison of experimental frequency of beams with different state of damages.				
Conclsions	- An increasing in flexuring strength and reducing in deflection have been indicated when CFRP sheet was used to strength the beams.				

Study 8	Title	**Static and dynamic response behaviour of RC beam model strengthened by CFRP sheets**			
Authors		Roberto Capozucca, M. Nilde Cerri			
Beams properties		Dimensions	Number	Width	Height	Span
			2	100mm	150mm	2.45 m
		Reinforcement	Longitudinal		.2-6mm Top., 3-8mm Bot.	
			Shear		Yes	
		FRP Type	One and two CFRP Sheets			
		Anchor	CFRP U-sheets at the ends			
		Materials Properties	Concrete Strength		32MPa	
			Concrete Elastic modulus		40.225 GPa	
			Steel Yield strength		315MPa	
			Steel Elastic modulus		2100GPa	

Study 8	**Title**	**Static and dynamic response behaviour of RC beam model strengthened by CFRP sheets**
Authors		Roberto Capozucca, M. Nilde Cerri

Beams properties

Dimensions	Number	Width	Height	Span
	2	100mm	150mm	2.45 m

Reinforcement		
Longitudinal	.2-6mm Top., 3-8mm Bot.	
Shear	Yes	

FRP Type	One and two CFRP Sheets
Anchor	CFRP U-sheets at the ends

Materials Properties		
Concrete Strength	32MPa
Concrete Elastic modulus	40.225 GPa
Steel Yield strength	315MPa
Steel Elastic modulus	2100GPa

Impact machine

Impacter type	Impact hammer
Frequencies	0-800 Hz
Resolution	0.5 Hz
Spring stiffness	8 N/mm
Instruments	Accelerometer

Beams classification

-B1: Strengthened with one layer of the CFRP-sheet and subjected to the maximum load max.=8 Kn and moment Mmax=4.5 kN.m.

-B2: Strengthened with two layers of the CFRP-sheet subjected to the maximum load max.=10 Kn and moment Mmax=5.38 kN.m corresponding to the Yielding moment=5.38

Brief explanation of the experimental work

The experimental work of static tests was as follows:
- Beams were statically tested to obtain a permanent state of cracking in tensile zone of the beam.
- After the beams were strengthened with CFRP-sheet, the static test was carried out on it.
- The beam was loaded through the static test.

Until to failure

The dynamic test programme was as follows:
- Before of the damage of the beams, beams were examined under dynamic load to obtain the natural frequency.
- After the beams were damaged, beams were tested under dynamic load. Also, all beams strengthened with CFRP sheet were tested under dynamic load
- The dynamic test was conducted on the beams after the static load was conducted on it

Test results

- Comparison between theoretical and experimental results of the Moment-deflection curve for beams with and without CFRP strengthening.
- Experimental frequency values for beams B1 and B2 for the following cases:

1-Initial before cracking

2-After cracking

3-After strengthening by CFRP

4-After test

Appendix B Instrumentation data sheets

B.1 Accelerometer

Figure B.1 Accelerometer

Model Number 353B11	ACCELEROMETER, ICP®		Revision J ECN #: 26610

Performance	ENGLISH	SI	
Sensitivity (±10 %)	5 mV/g	0.51 mV/(m/s²)	
Measurement Range	±1000 g pk	±9810 m/s² pk	
Frequency Range (±5 %)	1 to 10000 Hz	1 to 10000 Hz	
Frequency Range (±10 %)	0.7 to 15000 Hz	0.7 to 15000 Hz	
Frequency Range (±3 dB)	0.35 to 30000 Hz	0.35 to 30000 Hz	
Resonant Frequency	≥70 kHz	≥70 kHz	
Broadband Resolution (1 to 10000 Hz)	0.01 g rms	0.1 m/s² rms	[1]
Non-Linearity	≤1 %	≤1 %	[2]
Transverse Sensitivity	≤5 %	≤5 %	[3]
Environmental			
Overload Limit (Shock)	±10000 g pk	±98100 m/s² pk	
Temperature Range (Operating)	-65 to +250 °F	-54 to +121 °C	
Base Strain Sensitivity	≤0.005 g/με	≤0.05 (m/s²)/με	[1]
Electrical			
Excitation Voltage	18 to 30 VDC	18 to 30 VDC	
Constant Current Excitation	2 to 20 mA	2 to 20 mA	
Output Impedance	≤100 Ohm	≤100 Ohm	
Output Bias Voltage	8 to 12 VDC	8 to 12 VDC	
Discharge Time Constant	0.5 to 2.0 sec	0.5 to 2.0 sec	
Settling Time (within 10% of bias)	<5 sec	<5 sec	
Spectral Noise (1 Hz)	6400 µg/√Hz	62784 (µm/sec²)/√Hz	[1]
Spectral Noise (10 Hz)	1400 µg/√Hz	13734 (µm/sec²)/√Hz	[1]
Spectral Noise (100 Hz)	360 µg/√Hz	3532 (µm/sec²)/√Hz	[1]
Spectral Noise (1 kHz)	128 µg/√Hz	1256 (µm/sec²)/√Hz	[1]
Physical			
Size (Height)	0.43 in	10.9 mm	
Weight	0.07 oz	2.0 gm	[1]
Sensing Element	Quartz	Quartz	
Size (Hex)	0.31 in	7.9 mm	
Sensing Geometry	Shear	Shear	
Housing Material	Titanium	Titanium	
Sealing	Hermetic	Hermetic	
Electrical Connector	5-44 Coaxial	5-44 Coaxial	
Electrical Connection Position	Side	Side	
Mounting Thread	5-40 Male	5-40 Male	
Mounting Torque	8 to 12 in-lb	90 to 135 N-cm	

Typical Sensitivity Deviation vs Temperature

CE [4]

Optional Versions (Optional versions have identical specifications and accessories as listed for standard model except where noted below. More than one option maybe used.)

A - Adhesive Mount [5]
Supplied Accessory: Model 080A90 Quick bond Gel (for use with accelerometer adhesive mtg bases to fill gaps on rough surfaces)

B - Low bias electronics

Output Bias Voltage	4.5 to 7.5 VDC	4.5 to 7.5 VDC
Excitation Voltage	12 to 30 VDC	12 to 30 VDC
Constant Current Excitation	1 to 20 mA	1 to 20 mA
Measurement Range	±600 g pk	±5886 m/s² pk

J - Ground Isolated

Frequency Range (±5 %)	1 to 8000 Hz	1 to 8000 Hz
Frequency Range (±10 %)	0.7 to 15000 Hz	0.7 to 15000 Hz
Resonant Frequency	≥56 kHz	≥56 kHz
Electrical Isolation (Base)	≥10⁸ Ohm	≥10⁸ Ohm
Size (Hex x Height)	0.37 in x 0.57 in	9.5 mm x 14.5 mm
Weight	0.11 oz	3.2 gm

M - Metric Mount

Mounting Thread	M3 x 0.50 Male	(M3 x 0.50 Male)

Supplied Accessory: Model M080A15 Metric adhesive base, 0.31" hex x 0.125" thk, M3 x 0.50 thd, aluminum with insulating hardcoat finish replaces Model 080A15

Q - Extended discharge time constant [6]

Frequency Range (±5 %)	0.15 to 10000 Hz	0.15 to 10000 Hz
Frequency Range (±10 %)	0.1 to 20000 Hz	0.1 to 20000 Hz
Discharge Time Constant	>5 sec	>5 sec
Settling Time (within 10% of bias)	<45 sec	<45 sec

Supplied Accessory: Model ACS-4 Single-axis, low frequency phase and amplitude response calibration from 0.5 to 10 Hz

W - Water Resistant Cable

Electrical Connector	Sealed Integral Cable	Sealed Integral Cable
Electrical Connection Position	Side	Side

Notes

[1] Typical.

[2] Zero-based, least-squares, straight line method.

[3] Transverse sensitivity is typically <= 3%.

[4] See PCB Declaration of Conformance PS023 for details.

[5] Adhesive mounting base is not required. "Quick Bonding Gel" has maximum temperature range of 180 ° F (82°C).

[6] ACS-4 starts at 1 Hz for sensitivities <20 mV/g.

Supplied Accessories
080A109 Petro Wax (1)
080A15 Adhesive Mounting Base (1)
ACS-1 NIST traceable frequency response (10 Hz to upper 5% point). (1)

Entered: BLS	Engineer: BAM	Sales: WDC	Approved: BLS	Spec Number:
Date: 07/10/2007	Date: 07/02/2007	Date: 07/02/2007	Date: 07/13/2007	353-2110-80
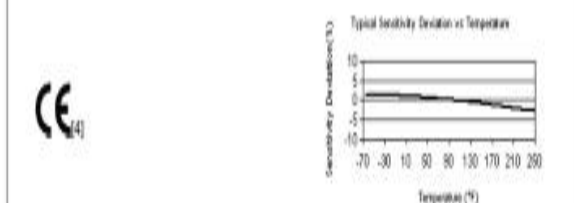
All specifications are at room temperature unless otherwise specified.

In the interest of constant product improvement, we reserve the right to change specifications without notice.

ICP® is a registered trademark of PCB group, Inc.

PCB PIEZOTRONICS
VIBRATION DIVISION
3425 Walden Avenue
Depew, NY 14043
UNITED STATES

Model Number 353B15		ACCELEROMETER, ICP®		Revision M ECN #: 35369

Performance	ENGLISH	SI	
Sensitivity (±10 %)	10 mV/g	1.02 mV/(m/s²)	
Measurement Range	±500 g pk	±4905 m/s² pk	
Frequency Range (±5 %)	1 to 10000 Hz	1 to 10000 Hz	
Frequency Range (±10 %)	0.7 to 18000 Hz	0.7 to 18000 Hz	
Frequency Range (±3 dB)	0.35 to 30000 Hz	0.35 to 30000 Hz	
Resonant Frequency	≥70 kHz	≥70 kHz	
Broadband Resolution (1 to 10000 Hz)	0.005 g rms	0.05 m/s² rms	[1]
Non-Linearity	≤1 %	≤1 %	[2]
Transverse Sensitivity	≤5 %	≤5 %	[3]
Environmental			
Overload Limit (Shock)	±10000 g pk	±98100 m/s² pk	
Temperature Range (Operating)	-65 to +250 °F	-54 to +121 °C	
Base Strain Sensitivity	≤0.002 g/με	≤0.02 (m/s²)/με	[1]
Electrical			
Excitation Voltage	20 to 30 VDC	20 to 30 VDC	
Constant Current Excitation	2 to 20 mA	2 to 20 mA	
Output Impedance	≤100 Ohm	≤100 Ohm	
Output Bias Voltage	8 to 12 VDC	8 to 12 VDC	
Discharge Time Constant	0.5 to 2.0 sec	0.5 to 2.0 sec	
Settling Time (within 10% of bias)	<5 sec	<5 sec	
Spectral Noise (1 Hz)	2800 µg/√Hz	27466 (µm/sec²)/√Hz	[1]
Spectral Noise (10 Hz)	700 µg/√Hz	6867 (µm/sec²)/√Hz	[1]
Spectral Noise (100 Hz)	180 µg/√Hz	1766 (µm/sec²)/√Hz	[1]
Spectral Noise (1 kHz)	64 µg/√Hz	628 (µm/sec²)/√Hz	[1]
Physical			
Size (Height)	0.43 in	10.9 mm	
Weight	0.07 oz	2.0 gm	[1]
Sensing Element	Quartz	Quartz	
Size (Hex)	0.31 in	7.9 mm	
Sensing Geometry	Shear	Shear	
Housing Material	Titanium	Titanium	
Sealing	Welded Hermetic	Welded Hermetic	
Electrical Connector	5-44 Coaxial	5-44 Coaxial	
Electrical Connection Position	Side	Side	
Mounting Thread	5-40 Male	5-40 Male	
Mounting Torque	8 to 12 in-lb	90 to 135 N-cm	

Optional Versions (Optional versions have identical specifications and accessories as listed for standard model except where noted below. More than one option maybe used.)

A - Adhesive Mount
Supplied Accessory: Model 080A90 Quick bond Gel (for use with accelerometer adhesive mtg bases to fill gaps on rough surfaces)

B - Low bias electronics

Output Bias Voltage	4.5 to 7.5 VDC	4.5 to 7.5 VDC
Excitation Voltage	12 to 30 VDC	12 to 30 VDC
Constant Current Excitation	1 to 20 mA	1 to 20 mA
Measurement Range	±300 g pk	±2943 m/s² pk

J - Ground Isolated

Frequency Range (±5 %)	1 to 8000 Hz	1 to 8000 Hz	
Frequency Range (±10 %)	0.7 to 15000 Hz	0.7 to 15000 Hz	
Resonant Frequency	≥56 kHz	≥56 kHz	
Electrical Isolation (Base)	≥10⁸ Ohm	≥10⁸ Ohm	
Size (Hex x Height)	0.37 in x 0.57 in	9.5 mm x 14.5 mm	[1]
Weight	0.11 oz	3.2 gm	[1]

M - Metric Mount
Mounting Thread — M3 x 0.50 Male (M3 x 0.50 Male)
Supplied Accessory: Model M080A15 Metric adhesive base, 0.31" hex x 0.125" thk, M3 x 0.50 thd, aluminum with insulating hardcoat finish replaces Model 080A15

Q - Extended discharge time constant

Frequency Range (±5 %)	0.15 to 10000 Hz	0.15 to 10000 Hz
Frequency Range (±10 %)	0.1 to 18000 Hz	0.1 to 18000 Hz
Discharge Time Constant	≥5 sec	≥5 sec
Settling Time (within 10% of bias)	≤45 sec	≤45 sec

Supplied Accessory: Model ACS-4 Single-axis, low frequency phase and amplitude response calibration from 0.5 to 10 Hz

W - Water Resistant Cable

Electrical Connector	Sealed Integral Cable	Sealed Integral Cable
Electrical Connection Position	Side	Side

Notes
[1] Typical.
[2] Zero-based, least-squares, straight line method.
[3] Transverse sensitivity is typically <= 3%.
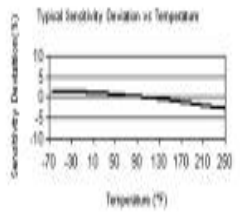[4] See PCB Declaration of Conformance PS023 for details.

Supplied Accessories
080A109 Petro Wax (1)
080A15 Adhesive Mounting Base (1)
ACS-1 NIST traceable frequency response (10 Hz to upper 5% point). (1)

CE [4]

Typical Sensitivity Deviation vs Temperature

Entered: DMW	Engineer: BAM	Sales: WDC	Approved: ECB	Spec Number:
Date: 03/25/2011	Date: 03/25/2011	Date: 03/25/2011	Date: 03/25/2011	353-2150-80

All specifications are at room temperature unless otherwise specified.
In the interest of constant product improvement, we reserve the right to change specifications without notice.
ICP® is a registered trademark of PCB group, Inc.

PCB PIEZOTRONICS
VIBRATION DIVISION

3425 Walden Avenue
Depew, NY 14043
UNITED STATES
Phone: 800-828-8840
Fax: 716-684-0987
E-mail: info@pcb.com

B.2 Load cell

Figure B.2 Force sensor

Model Number	FORCE SENSOR, ICP®	Revision F
204C		ECN #: 26908

Performance	ENGLISH	SI	
Sensitivity (±15 %)	0.12 mV/lb	27 mV/kN	
Measurement Range (Compression)	40000 lb	177.92 kN	
Maximum Static Force (Compression)	50000 lb	222.4 kN	
Broadband Resolution (1 to 10000 Hz)	0.80 lb-rms	3.6 N-rms	[1]
Low Frequency Response (-5 %)	0.0003 Hz	0.0003 Hz	[2]
Upper Frequency Limit	55 kHz	55 kHz	[3]
Non-Linearity	≤1.5 % FS	≤1.5 % FS	[4]
Environmental			
Temperature Range	-65 to +250 °F	-54 to +121 °C	
Temperature Coefficient of Sensitivity	≤0.08 %/°F	≤0.14 %/°C	
Electrical			
Discharge Time Constant (at room temp)	≥2000 sec	≥2000 sec	
Excitation Voltage	20 to 30 VDC	20 to 30 VDC	
Constant Current Excitation	2 to 20 mA	2 to 20 mA	
Output Impedance	≤100 Ohm	≤100 Ohm	
Output Bias Voltage	8 to 14 VDC	8 to 14 VDC	
Spectral Noise (1 Hz)	0.088 lb/√Hz	0.39 N/√Hz	[1]
Spectral Noise (10 Hz)	0.025 lb/√Hz	0.11 N/√Hz	[1]
Spectral Noise (100 Hz)	0.0060 lb/√Hz	0.0266 N/√Hz	[1]
Spectral Noise (1000 Hz)	0.0016 lb/√Hz	0.00719 N/√Hz	[1]
Output Polarity (Compression)	Positive	Positive	
Physical			
Preload	8000 lb	35.585 kN	
Stiffness	29 lb/μin	5 kN/μm	[1]
Size (Diameter x Height x Bolt Diameter)	1.34 in x 0.47 in x 0.625 in	34 mm x 12 mm x 16 mm	
Size (ID) (Hole Diameter)	0.660 in	16.76 mm	
Size (OD) (Sensor)	1.340 in	34 mm	
Size (Sensing Surface)	1.10 in	28 mm	
Weight	2.0 oz	57 gm	
Housing Material	Stainless Steel	Stainless Steel	
Sealing	Hermetic	Hermetic	
Electrical Connector	10-32 Coaxial Jack	10-32 Coaxial Jack	
Electrical Connection Position	Side	Side	

Optional Versions (Optional versions have identical specifications and accessories as listed for standard model except where noted below. More than one option maybe used.)

M - Metric Mount
  Supplied Accessory: Model M081A14 Mounting stud, M14 x 1.25 x 1.400, BeCu (for M204C and M214B)
  Supplied Accessory: Model M083B04 Pilot Bushing (for Models M204C and M214B)

N - Negative Output Polarity
  Output Polarity (Compression)   Negative   Negative

W - Water Resistant Cable
  Electrical Connector   Sealed Cable   Sealed Cable
  Electrical Connection Position   Side   Side

Notes
  [1] Typical.
  [2] Calculated from discharge time constant.
  [3] Estimated using rigid body dynamics calculations.
  [4] Zero-based, least-squares, straight line method.
  [5] See PCB Declaration of Conformance PS023 for details.

Supplied Accessories
080A82 Assembly Lubricant (1)
081A14 Mounting Stud,1/2-20 x 1.400, BeCu (1)
082B04 Anti-friction washer (for Models 204C and 214B) (1)
083B04 Pilot bushing (for Models 204C and 214B) (1)

CE [5]

Entered: BLS	Engineer: MJK	Sales: DPC	Approved: BLS	Spec Number:
Date: 07/20/2007	Date: 07/19/2007	Date: 07/19/2007	Date: 07/20/2007	5874

All specifications are at room temperature unless otherwise specified.
In the interest of constant product improvement, we reserve the right to change specifications without notice.
ICP® is a registered trademark of PCB group, Inc.

PCB PIEZOTRONICS
FORCE / TORQUE DIVISION
3425 Walden Avenue
Depew, NY 14043
UNITED STATES
Phone: 800-828-8840
Fax: 716-684-0987
E-mail: info@pcb.com
Web site: www.pcb.com

NAC Image Technology, the most experienced name in high-speed video, presents the HotShot 1280 pci, putting high-performance, high resolution high-speed video within the reach of more research, test and production users.

NAC's HotShot 1280 pci Digital High-Speed Video System

NAC's HotShot **1280** pci was designed from the beginning to be an easy-to-use, high-speed video solution for research, test and production customers. The Hot Shot 1280 PCI camera and recording system provides the user with a versatile and reliable high-speed video system.

The HotShot **1280** pci records brilliant color images or crisp monochrome images at resolutions up to 1280 X 1024 pixels. Using its advanced CMOS image sensor, the HotShot **1280** pci is capable of recording speeds in excess of 20,000 fps at reduced resolutions. The camera system's global electronic shutter allows the user to vary the exposure time, independent of the frame rate to be able to eliminate motion blur or to permit low-light recording. The HotShot **1280** pci image recording can be started or stopped remotely via a handheld switch, a direct signal from the subject or an external trigger. Images can be quickly reviewed and downloaded to a PC for more detailed analysis or image archiving and storage.

The HotShot **1280** pci is a PCI based computer peripheral that can also be purchased as a fully integrated standalone instrumentation system. The HotShot **1280** pci system is an easy-to-use window based motion analysis tool that includes onboard memory and camera control boards as well as user interface software and documentation. The HotShot **1280** pci can be integrated with a Control Console and keyboard making it a complete imaging system that is simple to operate and is adaptable to a variety of laboratory and production environments. The **1280** pci features a compact remote camera head that allows the system to operate in difficult-to-reach, confined spaces.

The HotShot **1280** pci also gives the user more control over the system's frame rate/resolution/ recording time parameters. This makes the system dramatically more flexible in of research, test and production environments.

Choose NAC to help address your high-speed imaging needs and you'll see *The Visible Difference*.

Visit our web site at www.nacinc.com

Appendix C Materials properties

C.1 properties of CFRP strip

weber

*High-performance carbon fibre
plate reinforcement for structural
strengthening*

weber.tec force
carbon plate

enforce carbon fibre plate

About this product

weber.tec force carbon plate is high-performance, corrosion-resistant carbon fibre laminate. Manufactured by S&P, Switzerland, these laminates have a fibre volumetric content up to 70% in an epoxy resin matrix. When used with **weber.tec EP structural adhesive**, the laminates form part of the **weber.tec force composite strengthening system**. For use in accordance with Concrete Society Technical Report 55 *Design Guidance for Strengthening Concrete Structures*.

Technical data

Physical parameters

Composition	Carbon fibre reinforced laminate in epoxy resin matrix
Colour	Black
Fibre content v_f	70%
Density	1.7 g/cm³
Temperature resistance T_{GM}	100 – 130°C
Thickness	1.2 mm and 1.4 mm standard
Width	10, 50, 80, 90, 100, and 120 mm standard Other widths available on request

Mechanical properties

	Grade 150	200
Elastic modulus E_f	> 165 kN/mm²	> 210 kN/mm²
Characteristic elastic modulus E_{fk}	150 kN/mm²	200 kN/mm²
Tensile strength f	2800 – 3000 N/mm²	2400 – 2600 N/mm²
Characteristic tensile strength f_k (where $f_k = f - 2s$)	2850 N/mm²	2500 N/mm²

Uses

To strengthen reinforced concrete, or masonry structures and timber

- Increasing load capacity
- Improving serviceability
- Reducing deflection
- Repairs to damaged concrete
- Change in use of structure:
  Removal of walls
  Removal of columns
  Openings in floor slabs
- Flexural strengthening

Typical applications

- Reinforced concrete beams, columns and walls
- Floor slabs to buildings, car parks
- Bridge decks, culverts and retaining walls

Features and benefits

- Can be used in conjunction with the **weber.tec force** CD design software package
- Precise performance with high strength and high modulus of elasticity in quality controlled manufacture
- Various strengths and modulus available for selection
- No corrosion, excellent durability and minimal maintenance
- Lightweight and easy to apply
- Range of dimensions for designer to choose from
- Available in any length
- Factory lamination with 70% carbon fibre content
- Good fire resistance of CFRP
- High fatigue strength of unidirectional laminate
- Excellent creep strength of CFRP over other fibre composites
- S&P can manufacture any special width for specific projects

230

weber.tec force carbon plate

Carbon fibre plate grades and types

S&P CFK 150/2000 E_{fk} = 150 kN/mm²   **Tensile load**

Width, mm	Thickness, mm	0.6% ε	0.8% ε
10	1.4	13 kN	17 kN
50	1.2	54 kN	77 kN
50	1.4	63 kN	90 kN
80	1.2	86 kN	123 kN
80	1.4	100 kN	134 kN
90	1.4	113 kN	151 kN
100	1.2	108 kN	144 kN
100	1.4	126 kN	168 kN
120	1.4	151 kN	202 kN

S&P CFK 200/2000 E_{fk} = 200 kN/mm²   **Tensile load**

Width, mm	Thickness, mm	0.6% ε	0.8% ε
50	1.4	84 kN	112 kN
80	1.4	134 kN	179 kN
90	1.4	151 kN	202 kN
100	1.4	168 kN	224 kN
120	1.4	201 kN	269 kN

Preparation

Tensile forces are transferred from the carbon fibre plate through the adhesive into the bearing substrate. The substrate should therefore have an inherent surface tensile strength greater than 1.5 N/mm². Testing of the tensile strength f_{ctm} of the substrate should be carried out prior to application of carbon fibre plate by a bond test.

The surface of the substrate must be roughened by grinding or sandblasting to remove any weak surface laitance or deleterious friable material. In order to prevent peeling due to deviation forces, the evenness of the prepared surface must be tested with a 2 m straight edge. Maximum allowable deviation is 5 mm over a 2 m length.

If the substrate is uneven, then it will need to be re-profiled using **weber.tec EP highbuild** or **weber.tec EP structural adhesive**. If the substrate is poor and the tensile bond strength is less than 1.5 N/mm², the surface may need to be primed. Please contact Technical Services for recommendations.

Immediately prior to the application of **weber.tec EP structural adhesive**, solvent-wipe the carbon fibre plate with **weber.tec solvent 1** to remove carbon dust and any contaminants. Wait until surface is dry before applying adhesive.

Application

Apply mixed **weber.tec EP structural adhesive** to the prepared concrete at 2 mm thickness and carbon fibre plate at 2 – 3 mm thickness within the pot life of the adhesive.

Place the carbon fibre plate onto the prepared substrate with the two adhesive layers in contact. Use a hard rubber roller to press the laminate onto the substrate until adhesive squeezes out from both sides of the laminate. Roller along the centre of the plate to achieve a void-free bond line of approximate thickness of 2 – 4 mm.

Remove the surplus adhesive from the sides of the laminate.

After 24 hours, when the adhesive has cured, test for voids by lightly tapping the laminate with a small hammer.

Cleaning

Clean tools and remove any uncured adhesive using **weber.tec solvent 3**.

Packaging

Supplied in 150 m rolls ready for use. The **weber.tec force** trestle is available seperately to safely unroll the carbon fibre plate laminate. The laminate can be pre-cut at the factory to suit the project needs.

Please advise at the time of order whether the laminate is required in cut lengths or in a roll.

Storage and shelf life

Store in dry conditions.
Protect from exposure to direct sunlight.

Unlimited shelf life.

Health and safety

Carbon-fibre reinforced plate.

Loose fibres are sharp, strong and irritating. Always wear leather gloves when handling carbon-fibre plates and avoid contact with the skin.

Laminate plate is naturally flat, and when delivered in roll form, is under significant tension. To avoid injury to personnel, unroll and dispense CFRP laminates with a purpose made **Weber** trestle.

For further information, please request the Material Safety Data Sheet for this product.

weber.tec force trestle

Technical services

Weber's Customer Services Department has a team of experienced advisors available to provide on-site advice both at the specification stage and during application. Detailed specifications can be provided for specific projects or more general works. Site visits and on-site demonstrations can be arranged on request.

Technical helpline
Tel: (01525) 722110
Fax: (01525) 718988

Sales enquiries

Weber products are distributed throughout the UK through selected stockists and distributors. For UK sales enquiries and overseas projects, contact **Weber's** Sales office.

Sales office
Tel: (01525) 722100
Fax: (01525) 718988

C.2 properties of the epoxy

weber
SAINT-GOBAIN

*Moisture-tolerant epoxy adhesive
for structural bonding applications*

weber.tec
EP structural adhesive

Uses

- Adhesive for structural bonding
- Jointing of precast segmental bridge units
- Adhesive for external steel plate bonding
- Adhesive for **weber.tec force carbon plate** composite strengthening
- Adhesive for bonding rubber bearing pads for highways and railways

About this product

weber.tec EP structural adhesive is a two-component, bisphenol epoxy resin and polyamine hardener, highly moisture-tolerant structural adhesive for structural jointing and structural strengthening. Used for application thicknesses of 2 – 10 mm.

Conforms with BS EN 1504-4.

Features and benefits

- Excellent cohesive bond to prepared surfaces
- Good adhesion to concrete, steel, timber, glass, rubber and carbon fibre
- Negligible shrinkage on curing
- Moisture tolerant for all year round work
- Three grades available: standard, winter and tropical
- Fully complies with BA 30/94 *Strengthening of Concrete Highway Structures Using Externally Bonded Plate*

Technical data

The following test results were obtained in laboratory condidtions at 20°C.

Physical properties

Colour		Mid grey when mixed Components different colours
Density		1685 kg/m³
Grades	Standard	10°C – 25°C
	Winter	5°C – 15°C
Cure temperature		+5°C to 30°C
Moisture resistance		0-5% water absorption at 1-1 mm
		0-3% water absorption at 1-6 mm
Workable life	Standard	30 minutes at 20°C
	Winter	30 minutes at 10°C

FM 1205

weber.tec EP structural adhesive

Preparation

No adhesive will develop full bond adhesion strength without the surface substrate being carefully prepared to give a mechanically sound, clean surface.

Concrete and masonry
The surface must be prepared by mechanical means, such as grinding or grit blasting, to remove any weak surface laitance or deletrious, friable material.

The substrate should have an inherent tensile strength greater than 1.0 N/mm².

Pull-off tests should be carried out prior to application of the adhesive.

If the substrate is uneven, then the surface must be re-profiled with a levelling mortar. Check for evenness of substrate.

Timber
Timber surfaces should be prepared by sanding and planing with all dust removed under vacuum.

Steel substrates
These should be grit blasted to Swedish Standard SA 2½, equivalent to BS 7079-A1 and de-greased immediately prior to application. Where corrosion is absent, wire brushing to a clean, bright surface may be adequate. Care must be taken not to polish the rust.

Mixing

Mix by adding the dark grey hardener to the white resin and mix for 3 to 5 minutes with a low speed drill and spiral mixing head (EPI MR4 100). Mix until a uniform consistency and colour is obtained.

In cold weather, it is advisable to store the product unopened in a warm environment for several hours before mixing.

Application

The mixed adhesive must be placed within its pot life. Apply the adhesive to the prepared substrate with a grooved trowel or by gloved hands. Apply material to both surfaces before joining together.

In some cases, only one face needs to be coated with adhesive, provided that at least 3 mm thickness is applied (e.g. segmental bridge construction).

Plate bonding
Push the glued plates onto the glued substrate within the open life of the material.

Apply a hard rubber roller to squeeze the adhesive from both sides of the plate edge and ensure no air voids.

Roller to achieve a bond line of approximately 2 – 3 mm thickness. Remove the surplus adhesive from the sides of the plate.

Setting time

Temp	Standard	Winter
5°C	Do not use	75 min.
10°C	80 min.	60 min.
15°C	65 min.	41 min.
20°C	44 min	Do not use
25°C	31 min.	–

Cleaning

Clean tools and any uncured adhesive using **weber.tec solvent 3.**

Packaging

weber.tec EP structural adhesive is available in 5 kg pails with hardener compound recessed in the lid.

Coverage

Yield 5 kg approximately 2.9 litres.

Thickness of adhesive	kg/m²
2 mm	3-3
4 mm	6-7
10 mm	17-0

Storage and shelf life

Shelf life is at least 12 months when it is kept unopened and stored in cool, dry conditions.

Store at between 5°C and 25°C.

Protect from frost.

Health and safety

Contains epoxy constituents. Refer to information supplied by manufacturer (see Material Safety Data Sheet).

All skin contact with epoxy resin products should be avoided. Barrier creams should be used and operatives should wear protective clothing including gloves. Working areas should be well ventilated.

The hardener content is alkaline and labelled as corrosive. The resin content is labelled as an irritant. The flash point of all components is in excess of 100°C. In the event of fire use foam, dry chemical, carbon dioxide (CO_2) or water fog extinguishers.

For further information, please request the Material Safety Data Sheet for this product.

Technical services

Weber's Customer Services Department has a team of experienced advisors available to provide on-site advice both at the specification stage and during application. Detailed specifications can be provided for specific projects or more general works. Site visits and on-site demonstrations can be arranged on request.

Technical helpline
Tel: 08703 330 070
e-mail solutions@netweber.co.uk

Sales enquiries

Weber products are distributed throughout the UK through selected stockists and distributors. Please contact the relevant Customer Services Team below for all product orders and enquiries.

UK and Ireland
Tel: 08703 330 070
Fax: 01525 718988
e-mail sales@netweber.co.uk

weber
SAINT-GOBAIN

Appendix D : Equation 5.16 Integration steps

$$\int sin^2(\frac{\pi x}{l})dx$$

$$Substitute\ u = \frac{\pi x}{l} \longrightarrow \frac{du}{dx} = \frac{\pi}{l}:$$

$$= \frac{l}{\pi}\int sin^2(u)du$$

$Now\ solving:$

$$\int sin^2(u)du$$

$Apply\ reduction\ formula:$

$$\int sin^n(u)du = \frac{n-1}{n}\int sin^{n-2}(u)du - \frac{cos(u)sin^{n-1}(u)}{n}$$

$with\ n = 2:$

$$= -\frac{cos(u)sin(u)}{2} + \frac{1}{2}\int 1du$$

$Now\ solving:$

$$\int 1du$$

$Apply\ constant\ rule:$

$$= u$$

$Plug\ in\ solved\ integrals:$

$$-\frac{cos(u)sin(u)}{2} + \frac{1}{2}\int 1du$$

$$= -\frac{cos(u)sin(u)}{2} + \frac{u}{2}$$

$Plug\ in\ solved\ integrals:$

$$\frac{l}{\pi}\int sin^2(u)du$$

$$= -\frac{lcos(u)sin(u)\pi}{2} + \frac{lu}{2\pi}$$

Undo substitution $u = \dfrac{\pi x}{l}$:

$$= \frac{-l cos(\frac{\pi x}{l}) sin(\frac{\pi x}{l})}{2\pi} + \frac{x}{2} + C$$

$$= -\frac{l cos(\frac{\pi x}{l}) sin(\frac{\pi x}{l})}{2\pi}) + \frac{x}{2} + C$$

Rewrite/simplify:

$$= -\frac{l sin\left(2\frac{\pi x}{l}\right)}{4\pi} + \frac{x}{2} + C$$

So:

$$\int_0^{l/2} sin^2(\frac{\pi x}{l}) dx = [-\frac{l sin\left(2\frac{\pi x}{l}\right)}{4\pi} + \frac{x}{2}]_0^{\frac{l}{2}} = \frac{l}{4}$$

Appendix E Experimental results of strengthened beams

E.1 Control beam
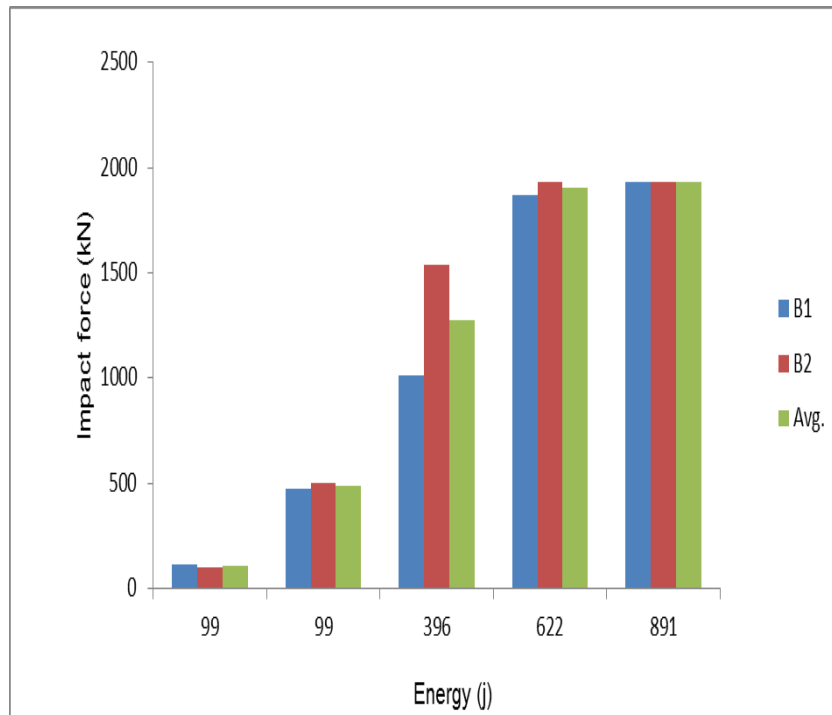
Figure E.1 beam impact force under different single impact energy
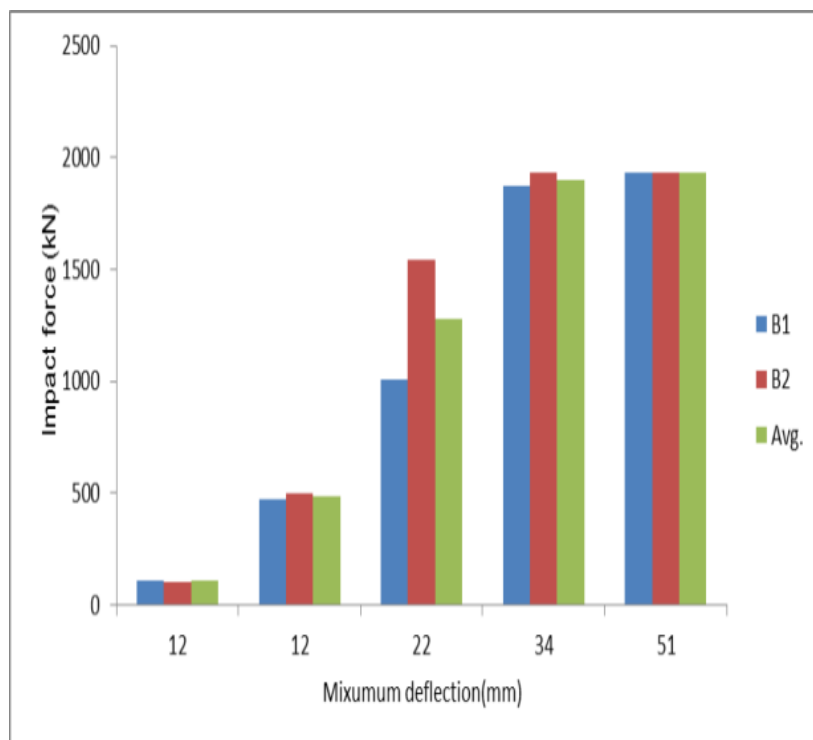
Figure E.2 beam maximum deflection under different single impact energy

236
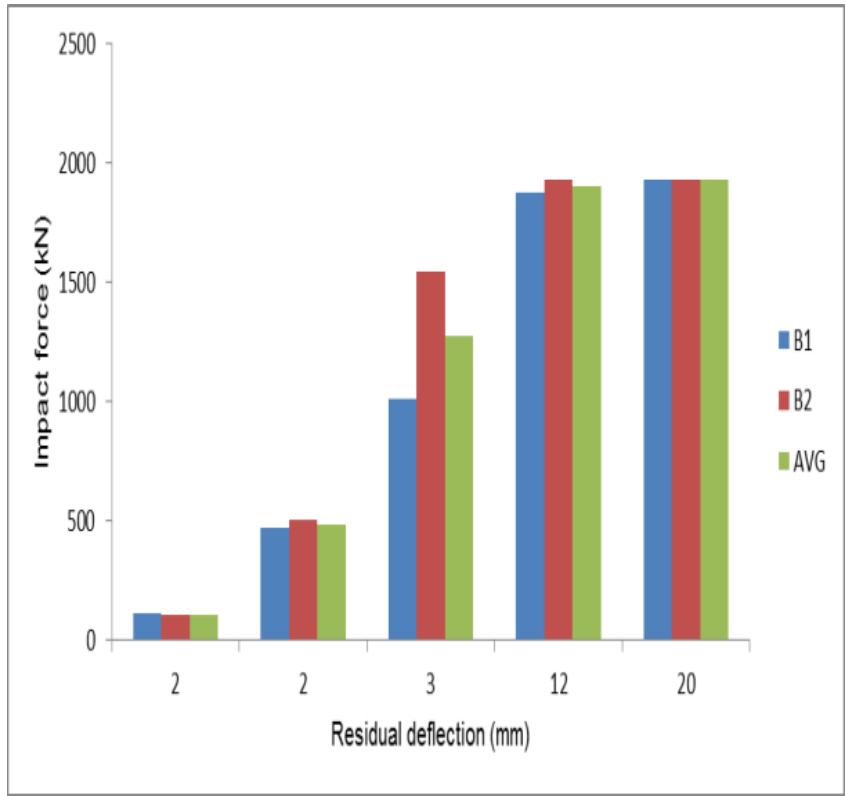
Figure E.3 beam residual deflection under different single impact energy
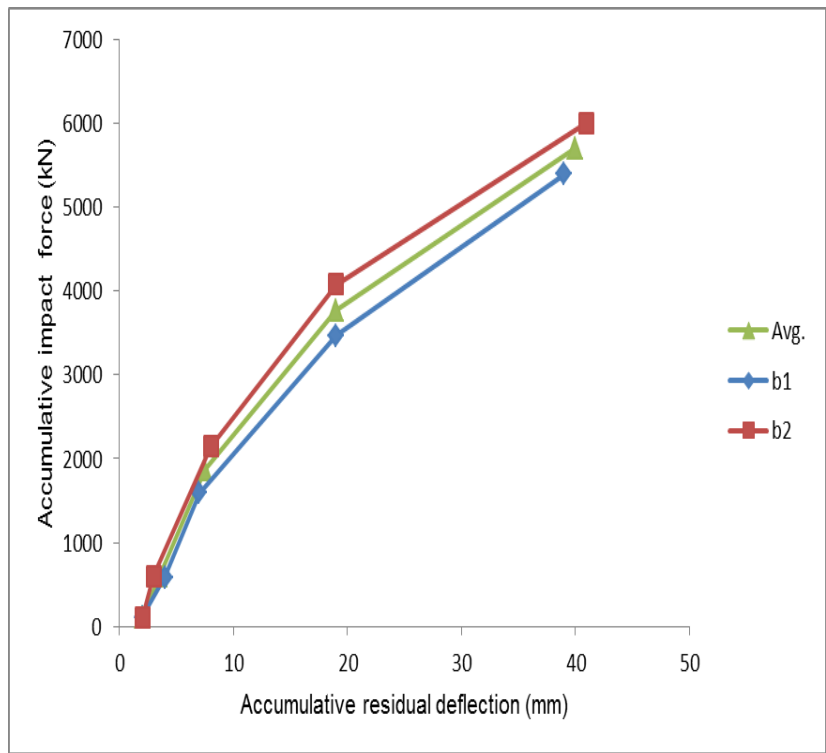
Figure E.4 accumulative impact force vs accumulative residual deflection
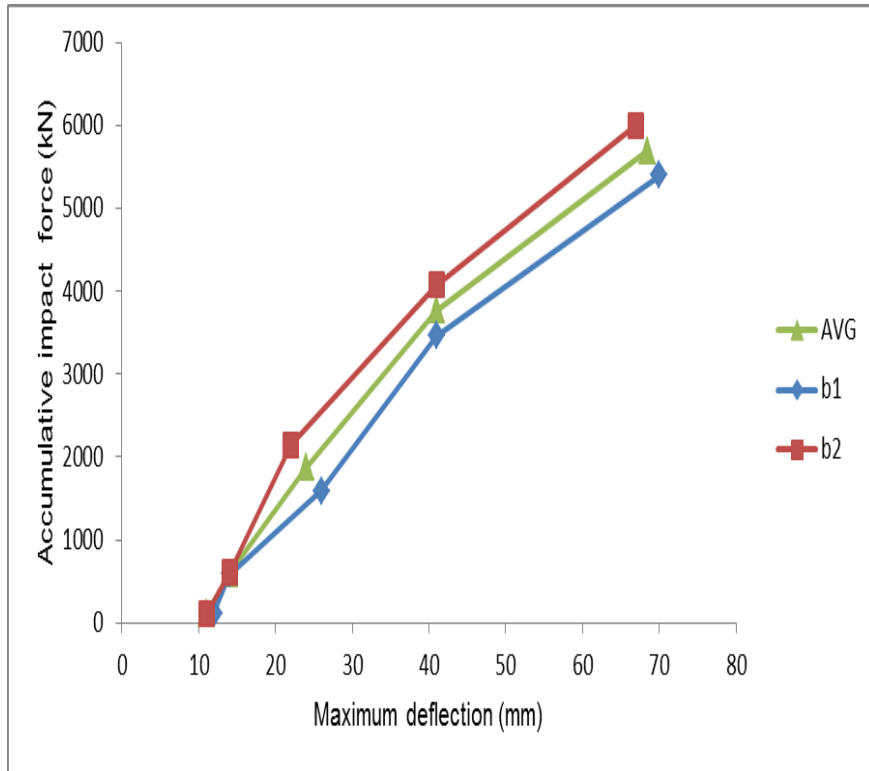
Figure E.5 accumulative impact force vs maximum deflection
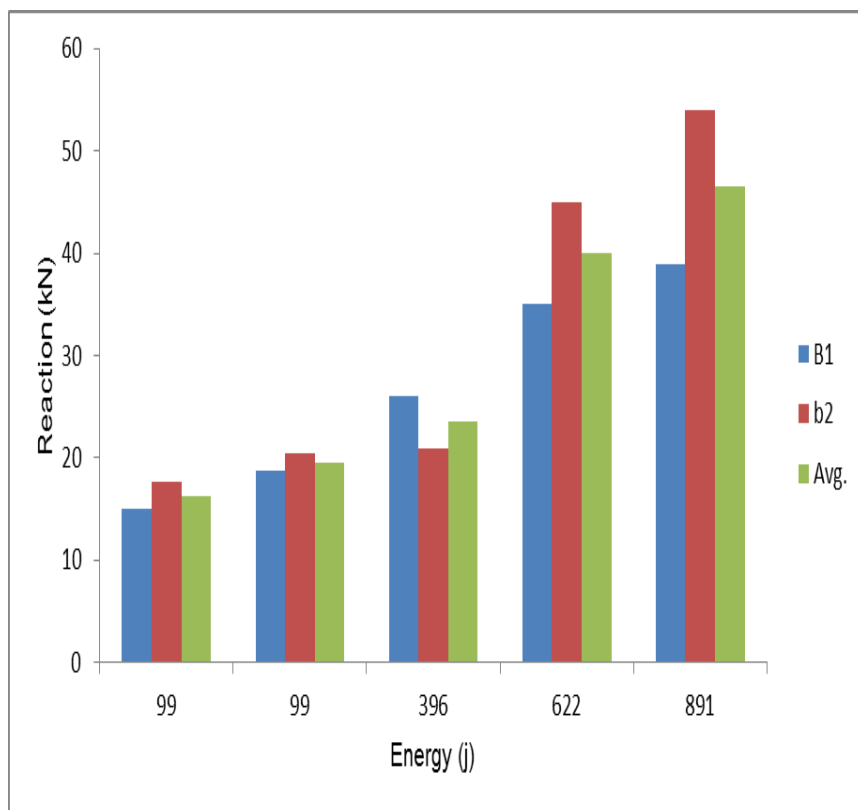
Figure E.6 beam reaction force under different single impact energy
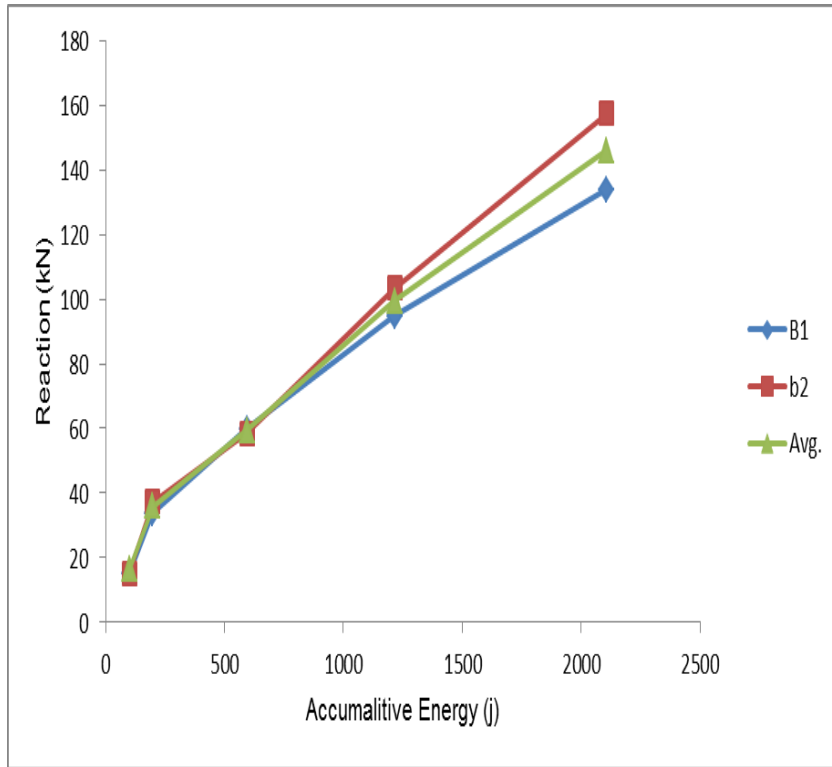
Figure E.7 beam accumulative reaction force vs accumulative impact energy
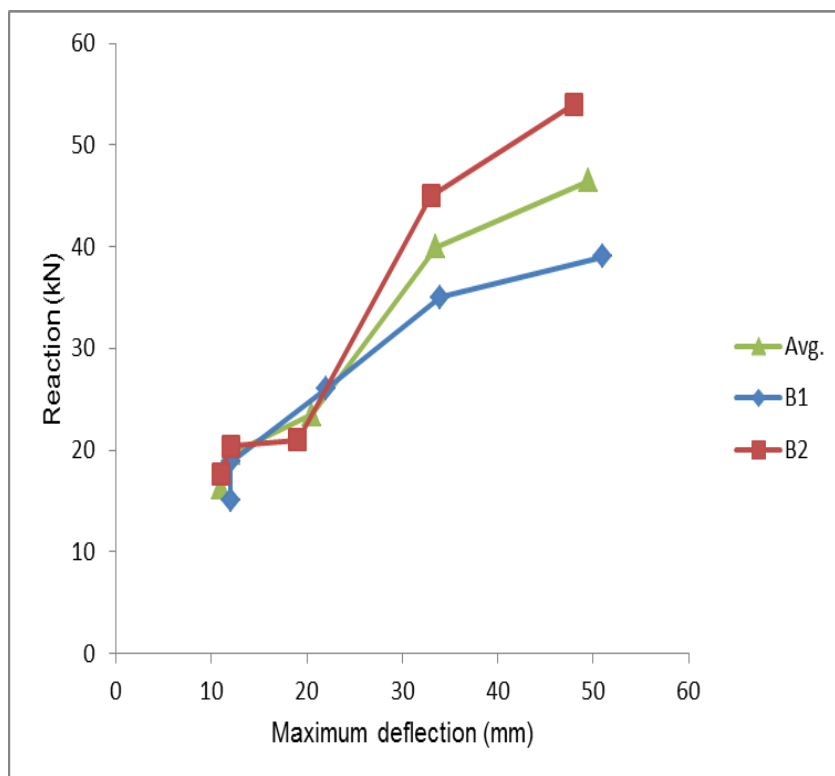
Figure E.8 accumulative reaction force vs maximum deflection
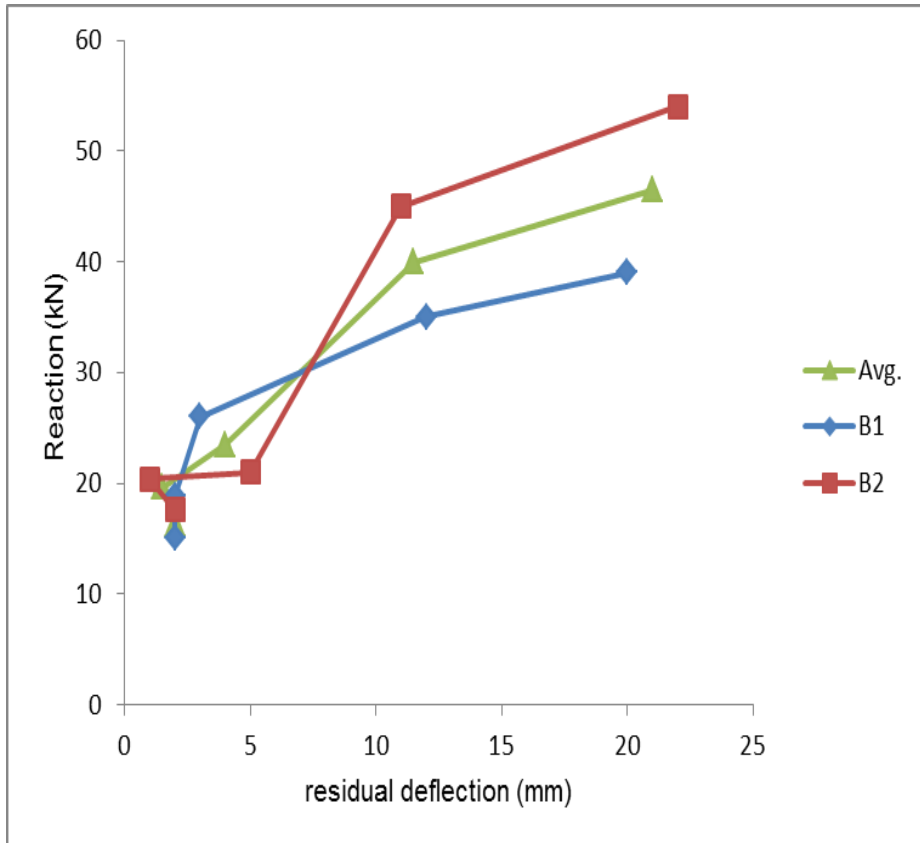
Figure E.9 reaction force vs residual deflection
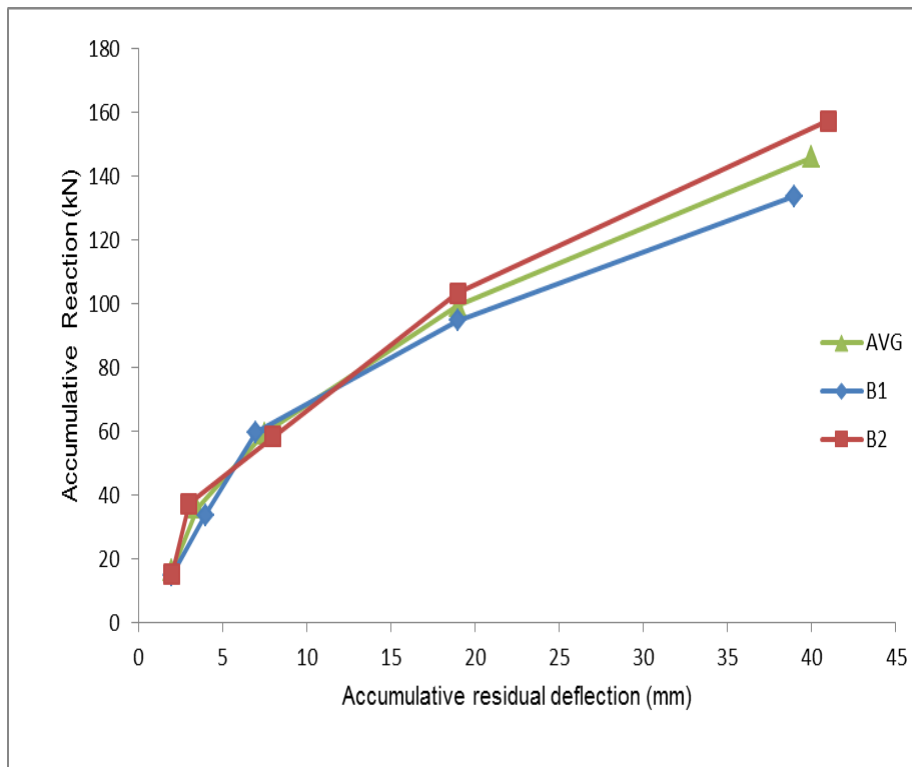
Figure E.10 accumulative reaction force vs accumulative residual deflection
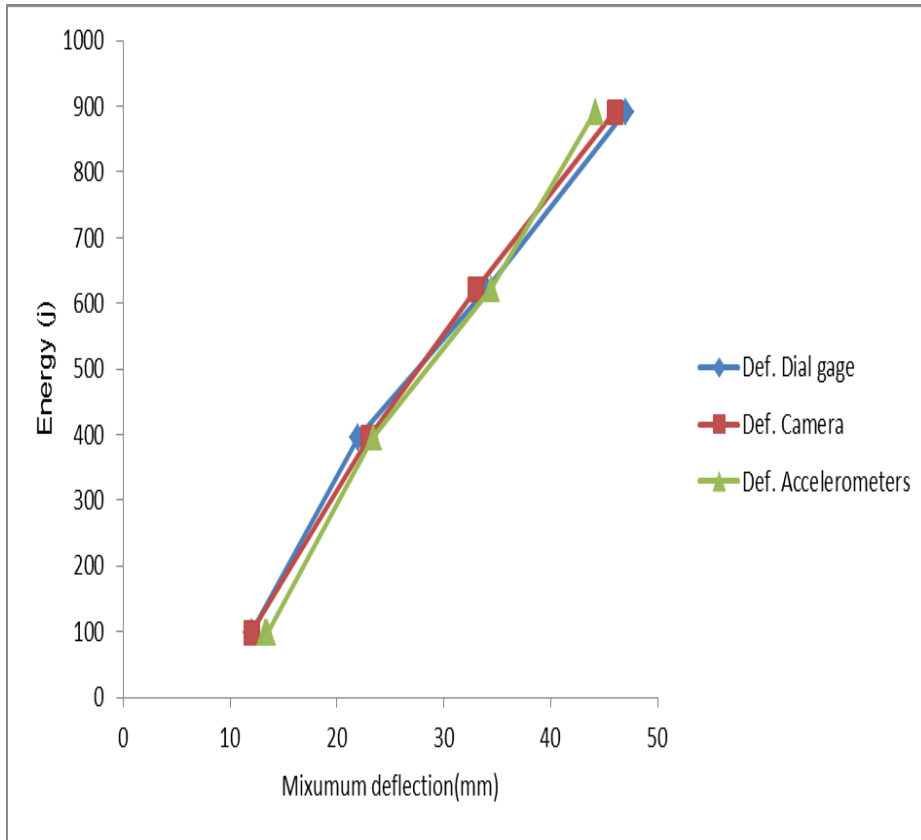
Figure E.11 Maximum deflection of B1 recorded by different methods
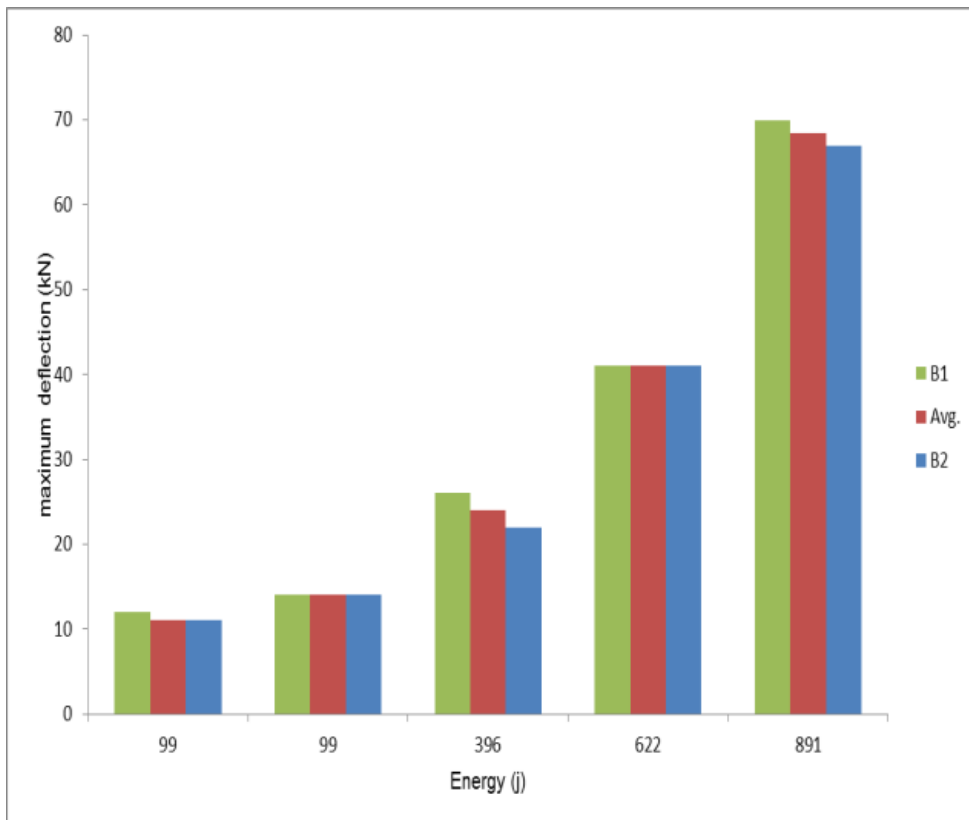
Figure E.12 residual deflections under different single impact energy
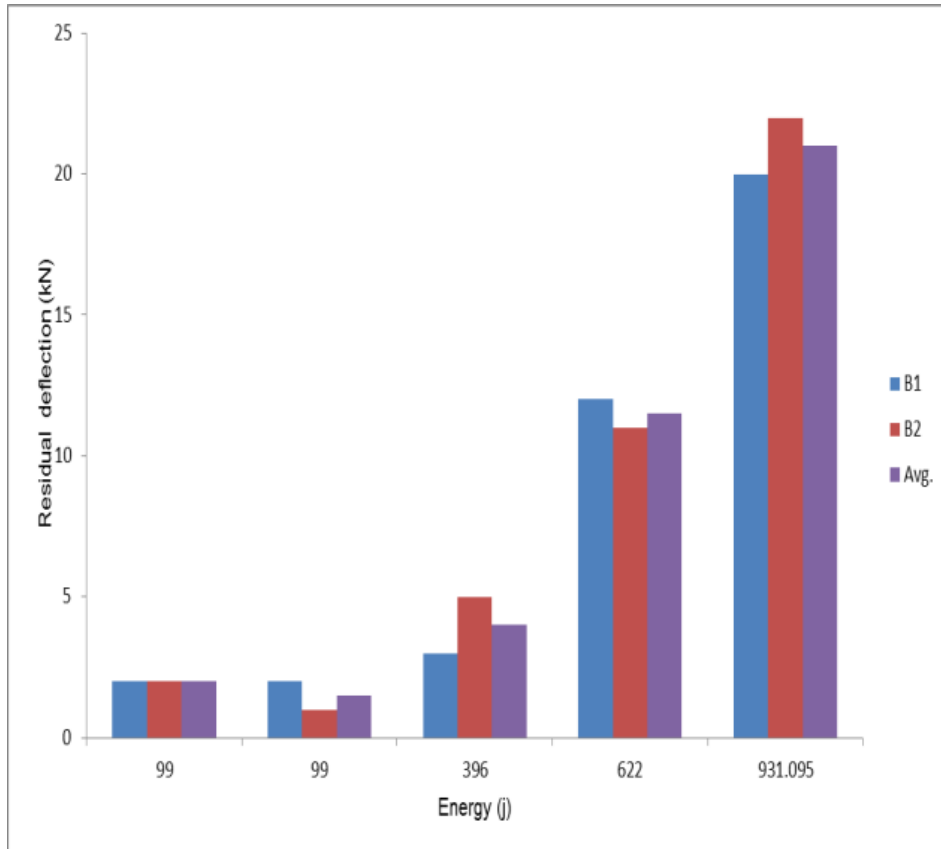
Figure E.13 maximum deflections under different single impact energy
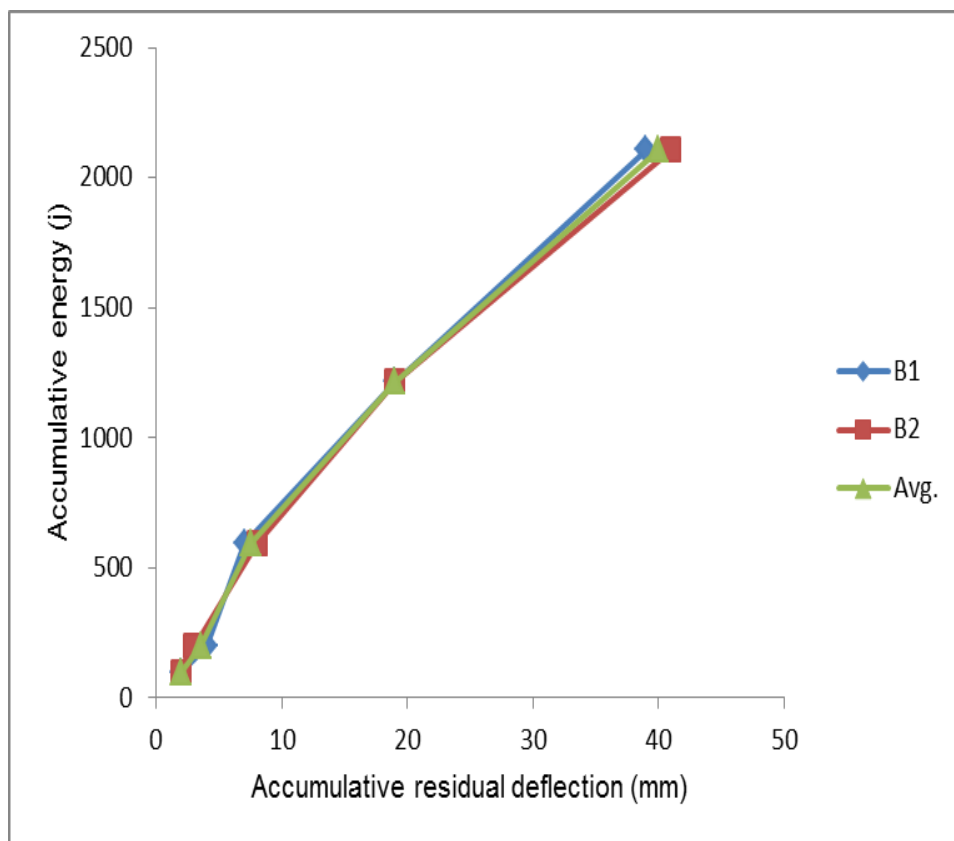
Figure E.14 accumulative energy vs accumulative residual deflection

242

E.2 External bonded technique EBR
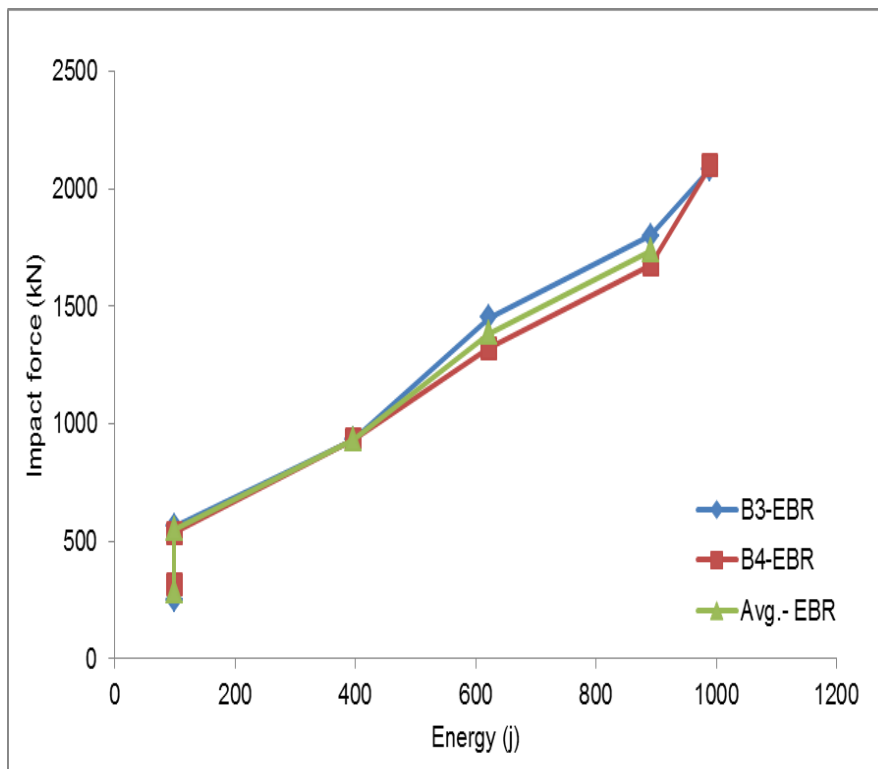
Figure E.15 beam impact force under different single impact energy
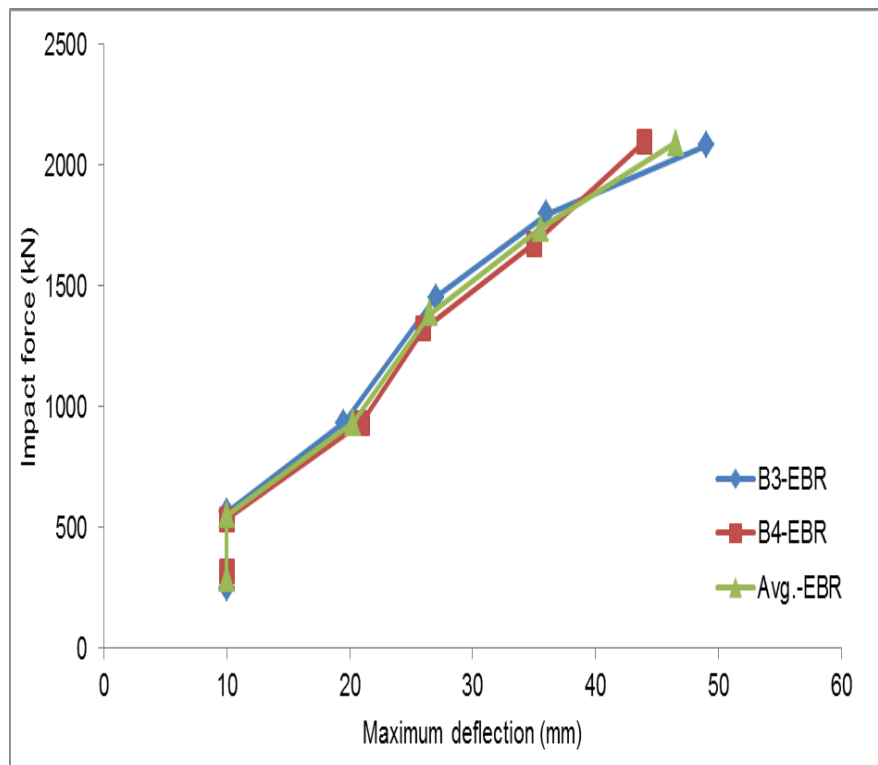
Figure E.16 impact force vs maximum deflection
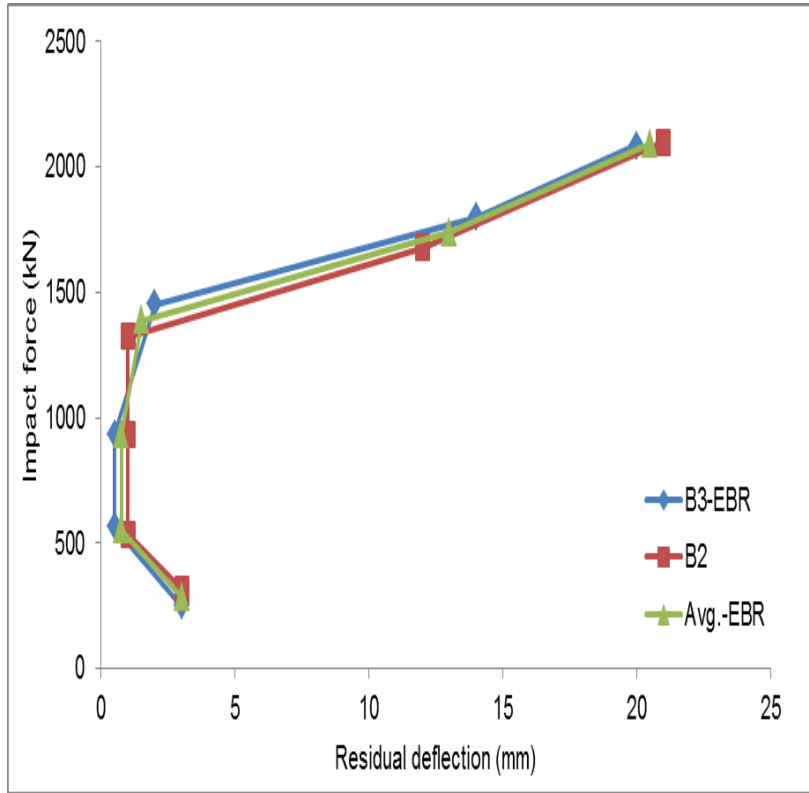
Figure E.17 impact force vs accumulative residual deflection
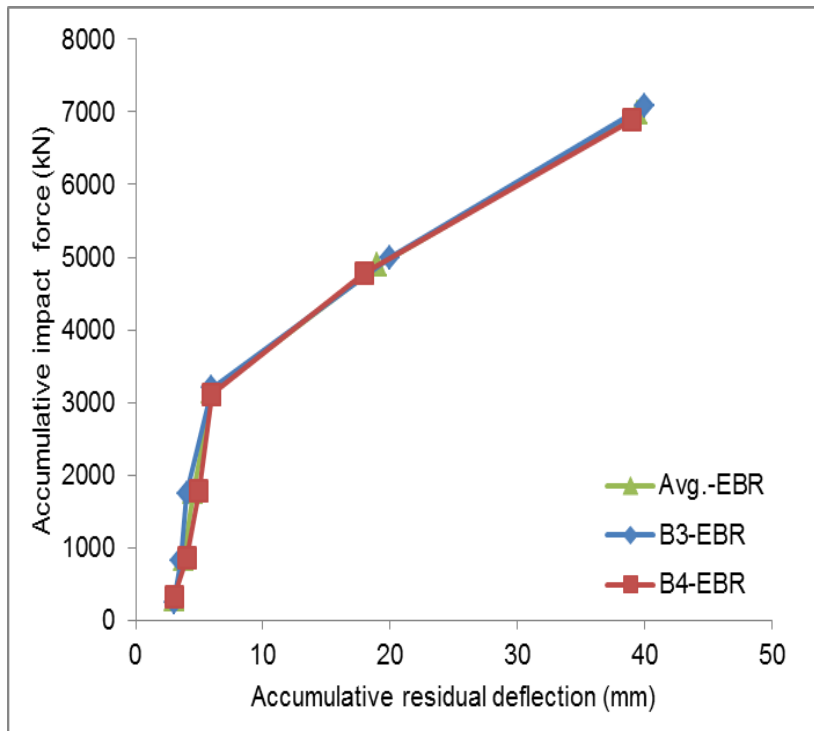
Figure E.18 accumulative impact force vs accumulative residual deflection
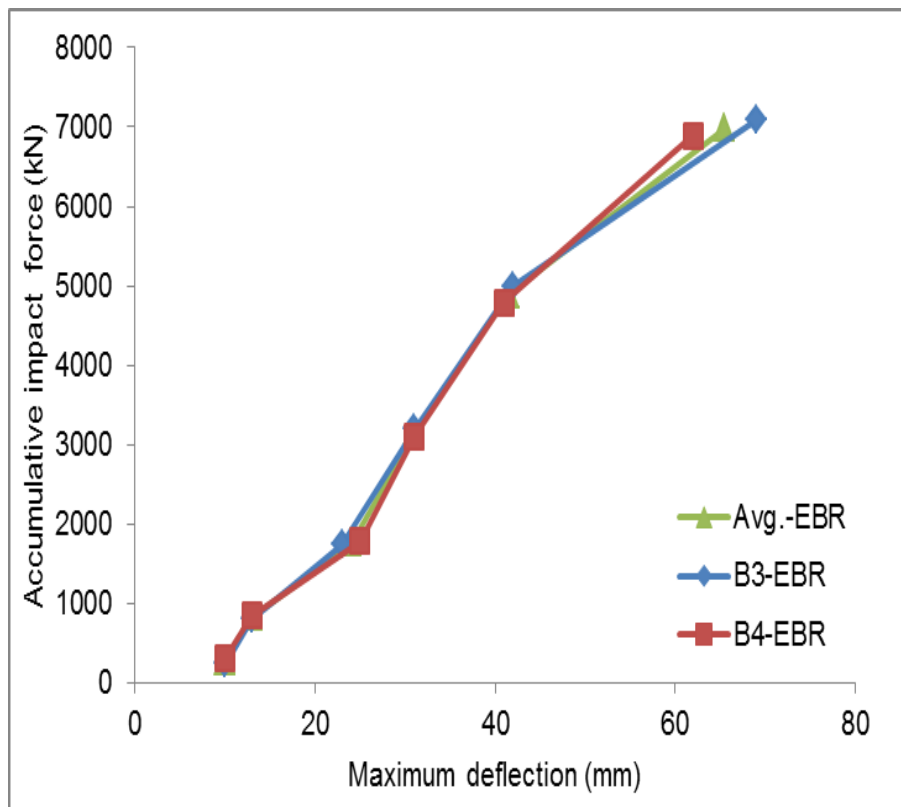
Figure E.19 accumulative impact force vs maximum deflection
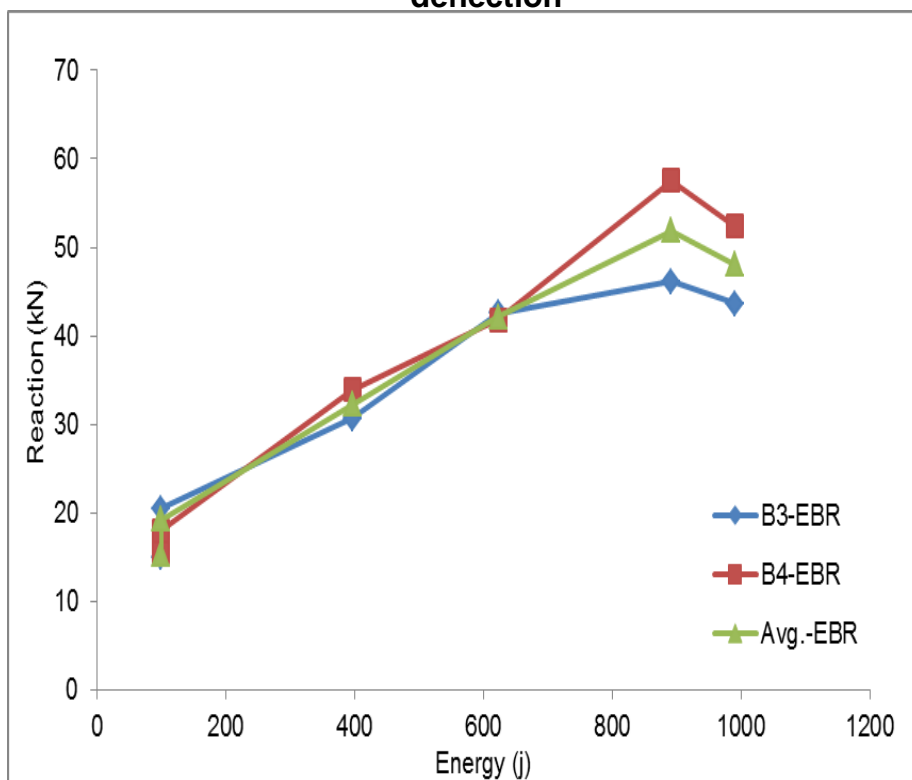
Figure E.20 beam reaction vs impact energy
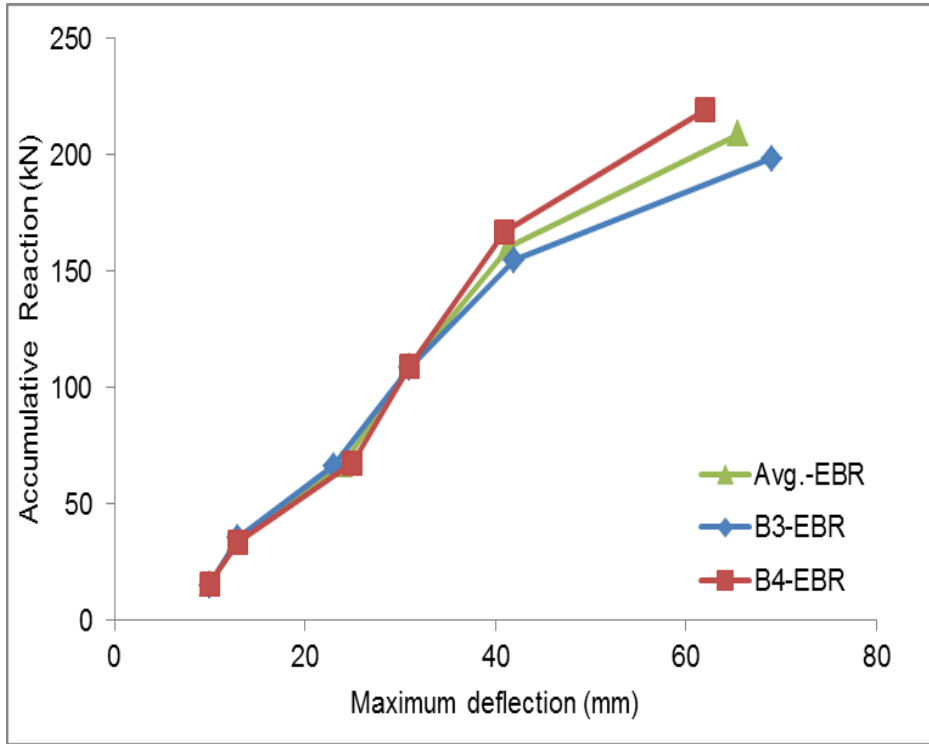
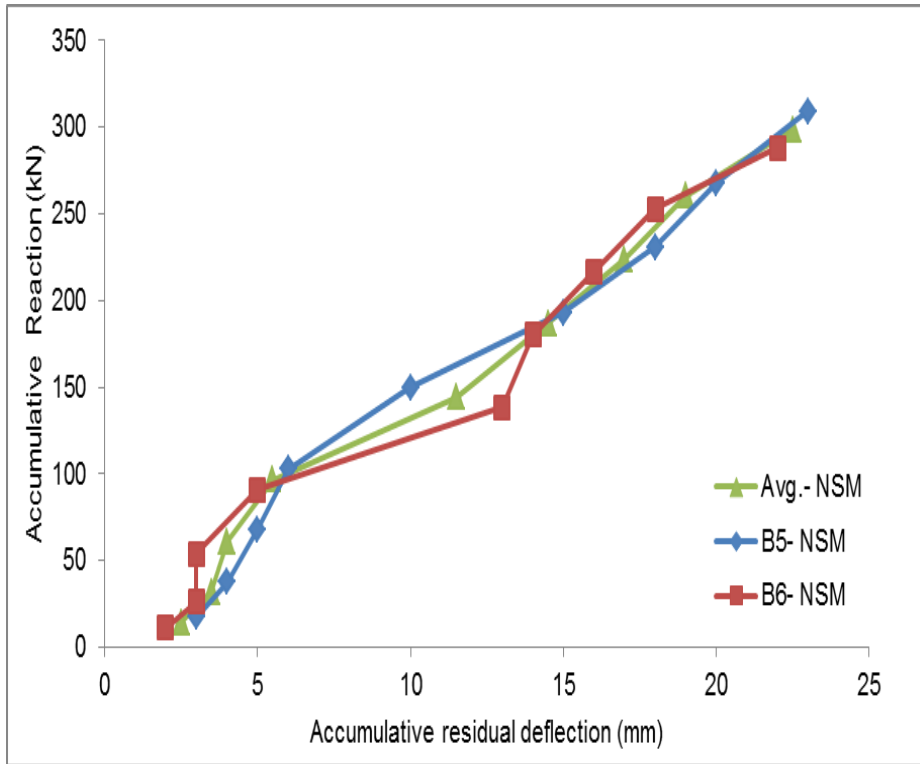**Figure E.21 accumulative reaction force vs maximum deflection**
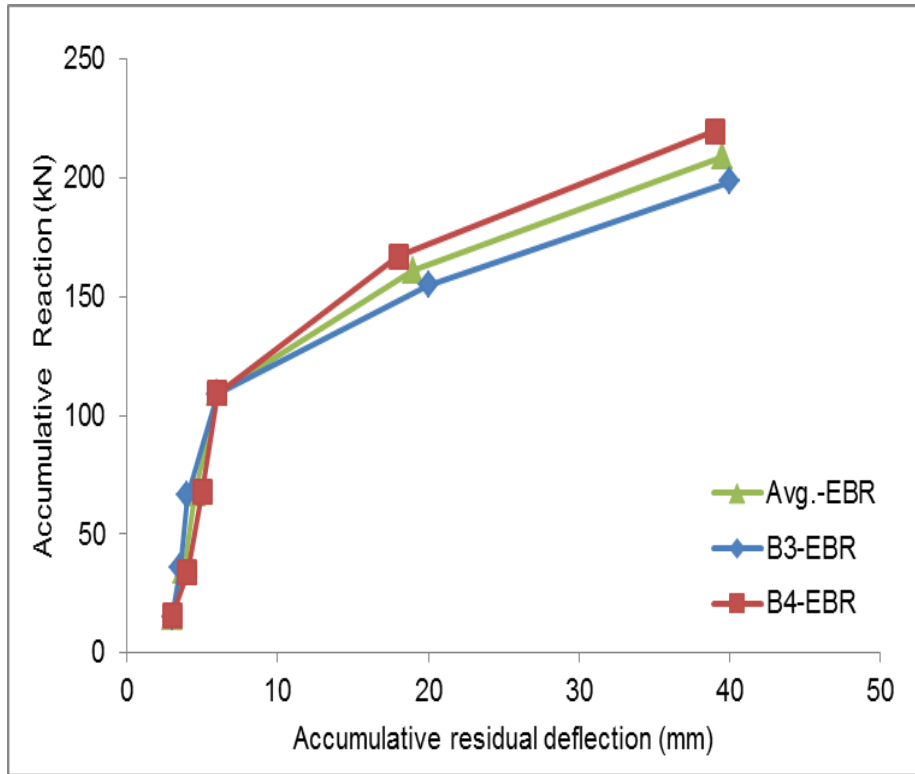
Figure E.22 accumulative reaction force vs accumulative residual deflection
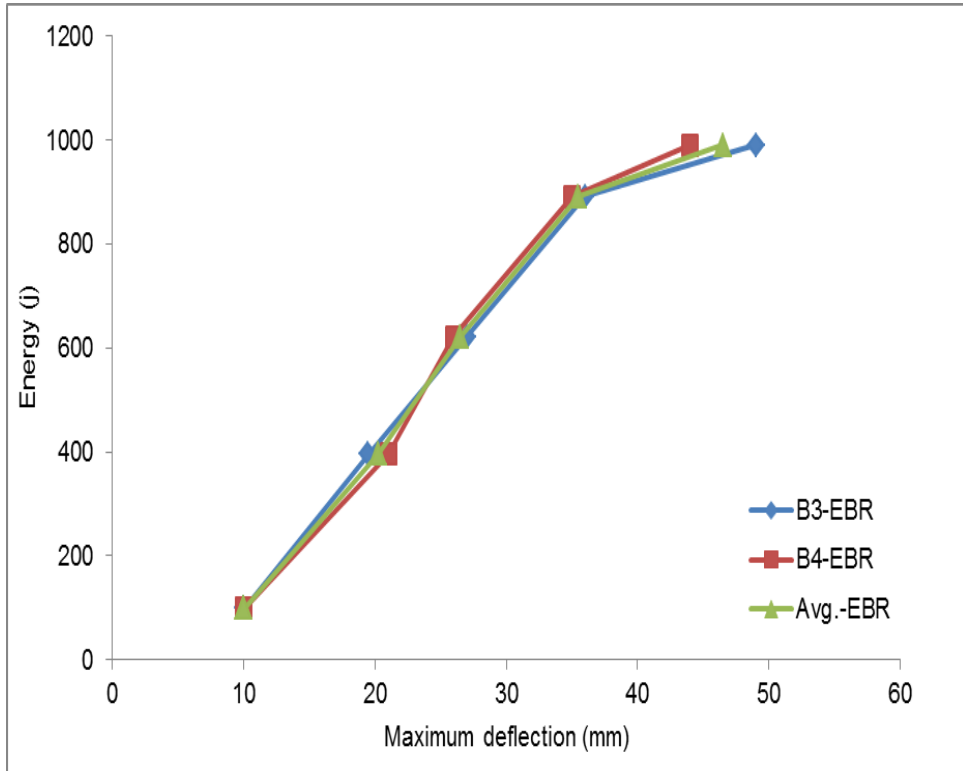
Figure E.23 maximum deflections vs impact energy
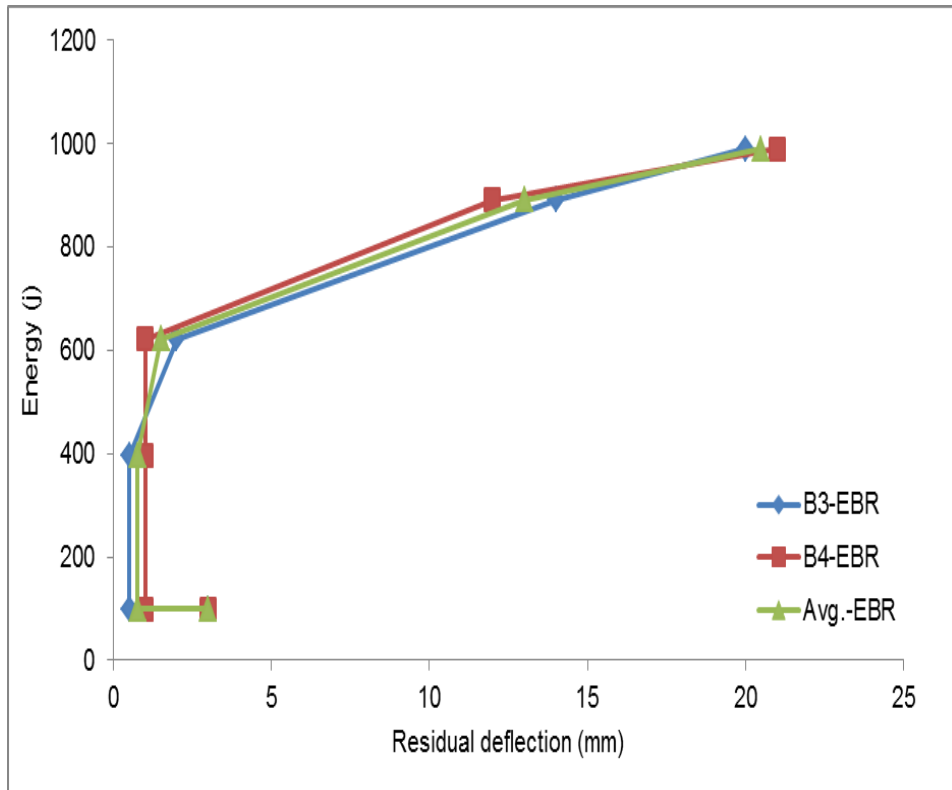
Figure E.24 residual deflections vs impact energy

247
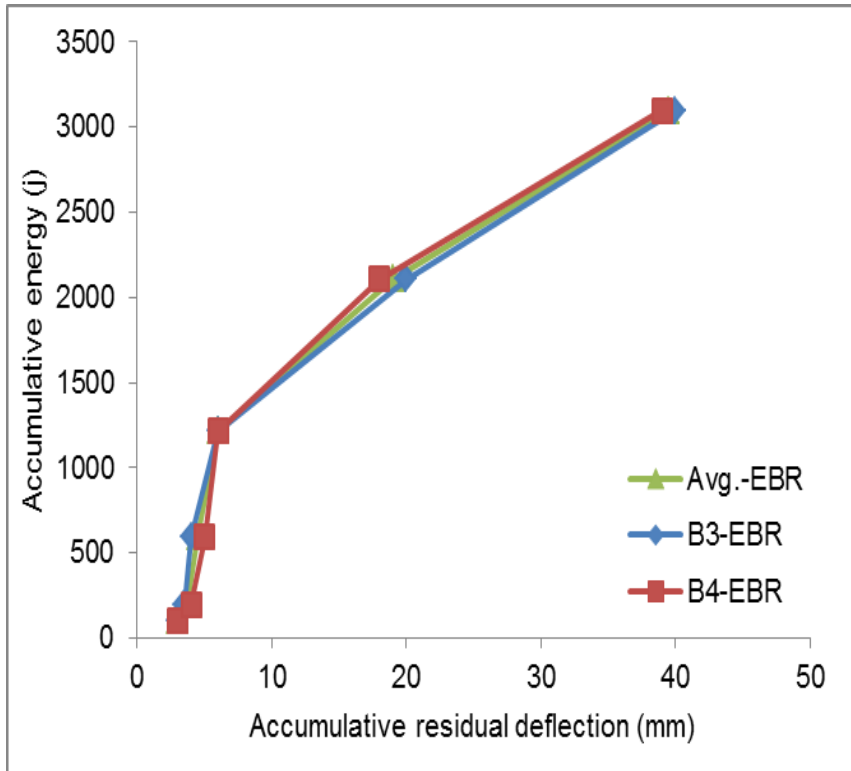
Figure E.25 accumulative energy vs accumulative residual deflection

E.3 Near surface mounted technique NSM
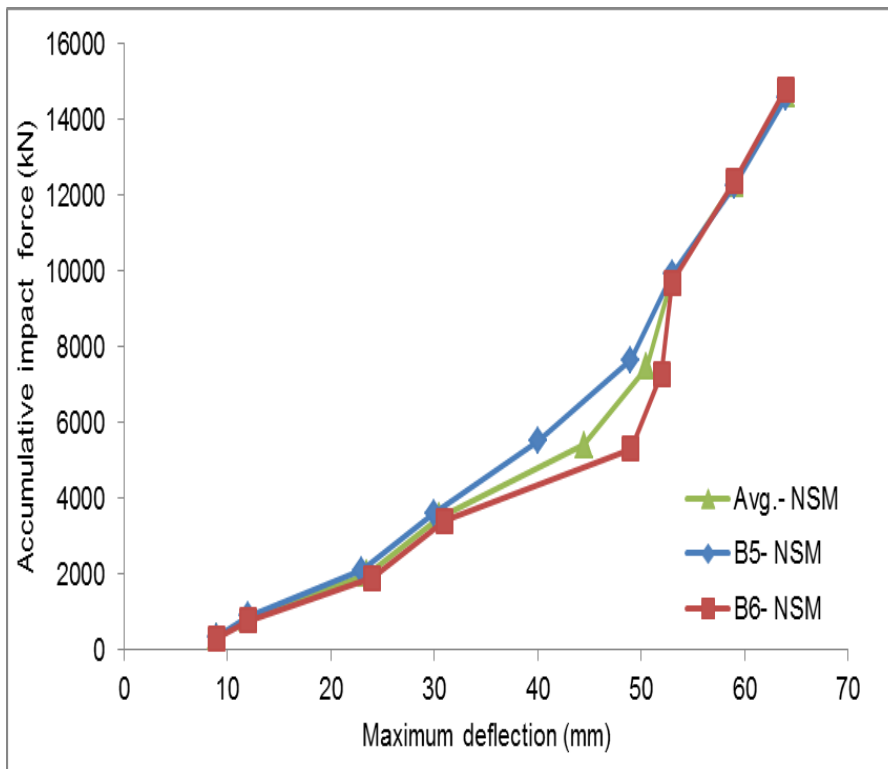
Figure E.26 accumulative impact force vs maximum deflection
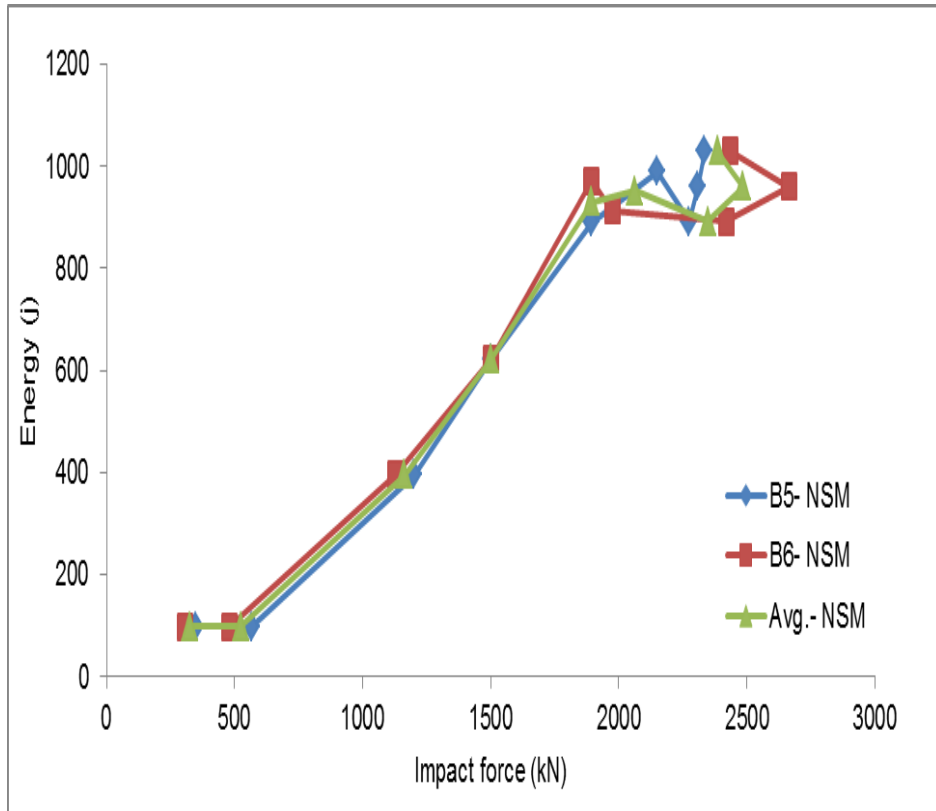
Figure E.27 beam impact force vs impact energy
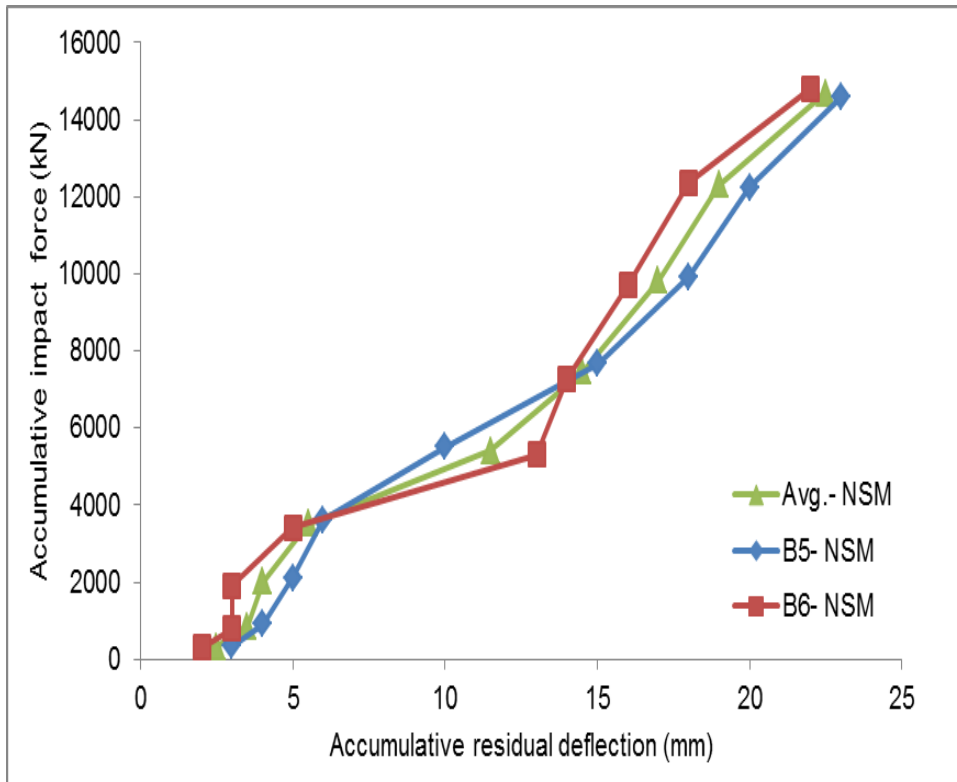
**Figure E.28 accumulative impact force vs accumulative residual deflection**
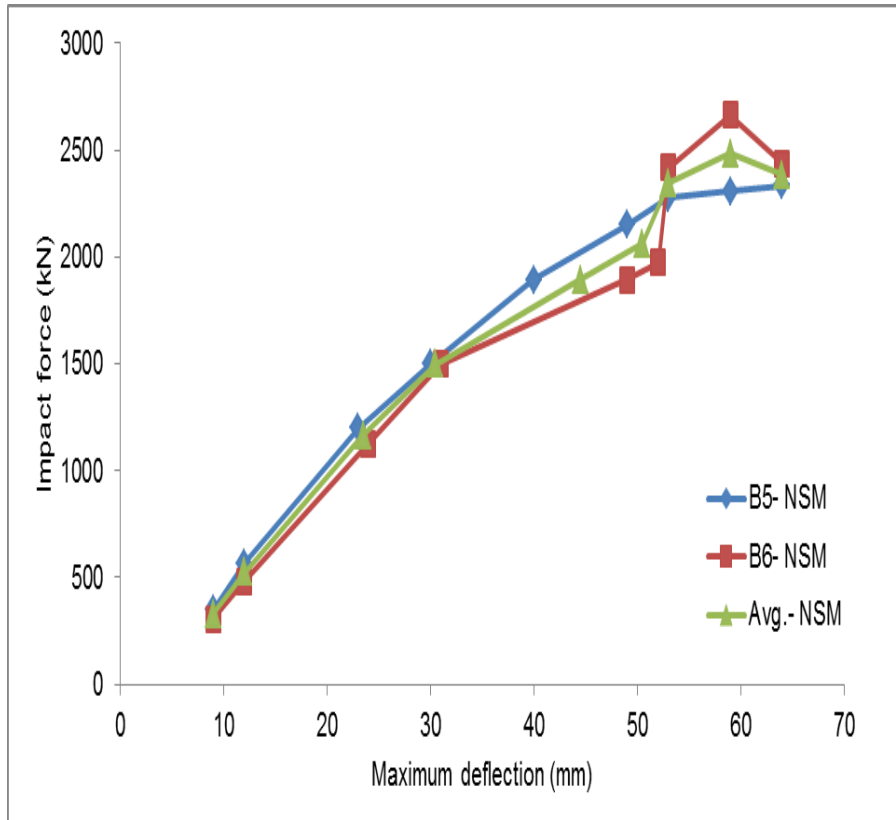
Figure E.29 impact force vs maximum deflection
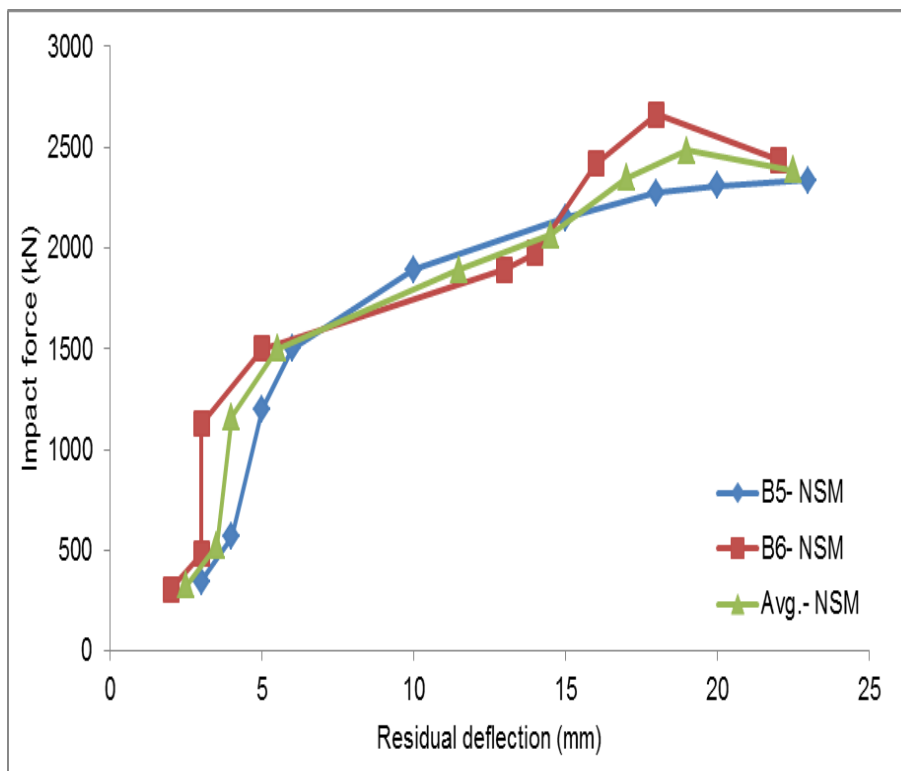
Figure E.30 impact force vs residual deflection

250
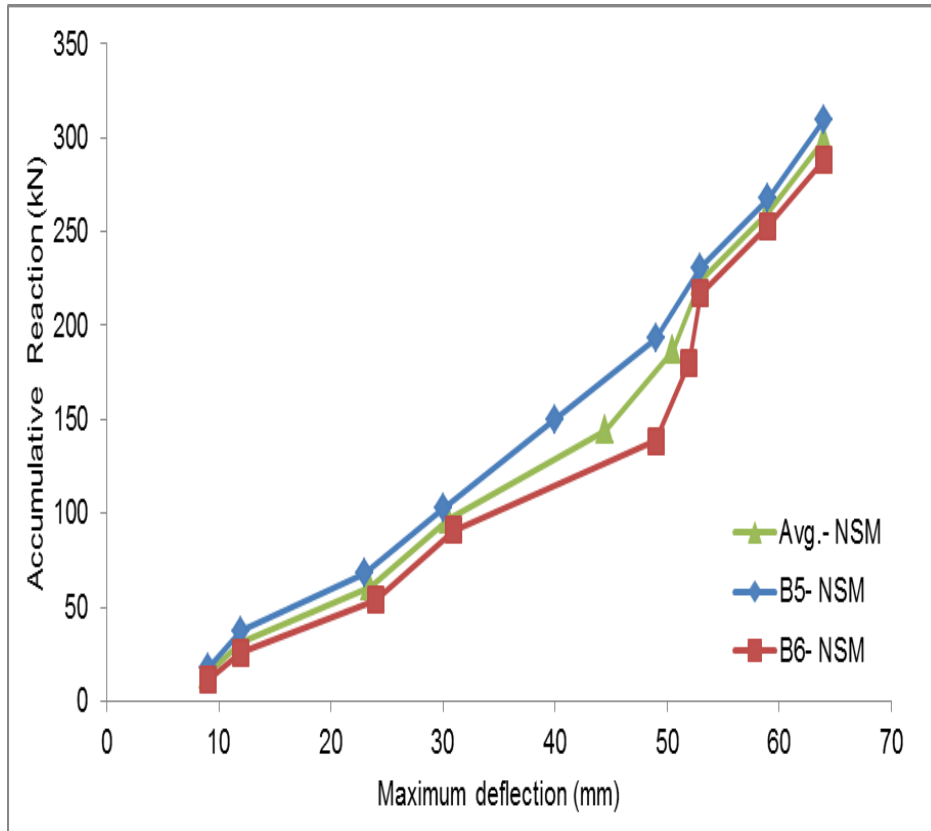
Figure E.31 accumulative reaction force vs maximum deflection
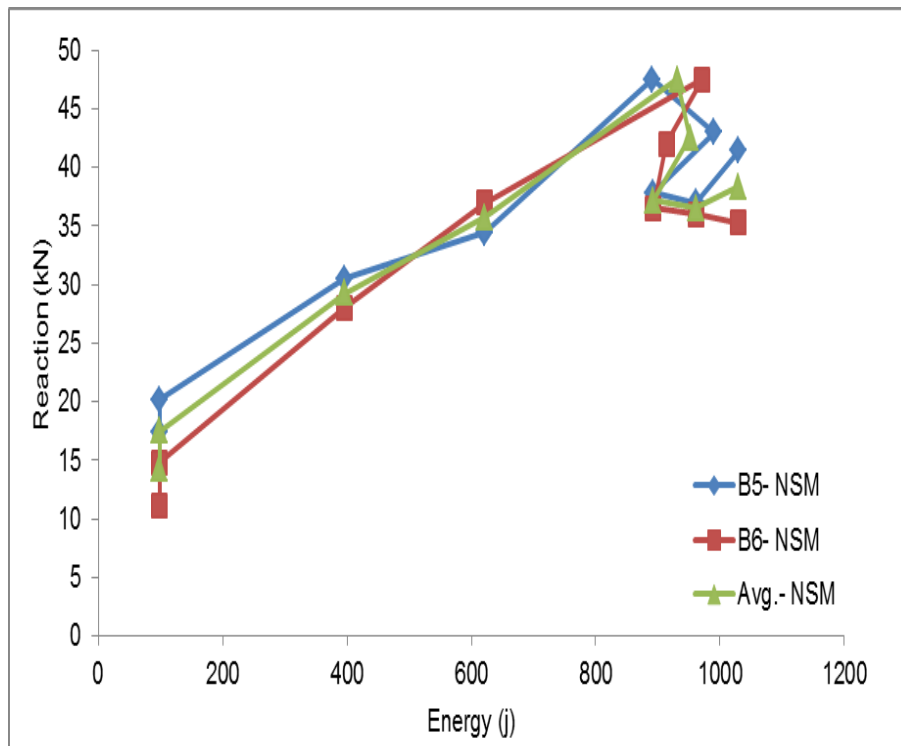
Figure E.32 beam reaction force vs impact energy

251

Figure E.33 accumulative reaction force vs accumulative residual deflection
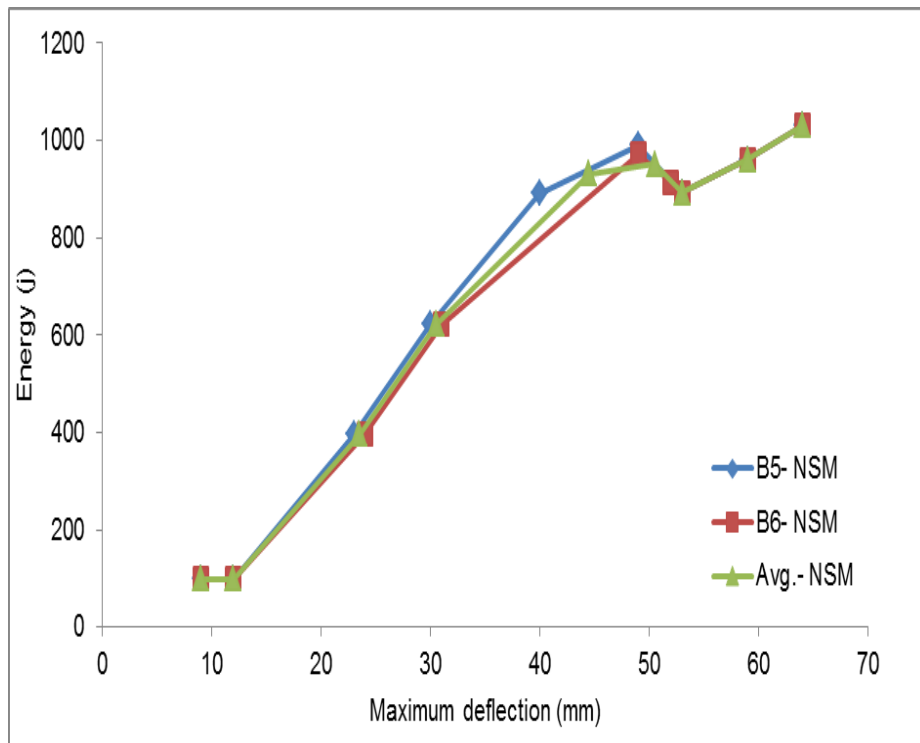
Figure E.34 maximum deflections vs impact energy
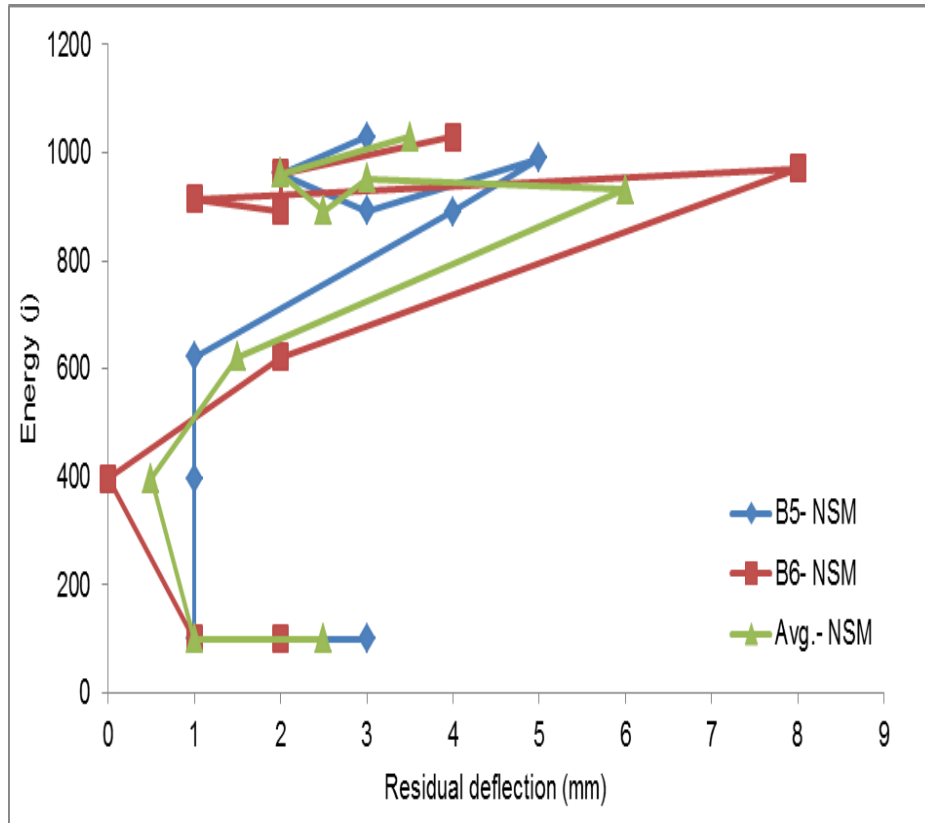
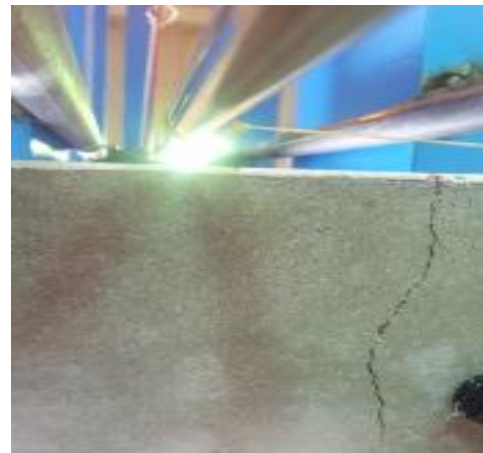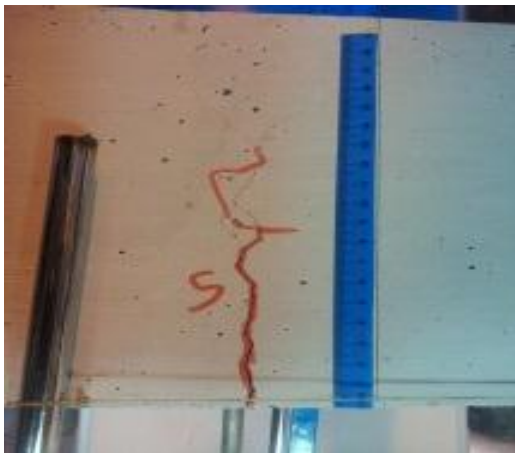**Figure E.35 impact energy vs accumulative residual deflection**
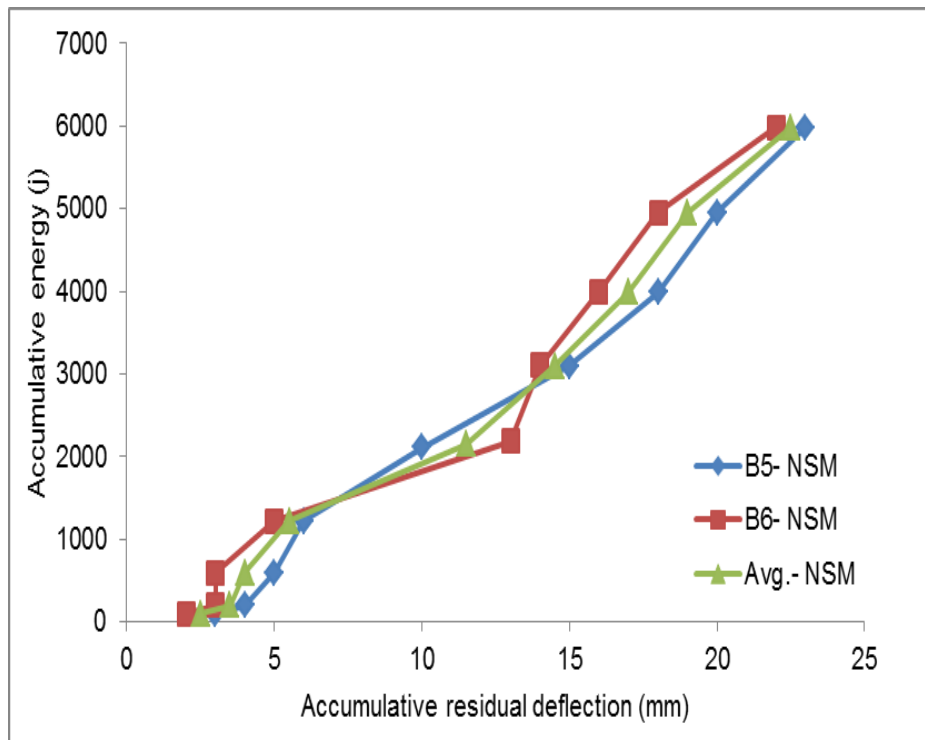
Figure E.36 accumulative energy vs accumulative residual deflection
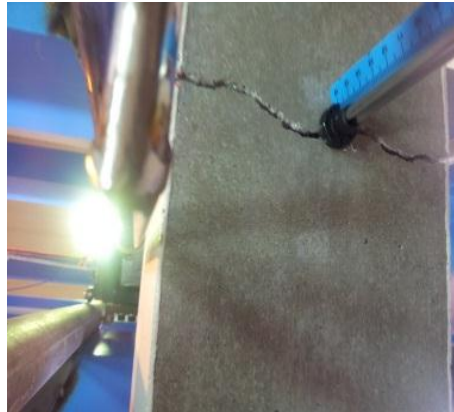
Appendix F control, EBR and NSM beams cracks development

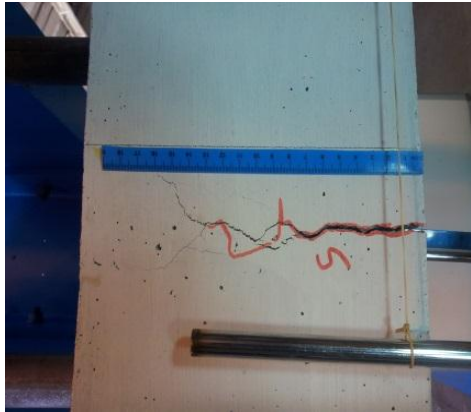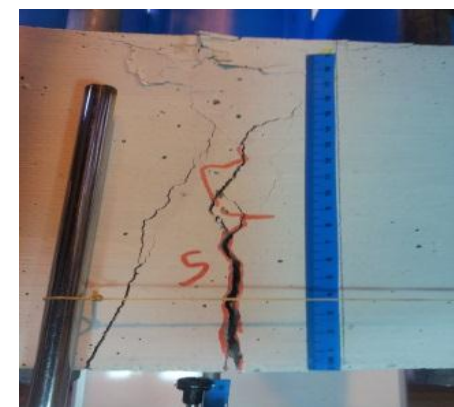**Control beam,** T2: h=0.05 m , w=200 kg

T3: h=0.2 m , w=200 kg

T4: 2: h=0.32 m , w=200 kg

T5: 2: h=0.46 m , w=200 kg

EBR Beam

T1: h=0.05 m , w=200 kg

T2: h=0.05 m , w=200 kg ,   T3: h=0.32 m, w=200 kg
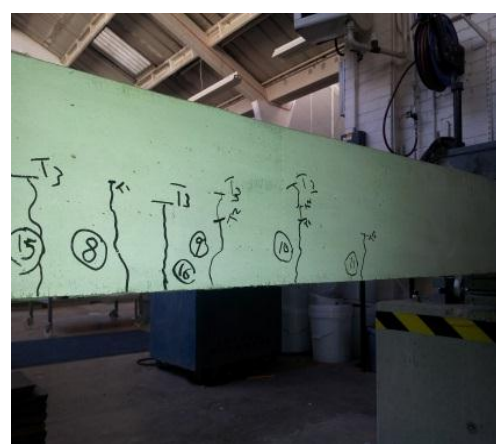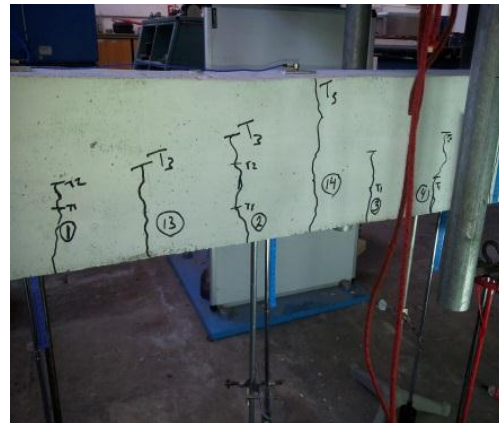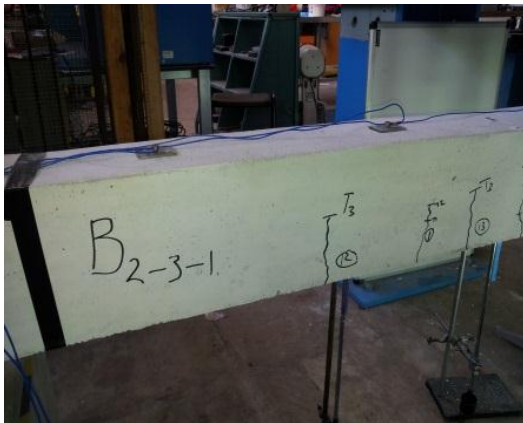
T4: h=0.32 m , w=200 kg
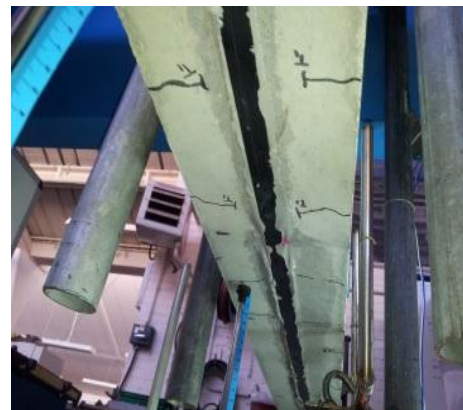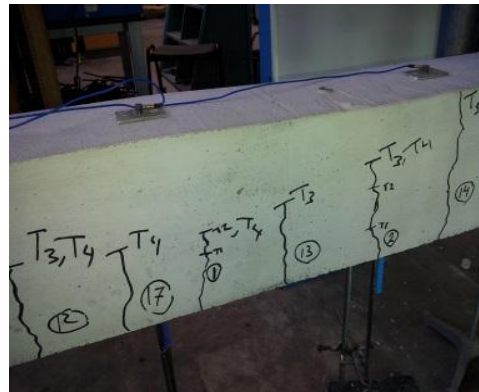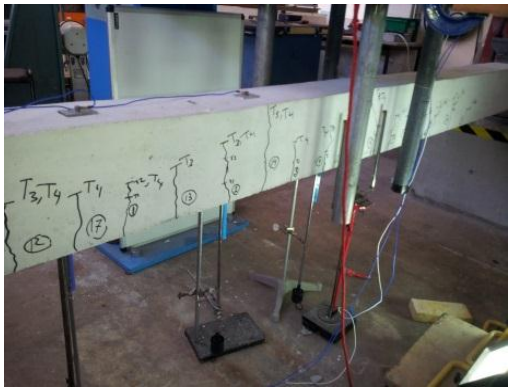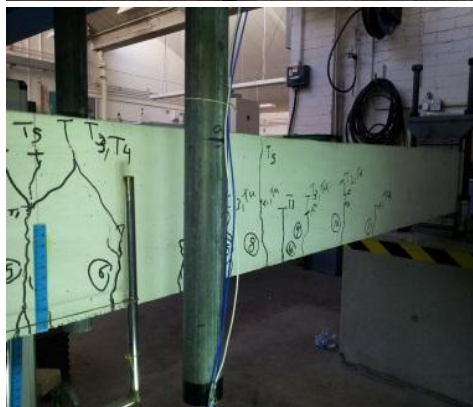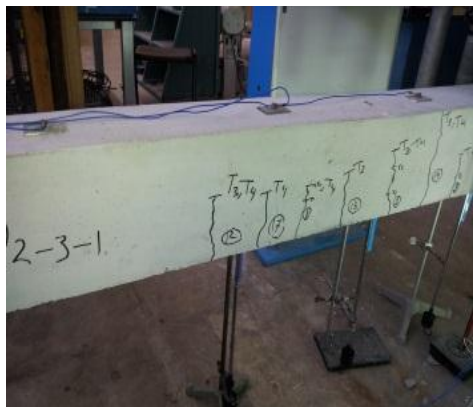
T5: h=0.46 m , w=200 kg
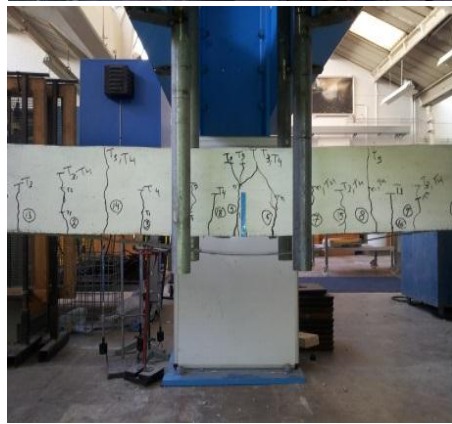
T6: h=0.46 m , w=220 kg

NSM beam

T3: h=0.2 m , w=200 kg
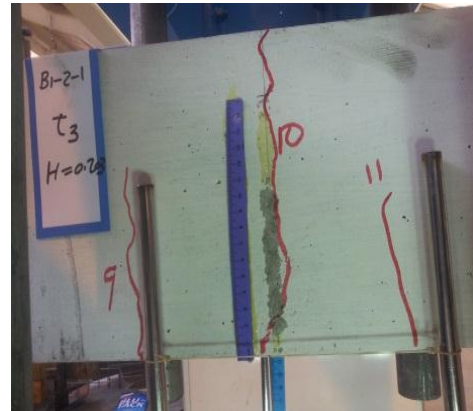
T4: h=0.32 m , w=200 kg
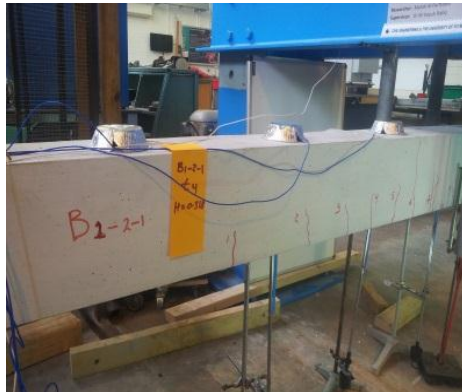
T5: h=0.46 m , w=200 kg
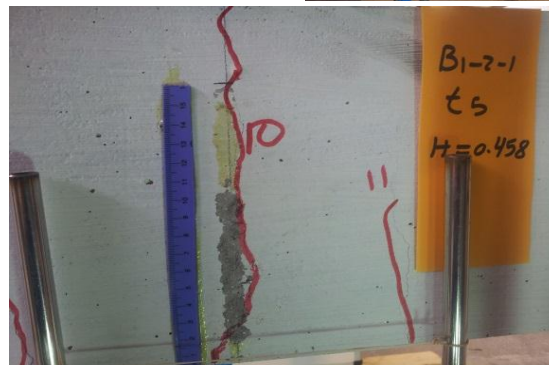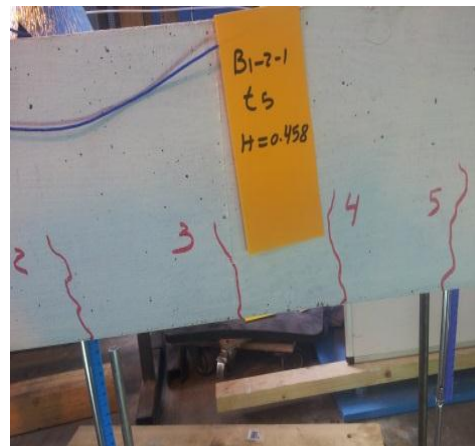
T6: h=0.46 m , w=220 kg

T7: h=0.35 m , w=260 kg

T8: h=0.35 m , w=280 kg

T9: h=0.35 m , w=300kg
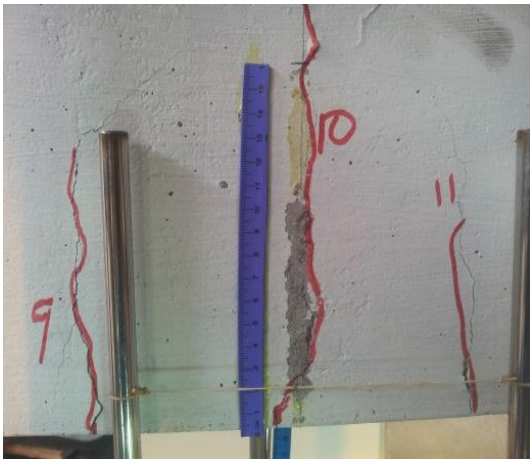
References

ABBAS, H., GUPTA, N. K. & ALAM, M. 2004. Nonlinear response of concrete beams and plates under impact loading. International Journal of Impact Engineering, 30, 1039-1053.

ACI, A. C. I. 2002. 440.2 R-02: Guide for the design and construction of externally bonded FRP systems for strengthening concrete structures. Farmington Hills, MI: American Concrete Institute.

ACI Committee 224.ACI 224.1R-93, 1994. Causes, evaluation and repair of cracks in concrete structures.Manual of Concrete Practice, American Concrete Institute. Detroit.

ACI Committee544 (ACI544.1R-82), 1982. Concrete International. 4, 9–30.

ALZOUBI, FERAS, QI ZHANG, AND ZHENG-LIANG LI. (2007). Shear Strengthening of pre-damaged Reinforced Concrete Beams with Carbon Fiber Reinforced Polymer Sheet Strips. Journal of Chongqing University. 6.4 305-310.

AL-FARTTOOSI, M., RAFIQ, Y., SUMMERSCALESJ.AND WILLIAMSC.2014. Using Model Updating Techniques to assess bond-slip effects on the behaviour of reinforced concrete beams externally strengthened with CFRP. intelligent Computing in Engineering, Cardiff, UK, July 16-18.

AL-MAHMOUD, F., CASTEL, A., FRANÇOIS, R. & TOURNEUR, C. 2010. RC beams strengthened with NSM CFRP rods and modeling of peeling-off failure. Composite Structures, 92, 1920-1930.

AL-SAIDY, A. H., AL-HARTHY, A. S., AL-JABRI, K. S., ABDUL-HALIM, M. & AL-SHIDI, N. M. 2010. Structural performance of corroded RC beams repaired with CFRP sheets. Composite Structures, 92, 1931-1938.

AMORN, P. 2010. Strengthening R/C beams with opening by externally installed FRP rods: Behavior and analysis. Composite Structures, 92, 1957-1976.

ANDREOU, E., DELPAK, R. & TANN, D. 2001. Strengthening of r/c beams with different frps–a comparative study. Structural Faults and Repair.

ARAM, M. R., CZADERSKI, C. & MOTAVALLI, M. 2008. Debonding failure modes of flexural FRP-strengthened RC beams. Composites Part B: Engineering, 39, 826-841.

AU, C. & BÜYÜKÖZTÜRK, O. 2006. Debonding of FRP plated concrete: A tri-layer fracture treatment. Engineering Fracture Mechanics, 73, 348-365.

Azizinamini, A.; Stark, M.; Roller, J. H.; and Ghosh, S. K., 1993, "Bond Performance of Reinforcing Bars Embedded in High-Strength Concrete," *ACI Structural Journal,* V. 90, No. 5, Sept.-Oct., pp. 554-561.

Azizinamini, A.; Chisala, M.; Roller, J. H.; and Ghosh, S. K., 1995, "Tension Development Length of Reinforcing Bars Embedded in High-Strength Concrete," *Engineering Structures*, V. 17, No. 7, pp. 512-522.

A. BADR, A.F. ASHOUR, A.K. PLATTEN. 2006. Statistical variations in impact resistance of polypropylene fiber-reinforced concrete. International Journal of Impact Engineering, 32,1907–1920

A. BILOTTA, F. CERONI, E. NIGRO, M. PECCE. (2015). Efficiency of CFRP NSM strips and EBR plates for flexural strengthening of RC beams and loading pattern influence. Composite Structure.

BANTHIA, N. 1987. Impact resistance of concrete. PhD, University of British Columbia.

BANTHIA, N., MINDESS, S., BENTUR, A. & PIGEON, M. 1989. Impact testing of concrete using a drop-weight impact machine. Experimental Mechanics, 29, 63-69.

BARR, B. & BAGHLI, A. 1988. A repeated drop-weight impact testing apparatus for concrete. Magazine of Concrete Research, 40.

BARROS, J. A. O., DIAS, S. J. E. & LIMA, J. L. T. 2008. Analytical and numerical analysis of the behaviour of RC beams flexural strengthened with CFRP. FRP Composites in Civil Engineering (CICE2008). Zurich, Switzerland.

BARROS, J. A. O., FERREIRA, D. R. S. M., FORTES, A. S. & DIAS, S. J. E. 2006. Assessing the effectiveness of embedding CFRP laminates in the near surface for structural strengthening. Construction and Building Materials, 20, 478-491.

BARROS, J. A. O. & FORTES, A. S. 2005. Flexural strengthening of concrete beams with CFRP laminates bonded into slits. Cement and Concrete Composites, 27, 471-480.

BELTRAMI, C. 2011. Bridge Girder Heavily Damaged by Impact Vehicle Load: A Case Strategy for Structure Assessment and FRP Strengthening. Applied Mechanics and Materials, 82, 606-611.

BENJEDDOU, O., OUEZDOU, M. B. & BEDDAY, A. 2007. Damaged RC beams repaired by bonding of CFRP laminates. Construction and Building Materials, 21, 1301-1310.

BIZINDAVYI L, N. K. 1999. Transfer lengths and bond strengths for composites bonded to concrete. Compos Construc, 3(4), 153-60.

BJÖRN, T. 2003. Strengthening concrete beams for shear with CFRP sheets. Construction and Building Materials, 17, 15-26.

BOROWICZ, D. 2002. Rapid strengthening of concrete beams withpowder-actuated fastening syst. and fiber reinforced polymer (FRP)composite material. MSc, University of Wisconsin-Madison.

BUYUKOZTURK O 1998. Hearing B. Failure behavior of precracked concrete beams retrofitted with FRP. Composite Constructual, 2(3), 44-138.

BÜYÜKÖZTÜRK, O. & LEE, K.-M. 1993. Assessment of interfacial fracture toughness in concrete composites. Cement and Concrete Composites, 15, 143-151.

BIJAN, SAMALI, AND LI JIANCHUN.2005.Stiffness Estimation and Damage Detection of Fibre Reinforced Polymer Strengthened Reinforced Concrete Beams Using a Vibration-Based Method.Australasian Congress on Applied Mechanics Conference.

CANTWELL, W. J. A. S., K. 1999. The static and dynamic response of CFRP-strengthenedconcrete structures. Materials Science Letters, 18(4), 309-310.

CAPOZUCCA, R. & NILDE , M. 2002. Static and dynamic behaviour of RC beam model strengthened by CFRP-sheets. Construction and Building Materials, 16, 91-99.

CERONI F, P. M. Ductility performance of RC Beams Strengthenedwith CFRP sheets. International Conference ERES, 2005 Skiatos, Greece. 89-579.

CHAJES, M. J., FINCH JR, W. W., JANUSZKA, T. F. & THOMSON JR, T. A. 1996. Bond and force transfer of composite-material plates bonded to concrete. ACI structural journal, 93.

CHEN, F. & HODGKINSON, J. M. 2011. Impact Damage. Wiley Encyclopedia of Composites.

CHEN JF, T. J. J. 2001. Anchorage strength models for FRP and steel plates bonded to concrete. Struct Engrg 127(7), 784–91.

CHEN, Y. & MAY, I. 2009. Reinforced concrete members under drop-weight impacts. Proceedings of the Institution of Civil Engineers. Structures and buildings, 162, 45-56.

Darwin, D.; Tholen, M. L.; Idun, E. K.; and Zuo, J., 1996a, "Splice Strength of High Relative Rib Area Reinforcing Bars,"ACI Structural Journal, V. 93, No. 1, Jan.-Feb., pp. 95-107.

Darwin, D.; Zuo, J.; Tholen, M. L.; and Idun, E. K., 1996b, "Development Length Criteria for Conventional and High Relative Rib Area Reinforcing Bars, " ACI Structural Journal, V. 93, No. 3, May-June, pp. 347-359.

Darwin, D.; Idun, E. K.; Zuo, J.; and Tholen, M. L., 1998, "Reliability- Based Strength Reduction Factor for Bond," ACI Structural Journal, V. 95, No. 4, July-Aug., pp. 434-443.

DAVIES, E. & HUNTER, S. 1963. The dynamic compression testing of solids by the method of the split Hopkinson pressure bar. Journal of the Mechanics and Physics of Solids, 11, 155-179.

DE LORENZIS, L. & NANNI, A. 2001. Shear strengthening of reinforced concrete beams with near-surface mounted fiber-reinforced polymer rods. ACI structural journal, 98, 60-68.

DE LORENZIS, L. & TENG, J. G. 2007. Near-surface mounted FRP reinforcement: An emerging technique for strengthening structures. Composites Part B: Engineering, 38, 119-143.

DUAN, M., PERDIKARIS,P.C.,CHEN,W. 2000. Impact Effect of Moving Vehicles, Boca Raton, Wai-Fah Chen and Lian Duan.

EL-ARISS, B. 2011. Instrumented drop weight impact test set-up design and assessment. International Journal of Structural Engineering, 2, 85-99.

El-Hacha, R., El-Agroudy, H., and Rizkalla, S. H.,2006,2 Bond characteristics of high-strength steel reinforcement". *ACI Structural Journal*, 103(Compendex), 771-782.

ERKI, M. & MEIER, U. 1999. Impact loading of concrete beams externally strengthened with CFRP laminates. Journal of Composites for Construction, 3, 117.

ESFAHANI, M. R., KIANOUSH, M. R. & TAJARI, A. R. 2007. Flexural behaviour of reinforced concrete beams strengthened by CFRP sheets. Engineering Structures, 29, 2428-2444.

Esfahani, M. R., and Rangan, B. V., 1996, "Studies on Bond between Concrete and Reinforcing Bars," School of Civil Engineering, Curtin University of Technology, Perth, Western Australia, 315 pp.

F.CERONI 2010. Experimental performances of RC beams strengthened with FRP materials. Construction and Building Materials, 24, 1547-1559.

FARDIS, M. N., AND KHALILI, H. 1981. Concrete Encased in Fiberglass Reinforced Plastic. ACI structural journal, 78(6), 440-446.

FORET, G. & LIMAM, O. 2008. Experimental and numerical analysis of RC two-way slabs strengthened with NSM CFRP rods. Construction and Building Materials, 22, 2025-2030.

FUJIKAKE, K., LI, B. & SOEUN, S. 2009. Impact response of reinforced concrete beam and its analytical evaluation. Journal of Structural Engineering, 135, 938.

GAO, B., KIM, J.-K. & LEUNG, C. K. Y. 2003. Effect of rubber modifier on interlaminar fracture toughness of CFRP-concrete interface. Composites Science and Technology, 63, 883-892.

GARDEN, H. N. & HOLLAWAY, L. C. 1998. An experimental study of the influence of plate end anchorage of carbon fibre composite plates used to strengthen reinforced concrete beams. Composite Structures, 42, 175-188.

GARDEN, H. N., QUANTRILL, R. J., HOLLAWAY, L. C., THORNE, A. M. & PARKE, G. A. R. 1998. An experimental study of the anchorage length of carbon fibre composite plates used to strengthen reinforced concrete beams. Construction and Building Materials, 12, 203-219.

GE, N., SU, Y. & WANG, X. 2010. Investigation on the failure mode of RC members subjected to impulsive loading. Journal of Xi'an University of Architecture & Technology (Natural Science Edition).

GOPALARATNAM, V., SHAH, S. & JOHN, R. 1984. A modified instrumented Charpy test for cement-based composites. Experimental Mechanics, 24, 102-111.

GRACE, N. F. 2004. Concrete repair with CFRP. Concrete international, 26, 45-52.

GRACE, N. F., ABDEL-SAYED, G. & RAGHEB, W. F. 2002. Strengthening of concrete beams using innovative ductile fiber-reinforced polymer fabric. ACI structural journal, 99, 692-700.

GRACE, N. F., SAYED, G., SOLIMAN, A. & SALEH, K. 1999. Strengthening reinforced concrete beams using fiber reinforced polymer (FRP) laminates. ACI Structural Journal-American Concrete Institute, 96, 865-874.

GRAVINA, R. J. & SMITH, S. T. 2008. Flexural behaviour of indeterminate concrete beams reinforced with FRP bars. Engineering Structures, 30, 2370-2380.

Grusova, M., Ibell, T. J., Darby, A. P., & Evernden, M. 2013. Shear transfer in CFRP strengthened reinforced concrete. Proceedings of the Advanced Composites in Construction (ACIC).

GUNES, O. 2002. Characterization and modeling of debonding in rc beams strengthened with frp composites. ASCE Engineering Mechanics. Columbia University, New York, NY.

GUNES, O., BUYUKOZTURK, O. & KARACA, E. 2009. A fracture-based model for FRP debonding in strengthened beams. Engineering Fracture Mechanics, 76, 1897-1909.

HAMED, E. & RABINOVITCH, O. 2005. Dynamic effects in continous RC beams strengthened with externally bonded FRP strips and subjected to dynamic loading. Composites in Construction. Lyon, France.

Hadje-Ghaffari, H., Choi, O. C., Darwin, D., and McCabe, S. L.,1994,2 Bond of epoxy-coated reinforcement: Cover, casting position, slump, and consolidation," *ACI Structural Journal*, 91(Compendex), 59-68.

Harajli, M. H., Hamad, B. and Kram, K. (2002). "Bond-slip response of reinforcing bars embedded in plain and fiber concrete" J. Mat. in Civ. Engrg., V. 14(6), 503-511.

HOPKINSON, B. 1914. A method of measuring the pressure produced in the detonation of high explosives or by the impact of bullets. Proceedings of the Royal Society of London. Series A, 89, 411-413.

Hamad, B.S., 1993.Evaluation and Repair of War-damaged Concrete Structures in Beirut. Concrete International: Design and Construction, v 15, pp. 47-51.

HOQUE, M. M. 2006. 3D Nonlinear Mixed Finite Element Analysis of RC Beams and Plates with and without FRP Reinforcement. MSc, Manitoba, Canada.

HOSNY, A., SHAHEEN, H., ABDELRAHMAN, A. & ELAFANDY, T. 2006. Performance of reinforced concrete beams strengthened by hybrid FRP laminates. Cement and Concrete Composites, 28, 906-913.

ISMAIL Z, ONG AZC AND RAHMAN AGA, (2011). Crack damage detection of reinforced concrete beams using local stiffness indicator. Scientific Research and Essays. 6(34): 6798–6803.

IMBEAU, P. P., D.; ALMANSOUR, H. 2011. State-of-the-art review of retrofit methodologies for concrete elements subjected to impact loading2nd international Engineering Mechanics and Materials Specialty Conference. Ottawa, Ontario.

I. Sharaky, L. Torres, J. Comas, C. Barris. (2014). Flexural response of reinforced concrete (RC) beams strengthened with near surface mounted (NSM) fibre reinforced polymer (FRP) bars. Compos Structure, p. 109

JEROME, D. M. & ROSS, C. A. 1997. Simulation of the dynamic response of concrete beams externally reinforced with carbon-fiber reinforced plastic. Computers & Structures, 64, 1129-1153.

Jefferson, A.D. 1999. "A multi-crack model for the FE analysis of concrete" Proceeding of *BCA Concrete Conference*, 275-286.

JIN, D. 2004. Shear Capacity of reinforced concrete beams without web. Journal of Chang'an University (Natural Science Edition), 5.

JOHN L. HUDSON, DAVID DARWIN. 2005. Evaluation and Repair of Blast Damaged Reinforced Concrete Beams. Technical Report, University of Kansas.

JUMAAT, M. & ALAM, A. 2008. Experimental and Analytical Investigations on the Structural Behaviour of Steel Plate and CFRP Laminate Flexurally Strengthened Reinforced Concrete Beams. Journal of Applied Sciences, 8, 4383-4389.

JUNG, W., PARK, Y., PARK, J., KANG, J. & YOU, Y. Experimental investigation on flexural behavior of RC beams strengthened by NSM CFRP reinforcements. 2005. 7–10.

JUNG WT, P. H., PARK JS, KANG JY, YOO YJ. Experimental Investigation on Flexural Behavior of RC Beams Strengthened by NSM CFRP Reinforcement.InternationalSymposium on Fiber-Reinforced (FRP) Polymer Reinforcement forConcrete Structures, 2005 ACI Symp. SP-230-46, 795-806.

JUNG WT, P. J., PARK YH. A study on the Flexural Behavior ofReinforced Concrete Beams Strengthened with NSM PrestressedCFRP Reinforcement. International Symposium on

Fiber-Reinforced Polymer Reinforcement in Concrete Structures, 2007 FRPRCS-8, Partas, Greece,PP.8-10. pp. 8-10.

KABIR, M. Z. & SHAFEI, E. 2009. Analytical and Numerical Study of FRP Retrofitted RC Beams Under Low Velocity Impact. Scientia Iranica Transaction A: Civil Engineering, 16, 415-428.

Karabinis, A.I. and Rousakis, T.C.,2002."Concrete confined by FRP material: a plasticity approach" ,Engineering Structures, Vol. 24, pp. 923-932.

KACHLAKEV, D. & MCCURRY, D. D. 2000. Behavior of full-scale reinforced concrete beams retrofitted for shear and flexural with FRP laminates. Composites Part B: Engineering, 31, 445-452.

KANTAR, E., ERDEM, R. T. & ANıL, Ö. 2011. Nonlinear finite element analysis of impact behavior of concrete beam. Mathematical and Computational Applications, 16, 183-193.

KATSUMATA, H., KOBATAKE, Y. & TAKEDA, T. A study on the strengthening with carbon fiber for earthquake-resistance capacity of existing reinforced concrete columns. Earthquake Engineerig, 1988 Tokyo-Kyoto, JABA.

KHALIFA, A. & NANNI, A. 2000. Improving shear capacity of existing RC T-section beams using CFRP composites. Cement and Concrete Composites, 22, 165-174.

KHALIFA, A., TUMIALAN, G., NANNI, A. & BELARBI, A. 1999 , Shear strengthening of continuous RC beams using externally bonded CFRP sheets. FRP for Reinforcement of Concrete Structures (FRPRCS4), Baltimore. 689-696.

KIM, Y. J., GREEN, M. F. & FALLIS, G. J. 2008. Repair of bridge girder damaged by impact loads with prestressed CFRP sheets. Journal of Bridge Engineering, 13, 15.

KISHI, N., OHNO, T., KONNO, H. & BHATTI, A. 2006. Dynamic Response Analysis for a Large-Scale RC Girder under a Falling-Weight Impact Loading. Advances in Engineering Structures, Mechanics & Construction, 99-109.

KOLSKY, H. An Investigation of the Mechanical Properties of Materials at very High Rates of Loading Phys, 1949 Soc.

KOTYNIA, R. 2011. NSM FRP shear contribution in the strengthened RC beamsSmart Monitoring, Assessment and Rehabilitation of Civil Streuctures. Dubai, UAE.

LAKSHMIKANDHAN K. N, SIVAKUMAR P, RAVICHANDRAN R.2013.Damage Assessment and Strengthening of Reinforced Concrete Beams. International Journal of Material and Mechanical Engineering,v2.

LAMANNA, A. J., BANK, L. C. & BOROWICZ, D. T. 2004a. Mechanically fastened FRP strengthening of large scale RC bridge T beams. Advances in structural engineering, 7, 525-538.

LAMANNA, A. J., BANK, L. C. & SCOTT, D. W. 2001. Flexural strengthening of reinforced concrete beams using fasteners and fiber-reinforced polymer strips. ACI structural journal, 98, 368-376.

LAMANNA, A. J., BANK, L. C. & SCOTT, D. W. 2004b. Flexural strengthening of reinforced concrete beams by mechanically attaching fiber-reinforced polymer strips. Journal of Composites for Construction, 8, 203-210.

LIU, I. S. T., OEHLERS, D. J. & SERACINO, R. 2006. Tests on the ductility of reinforced concrete beams retrofitted with FRP and steel near-surface mounted plates. Journal of Composites for Construction, 10, 106.

LOPEZ, A. & NANNI, A. 2006. Composite Strengthening Technologies. CONCRETE INTERNATIONAL, 28, 74.

LUC, T. & STIJN, M. 2011. USE OF FRP IN CONCRETE STRUCTURES: TRENDS AND CHALLENGES. FIB symposium on concrete engineering for excellence and efficiency. Prague, Czech Republic: Czech Concrete Society.

LUSAS. 2012. Finite Element Analysis Ltd. Surray, United Kindom, version 14.

MASOUD, S., SOUDKI, K. & TOPPER, T. 2001. CFRP-strengthened and corroded RC beams under monotonic and fatigue loads. Journal of Composites for Construction, 5, 228.

MAY, I. M., CHEN, Y., OWEN, D. R. J., FENG, Y. & BERE, A. T. 2005. Experimental testing and finite element simulation of the behaviour of reinforced concrete beams under impact loading. Proc., COMPLAS VIII.

MAECK, JOHAN, ET AL. 2000."Damage identification in reinforced concrete structures by dynamic stiffness determination.Engineering structures.22.10 : 1339-1349.

MEIER, U. 1987. Bridge Repair with High PerformanceComposite Materials. Material und Technik, 4, 125-128.

MOHAMMED, T. & PARVIN, A. 2011. Impact Load Response of Concrete Beams Strengthened with Composites.

MUKHOPADHYAYA, P., AND SWAMY, N. 2001. Interface shear stress: a new design criterionfor plate debonding. Journal of Composites for Construction, ASCE, 5(1), 35-43.

NGUYEN, D. M., CHAN, T.K., AND CHEONG, H.K. 2001. Brittle failure and bond development length of CFRP concrete beams. Journal of Composites for Construction, ASCE, 5(1), 12-17.

NORDIN, H. 2003. Fibre reinforced polymers in civil engineering: flexural strengthening of concrete structures with prestressed near surface mounted CFRP rods. licentiate, Lulea University of Technology.

OBAIDAT, Y. T. 2011. Structural Retrofitting of Concrete Beams Using FRP. Canadian Journal of Civil Engineering.

OBAIDAT, Y. T., HEYDEN, S., DAHLBLOM, O., ABU-FARSAKH, G. & ABDEL-JAWAD, Y. 2011. Retrofitting of reinforced concrete beams using composite laminates. Construction and Building Materials, 25, 591-597.

OEHLERS, D. J., RASHID, R. & SERACINO, R. 2008. IC debonding resistance of groups of FRP NSM strips in reinforced concrete beams. Construction and Building Materials, 22, 1574-1582.

Ogura, N., Bolander, J. E., and Ichinose, T. 2008, "Analysis of bond splitting failure of deformed bars within structural concrete". *Engineering Structures*, 30(Compendex), 428-435.

RAFIQ, Y. AND AL-FARTTOOSI, M. (2013). "Using Model Updating to Predict the Failure of Reinforced Concrete Elements". Computing in Civil Engineering (2013), ASCE Conference in LA: pp. 459-467.

RAFIQ, Y. AND AL-FARTTOOSI, M. (2014). "Predicting the behaviour of reinforced concrete elements strengthened with CFRP using model updating techniques",ASCE, ICCCBE, CIBW74 conference.

RAMI A, H. 2012. Nonlinear finite element modeling of RC beams strengthened with NSM FRP rods. Construction and Building Materials, 27, 461-471.

REINHARDT, H., KÖRMELING, H. & ZIELINSKI, A. 1986. The split Hopkinson bar, a versatile tool for the impact testing of concrete. Materials and structures, 19, 55-63.

RENATA, K. Bond between FRP and concrete in reinforced concrete beams strengthened with near surface mounted and externally bonded reinforcement. Construction and Building Materials.

RITCHIE, P. A., THOMAS, D. A., LU, L. W. & CONELLY, G. M. 1991. External reinforcement of concrete beams using fiber reinforced plastics. ACI structural journal, 88.

RIZZO, A. & DE LORENZIS, L. 2009a. Behavior and capacity of RC beams strengthened in shear with NSM FRP reinforcement. Construction and Building Materials, 23, 1555-1567.

RIZZO, A. & DE LORENZIS, L. 2009b. Modeling of debonding failure for RC beams strengthened in shear with NSM FRP reinforcement. Construction and Building Materials, 23, 1568-1577.

ROBERTO, C. 2009. Static and dynamic response of damaged RC beams strengthened with NSM CFRP rods. Composite Structures, 91, 237-248.

SAADATMANESH, H. & EHSANI, M. R. 1991. RC beams strengthened with GFRP plates. I: Experimental study. Journal of Structural Engineering, 117, 3417-3433.

SAATCI, S. 2007. Behaviour and modelling of reinforced concrete structures subjected to impact loads.

SAATCI, S. & VECCHIO, F. J. 2009a. Effects of shear mechanisms on impact behavior of reinforced concrete beams. ACI structural journal, 106, 78-86.

SAATCI, S. & VECCHIO, F. J. 2009b. Nonlinear Finite Element Modeling of Reinforced Concrete Structures under Impact Loads. ACI structural journal, 106, 717.

SENA-CRUZ, J., BARROS, J. A. O., COELHO, M. R. F. & SILVA, L. F. F. T. 2011. Efficiency of different FRP-based flexural strengthening techniques in beams submitted to fatigue loading. Construction and Building Materials, 29, 175-182.

SHAHAWY, M. & BEITELMAN, T. E. 1999. Static and fatigue performance of RC beams strengthened with CFRP laminates. Journal of Structural Engineering, 125, 613.

SHAHAWY, M. A., AROCKIASAMY, M., BEITELMAN, T. & SOWRIRAJAN, R. 1996. Reinforced concrete rectangular beams strengthened with CFRP laminates. Composites Part B: Engineering, 27, 225-233.

SMITH, S. T. & TENG, J. G. 2001. Interfacial stresses in plated beams. Engineering Structures, 23, 857-871.

SMITH P.D.,HETHERINGTON J.G.1994.Blast and Ballistic Loading of Structures. Oxford, , UK: Butterworth-Heinemann.

SOEUM, S., FUJIKAKE, K., MATSUI, T. & SUZUKAWA, K. 2008. Resistance of CFRP strengthened RC beams under impact loadings.

SOLEIMANI, S. & BANTHIA, N. 2012. A Novel Drop Weight Impact Setup for Testing Reinforced Concrete Beams. Experimental Techniques.

STRUCK, W. & VOGGENREITER, W. 1975. Examples of impact and impulsive loading in the field of civil engineering. Materials and structures, 8, 81-87.

SWAMY, R. N. & JOJAGHA, A. H. 1982. Impact resistance of steel fibre reinforced lightweight concrete. International Journal of Cement Composites and Lightweight Concrete, 4, 209-220.

TÄLJSTEN, B., CAROLIN, A. & NORDIN, H. 2003. Concrete structures strengthened with near surface mounted reinforcement of CFRP. Advances in structural engineering, 6, 201-213.

TANARSLAN, H. 2011. The effects of NSM CFRP reinforcements for improving the shear capacity of RC beams. Construction and Building Materials, 25, 2663-2673.

TANARSLAN, H. MURAT. 2010. Repairing and strengthening of earthquake-damaged RC beams with CFRP strips. Magazine of Concrete Research.62.5 ,pp. 365-378.

TANG, T. & HAMID SAADATMANESH, P. 2003. Behavior of concrete beams strengthened with fiber-reinforced polymer laminates under impact loading. Journal of Composites for Construction, 7, 209.

TANG, T. & SAADATMANESH, H. 2005. Analytical and experimental studies of fiber-reinforced polymer-strengthened concrete beams under impact loading. ACI structural journal, 102.

TRIANTAFILLOU, T. & PLEVRIS, N. 1992. Strengthening of RC beams with epoxy-bonded fibre-composite materials. Materials and structures, 25, 201-211.

VALERIO, P., IBELL, T. J., & DARBY, A. P. (2009). Deep embedment of FRP for concrete shear strengthening. Proceedings of the ICE-Structures and Buildings, 162(5), 311-321.

WANG, N., MINDESS, S. & KO, K. 1996. Fibre reinforced concrete beams under impact loading. Cement and concrete research, 26, 363-376.

WANG, S.-P., HOU, S.-L. & WANG, B. The effect of bond length on the flexural behavior of RC beam strengthened with NSM CFRP Bar. Electric Technology and Civil Engineering (ICETCE), 2011 International Conference on, 22-24 April 2011 2011. 6278-6281.

Wang, X., Liu, L. (2003). "A strain-softening model for steel–concrete bond" Cement and Concrete Research 33, 1669-1673.

WOLF, R., AND MIESSLER, H. J. 1989. HLV-Spannglieder in der Praxis. Erfahrungen Mit Glasfaserverbundstaben, 2, 47-51.

W.K.K.G. Kalupahana, T.J. Ibell, A.P. Darby. 2013. Bond characteristics of near surface mounted CFRP bars. Construction Build Materials, pp. 58–68.

YOSHITAKE, I., KIM, Y. J., YUMIKURA, K. & MIMURA, Y. 2011. Composite strips with various anchor systems for retrofitting concrete beams. International Journal of Concrete Structures and Materials, 5, 43-48.

YOSHITAKE I., Y. J. K., KEIYU YUMIKURA,YOICHI MIMURA 2011. Composite Strips with Various Anchor Systems for Retrofitting Concrete Beams. International Journal of Concrete Structures and Materials5(1), 43-48.

Yu ,T., Teng ,J. G., Wong ,Y. L., Dong ,S. L.,2010. " Finite element modelling of confined concrete-I:

Drucker-Prager type plasticity model" *Engineering Structures*,32(3): 665-679.

ZHANG, X. X., RUIZ, G. & YU, R. C. 2010. A New Drop-Weight Impact Machine for Studying Fracture Processes in Structural Concrete. Strain, 46, 252-257.

ZHOU, L., HAN, L. & LI, Y. 2009. Finite element simulation on collision of ship with cross-sea bridge and protection of marine structures. Computer Aided Engineering, 04.